
CHAPTER – 1

INTRODUCTION

1.1 Motivation

Among many other factors, process systems engineering (in which CFD can be considered a tool) can aid industrial growth. This is the belief and motivation of the author outlined in this section. Process industries include among others, the chemical, petrochemical, food, agrochemical, automotive, electronic, metallurgical, and ship building industries. The terms ‘industrial design’ and ‘process design’ are allied terms usually applied to products which are *mass produced*. Industrial design is the *process of design* required to obtain the final product which is distinguished from, and precursor of the actual physical manufacture of the product. It entails conceptualizing and determining all the steps required to create the specified product. Hence all industrial production is the result of process design. Chemical engineers more commonly use the term ‘process design’ to describe all the physical and chemical transformations applied to the raw materials before final product formation. For process design, design tools are required. Design tools usually include experimentation on lab-scale and pilot plant scale, as well as mathematical or numerical modeling. In this context Computational Fluid Dynamics (CFD) has a role to play as a numerical or computational design tool (Davidson, 2001a).

Industrialization increasingly occupies a pivotal position in meeting basic needs of a nation. The quality of life and standard of living of individuals in particular and society as a whole is dependent on the abundance and quality of commercial products. These products are in turn dependent on the health of the industrial sectors. Another

factor related to the standard of living is the jobs creation in the economy. A larger number of jobs and also better paying jobs in turn pump up the economy creating larger investment in the industrial sector. The starting point of this economic growth cycle is therefore the performance of process industries. The performance of major chemicals in India from 2006 to 2014 showing the chemical growth rate (CGR) in this period as released by Government of India report (2014) is given in Table 1.1. (<http://chemicals.gov.in/>: 26/Oct/2014)

Table 1.1 Performance of major chemicals in India from 2006-2014

(Statistics are in metric tones $\times 10^3$)									
HEAD	2006-07	2007-08	2008-09	2009-10	2010-11	2011-12	2012-13	2013-14	CGR (%) (2006-2014)
Capacity	10190	10661	10709	11345	11578	11926	11888	12039	2.41
Production	7713	7945	7564	7895	8509	8730	8690	8839	1.97
Imports	1446	1922	2378	2651	2514	3162	6820	3721	14.46
Exports	581	626	599	1187	1268	1317	1087	1087	9.37

Production growth has only increased by about 1.97% in the period from 2006 to 2014 (Table 1.1). The data indicates a need for increase in the chemical growth rate (CGR). The answer lies not just in improving plant capacity but also in increasing the number of plants in total. The former relates to ‘process systems engineering’ which deals with overall behavior of a system such as a manufacturing plant or even a part of it. Models developed can then be integrated to predict and test outcome of various design options and process changes. CFD is a useful tool in this context as well as for design, scale-up

and start-up of new plants. It can reduce the amount of experimentation and potentially the cost of pilot-plant investments. CFD simulations may never completely replace experimentation and pilot-plant runs, but it has the potential to supplement them. Other benefits are improved design reliability and shortened to market time (Davidson, 2001b). The benefit of design reliability is exemplified by the fact that CFD design of equipment may be made *without* any assumptions about the macroscopic flow pattern. This leads to nearly accurate and comprehensive design of the flow equipment *the very first time*, instead of a slow process of improving design by monitoring the equipment after installation. There is evidence that CFD is generally superior as a design tool for geometrically complicated parts when compared to rules-of-thumb or experiments. These advantages have been documented in the USA for fiber spinning operations resulting in ‘right the first time’ designs (Davidson, 2001b). Documentation of the extent to which CFD is already aiding production in India is not currently open source, to the best of our knowledge. The fact that commercially produced CFD codes such as ANSYS FLUENT have been available only for the last decade or so in India might imply that process industries are yet to significantly benefit from the use of CFD. There is evidence that the USA is already ahead in this. A case study of the economic benefit of the application of CFD in one chemical and engineered-material company over a six-year period conservatively estimated that the application of CFD generated approximately a six-fold return on the total investment in CFD (Davidson, 2001b).

1.2 Computational Fluid Dynamics: a potent research tool

In this section we define CFD and bring out its potential as a valuable research tool which this work as a whole demonstrates. Computational fluid dynamics is an offshoot of fluid mechanics. In fluid mechanics the fundamental principles that govern the physical aspects of fluid flow are (i) mass conservation (ii) Newton's second law or momentum conservation and (iii) energy conservation. These laws are expressed either as integral equations or partial differential equations. In some engineering applications these laws can be simplified considerably using assumptions so that analytical solutions are possible. It is clear that such an approach has limited applicability. The predictions derived might also be limited in their validity due to the many simplifying assumptions made. Despite this, analytical solutions still play an important role in modeling (Anderson, 1995). Lab-scale experimental measurements usually enable realistic predictions to model simple to complex engineering problems. CFD predictions can supplement laboratory data in research work. Using CFD as a tool, researchers can carry out *numerical experiments* for system size ranging from lab-scale to industrial scale. The latter would consume considerable computational resources. Hence in addition to being an engineering scale-up tool, CFD is used as a research tool to study, model or illuminate the science of various flow phenomenon like mixing, swirling flows, boundary layer development, cavitation, capillary action, multi-phase flow, non-Newtonian flows, reacting flows etc.

The concept behind the solution method in CFD is to find numerical values of the flow variables at a large number of points in the flow. These points are connected together to form a 'mesh' or 'grid' which could be square, rectangular or polyhedral in two or three spatial dimensions. The refinement of the mesh controls the number of

calculations. The system governing equations are converted to a set of algebraic equations representing the interdependency of flow at the grid points. The procedure for converting partial differential equations to algebraic equations is referred to as ‘discretization’. We now have a system where the unknowns are the flow variables at the grid points. Using other system relevant information like boundary conditions, initial conditions and species stoichiometry, the numbers of equations are made equal to the unknowns. The resulting set of algebraic equations in matrix form may be linear or non-linear. Solution to these equations involves matrix manipulations which are efficiently accomplished by digital computer. The number of calculations is of course dependent on the number of grid points and is limited by the computational resources. The solution procedure is repeated at increasing discrete time intervals to predict the evolution in time of the flow variables at the grid points. The CFD solution is therefore given in terms of ‘fields’ of the flow variables at different time intervals. In summary the three basic steps common to all CFD solution methods include (i) subdivision or discretization of the flow domain into cells or elements (ii) discretization of the governing equations and (iii) solution of the resulting algebraic equations. These three basic steps are elaborated into ten workable points that constitute the general CFD solution procedure as given in Table 1.2.

As commercial and open-source CFD solvers become more accessible, we are seeing a growing number of publications which use CFD as a tool for data generation and analysis. These research works cut across the disciplines of chemical, civil, mechanical, and environmental engineering. The use of CFD as a tool can be loosely linked with the concept of ‘thought experiment’. The goal of a thought experiment is to explore the

potential consequences of the principle or hypothesis in question by using the mind and imagination.

Table 1.2 The generalized CFD solution procedure (Anderson, 1995).

1.	Problem statement	Define all relevant information about the flow or system
2.	Governing equations formulation	Formulate Initial Boundary Value Problem from : Partial Differential Equations + Initial Conditions + Boundary Conditions
3.	Mesh generation	Define grid points, their pattern and density in the flow domain
4.	Space discretization	Derive a linear algebraic system of equations: $Ax = b$
5.	Time discretization	
6.	Iterative solution	The algebraic system of equations is solved using solution values from the previous iteration. This is done in a coupled or segregated manner until a convergence criterion is met
7.	Simulation Monitoring	The progress of the simulation is monitored by plotting residuals for progressive iterations. Key flow variables can also be monitored
8.	Simulations display	The numerical solution is usually displayed in the form of contours of the flow variables also called fields of the variables or simply simulations
9.	Postprocessing	Required data in the form of various plots may be extracted from the simulations
10.	Validation	The extracted data or simulations may be compared to experimental or other modeling results

In CFD one does a ‘virtual experiment’ by implementing specific physical laws in the form of equations. These equations are solved by computers and reveal the effects of these equations in a physical domain. Take for example the problem of finding the velocity profile of fluid flow through a pipe of complex geometry. The researcher mainly inputs the domain dimensions in the form of a mesh and codes or activates mainly the

Navier-Stokes equation for viscous. The computer carries the problem to completion by calculating the consequence of the given equations on the mesh. The velocity profile is then revealed from the simulation of velocity field. This process, as directed by the researcher, becomes a ‘virtual experiment’. The computer along with the case developed, now becomes a ‘transportable experimental set-up’. It might be argued that the solutions obtained from the CFD case study, are free from many errors that experimental systems are difficult to insulate from. Take for example errors of measurement and other human errors. However, errors do exist in CFD computation as well. These commonly include (i) truncation error in discretization (ii) residual error in satisfying the model equations and (iii) round-off or chopping error in calculated values due to the fact that computer resources are not infinite. Most importantly, the reliability of the CFD solution depends on how accurately the models are able to capture the real life phenomenon in question. Even with well accepted models non-idealities of this nature do exist and these are usually referred to as ‘physical modeling errors’. These include uncertainty in model assumptions, boundary conditions, initial conditions and data input. Another example is simplification in the analysis like modeling a viscous flow as inviscid. In spite of these limitations, CFD virtual experimentation has certain unique features over laboratory experimentation:

i. Measurement of entire fields Vs measurements at limited points:

CFD gives unique insight into a particular phenomenon or flow because the simulations obtained are in terms of fields. For example, in a fluidized bed, CFD can reveal the entire solid particle concentration in the reactor by displaying the solid packing contours. In experiment, an average bed voidage is usually calculated from measuring the height of

the bed. Here, even if the solid packing is visible, the speed of the flow makes it difficult to inspect. This is not a limitation in CFD simulations where snapshots after every time step can be inspected at length. Further, *invisible* field variables like temperature, pressure, velocity, granular temperature etc. are revealed by CFD snapshots. In experimentation there are limitations on the number of points at which measurements can be made in time and space. Take another example of finding the velocity profile of pipe flow in experimental set-up using a Pitot-tube. The number of points at which the local velocity can be measured is very limited. In addition, the very presence of the Pitot-tube hampers the flow. These difficulties do not arise when using CFD to find the solution.

ii. multi-quantity measurement Vs single quantity measurement:

In CFD the flow quantities are measured all at once i.e. one simulation run is sufficient to obtain all flow fields. This is not so with experiment, where usually only one quantity at a time can be measured. Take for example the problem of a mixing elbow. Using CFD we can ascertain velocity, pressure, temperature etc. simultaneously in one simulation run. In experiment we would need to design multiple trials to measure different quantities at different times.

iii. Unlimited flow conditions Vs limited flow conditions

In a CFD case study, the material properties, operating variables and domain dimensions can all be easily changed. For experiment, flow properties are fixed by the materials taken and the experimental setup. Also in the case of experiments only realistic operating variables can be implemented. In CFD, virtually any value of operating variable can be trialed, as long as model convergence is attained. Further, even abstract quantities like forces can be changed, scaled or introduced in CFD. This is impossible in an

experimental setup! Take the example of finding the effect of electric field forces on particles in a fluidized bed. In CFD virtually any value can be assigned to the electric field forces to test their effect on the particles.

Table 1.3 summarizes the unique features offered by CFD as a research tool. The comparison of CFD with other numerical modeling methods is also relevant to this discussion but out of its scope.

Table 1.3 Unique features offered by CFD as a research tool

1.	Measurement of fields	Quantitative predictions of invisible flow field variables (like temperature, pressure, velocity etc.) over the entire domain
2.	Multi-quantity measurement	Simultaneous rather than sequential measurement of multiple quantities
3.	Testing wide operating conditions range	Possibilities for parametric studies are extensive. These include the testing of (i) hypothetical materials (ii) complex and difficult to construct flow domains and (iii) unrealistic and unstable operating points

1.3 Fluidization regimes: ripe for exploration using CFD

A particulate system commonly employed as industrial reactors is the fluidized bed which has wide application in chemical, petrochemical and pharmaceutical industry. Industrially, fluidized beds are widely used in both unit operations and unit processes. Examples where the operations involve purely physical mechanisms include powder drying, solvent adsorption, granulation, tablet coating and other heat treatment processes. Some of the industrial applications where chemical reactions occur are presented in Table 1.4.

Table 1.4 Common industrial applications of fluidized beds in unit processes

Reaction where solids act as catalyst	Reaction where solids are transformed
<ul style="list-style-type: none">▪ oil cracking▪ oil reforming▪ manufacture of polyethylene, chlorinated hydrocarbons and acrylonitrile	<ul style="list-style-type: none">▪ coal combustion▪ gasification of wood, coal and bio-mass▪ fluidized bed coking▪ incineration of liquid and solid waste▪ titanium oxide manufacture

Gas–solid fluidized beds in particular are extensively applied in the process industry because of their advantageous properties including isothermal conditions throughout the bed and superior gas-solids contacting which are closely related to reactor performance (Kunii and Levenspiel, 1991).

Stationary solid particles placed in a vertical vessel and supported at the bottom by a horizontal plate are called fixed beds or packed beds. If the plate is porous and allows for incoming fluid it is called a distributor. On increasing flow rate, there comes a point when the fluid drag on the particles is entirely counterbalanced by the effective weight of particles (real weight minus buoyancy force). This is the *incipient fluidization point*. The corresponding flow rate is an extensive quantity, since it is proportional to the cross-sectional area of the distributor, and therefore does not represent a property of the fluid-particle system. On dividing the flow rate by area we obtain the minimum fluidization velocity which represents the minimum fluidization flow rate per unit cross-sectional area of the vessel. The minimum fluidization velocity represents a property of the fluid-particle system (Davidson, 1985).

In liquid-solid systems, if we further increase the flow rate of fluid, the bed apparently expands homogeneously or uniformly (see particulate regime in Fig. 1.1), and the corresponding fluidization regime is called smooth, bubble-free, homogeneous or particulate. *We shall refer to it throughout this work as homogeneous regime.* In gas-solid systems, we observe this behavior only under special operating conditions and for small and light particles called Geldart A powders described in section 1.5. If the flow rate is further increased the homogeneous regime gives way to the bubbling regime. The corresponding velocity is known as minimum bubbling velocity and is a representative property of the bed.

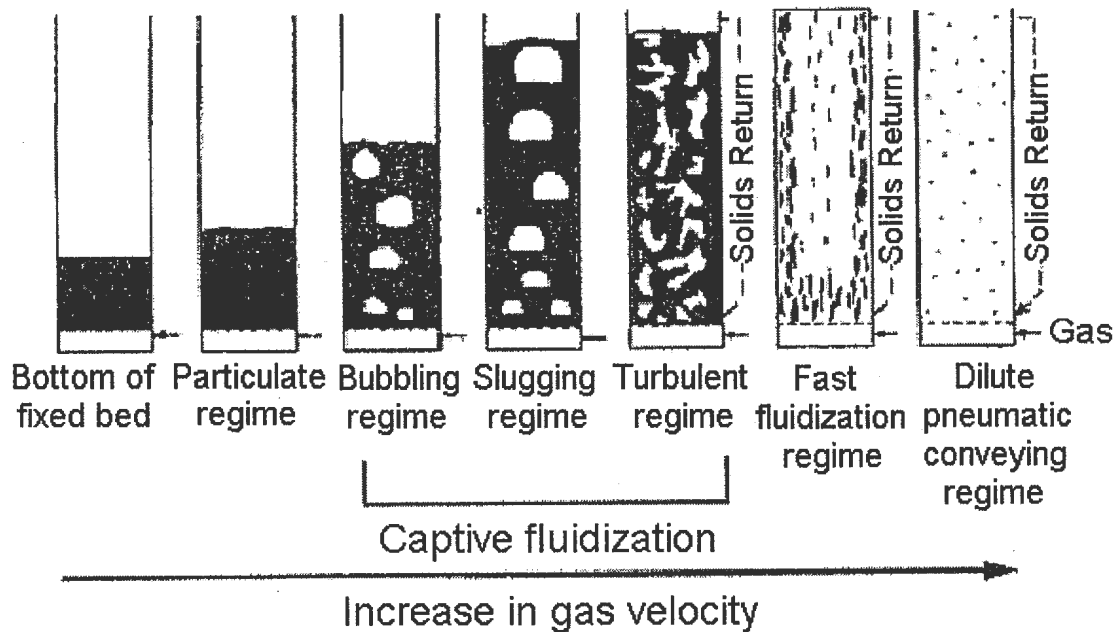


Fig. 1.1 Representative patterns of the major flow regimes in fluidized bed (Kunii and Levenspiel, 1991)

Hence homogeneous fluidization occurs in the window after minimum fluidization but before minimum bubbling. Minimum bubbling conditions marks the transition of the bed to bubbling regime and its identification is paramount in industrial applications where regime change may drastically affect reactor performance. The homogeneous expansion is technologically the most attractive of the processes when uniform conditions are desirable because gas by passing and solid-phase dead zone are carefully avoided and each particle is used efficiently (Zhang et al., 2008).

For Geldart B and D particle systems, bubbling ensues at incipient fluidization point, and there is no window of homogeneous fluidization. On further increasing flow rate the bubbles coalesce as they rise through the bed bubbles may eventually become as large as the cross-sectional area of the vessel. We call this fluidization regime slugging. If the fluid flux exceeds the terminal velocity of the particles, these start moving faster and more chaotically. Streamers and clusters of particles continuously form and break, and the overall structure of the bed becomes more homogeneous. This regime therefore resembles the homogeneous regime but is less dense and occurs at much higher gas velocities. We call this new fluidization regime turbulent. On increasing the flow rate further a lean fluidized bed with pneumatic transport is obtain. Fig. 1.1 schematically displays the various regimes just described and Fig 1.2 gives the regime sequence displayed by each Geldart powder

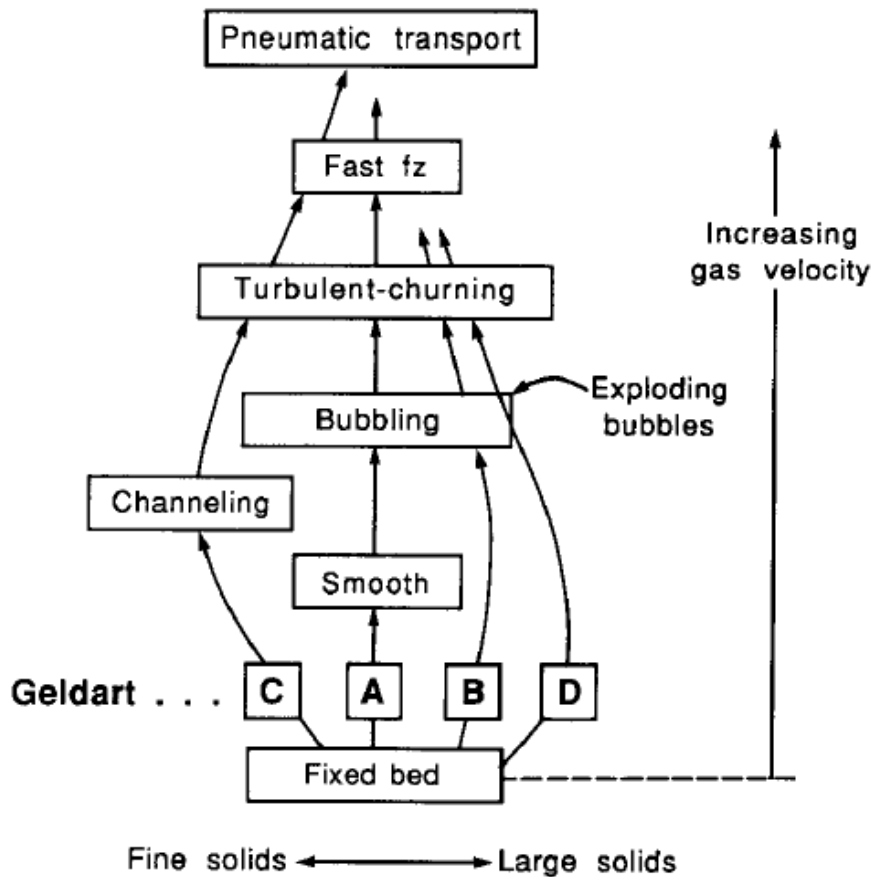


Fig. 1.2 The various fluidization regimes demonstrated by the different Geldart powders (Kunii and Levenspiel, 1991)

Of importance to this work is the theory that gas-solid fluidization of the fine Geldart A particles (Geldart, 1973) can be broadly divided into two classes, namely homogeneous fluidization and all other forms of aggregative fluidization. The homogeneous fluidization is a striking feature of fluidized beds of Geldart A particles and it is identified by the apparently uniform distribution of particles in the gas phase *without* the formation of bubbles and agglomerates which characterize heterogeneous beds.

As discussed in section 1.2 CFD simulations provide insight into flow patterns that are difficult, expensive or impossible to study using experiments. The flow regimes in gas-solid fluidization have unique patterns that are ideal to be researched using CFD. The literature survey in chapter 2, shows that some regimes like bubbling and turbulent regimes have hitherto received the bulk of scientific attention, probably because of their current applications industrially. This by no means discourages exploration of other regimes which may in future prove to be viable alternatives for industry.

There exists currently no comprehensive theoretical approach, which is capable of describing both the homogeneous fluidization *and* bubbling behavior on the basis of gas and particle properties (Ye et al., 2005). This statement underlines one of the many gaps that need to be bridged by further investigation.

1.4 Modeling multi-phase flows

An analogy from nature for the two approaches is proposed. The Eulerian-Eulerian approach envisions the two phases analogous to a honeycomb. The honey is the fluid phase and the comb is the solid phase. The honeycomb exists as two interpenetrating phases occupying the same volume. This means that any volume chosen, which is larger than the microscopic scale (size of particles comprising the comb material), will contain both phases. To separate the phases one would have to squeeze out the honey which would come out as a continuous phase, confirming that the honey interpenetrates the comb. In contrast, the Eulerian-Lagrangian approach envisions the two phases analogous to a swarm of bees. Here the air is the continuous phase analogous to the fluid. The bees represent the solid phase, and they need to be tracked individually to gather information

about the solid phase. Each bee moves in the air like all other bees, but its motion locally is independent of all other bees making it a discrete entity.

1.4.1 The Eulerian-Lagrangian approach

The two approaches for modeling multi-phase flows differ fundamentally in the level of detail offered by their solutions. In the Lagrangian approach each particle is treated *discretely*. The motion of the individual particles is governed by the classical equations of rigid-body Newtonian mechanics where particle forces mainly contact force, body force and drag force are accounted for. The interstitial fluid is assumed to be the continuous phase and is hence treated like a continuum whose dynamics is described by the equations of conservation of mass and linear momentum to be satisfied at each point of the fluid itself. The fluid field then needs to be resolved at a length scale which is smaller than the particle diameter. This is referred to as microscopic length scale. The no-slip boundary conditions assigned on the surface of each particle is coupled to the fluid equations. This means that quantities calculated for the individual particles affect the fluid equations. The approach is therefore called Eulerian-Lagrangian indicating that the fluid phase is considered continuous as per Eulerian approach, and the particles are considered discrete as per Lagrangian approach. The simulation technique based on Eulerian-Lagrangian approach is called discrete element method (DEM) which has been used to investigate gas-particle systems (Kobayashi et al., 2002; Li et al., 2012; Renzo and Maio, 2007). There are two approaches for simulating particle-particle collisions in DEM. They are the soft sphere approach e.g. by Tsuji et al. (1993) and the hard sphere

approach e.g. by Hoomans et al.(1996). In the soft sphere model it is possible to estimate the interaction forces using multiple particle contacts.

The main advantage of the DEM technique lies in the simplicity of the equations that need to be solved. By simplicity it is meant that the equations have no indeterminate terms that need other semi-empirical models or *closures* to be solved. This is with the exception of the fluid stress tensor, for which the classical Newtonian constitutive equation holds, and of the coefficients of restitution that account for the inelastic collisions between pairs of particles. The disadvantage of DEM is the massive computational resources that are spent in tracking and recording quantities for individual particles. The discrete particle model (DPM), which also follows the Eulerian-Lagrangian approach, is an attempt to overcome this debilitating drawback. For DPM simulation technique as in DEM, the fluid phase is considered a continuum and classical Newtonian equations for motion are solved for each particle. However, the particles do not interact with the fluid via its microscopic velocity field as in DEM, but with the averaged value of the microscopic velocity field i.e. field of individual particle velocities. For instance, the overall force exerted by the fluid on each particle is not computed from the effect of local fluid velocity gradients as in DEM. The force is instead evaluated in terms of slip velocity between the averaged fluid velocity and particle velocity. This simplification reduces computational requirements to some extent. DPM was also used to study gas-particle systems (Ye et al., 2004, 2005). It must be noted that all DEM and DPM studies have been conducted for *theoretical domains* of the order of mm. It is difficult to foresee DEM and DPM studies on an industrial scale even in the near future. Though with rapidly developing computer resources, this might become possible for very dilute flows

or larger particles like Geldart group B and D particles, but remains unlikely for Geldart A particles. The Geldart classification of particles is discussed in section 1.5.

1.4.2 The Eulerian-Eulerian approach

Even if the Eulerian-Lagrangian techniques are made feasible for a large scale (lab-scale up to industrial scale), the amount of information provided would be far too detailed, and in any case a method of filtering or averaging would be required to extract useful results. In the Eulerian-Eulerian approach *averaged* transport equations for both phases are formulated. This amounts to considering both phases as inter-penetrating continua. In the Eulerian-Lagrangian techniques only the fluid was considered continuous. The concept of continuum mechanics is that matter is *not* perceivably concentrated in individual packets called molecules but is rather continuous in nature. This can be assumed for length scales larger than the dimensions of molecules.

Several studies have been conducted in the pursuit of averaged equations of the fluid and solid phases. Different mathematical techniques were employed to elicit such equations, and several claims were advanced as to the superiority of the averaging technique used. Regardless of the specific mathematical scheme adopted, however, the resulting transport equations are very similar and present many common features. The most well known of these works was that of Gidaspow (1994) where the well known Two-fluid model (TFM) equations originating from Kuipers et al. (1992) were derived. The TFM is a refined form of the mentioned work and the resulting averaged equations resemble those that one would write for 'x' number of imaginary fluids capable of interpenetrating each other while simultaneously occupying the same volume. *The TFM*

was used throughout our studies and the set of model equations implemented is presented in section 2.2.2.1. TFM is sometimes referred to in the literature as Eulerian-Eulerian or multi-fluid model, but we shall always call it TFM in this work. The TFM takes the form of partial differential equations coupled between the phases and subjected to initial and boundary conditions assigned only on the system boundaries but *not* between the phases. Both solid and fluid must meet the requirement of other boundary conditions at the surface of the reactor, inlet and exit.

Hence the Eulerian-Lagrangian approach is computationally expensive when compared to the Eulerian-Eulerian approach and offers a detailed description of the particle phase. It is currently suitable for theoretical study and not for realistic sized domains, but this might change in the future. The averaged equations of the Eulerian-Eulerian approach offer solutions that are less detailed and hence use considerably less computational resources than Eulerian-Lagrangian approach. Therefore, this approach is suitable for application on lab-scale and even industrial sized domains.

1.5 Geldart Classification of powders

The behavior of a fluidized bed is highly dependent on the properties of the solid particles. The well known properties are size, density, sphericity, fine content and cohesiveness. Geldart (1973) was the first to propose a powder classification (Fig. 1.3) based solely on the mean particle diameter of the particles and the difference in density between the fluid and the solid particles. The advantage of having a powder classification is that the properties, behavior or phenomenon observed for one powder may be reasonably extended to all other powders within that group. In simulation context also,

the powder classification provides a basis by which we may generalize our observations for a particular group. Conversely, conclusions drawn from observations made on one powder in one group should not in general be used to predict the behavior of a powder in another group.

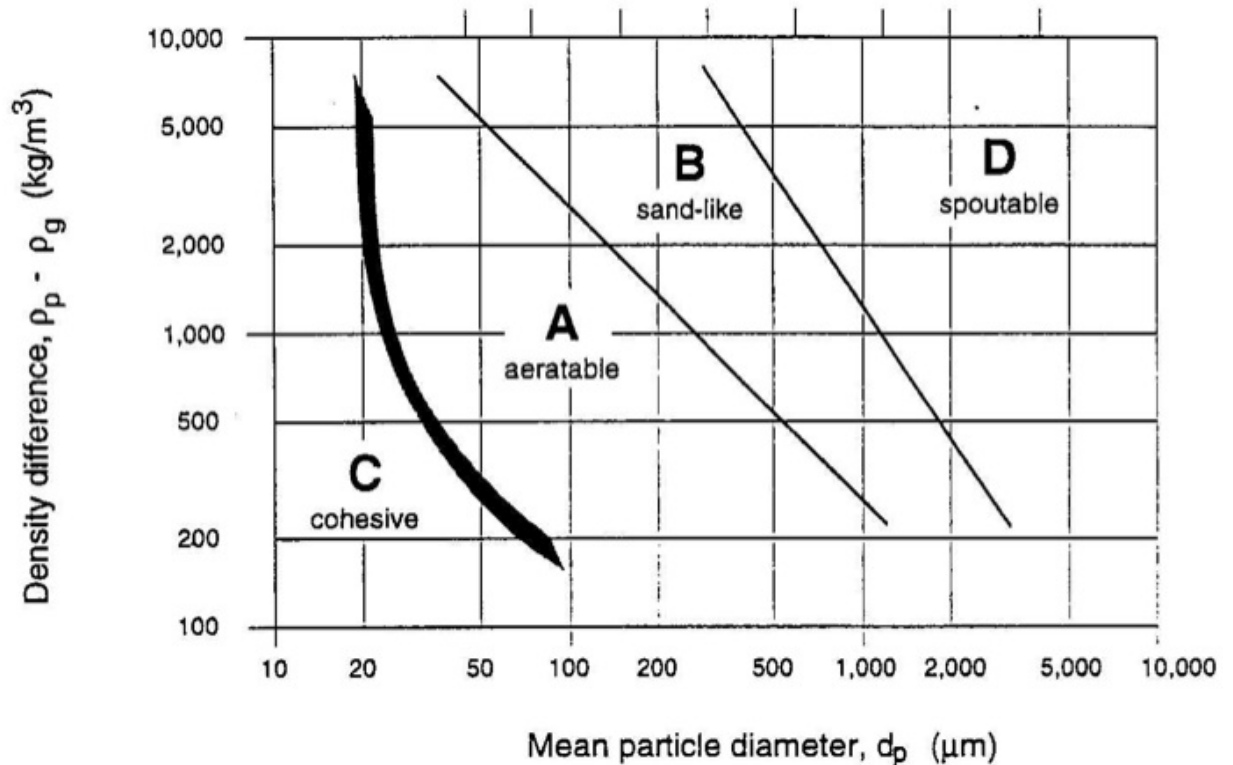


Fig. 1.3 Geldart (1973) powder classification chart.

(Source: <http://jenike.com/files/2012/11/Powder-fluidization-geldart-chart.jpg>)

The main characteristics of the four groups of powders proposed by Geldart are given in Table 1.4. A more detailed description of each powder follows.

\

Table 1.4 Main characteristics of the four Geldart powders

Item	Group C	Group A	Group B	Group D
Defining feature	Cohesive, difficult to fluidize	Ideal for fluidization. Exhibits range of non-bubbling fluidization called homogeneous expansion before bubbling	Starts bubbling at minimum fluidization	Course solids with slow bubbles
Common examples	Flour, cement	Cracking catalyst	Building sand	Gravel, coffee beans
Bed expansion	Low because of channeling	High	Moderate	Low
De-aeration rate	Initially fast, then exponential	Slow, linear	Fast	Fast
Bubble properties	No bubbles, only channels	Bubbles split and coalesce, Maximum bubble size exists	No limit to size	No limit to size
Solid mixing	Very low	High	Moderate	Low
Gas back-mixing	Very low	High	Moderate	Low
Spouting	No	No	Only in shallow beds	Yes, even in deep beds

Group A: These particles are recognized by their aeratable quality. Group A particles are most widely employed in fluidized catalytic cracking. They exhibit what is known as homogeneous or particulate expansion. This expansion is exhibited in the velocity range after minimum fluidization but before minimum bubbling velocity. Minimum bubbling was defined by Abrahamsen and Geldart (1980), as the inlet gas velocity at which the *first* bubble is observed. Homogeneous expansion is so named because of the apparent lack of bubbles in the bed. The particles *appear* to be uniformly distributed in the gas-phase and this is also referred to as emulsion phase or dense phase. The homogeneous

expansion of Group A powders has been described using the Richardson and Zaki (1954) empirical expression:

$$\ln u = n \ln \varepsilon + \ln u_t \quad (1.1)$$

Where u is gas velocity, ε is bed voidage, u_t is particle terminal velocity and n is an experimentally defined parameter. This equation was originally developed to describe the sedimentation and fluidization of uniformly sized particles with diameters larger than 100 μm and fluidized with different liquids. This expression was also found to fit experimental data of gas-solid fluidization with different values of n . The most widely accepted empirical correlation for minimum bubbling velocity was given by Abrahamsen and Geldart (1980), who experimented with 23 different group A powders fluidized by 5 different gases.

$$u_{mb,e} = \frac{2.07 d_p \rho_g^{0.06}}{\mu_g^{0.347}} \exp(0.716 F_{45}) \quad (1.2)$$

The notations have their usual meaning and F_{45} is the fraction of fines which are those particles with diameter less than 45 μm . In the bubbling regime a maximum bubble size does exist, but most bubbles rise more rapidly than the interstitial gas. When the gas supply to the bed is suddenly cut off the bed collapses slowly. Gross circulation of the powder which is similar to convection currents in liquids occurs even when few bubbles are present, producing rapid mixing. Hence group A particles demonstrate the best heat transfer characteristics. The criterion devised to distinguish group A powders from group B powders is given by Eq. (1.3) where the particle and fluid densities are in g/cc and particle diameter is in μm .

$$(\rho_p - \rho_f)d_p \leq 225 \quad (1.3)$$

Eq. (1.3) is represented on the Geldart classification chart by the line separating areas marked A and B in Fig. 1.3. From experimental observation the boundary between A and C is not as sharp as between A and B and is represented by the black area.

Group B: For these powders there is no window of homogeneous or particulate fluidization and bubbling commences at incipient or minimum fluidization conditions itself. When the gas supply is cut off the bed collapses quite rapidly as the bed expansion is quite small. This again is in contrast to Geldart A particles. There is little or no circulation of particles in the absence of bubbles. Hence the heat transfer characteristics are second best to powders of group A. Most bubbles rise with a higher velocity than the interstitial gas and bubble size increases linearly with both bed height and excess gas velocity. There is no evidence of a maximum bubble size.

Group C: These powders are cohesive and do not fluidize easily. The presence of inter-particle forces (IPFs) is believed to be responsible for this. This difficulty in fluidization arises because the inter-particle forces are greater than those which the fluid can exert on the particle. In small diameter tubes, or channels these powders lift as a plug. IPFs are mainly the result of very small particle size, strong electrostatic charges or the presence of wet or sticky material in the bed. Particle mixing and therefore heat transfer within the bed is much poorer than with powders of groups A or B.

Group D: These particles are the largest and densest of all the other powders in the Geldart classification. They are similar to B group powders in that they bubble at minimum fluidization conditions. However, all but the largest bubbles rise more slowly than the interstitial gas. The gas mostly flows into the base of the bubble and out of the top and in this way creating a by-passing which is different from that observed with group A or B powders. The mixing and heat transfer characteristics are therefore poorer than A or B powders. If the inlet gas is allowed through a centrally positioned hole in the bottom plate of the bed, D group particles can be made to spout.

1.6 Objectives of research

The objectives of the present research work are:

1. To simulate and study the hydrodynamics of homogeneous fluidization of Geldart A particles.
2. To study and predict regime transition to bubbling.
3. To simulate and study the fluidized system with reaction (introduced in section 2.3 and 2.4).
4. To validate the simulations with experimental/ computational results from literature

1.7 Organization of thesis

The thesis is presented in five chapters. An exhaustive review of literature on experimental and CFD works which investigate the various fluidization regimes is given in chapter 2. A major part of the literature survey deals with the hydrodynamics of inert

or non-reacting beds and in the latter part (section 2.3) reactive systems are considered. For the most part, modeling studies apart from CFD works are out of scope of the literature survey. The standard TFM equations used in this work without modification are tabulated in the literature survey itself (Tables 2.3 - 2.6) and all relevant nomenclature are repeated here for easy access. The complete solution procedure followed using FLUENT 6.3.26 solver is presented in chapter 3. The obtained simulation results are presented and discussed in chapter 4. Conclusions drawn from the work are presented in chapter 5.

CHAPTER – 2

LITERATURE REVIEW

In this section the literature review is presented under the headings of experimental works and works of modeling and simulation. Following the scope of our work, the literature survey is limited to fluidization of Geldart A particles. The modeling and simulation works have been divided on the basis of Eulerian-Lagrangian and Eulerian-Eulerian models. For Eulerian-Eulerian two-fluid model (TFM) works the survey covers bubbling flows, riser flows and homogeneous expansion. For Eulerian-Lagrangian models only bubbling beds and homogeneous expansion have been covered.

Standard TFM and selected closures were adopted directly from literature for our simulation studies. No modifications were made. The model equations are presented in section 2.2.2.1. All models were implemented in the FLUENT 6.3.26 solver as described in chapter 3.

2.1. Experimental works on gas-solid fluidization of Geldart A particles

Fluidization of Geldart A particles has been the subject of experimentation since the 1950s; mainly because of their wide spread commercial use in fluidized catalytic crackers. Some of the early works included studies on effect of moisture for glass microspheres and catalytic particles in homogeneous expansion regime (D'Amore et al., 1979), indirect measurement of cohesive forces: said to be capillary and van der Waals forces using centrifugal method for 40-45 μ m diameter particles (Donsi et al., 1975) and observation of homogeneous bed structure (Massimilla et al., 1972). Cavities (1 to $5d_p$

size) were reported from microscopic observation of expanded particles in size range 120 to 40 μm and existence of a cellular structure was proposed, consistent with the apparent lack of solids mobility in the bed. In a later work (Geldart and Wong, 1984) for similar catalyst particles, a structure which resembles a honeycomb having cells 2-3 cm across was observed. Also, with naked eye vertical channels approximately 1 mm diameter and about 10 mm long were observed. Some areas of the bed appeared to be more dilute than others while some regions were darker and therefore denser. For inlet velocity slightly above minimum bubbling, the passage of bubbles destroyed the mentioned structures. Geldart and Wong (1984), unlike Massimilla et al. (1972), concluded that homogeneous beds were not lacking in mobility but subject to slow instabilities making them far from absolutely homogeneous. Apart from bed structure, the study of minimum bubbling velocity received a lot of attention. Geldart (1973) who defined minimum bubbling velocity as the gas velocity at which the *first* bubble appears in the homogeneously expanded bed. This way of quantifying a transition point to bubbling regime, namely minimum bubbling velocity, has remained more or less unchanged in experimentation till date.

The most quoted correlation on minimum bubbling velocity is from the experimental work of Abrahamson and Geldart (1980). They correlated the minimum bubbling velocity from experimental results on 48 gas-solid systems and found it to be a function of the density and viscosity of the fluidizing gas, the mean sieve size of the powder and the fraction of fines less than 45 μm which is represented as F_{45} . A correlation for the ratio of the height of the bed at minimum bubbling conditions to minimum fluidization conditions was also presented. From this correlation the bed

voidage at minimum bubbling conditions might be found. This voidage is important as it is *maximum* voidage that the homogeneously expanded bed can attain before bubbling sets in. It was also referred to as the maximum dense phase voidage. Authors reported that the correlation (Abrahamsen and Geldart, 1980) required an accurate value of particle density.

Cohesiveness of the aeratable Geldart A particles has mostly been studied in conjunction with the cohesive Geldart C particles (Table 2.1). For Geldart A particles there has been much debate on the role of cohesiveness or inter-particle forces (IPFs): a term we use throughout this work. The early researches seemed to propagate two views on IPFs: one view was that IPFs present in Geldart A particles made them *slightly* cohesive (compared to Geldart C particles) and were actually responsible for the stability and hence the existence of the homogeneous expansion regime (Geldart and Wong, 1984; Rietema et al., 1993; Rietema and Piepers, 1990). The other view was that IPFs were *not* of significance for the case of dry fluidized Geldart A powders since this would not explain why the range of homogeneous expansion extended with increased pressure. Hence a purely hydrodynamic modeling criterion for homogeneous expansion (Foscolo et al., 1983) and the onset of bubbling (Foscolo and Gibilaro, 1984) was put forward. It is important to note that even though evidence of IPFs in homogeneous expansion of Geldart A particles was reported (Table 2.1), the extent of cohesion was always reported to be low. In fact the distinction of type A powder from type C powder follows from the condition that free particle motion is not dominated by cohesion in the case of powder type A (Molerus, 1982). It was concluded that IPFs would be present even in FCC which

possess ideal qualities of fluidization, but particles with a size larger than 55 μm , were reportedly only *slightly* cohesive (Donsi et al., 1975; Geldart and Wong, 1984).

Table 2.1 Major founding works reporting evidence of Inter-particle force in fluidization of Geldart A particles

Sl. No.	Method	Findings on Inter-particle Forces	Reference
1.	Observation of particle Radii of curvature	Capillary and van der Waals forces were predicted and compared with experimental values of cohesive forces between particles. Particles size range was 40-45 μm	(Donsi et al., 1975)
2.	Measurement of bed permeability and settled and fluidized bed voidages.	Sensitivity to moisture drastically changed from porous to non-porous materials. There were differences among the porous materials with regard to the effect of water on major fluidization characteristics	(D'Amore et al., 1979)
3.	Measurement of bed height to calculate voidage profiles	Homogeneous expansion characteristics of particles in range 125 to 3 μm were measured. The ratio of the tapped bulk density to most loosely packed bulk density gave an indication of the cohesiveness of the powder	(Geldart and Wong, 1984)
4.	Observations of bed behavior under various conditions	These were attributed to IPFs: Electric conductivity of fluidized particles. Observation of stable bed surface during tilting until critical angle was reached. observation and measurement of surpressure just beyond incipient fluidization	(Rietema and Piepers, 1990)
5	Collapse tests and shear characterization of particles	Behavior of three size distributions of identical surface-volume mean diameter (53 and 73 Fm) but different 'fines' contents and size spectra was studied. Fines and size spectra affect the flow and fluidization properties. interparticle forces are not overcome completely at minimum bubbling	(Khoe et al., 1991)

More recent experimental works have been comparatively fewer, probably due to focus on modeling and simulation aided by a variety of tools available to researchers. Some noteworthy works reported on effect of temperature in fluidization of Geldart A particles. Experimental observations of homogeneous expansion of three FCC catalysts with increasing temperature from ambient up to 650°C were studied (Lettieri et al., 2002). Also the conditions under which the hydrodynamic forces dominated or under which IPFs dominated were studied in order to predict the fluidization behavior at elevated temperatures (Lettieri et al., 2001). Bed collapse test was used as a quantitative test to characterize fluidization behavior. It provided a means of assessing the changes in aeratability of materials between ambient and high temperature fluidization (Lettieri et al., 2000).

2.2. Modeling and simulation of gas-solid fluidization of Geldart A particles

2.2.1 Eulerian- Lagrangian approach

Literature reports on CFD simulations of Geldart A particles following Eulerian-Lagrangian approach in homogeneous and bubbling regime. Effect of IPFs was also studied. As mentioned in the introduction chapter, the Eulerian- Lagrangian approach comprises the Discrete Element Model (DEM) and Discrete Particle Model (DPM). Major contributions of DEM and DPM to simulation of fluidization of Geldart A particles are summarized in Table 2.1. As mentioned in introduction chapter the Eulerian-Lagrangian approach is very expensive computationally. Hence the size of the systems simulated is very limited, as seen from the number of particles in Table 2.2.

Table 2.2 Major works on DPM/DEM simulation of fluidization of Geldart A particles

Sl. No.	Simulated:-	Maximum No. of particles	Reference
1	Three powders in homogeneous expansion with and without imposed IPF	106,400	(Rhodes et al., 2001)
2	Effect of adhesion and lubrication forces between particles for Group A and B powder	870	(Kobayashi, 2002)
3	Typical features of Geldart A particles, including homogeneous expansion, gross particle circulation in the absence of bubbles, and fast bubbles. All this was seen only for the relatively weak van der Waals forces	36,000	(Ye et al., 2004)
4	3D bed with effect of particle and gas properties. Minimum fluidization and minimum bubbling velocities. Ambiguity on visual detection of minimum bubbling was expressed	36,000	(Ye et al., 2005)
5	Homogeneous fluidization in liquid and gas fluidized beds in absence of any imposed inter-particle force. Minimum bubbling velocity predicted follow stability theory	10,000	(Renzo and Maio, 2007)
6	Flow structures induced by bubbles formed in 3D shallow rectangular gas-fluidized beds. Worm-like structures exist in addition to the conventional spherical cap.	4,500,000 (Geldart B particles)	(Tsuji et al., 2008)
7	Gas–solid flow in fixed-bed methanol-to-olefins (MTO) reactors. Particle motion exhibits a typical annulus–core structure, which promotes excellent transfer efficiency	8,000 to 40,000 (Geldart B particles)	(Zhuang et al., 2012)
8	Inter-particle adhesion force and compared with experimentally measured data. It was found from the results that there were considerable differences between their flow patterns	100,000	(Kobayashi et al., 2013)
9	A new hybrid approach to solve CFD–DEM problems in gas–solid fluidized beds systems applying an efficient coupling method suitable for large-scale simulations	107,000 to 25,000,000	(Jajcevic et al., 2013)

2D soft sphere DEM was used to study the effect of lubrication forces and van der Waals forces (Kobayashi, 2002). Particle diameters studied were 66 μm (Group A) and 500 μm (Group B). Density in both cases was 2470 kg/m^3 . Three cases were studied, the first neglecting both Lubrication and Adhesion forces, the second only with Adhesion force and the third only with Lubrication force. Adhesion and lubrication forces had no effect on the increasing profile of velocity vs. pressure drop and the value of minimum fluidization velocity, however on reducing velocity, fluidization point was found to increase slightly. More importantly the profile of RMS fluctuation in bed voidage was found to show minimum bubbling transition in all the three cases studied, i.e. even in absence of Adhesion and Lubrication forces, but the increase in RMS value of voidage was more stable in the case with adhesion force. Though detailed results and analysis were not presented in the paper, homogeneous expansion was clearly visible even in the case where both adhesion force and lubrication force were absent. This is in agreement with other DPM results (Ye et al., 2004) for group A particles of 100 μm diameter and 900 kg/m^3 density. This implies that IPFs were not *solely* responsible for homogeneous expansion as previously hypothesized by experimental works (Geldart and Wong, 1984; Rietema and Piepers, 1990). Ye et al. (2004) also concluded that in bubbling regime bubbles are typically fast with circulation of gas flow around them and the important features of homogeneous fluidization can be qualitatively described by DPM.

Ye et al. (2005) studied the effect of various gas and particle properties on minimum bubbling velocity using 3D DPM simulations of domain size 12 \times 3 \times 1.2mm. They found their predicted minimum fluidization values to be in good agreement with the correlation by Abrahamsen and Geldart (1980), but the minimum bubbling velocities

showed only qualitative agreement ($d_p = 75\mu\text{m}$) with the simulated values increasing slightly from 0.0082 to 0.0094 m/s when particle density increased from 900 to 4195 kg/m³. Experimental correlation by Abrahamsen and Geldart (1980) of minimum bubbling velocity does not contain density as a variable, indicating negligible dependence of minimum bubbling on density. The simulated values of minimum bubbling were all higher than the value predicted by the correlation. Non-visual method of predicting minimum bubbling velocity was carried out by plotting local porosity fluctuation against superficial velocity. The plot showed two transition points indicating those of minimum fluidization and minimum bubbling. The predicted minimum bubbling velocity simulated using free-slip boundary condition for gas phase was found to be 15–25% higher than value calculated by the correlation, while using no-slip boundary conditions this accounted to 80%. The overshoot of pressure drop near the minimum fluidization point was found to be affected by both the particle-wall friction and the inter-particle van der Waals forces, which confirm previous experimental observations (Rietema and Piepers, 1990). It was found that increasing inter particle van der Waals forces delayed the onset of bubbling and hence increases the velocity interval of homogeneous expansion. Simulations without inter particle van der Waals forces, also captured homogeneous expansion and minimum bubbling as in other modeling works (Kobayashi, 2002; Ye et al., 2004).

The 2D soft-sphere DEM simulations were performed in the absence of any inter-particle cohesive force and with an imposed cohesive force equivalent in magnitude to several times the single particle weight (Rhodes et al., 2001). Homogeneous fluidization was observed for a significant range of gas velocity even with no inter-particle force. The

authors noted this as evidence of true Group A behavior in the absence of inter-particle cohesive force. Greater expansion was seen for powders more into Group A and away from Group A/B boundary. Simulations performed with imposed inter-particle force showed little change in fluidized bed until the magnitude of force was many times the single particle buoyant weight.

A more recent DEM 2D soft-sphere DEM study (Renzo and Maio, 2007), simulated bed voidage for different gas velocities in homogeneous regime. Two systems were studied: glass beads of 200 μm fluidized by water and air fluidization of group A powder of 70 μm diameter and 1000 kg/m^3 density. The appearance of bubbles in the fluidized bed behavior is shown to occur at velocities in quantitative agreement with the theory of fluidized bed stability (Foscolo and Gibilaro, 1984). In this context, the transient behavior of the two systems was analyzed, validating the capability of the numerical model to capture the propagation of voidage shocks along bed height.

2.2.2 Eulerian approach

The Eulerian approach is a multi-phase modeling approach which treats the phases mathematically as interpenetrating continua. Since the volume of one phase cannot be occupied by the other phases, the concept of phase-volume fraction is introduced here. These volume fractions are continuous functions of space and time and their sum is equal to one. Conservation equations of mass, momentum and granular pressure (if granular phase is present) are therefore the governing equations of flow. The well known multi-phase models which follow Eulerian approach are the Volume of Fluid (VOF), Mixture and Eulerian-Eulerian model (Two-fluid model). The VOF model is most suitable for two or more immiscible fluids where the position of the interface between the fluids is mainly of interest. In the VOF model, a single set of momentum equations is shared by all the fluids. VOF model in conjunction with other models was recently applied to three phase gas-solid-liquid bubbling flows (Ma et al., 2012; Xu et al., 2013; Yujie et al., 2012). Some other applications include disintegration of cavitating turbulent liquid jets (Srinivasan et al., 2010) and analysis of bubble impact on flat horizontal surface (Albadawi et al., 2014). The mixture model solves for the mixture momentum equation and prescribes relative velocities to describe the dispersed phases. Applications of the mixture model include particle-laden flows with low loading, bubbly flows, sedimentation, and cyclone flows. Recent applications of mixture model in conjunction with other models include two-phase flow in horizontal pipe (Shang et al., 2013) and turbulent flow of Alumina nano-fluid inside a horizontal tube (Hejazian et al., 2014).

2.2.2.1 State-of-the-art TFM

In the Eulerian-Eulerian model *averaged* transport equations for both solid and fluid phases are formulate. Both phases are considered as inter-penetrating continua. Irrespective of the specific mathematical scheme adopted for averaging, the resulting transport equations are very similar. The averaged transport equations along with their boundary conditions require the values of certain quantities such as the interphase drag coefficient, solid phase stress tensor and solids pressure. These quantities are described by models called closures which are empirical in nature. Theses averaged transport equations along with their closures developed since the 1960s to give what is now called the Two-Fluid Model (TFM). TFM is the common name for the Eulerian-Eulerian model, which we shall use throughout this thesis. Origins of the governing equations can be traced from the 1960s (Anderson and Jackson, 1967) to 1990s (D.Gidaspow, 1994.; J. Kuipers, 1998; Jackson, 1997). The most quoted work is that of Gidaspow (1994) which for the most part forms the state-of-the-art TFM that is used in current literature. The TFM adopted the kinetic theory to close the particle stresses. What follows is a detailed account of the equations which constitute the state-of-the-art TFM. Theses model equations are readily available in current literature (Loha et al., 2012; van Wachem et al., 2001; Wang et al., 2010). The governing equations and closures which were implemented in this work using the FLUENT 6.3.26 solver are described in Tables 2.3, 2.5 and 2.6.

2.2.2.1.1 Governing equations and Kinetic Theory of Granular Gases

The governing equations in TFM constitute the equations for conservation of mass, linear momentum and granular temperature (Table 2.3).

Table 2.3 TFM governing equations of the form implemented in FLUENT 6.3.26 solver

<p>Conservation of mass for gas phase</p> $\frac{1}{\rho_{r,g}} \left(\frac{\delta}{\delta t} (\varepsilon_g \rho_g) + \nabla \cdot (\varepsilon_g \rho_g \vec{v}_g) = \sum_{p=1}^n (m'_{sg} - m'_{gs}) \right)$	(2.1)
<p>Analogous Conservation of mass for solid phase</p> $\frac{1}{\rho_{r,s}} \left(\frac{\delta}{\delta t} (\varepsilon_s \rho_s) + \nabla \cdot (\varepsilon_s \rho_s \vec{v}_s) = \sum_{p=1}^n (m'_{gs} - m'_{sg}) \right)$	(2.2)
<p>Solid volume fraction constraint</p> $\varepsilon_s + \varepsilon_g = 1$	(2.3)
<p>Momentum conservation equation for gas phase</p> $\begin{aligned} \frac{\delta}{\delta t} (\varepsilon_g \rho_g \vec{v}_g) + \nabla \cdot (\varepsilon_g \rho_g \vec{v}_g \vec{v}_g) \\ = -\varepsilon_g \nabla p + \nabla \cdot \bar{\tau}_g + \varepsilon_g \rho_g \vec{g} + \sum_{p=1}^n (K_{sg} (\vec{v}_s - \vec{v}_g) + m'_{sg} \vec{v}_{sg} - m'_{gs} \vec{v}_{gs}) \end{aligned}$	(2.4)
<p>Analogous momentum conservation equation for solid phase</p> $\begin{aligned} \frac{\delta}{\delta t} (\varepsilon_s \rho_s \vec{v}_s) + \nabla \cdot (\varepsilon_s \rho_s \vec{v}_s \vec{v}_s) \\ = -\varepsilon_s \nabla p - \nabla p_s + \nabla \cdot \bar{\tau}_s + \varepsilon_s \rho_s \vec{g} \\ + \sum_{p=1}^n (K_{gs} (\vec{v}_g - \vec{v}_s) + m'_{gs} \vec{v}_{gs} - m'_{sg} \vec{v}_{sg}) \end{aligned}$	(2.5)
<p>Conservation of granular energy</p>	(2.6)

$\frac{3}{2} \left[\frac{\partial}{\partial t} (\rho_s \varepsilon_g \theta_s) + \nabla \cdot (\rho_s \varepsilon_g \bar{v}_s \theta_s) \right] = (-p_s \bar{I} + \bar{\tau}_s) : \nabla \bar{v}_s + \nabla \cdot (k_{\theta_s} \nabla \theta_s) - \gamma_{\theta_s} + \phi_{gs}$ <p> $(-p_s \bar{I} + \bar{\tau}_s) : \nabla \bar{v}_s = \text{Generation of energy by solid stress tensor}$ </p> <p> $k_{\theta_s} \nabla \theta_s = \text{Energy diffusion } (k_{\theta_s} \text{ is diffusion coefficient of the particles})$ </p> <p> $\gamma_{\theta_s} = \text{Collision dissipation of energy}$ </p> <p> $\phi_{gs} = \text{Energy exchange between gas and solid phase}$ </p> <p>Under steady state convection and diffusive terms are usually neglected to give:</p> $(p_s \bar{I} + \bar{\tau}_s) : \nabla \bar{v}_s = -\gamma_{\theta_s} + \phi_{gs}$	
<p>Solids pressure</p> $p_s = \varepsilon_s \rho_s \theta_s + 2\rho_s (1 + e_s) \varepsilon_s^2 g_{o,s} \theta_s \quad (\text{Lun et al., 1984}) \quad (2.7)$ $p_s = 2\rho_s (1 + e_s) \varepsilon_s^2 g_{o,s} \theta_s \quad (\text{Syamlal et al., 1993}) \quad (2.8)$ <p> $\varepsilon_s \rho_s \theta_s = \text{pressure due to kinetic energy of particles, neglected in Syamlal model}$ </p> <p> $2\rho_s (1 + e_s) \varepsilon_s^2 g_{o,s} \theta_s = \text{pressure due to particle collision}$ </p>	
<p>Radial distribution function</p> $g_{o,s} = \left[1 - \left(\frac{\varepsilon_s}{\varepsilon_{s,\max}} \right)^{\frac{1}{3}} \right]^{-1} \quad (\text{S. Ogawa, 1980}) \text{ and later by } (\text{Syamlal et al., 1993}) \quad (2.9)$	

Table 2.4 Notation used for TFM equations in Table 2.3

$\rho_{r,g}$ = Reference density or volume averaged density of gas phase (kg/m^3)

ε_g = Volume fraction of gas phase (-)

ε_s = Volume fraction of solid phase (-)

ρ_g = Density of gas phase (kg/m^3)

ρ_s = Density of solid phase (kg/m^3)

\vec{v}_g = Velocity of gas phase (m/s)

\vec{v}_s = Velocity of solid phase (m/s)

\dot{m}_{sg} = Mass transfer rate from solid to gas phase (kg/s)

\dot{m}_{gs} = Mass transfer rate from gas to solid phase (kg/s)

p = Gas pressure (Pa)

p_s = Solids pressure (Pa)

$\vec{\tau}_s$ = solid phase stress tensor (N/m^2)

\vec{g} = Acceleration due to gravity (m/s^2)

\vec{v}_{gs} = Interphase velocity .If $\dot{m}_{gs} > 0$, $\vec{v}_{gs} = \vec{v}_g$ else if $\dot{m}_{gs} < 0$, $\vec{v}_{gs} = \vec{v}_s$

\vec{v}_{sg} = Interphase velocity .If $\dot{m}_{sg} > 0$, $\vec{v}_{sg} = \vec{v}_s$ else if $\dot{m}_{sg} < 0$, $\vec{v}_{sg} = \vec{v}_g$

$K_{gs} = K_{sg}$ = Momentum exchange coefficient between gas and solid phase

Θ = Granular temperature (m^2/s^2)

e_s = Restitution coefficient for particle collisions (-)

$g_{o,s}$ = Radial distribution function (-)

Analogous to the thermodynamic temperature for gases from Kinetic theory, the granular temperature is a measure of the particle velocity fluctuations and defined as one third of the average particle velocity fluctuations:

$$\theta = \frac{1}{3} \langle v'^2 \rangle \quad (2.10)$$

The granular energy is defined as follows:

$$\frac{2}{3} \theta \quad (2.11)$$

The conservation of granular energy for the solid phase is analogous to conservation of energy from Kinetic theory. The solids pressure that appears in the solids momentum and granular energy balance is the normal forces due to particle-particle interactions. In the literature there is general agreement on the form of the solids pressure in Eq. 2.7 (Lun et al., 1984). The first term represents the kinetic contribution, and the second part represents the collisional contribution. The kinetic part of the stress tensor physically represents the momentum transferred through the system by particles moving across imaginary shear layers in the flow. The collisional part of the stress tensor denotes the momentum transferred by direct collisions. The Syamlal model (Eq. 2.8) which we used, neglects the kinetic part which dominates in dilute-phase flows but not in dense flows which we simulated. The solid-phase stress is dependent on the radial distribution function at contact. Radial distribution function is a correction factor which accounts for the higher probability of collision between particles when the granular phase becomes denser and denser. As can be seen from Eq. 2.8, as ϵ_s tends to $\epsilon_{s,\max}$ the radial distribution function tends to an infinite value, and hence the pressure due to collisions dominated

over pressure due to kinetic energy. Radial distribution function can also be interpreted as the non-dimensional distance between phases

$$g_{o,s} = \frac{s + d_p}{s} \quad (2.12)$$

Where 's' is the average distance between particles of the granular phase. Hence as s becomes zero the radial distribution function tends to infinity. Other formulations for radial distribution function are available (D.Gidaspow, 1994.; Lun and Savage, 1986; Sinclair and Jackson, 1989).

The application of kinetic theory enables us to model the granular phase as a 'granular gas' which can be defined as a many-particle system in which the mean free path of the particles is much larger than the typical particle size, and where particle collisions occur dissuasively (Lun et al., 1984). Historically we know that the idea of granular gases was given by Einstein in 1956, when he compared the observable agitated motion of pollen grains in water to Brownian motion of molecules. The main analogy between gas-solid fluidization and kinetic theory of ideal gas is the existence of a velocity distribution function, similar to the Maxwell velocity distribution function for ideal gas. Also, collisions occur in pairs and are brief or momentary with no interstitial fluid. Unlike molecules, grains do not collide in an elastically and therefore energy needs to be pumped into a granular gas in order to keep it fluidized. Consequently, granular gases are always in non-equilibrium states (Goldhirsch, 2008). Furthermore, unlike molecules, grains undergo attrition, breakup, coagulation and other processes (Klinzing et al., 2011). The main difference between real gases and granular gases are summarized as follows:

- i. Solid particles are orders of magnitude larger than molecules.
- ii. Velocity fluctuations of solids are much smaller than their mean velocity.

- iii. The kinetic contribution of solids fluctuation is anisotropic.
- iv. Velocity fluctuations of solids, dissipates into heat at a faster rate than molecules as a result of inter particle collision.
- v. Granular temperature is a byproduct of flow and not purely a consequence of thermal energy as in the case of molecular motion.

Notwithstanding the above difference, one can use all the tools and concepts that pertain to molecular assemblies to obtain similar properties for granular particles in fluidized beds. This outlines ‘the kinetic theory of granular flow’ (Ding and Gidaspow, 1990; Lun et al., 1984).

2.2.2.1.2 Closures for stress tensors and solid shear

The solid phase stress tensor accounts for interactions within the solid phase and is derived from granular kinetic theory. The momentum balance equations require closure for the solid and gas phase stress tensors. For the gas phase these are fluid properties available in standard tables. For granular phase the shear and bulk viscosity components need to be described by separate closures. For the solids bulk viscosity, which describes the resistance of the particle suspension to compression, there is general agreement on the Eq. (2.14) (Lun et al., 1984) in Table 2.5.

The solids shear viscosity comprises the collision term, the kinetic term and the frictional term. The collisional term is usually modeled by the combined Gidaspow and Syamlal model. Syamlal model for kinetic shear viscosity is suitable to be used with the former, but there are other forms available (Hrenya and Sinclair, 1997; Lun et al., 1984). Frictional viscosity needs to be considered when the particles are in contact with each

other as in the case of granular flow eg: powder flowing out of a conduit. Here the application of kinetic theory does not become relevant and instantaneous collisions are almost absent. Mathematically frictional viscosity operates between the packing limit when frictional viscosity is significant (ϵ_s^{\min}) and maximum packing limit or packed bed state (ϵ_s^{\min}). Both frictional viscosity models given in Table 2.5 were trialed by us.

Table 2.5 Closures for stress tensors implemented

<p>Stress tensor for solid phase</p> $\overline{\tau}_s = \epsilon_s \mu_s \left(\nabla \overline{v}_s + \nabla \overline{v}_s^T \right) + \epsilon_s \left(\lambda_s - \frac{2}{3} \mu_s \right) \nabla \cdot \overline{v}_s \overline{I}$	(2.13)
<p>Analogous stress tensor for gas-phase</p> $\overline{\tau}_g = \epsilon_g \mu_g \left(\nabla \overline{v}_g + \nabla \overline{v}_g^T \right) + \epsilon_g \left(\lambda_g - \frac{2}{3} \mu_g \right) \nabla \cdot \overline{v}_g \overline{I}$	(2.14)
<p>Solid bulk viscosity</p> $\lambda_s = \frac{4}{3} \epsilon_s \rho_s d_p g_{o,s} (1 + e_s) \sqrt{\frac{\theta_s}{\pi}} \text{ (Lun et al., 1984)}$	(2.15)
<p>Components of solids shear viscosity appearing in Eq. (2.11) are collisional, Kinetic and frictional: $\mu_s = \mu_{s,col} + \mu_{s,Kin} + \mu_{s,fr}$</p>	(2.16)
<p>Collision shear viscosity given by the combined Gidaspow and Syamlal models</p> $\mu_{s,col} = \frac{4}{5} \epsilon_s \rho_s d_p g_{o,s} (1 + e_s) \sqrt{\frac{\theta_s}{\pi}} \text{ (D.Gidaspow, 1994.; Syamlal et al., 1993)}$	(2.17)
<p>Kinetic shear viscosity given by the Syamlal model</p> $\mu_{s,kin} = \frac{\epsilon_s d_p \rho_s \sqrt{\theta_s \pi}}{5} \left[1 + \frac{2}{3} (1 + e_s) (3e_s - 1) \epsilon_s g_{o,s} \right] \text{ (Syamlal et al., 1993)}$	(2.18)

<p>Frictional viscosity</p> $\mu_{s,fr} = \frac{p_f \sin \phi}{2\sqrt{I_{2D}}} \text{ (Schaeffer, 1987)}$	(2.19)
<p>Frictional pressure</p> $p_f = Fr \frac{(\bar{\epsilon}_s - \epsilon_s^{\min})^n}{(\epsilon_s^{\max} - \epsilon_s)^p} \text{ (Johnson and Jackson, 1987)}$	(2.20)
<p>Frictional pressure</p> $p_f = \bar{A}(\bar{\epsilon}_s - \epsilon_s^{\min})^n \text{ (Syamlal et al., 1993)}$	(2.21)

2.2.2.1.3 Closures for Interphase drag coefficient

As seen from equations of momentum balance (Eq. 2.4 and Eq. 2.5 in Table 2.3), coupling between the gas and solid phase is achieved through the interphase forces include drag force, external body force, lift force and virtual mass force. Usually in fluidized beds only the drag force is significant and the remaining interphase forces are neglected (Li et al., 2008; Loha et al., 2012; van Wachem et al., 2001). The commonly applied drag models include Gidaspow model (which is a combination of Wen Yu and Ergun equations) and Syamlal O'Brien model. Along with these two models we trialed the stand alone Wen Yu model in this work (Table 2.6). Though Wen Yu model is used in conjunction with Ergun model and when void fraction exceeds 0.8, we trialed it as stand alone because it was suggested (Mazzei and Lettieri, 2008) that this threshold value is not constant, but system depended and in many cases was more precise than other drag laws even for void fractions lower than 0.8.

Table 2.6 Closures for drag coefficient implemented

<p>Gidaspow drag law</p> <p>If $\varepsilon_g < 0.8$</p> $K_{gs} = \frac{3}{4} C_D \frac{\varepsilon_s \varepsilon_g \rho_g \vec{v}_s - \vec{v}_g }{d_p} \varepsilon_g^{-2.65} \quad (\text{Ergun, 1952})$ $C_D = \frac{24}{\varepsilon_g Re_p} \left[1 + 0.15 (\varepsilon_g Re_p)^{0.687} \right]$ $Re_p = \frac{d_p \rho_g \vec{v}_s - \vec{v}_g }{\mu_g}$	(2.22)
<p>If $\varepsilon_g > 0.8$ (C.Y. Wen, 1966)</p> $K_{gs} = 150 \frac{\varepsilon_s (1 - \varepsilon_s) \mu_g}{\varepsilon_s d_p^2} + 1.75 \frac{\varepsilon_s \rho_g \vec{v}_s - \vec{v}_g }{d_p}$	(2.23)
<p>Syamlal O'Brien drag law (Syamlal et al., 1993)</p> $K_{gs} = \frac{3 \varepsilon_s \varepsilon_g \rho_g}{4 v_t^2 d_p} C_D \frac{Re_p}{v_t} \vec{v}_s - \vec{v}_g $ $C_D = \left(0.63 + \frac{4.8}{\sqrt{\frac{Re_p}{v_t}}} \right)^2$ $v_t = 0.5 \left(A - 0.06 Re_p + \sqrt{(0.06 Re_p)^2 + 0.12 Re_p (2B - A) + A^2} \right)$ $A = \varepsilon_g^{4.14}$ <p>If $\varepsilon_g \leq 0.85$ $B = 0.8 \varepsilon_g^{1.28}$ If $\varepsilon_g > 0.85$ $B = \varepsilon_g^{2.65}$</p>	(2.24)

The Ergun equation is derived for dense beds and relates the drag to the pressure drop through porous media. The Wen Yu drag model uses correlation from the experimental results (Richardson and Zaki, 1954). The Syamlal–O’Brien model is based on the measurement of terminal velocity of solid particle in the fluidized bed. Another drag law commonly used in DPM studies is expressed as the product of the drag force on an unhindered particle subject to the same volumetric flux of fluid as the hindered particles, and a voidage function (Di Felice, 1994). A more recent drag coefficient model was proposed (Yang et al., 2003) based on the concept of energy minimization multi-scale (EMMS) for bubbling fluidized beds and riser flows (Li et al., 2013). Several modifications have been proposed along the same lines as the EMMS model. Correlative multi-scale methods to estimate drag laws have also been proposed (Andrews et al., 2005; Igci et al., 2008) but these are out of the scope of this work, and as in the case of drag models based on EMMS, they are applicable to riser and bubbling flows.

For comparison with TFM the main particle equations for DPM simulation are given in Table 2.7. The gas phase equations are the same as for TFM. The particles are tracked by Newton’s laws for individual particles. The main forces considered in standard DPM are the drag force obtained from first principles. Contact forces given by spring and dashpot model (Cundall and Strack, 1979) is commonly used. To account for the IPF, which is assumed to be van der Waals force, the Hamaker expression (Chu, 1967) is used

Table 2.7 DPM Equations (Newtonian equation of particle motion) and closures

$m_a \frac{d^2 D_a}{dt^2} = F_{c,a} + F_{vdw,a} + F_{drag,a} - V_a \nabla p + m_a g$	(2.25)
$F_{drag,a} = 3\pi\mu_g \epsilon_g^2 d_p (u_g - v_p) f(\epsilon_g)$	(2.26)
$F_{vdw,a}(S) = \frac{H_{ab}}{3} \frac{2r_a r_b (S + r_a + r_b)}{[S(S + 2r_a + 2r_b)]^2} \times \left[\frac{S(S + 2r_a + 2r_b)}{(S + r_a + r_b)^2 - (r_a - r_b)^2} - 1 \right]^2$ (Chu, 1967)	(2.27)

Table 2.8 Notation used for TFM equations in Tables 2.5 to 2.7

<p>μ_s = Shear viscosity of solids (Pa s)</p> <p>λ_s = Bulk viscosity of solid (Pa s)</p> <p>\bar{I} = Unit stress tensor (-)</p> <p>$\vec{\nabla}_s$ = Divergence of solid velocity vector (-)</p> <p>$\vec{\nabla}_s^T$ = Transpose of divergence of solid velocity vector(-)</p> <p>p_f = Solids pressure due to friction (Pa) to be added to p_s of Eq. 2.7</p> <p>ϕ = Angle of internal friction (common value is 30°)</p> <p>I_{2D} = Second invariant of deviatoric stress tensor(-)</p> <p>ϵ_s^{\min} = Minimum bed solid volume fraction for frictional stress consideration(-)</p> <p>ϵ_s^{\max} = Maximum allowable bed packing (packed bed state)(-)</p> <p>$\overline{\overline{Fr}}, \overline{\overline{p}}, \overline{\overline{n}}$ = Empirical material constants required to calculate frictional pressure</p>

\bar{A} = Material constant required to calculate frictional pressure of typical value 10^{25}

K_{gs} = Interphase drag exchange coefficient

C_D = Drag function

v_t = Terminal velocity (m/s)

D_a, m_a, V_a = Displacement (m), mass (kg) and volume (m^3) of particle 'a'

$F_{c,a}, F_{vdw,a}, F_{drag,a}$ = Contact force, van der Waals force, drag force for the particle 'a' (N)

S, v_p, u_g = Intersurface particle distance (m), particle velocity (m/s), local gas velocity (m/s)

H_{ab} = Hamaker constant for interparticle force between the particles 'a', 'b' (J)

2.2.2.2 CFD simulations using TFM

Although the TFM which follows the Eulerian-Eulerian approach has been used to investigate bubbling regime, its success so far has been less than that of the Eulerian-Lagrangian approach models. Also, unlike in DEM/DPM studies, there have been fewer works on homogeneous expansion regime.

2.2.2.2.1 Application of Eulerian approach in Bubbling fluidization

Several Eulerian-Eulerian CFD studies have been devoted to understanding the hydrodynamics of bubbling fluidized beds (Gidaspow et al., 2004; Ye et al., 2008). However, although progress has been made in simulating gas-fluidization of Geldart B and D particles (Movahedirad et al., 2014; Wang and Liu, 2010; Wang et al., 2014) most of the studies on bubbling fluidized beds of Geldart A particles reported failure of the TFM to correctly predict the hydrodynamics (Mazzei and Lettieri, 2008; McKeen and Pugsley, 2003; Zimmermann and Taghipour, 2005). Mazzei and Lettieri (2008) reported agreement of their proposed drag law with empirical correlation of Richardson and Zaki (1954) in homogeneous expansion of liquid-fluidized bed, but reported minimum bubbling velocity to be ten times higher than the experimental value for gas-fluidization of Geldart A particles. They concluded that failure to predict the minimum bubbling was due to missing component in the constitutive laws of TFM rendering them faulty. McKeen and Pugsley (2003) argued that cohesive IPFs lead to agglomeration of FCC catalyst powder and significantly affect the fluidization quality. Bed voidage was accurately simulated for the freely bubbling bed only when a diameter of 135 μm to 170 μm was used in the drag law instead of the actual diameter of 75 μm . This was reported

as support for agglomeration of the FCC particles to form clusters, making the effective particle diameter equal to cluster diameter. When the actual bed particle diameter was used in the drag law the bed voidage prediction was over estimated. Many other works also reported on over prediction of voidage for bubbling beds using TFM. The consensus was that the effective drag on all the particles was being over predicted leading to higher bed voidage values. Hence various works used an ad hoc scaling-down of the drag laws employed, to match the experimental voidage. These works are reported in Table 2.9 along with the drag laws used and the scaling factors. One reason for this apparent failure was attributed to the existence of heterogeneous structure like clusters or voids which were not resolved in the simulations and which effected on the governing equations. The meshes used in all these works were of the order of a few mm and hence could not resolve the fine heterogeneous or sub-grid scale structures. It was suggested that simulations with fine enough meshes which could capture the sub-grid scale structures, would correctly predict the bed voidage (Wang et al., 2011).

The nature of these heterogeneous structures follows two views. One is that they are clusters of solid particles which form due to significant inter-particle cohesive forces (Das Sharma et al., 2006; Hosseini et al., 2009; McKeen and Pugsley, 2003) and the other view, which has more experimental support, is that they are bubbles in an emulsion phase (Barreto et al., 1983; Dry et al., 1983; Grace and Clift, 1974).

Table 2.9 Main works using Eulerian-Eulerian approach to simulate bubbling fluidization and reported failure to accurately simulate the hydrodynamics due to the coarse mesh used.

Sl. No.	Particle diameter (μm)	Particle density (kg/m^3)	Grid size (mm)	Drag law scaling factor (Drag law used)	Reference
1	75	1500	5	0.2-0.3 (Gibilaro et al., 1985)	(McKeen and Pugsley, 2003)
2	69.8	1310	3	0.25 (Gibilaro et al., 1985)	(Das Sharma et al., 2006)
3	125	2500	9.8	<i>Not reported</i> (Syamlal et al., 1993)	(Makkawi et al., 2006)
4	65	1500	10	0.06 (Gibilaro et al., 1985)	(Lindborg et al., 2007)
5	60	1530	4	<i>Not reported</i> (Wen, 1966)	(van Wachem and Sasic, 2008)
6	75	1500	5	0.15 (D.Gidaspow, 1994.)	(Ye et al., 2008)
7	58	1500	5	<i>Not reported</i> (Gidaspow, 1994.)	(Gao et al., 2008)
8	71.5	2500	5	<i>Not reported</i> (Mazzei and Lettieri, 2008)	(Mazzei and Lettieri, 2008)

The experimental studies on bubbling fluidization of fresh FCC Geldart A particles (Lettieri et al., 2001, 2002) have shown that the bed is dominated by hydrodynamic forces, and that inter-particle forces are negligible. Igci et al. (2008) studied the hydrodynamic characteristics of FCC particles in periodic domains using a standard two-fluid model (TFM) where the effect of inter-particle cohesive forces was not taken into account at all. Their conclusions suggested that predicted bed expansion data fit the experimental values even in absence of IPFs for the bubbling bed. DPM simulations also confirmed that IPFs are negligible in bubbling fluidized beds, though they might effect homogeneous fluidization and behavior in fixed beds (Kobayashi et al., 2013; Ye et al., 2004, 2005). Hence DPM studies also provide evidence that the apparent failure of TFM in bubbling regime may not be due to the absence of IPF contribution. but rather due to the absence of scale resolution i.e. the grid size commonly used are not small enough to capture heterogeneous structures which impact the constitutive laws and therefore the final solutions. It was therefore proposed that with a fine enough mesh, bubbling fluidization could be adequately captured, and that IPFs were negligible in the bubbling regime. Thus making TFM adequate for bubbling regime (Wang et al., 2011). TFM as yet has no closure for IPFs because of the lack of a physical basis for these forces.

2.2.2.2.2 Application of Eulerian-Eulerian approach in riser flows

FCC riser flows belong to the turbulent regime which is beyond bubbling regime. Due to computational limitations, a highly resolved simulation of industrial scale reactors is still unfeasible (Schneiderbauer et al., 2013). It is common to use coarse grids to reduce the demand on computational resources. Several approaches have been proposed to account for

the effect of these unresolved scales, especially on the drag correlation, by applying corrective formulations on the TFM. The Energy minimization multi-scale (EMMS) model (Liu et al., 2001; Yang et al., 2003) was one of the first approaches to formulate these corrections called sub-grid scale laws. It was assumed that heterogeneities in the riser flows appear as distinct particle clusters within an interstitial dilute particle phase. The clusters and the dilute phase consist individually of homogeneously distributed particles, enabling the application of a homogenous drag correlation to these structures. The resulting set of equations is solved by *minimizing* the energy consumed by the transport of the particles, referred to as a main stability condition. Modifications of the EMMS model have also been proposed (Shuai et al., 2011; Wang and Li, 2007). The groups of Simonin (Parmentier et al., 2012) and Sundaresan (Igci et al., 2008; Igci and Sundaresan, 2011) proposed a different route to achieving the sub-grid formulations. They derived residual correlations from filtering highly resolved simulations. The concept behind filtered equations is to recreate the TFM via an operation that amounts to spatially averaging the highly resolved simulations over some chosen filter length scale. In these filtered or coarse grid equations, the consequences of the flow structures occurring on a highly resolved scale is reproduced. If the several assumptions innate to the filtering methodology hold true, the filtered equations can produce a solution with the same macroscopic features as the finely resolved TFM solution, but this solution should come at less cost computationally. Homogeneous expansion regime is yet to be investigated for sub-grid scale equations. These coarse grid approaches hold promise for the future in producing accurate CFD simulations for industrial scale. However the general validity of the models must be further studied.

2.2.2.2.3 Application of Eulerian approach in Homogeneous expansion and benchmarking of CFD tools

Simulation of homogeneous expansion in gas-solid beds have been largely lacking in the literature. Mazzei and Lettieri (2008) analyzed the behavior of homogeneous expansion in liquid-fluidized with their proposed drag law and elastic stress model. The beds were subjected to sudden changes in fluid flux, and results found comparable with the theoretical predictions of the mechanistic one-dimensional model of Gibilaro et al, (1985). They also reported their predicted minimum bubbling velocity in gas-fluidized beds to be one magnitude higher than the experimental value. A short communication by Wang et al. (2009) reported that the apparent failure of TFM to predict minimum bubbling was not due to any fault in the standard equations but because of insufficient grid resolution, (The importance of grid resolution has already been discussed in the previous two sections 2.2.2.21 and 2.2,2.2.2 in context of other flow regimes). Wang et al. (2009) reported their simulated bed expansion, using TFM with grid size of 2-4 particle diameters, matched with that of DPM simulations. However, the main drawback of the work was that the size of the bed was only 3mm x 1.2mm x 12mm, making it a hypothetical bed. Further, only one set of simulations was shown and results were not compared to experimentally obtained values. Wang et al. (2010) used similar grid resolution to predict minimum bubbling velocity using TFM and reported agreement with the experimental work of Abraham and Geldart (1980). An in press article by Liu et al. reports on minimum bubbling velocity in micro-bed using very fine mesh ($1-2d_p$) simulations with Gidaspow (1994) and Gibilaro (1985) drag laws and reported the latter to better predict the hydrodynamics. Summary of these main works are given in Table 2.10.

Table 2.10 Major works using TFM to investigate homogeneous expansion and minimum bubbling transition with their limitations

Sl. No.	Investigated	Limitation	Reference
1	Homogeneous expansion for liquid-fluidized bed with new closure for drag and accounting of elastic forces. Tested minimum bubbling velocity for gas-solid fluidization	Closures not applied to gas-solid homogeneous expansion. Minimum bubbling predicted 10 times higher than experimental value	(Mazzei and Lettieri, 2008)
2	Proposed that the mesh size rather than fault in constitutive TFM was the reason for over prediction of minimum bubbling velocity	Domain size theoretical (3mm × 1.2mm). Only a trial simulation on gas-solid homogeneous expansion as it was a short communication	(Wang et al., 2009)
3	Minimum bubbling velocity using fine mesh (2-4d _p) simulations	Small domain size (2cm × 3cm) and only 2s of flow time simulated for each trial without reaching steady state	(Wang et al., 2010)
4	Minimum bubbling velocity using fine mesh (1-2d _p) simulations with Gidaspow (1994) and Gibilaro (1985) drag laws	Theoretical domain (micro-bed) was used.	(Liu et al., In press)

A study on capability of software tools (Herzog and Egbers, 2013) concludes that the CFD codes of MFIx and Fluent 6.3 were technically mature to predict the fluidization phenomenon based on Eulerian-Eulerian method. OpenFOAM was the third code that was benchmarked, but it did not agree with the results obtained from MFIx and Fluent 6.3. It is worth noting that there was an overall agreement of all three codes with experimental data, but not below 0.1m/s inflow gas velocity. Experimental data showed expansion for all values of gas flow, even values below 0.1m/s, but none of the codes were able to capture this. Instead simulated expansion starts only after 0.1 m/s, and below this value there was no bed expansion. This may have been because of the coarse mesh size (5mm ×5mm) used

was not able to capture the small scale fluctuations of local porosity, which is Both Gidaspow (1994) and Syamlal-O'Brien (1993) drag laws were benchmarked in this work.

2.2.3 Linear stability analysis approach

'Linear stability analysis' was used to predict minimum bubbling voidage, which is the gas volume fraction of the fluidized bed at the instant of time that the first bubble is formed in the bed. Owoyemi and Lettieri (2008) studied thirteen group A powders fluidized by mono-component gases. They developed expressions for the kinematic and dynamic velocities from their new stability criteria and compared the obtained minimum bubbling voidage values with those of the Foscolo and Gibilaro (1984) criterion and experimental data obtained by Xie and Geldart (1984). Their values, like in the previous study (Foscolo and Gibilaro, 1984), clearly underestimated minimum bubbling voidage for particle diameters more than 80 μm and overestimated the same below 80 μm . This might indicate the role of IPFs for diameters below 80 μm . The proposed drag law closure (Owoyemi and Lettieri, 2008) was validated against the equation of Richardson and Zaki (1954).

2.3 Gas-solid fluidization with reaction

In theory, the simulation of reactive beds needs to follow after the inert bed simulations are well established. This is because a bed with simultaneous reaction and fluidization has more complex hydrodynamics than one carrying out fluidization alone. But even though there are issues yet to be resolved for inert bed simulations, some researchers have initiated reactive bed simulations with at least some major approximations. Simulation of reactive beds is therefore a very current topic and calls for much investigation in the coming years. The following literature survey covers all major works

currently available in this area. The most studied reaction using CFD is that of ozone decomposition. Zimmermann and Taghipour (2005) simulated such a system for a bed of 60 μm particle size in bubbling fluidization. The model treated the reaction as purely gas phase, mimicking the situation where ozone species undergo physisorption onto the solid sand particles which acts as reaction sites, but which do not chemically taking part in the reaction. They (Zimmermann and Taghipour, 2005) used Eulerian-Eulerian approach with a modified form of Syamlal and O'Brien drag law to allow for minimum fluidization velocity of 0.0027m/s. The simulated ozone conversions were higher than those measured experimentally and the authors concluded that correct prediction of the reaction kinetics is highly dependent on modeling of the hydrodynamics, which needs further improvement. Ozone decomposition in 3D was also simulated (Hansen et al., 2004) using Eulerian description of the flow with focus on the ozone concentration which was found to be in better agreement with experimental data than 2D simulation results. The predicted pressure gradient showed agreement with the experimental data in the upper part of the riser but showed deviation in the lower part. Another 3D study (Snider and Banerjee, 2010) used the Eulerian-Lagrangian approach, and provided a detailed parameter study, but concluded that the reaction chemistry depended on the still unknown hydrodynamics of bubbling bed. Another CFD study of fluidized bed reaction was that of hydrogen production from steam reforming of glycerol (Dou and Song, 2010). They used Eulerian description of the flow coupled with laminar finite rate model for the simplified homogeneous gas phase reaction chemistry. Apart from pressure drop and velocity fields, Glycerol conversion, hydrogen production and selectivity were also studied. Wood gasification was modeled using Eulerian multiphase approach to bubbling fluidized bed

(Gerber et al., 2010). The detailed study covered operating as well as model parameters and concluded the need for further research especially with respect to the pyrolysis sub-model. Detailed methane chlorination chemistry was modeled (Raman et al., 2001) using Lagrangian composition probability density function (PDF) code with a novel chemistry tabulation algorithm and reported their CFD simulations in agreement with pilot plant data.

The kinetic studies of several other reactions which are commonly carried out in fluidized bed, but have not yet been modeled using CFD include the following. NO and N₂O reduction over coal chars in fluidized-bed combustion (Li et al., 1998), Hydrogen production from pyrolysis of biomass via catalytic steam reforming using commercial catalyst NiO/MgO (7.2 wt.% NiO) (Zhang et al., 2011), Hydrogen production from steam methane reforming (Go et al. 2009), Syngas production from reforming of methane over fluidized Ni/SrO–SiO₂ catalyst (Jing et al., 2004), methanation reaction using commercial Ni/ γ -Al₂O₃ catalyst of Group B (Kopyscinski et al., 2011), and oxidation of *n*-butane to maleic anhydride over δ -VOPO₄ and γ -VOPO₄ (Mills et al., 1999). Oxychlorination of ethylene is a very important reaction industrially as it produces ethylene dichloride (EDC) which is the precursor of one of the most mass produced thermoplastics- polyvinyl chloride (PVC). The reaction takes place over copper dichloride catalyst and is carried out industrially in fixed bed, and more popularly, fluidized bed mode. One of the first kinetic studies (Carrubba and Spencer, 1970) reported that the ethylene oxide mechanism, in which intermediate compound ethylene oxide, is chlorinated to EDC with hydrogen chloride, is validated by experimental data, where as the Deacon mechanism which proposed direct chlorination of ethylene evolved from the catalyst, was not

validated. Later Wachi and Asai (1994) reported a two step reaction where the formation of EDC was attributed to valency change of copper dichloride to give copper monochloride. Oxygen and hydrogen chloride only take part in subsequently catalyst regenerated. Also the interparticle diffusion effects of ethylene in catalyst were found to be negligible. Go et al. (2010) proposed it advantageous to carry out the two reactions of Wachi and Asai in two separate reactors and studied fluidization quality, conversion and selectivity. It is worth noting that there have been some modeling and simulation studies on EDC production (Al-Zahrani et al., 2001; Moreira and Pires, 2010; Sai Prasad et al., 2001) but none so far using CFD as a simulation tool. Sai Prasad et al. (2001) estimated the rate parameters using unsteady state assumption and found them to significantly differ from the steady state assumption. Here regeneration of catalyst was not modeled. They (Sai Prasad et al., 2001) validated the temperature behavior from experimental work. Al-Zahrani et al. (2001) used a one-dimensional transport and kinetic model to study oxychlorination of ethylene in bubbling bed and found that bubble diameter, ethylene mole fraction, residence time and height of bed at minimum fluidization had significant effect on the reactor performance.

2.4 Gaps in the literature

The Literature survey shows that efforts are being made to develop CFD models for fluidized beds and also to simulate the same. It is very evident that the bulk of the literature dealing with gas-solid fluidization is dedicated to the bubbling regime and riser flows, where investigations have been made using both the Eulerian-Eulerian approach (TFM) and Eulerian-Lagrangian (DPM, DEM) approach. Further, we see the most

success in bubbling beds, for simulation of the courser B and D group particles. Several authors reported that standard TFM failed to predict the main features of Geldart A particles in bubbling beds as discussed in section 2.2.2.3.

The number of CFD studies on homogeneous fluidization forms only a small fraction of the total number of published studies dealing with gas-solid fluidization. Of these DPM simulations reported on homogeneous expansion and minimum bubbling. However, DPM simulations are limited by the number of particles that can be tracked. Consider that the number of typical Geldart A particles in a standard lab-scale bed of radius 4cm and 12cm can be calculated to be 461,807,580 for a solid packing of 0.55. The maximum number of particles that DPM or DEM simulations handled so far (Table 2.2) is only of the order of 10^6 . Hence DPM or DEM simulations can track a flow domain of only mm size. On the other hand, most of the TFM studies on bubbling fluidization reported failure of the standard TFM (Tables 2.9 and 2.10) equations either to accurately capture hydrodynamics or predict minimum bubbling. To the best of our knowledge, there were about four major works so far using TFM to investigate homogeneous fluidization or minimum bubbling exclusively (Table 2.10). The work of Mazzei and Lettieri (2008) focused mainly on liquid fluidized beds and simulated homogeneous expansion within 2% error of experimental value. Gas-solid bed simulation was only carried out to predict minimum bubbling, which was 10 times the experimental value! They concluded that the standard TFM equations fail to predict onset of minimum bubbling due to fault in the constitutive laws, and that the elastic force contribution that they incorporated as a closure, had negligible effect. A short communication by Wang et al. (2009) reported high resolution bed simulations using the standard TFM coupled with

the combined Ergun and Wen and Yu drag correlation. Results were reported to match DPM simulations, but the results were not comprehensive, pertaining as they were to only one set of simulation runs. Moreover the domain size was $3\text{mm} \times 1.2\text{mm}$ which can only be considered a hypothetical case study. Wang et al. (2010) used similar grid resolution of 2-4 particle diameters to find minimum bubbling velocity and reported agreement with the experimental work of Abraham and Geldart (1980). However the bed expansion was not reported and the largest domain size simulated was $2\text{cm} \times 3\text{cm}$, which is smaller than even a lab scale system. Also the simulated flow time was only 2s which is a small time to justify persistence of bubbling or minimum bubbling. An in press article by Liu et al. on micro-bed reports that minimum bubbling velocity was correctly predicted with fine mesh ($1-2d_p$) simulations using Gibilaro (1985) drag law but not Gidaspow (1994) drag law.

The simulation of fluidized beds of Geldart A group particles with simultaneous reaction should logically be attempted once the issues regarding inert fluidized beds are resolved. This is because the simulation complexity is a level higher for reacting beds, and accurate hydrodynamic models are a prerequisite. However there have been some simulations of this type with at least some major assumptions, as detailed in section 2.3. In general all gas-solid reacting fluidized beds of Geldart A group particles can be viewed as two types, depending on the role of the fluidized bed. The first type is where the bed simply acts as a contacting surface for reaction. Physisorption of the reacting species may occur on the active sites of the particles which do not participate chemically in the reaction. The second type is where there is also chemical participation of the bed particles in the reaction, i.e. bed particles catalyze the reaction. This is called heterogeneous

catalytic reaction. Most simulations so far have been gas phase reactions of the first type, in particular ozone decomposition, which has received maximum attention. There have been few attempts to simulate heterogeneous catalytic reaction in a fluidized bed of fine Geldart A particles. The homogeneous expansion is technologically the most attractive of the processes when uniform conditions are desirable because gas bypassing and solid-phase dead zones are carefully avoided and each particle is surrounded by fluid and hence used efficiently (Zhang et al., 2008). It is therefore justifiable to use CFD as a tool of study in this context. Oxychlorination of ethylene for the production of ethylene dichloride, the precursor of polyethylene, renders itself suitable for investigation. It is industrially very important, and has established rate expressions and has already been modeled analytically in a few studies. It has not been studied so far using CFD simulations.

2.5 Scope of the work

From the gaps in the literature it is clear that there is scope for work to be done in the simulation of homogeneous fluidized beds of Geldart A particle. The Eulerian-Eulerian approach shows the most promise for large scale simulations. Hence we used the standard TFM described in section 2.2.2.1 for all simulations in this work. All equations were implemented in the FLUENT 6.3.26 commercial solver. No additional closures for TFM were required to be coded by us. The scope of the entire work includes a detailed mesh size effect study, fine mesh study and reaction study on the fluidization of Geldart A particle in homogeneous regime and transition to bubbling. Reaction was incorporated in the simulation studies by implementing user defined functions (UDFs) which we coded in visual basic C++. The reaction studied was oxychlorination of ethylene for the production

of ethylene dichloride. Analysis was based on visual insight of the simulations as well as bed averaged values calculated by solver. In this work over 200 simulations spanning various mesh sizes were conducted for 20-250s of flow time and it was always ensured that steady state was reached.

CHAPTER – 3

SIMULATION METHODOLOGY USING FLUENT 6.3.26

The problem mainly comprises a two-phase, gas-solid fluidized bed of Geldart A particles in 2D, described by the TFM equations presented in Tables 2.3 – 2.6. The bottom inlet simulates uniform gas inlet velocity and the side walls offer no-slip boundary condition to the gas phase and wall shear to the granular phase. At the outlet boundary, atmospheric pressure condition is imposed, to simulate the bed open to atmosphere. The procedure for simulation is presented in section 3.1. In section 3.2 the procedure for simulating the fluidized bed with reaction is presented. The reaction considered was the oxychlorination of ethylene to produce ethylene dichloride (EDC). In section 3.2 only modifications required in the procedure of section 3.1 are presented. A second approach to incorporate reaction (which yielded results) is present in section 3.3. Again only modifications required in the procedure of section 3.2 are presented.

3.1 CFD procedure for simulation of non-reacting fluidized bed using Two-fluid model

The simulation procedure comprises the various inputs, activations and selections required in FLUENT 6.3.26 commercial CFD solver. A summary of the major numerical inputs are provided in Table 3.1. The procedure is summarized in 10 main steps in Table 3.2. What follows include a description of the actions taken and snapshots of the panels that appear in FLUENT 6.3.26. These enable the reader to understand the procedure in more detail. For clarity, only main steps have been numbered and each sub- step is

preceded by an arrow to distinguish it from the main steps. Justifications for choice of inputs, if any, are given in *italics* at the end of each step or sub-step.

3.1.1 Problem description

Table 3.1 Summary of major numerical inputs used in the TFM simulation of non-reacting fluidized bed.

Parameter	Magnitude
Initial 2D packed bed dimensions (Diameter × Height) (cm)	4 × 12 (Std. lab-scale size of reactor)
Grid sizes tested (mm) <i>Reasons for choice are detailed in section 4.1</i>	i. 4 × 4 ii. 2 × 2 iii. 1.414 × 1.414 iv. 1 × 1 v. 0.4 × 0.4
Particle diameter (µm)	70 (typical Geldart A particle)
Gas phase density (kg/m ³)	1.138 (N ₂ at 300K and 1atm)
Gas phase viscosity (kg/m-s)	1.66×10 ⁻³ (N ₂ at 300K and 1atm)
Particle density (kg/m ³)	2000
initial packed bed solid volume fraction (ε_s^{max})	0.55 (Mazzei and Lettieri, 2007)
Solid packing range for frictional flow ($\varepsilon_s^{min} - \varepsilon_s^{max}$)	0.53 – 0.55 (estimated)
Specularity coefficient for solid-phase wall shear	0.5 (Johnson and Jackson, 1987)
Residuals tolerance limit	10 ⁻³ (Note: at steady state, residuals for coarse mesh simulations were in range 10 ⁻⁶ to 10 ⁻⁹ , fine mesh simulations were in range 10 ⁻⁴ to 10 ⁻⁷)
Maximum time step (s)	10 ⁻⁵ (required to always maintain residuals below 10 ⁻³)

Changes to numerical inputs in Table 3.1, if any, are mentioned wherever applicable in the results and discussions of Chapter 4. The Dirichlet boundary condition was used for the bottom gas inflow. Velocity vectors in x (horizontal) direction (always zero) and y (vertical) directions were defined to simulate gas inlet flow normal to distributor. The y velocity magnitude was varied in the range 4 to 12mm/s for each new simulation trial. Each unsteady state simulation trial was run for 10 to 20s of real flow time to ensure pseudo steady state. By pseudo steady state it is meant that average bed voidage calculated becomes nearly constant (fluctuations around mean) whereas the visualized dynamics of the bed could change. On left and right walls, the solid-phase shear was defined by boundary condition of Johnson and Jackson (1987), and for gas phase the no-slip boundary condition was used. At the gas exit boundary, zero gauge pressure was imposed to model the system open to atmosphere.

In the literature, values for the initial packed bed (maximum) solid volume fraction (ϵ_s^{max}) vary from 0.4 to 0.6, and higher values were shown to simulate more realistic drag predictions (Mazzei and Lettieri, 2007). Hence $\epsilon_s^{max} = 0.55$ was chosen, which also corresponds to frictional particles (Chialvo et al., 2012). Initial gas velocity for all interior cells was always set to 4mm/s. A time step as low as 10^{-8} s was required during the initial 1 to 2s to establish convergence, after which it was gradually increased to 10^{-5} s. The wall clocked run times of the simulations were dependent on coarseness of the mesh. A finer mesh necessitates a higher number of calculations. The time taken for a set of five simulations varied from one day to three weeks for the coarse mesh sizes (i to vi in Table 3.1). The fine mesh (v in Table 3.1) simulations required 6 to 12 months of wall clocked time. This included occasional power shutoffs and other non-idealities.

3.1.2 Simulation procedure

Preliminaries:

1. Create 2D mesh of required dimensions in GAMBIT meshing tool and save in file format (.msh) which is exportable to FLUENT 6.3.26
2. Start the 2D double-precision (2ddp) version of FLUENT

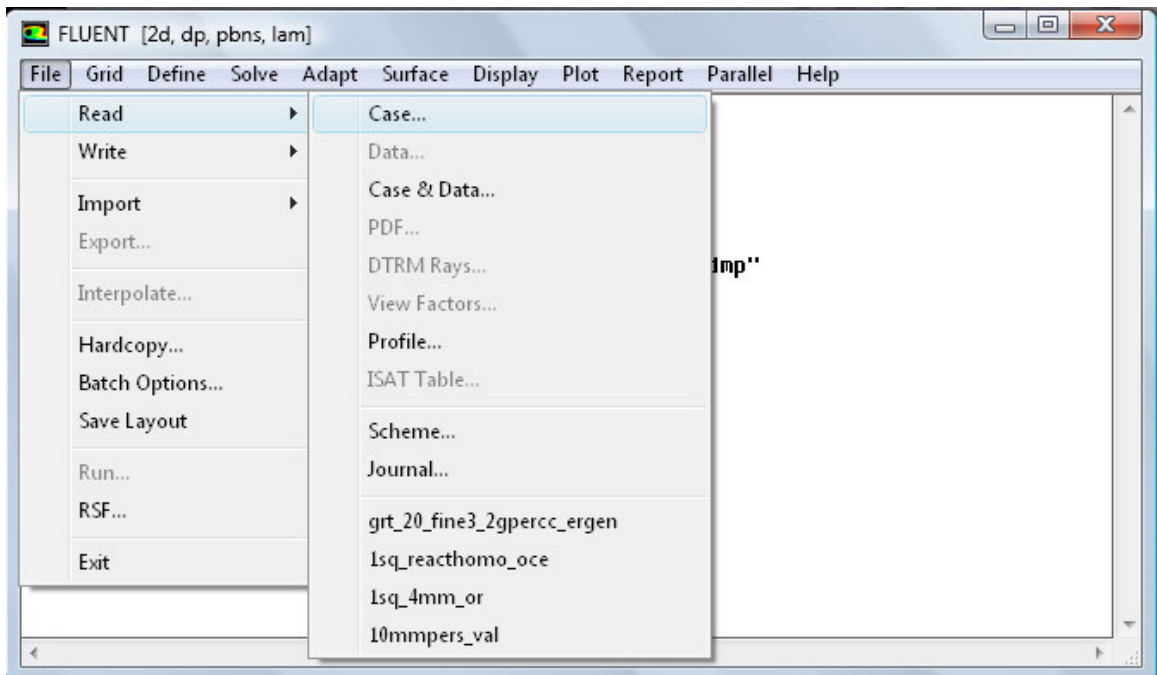
Table 3.2 Main steps of simulation procedure in FLUENT 3.6.26 for non-reacting bed

STEP No.	Function	Description
STEP 1	Mesh	The .msh file created in GAMBIT meshing tool is read into FLUENT. It is scaled to the dimensions of the reactor, checked and displayed
STEP 2	Solver	Solver options are defined. Main options are pressure based (segregated) solver method and unsteady formulation for time
STEP 3	Models	Eulerian multi-phase model with two phases is defined
STEP 4	Materials	Nitrogen gas (phase-1) and solid alumina (phase-2) properties are defined
STEP 5	Phases	Phases are confirmed. All solid phase and interphase interaction (drag) properties or models are defined
STEP 6	Operating conditions	Mainly gravity is defined. zero gauge pressure is defined for the interior of the reactor
STEP 7	Boundary conditions	Wall and inlet boundary conditions are set for gas phase. Only wall conditions are required for solids. For mixture (zero gauge pressure) at exit is defined
STEP 8	Monitors	Monitor of residuals of the conservation equations and Monitor of key bed variables are set-up
STEP 9	Solution controls	The equations to be solved and their discretization schemes are selected with under-relaxation factors
STEP 10	Iterate solution	Time-step related inputs are given. Enable data files saving from which required plots are extracted

STEP 1: MESH

→ **READ MESH**

File----Read----Case----Select the .msh file



A rectangular mesh with four faces was created in GAMBIT interface. The y-axis was the axis of the vessel domain. Since fine mesh for the entire domain was also tested, it was thought redundant to create fine mesh near boundaries for the coarse mesh simulations. The non-dimensional coordinates of the vessel domain were:

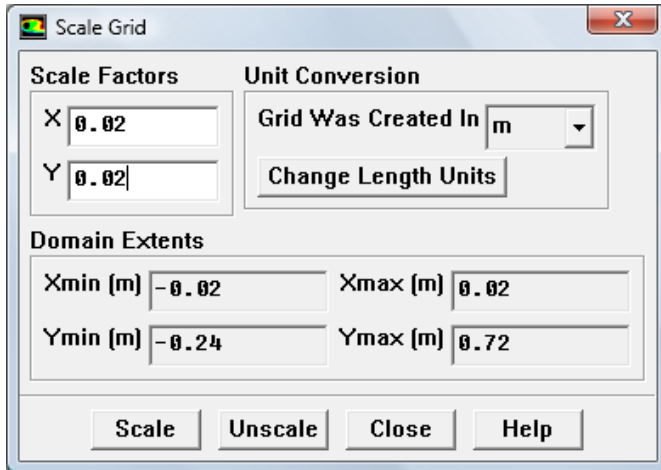
X coordinate: -1 to + 1

Y coordinate -12 to + 36

→ **SCALE MESH**

Grid----Scale----opens the Scale Grid panel----enter scale factors and **Scale**

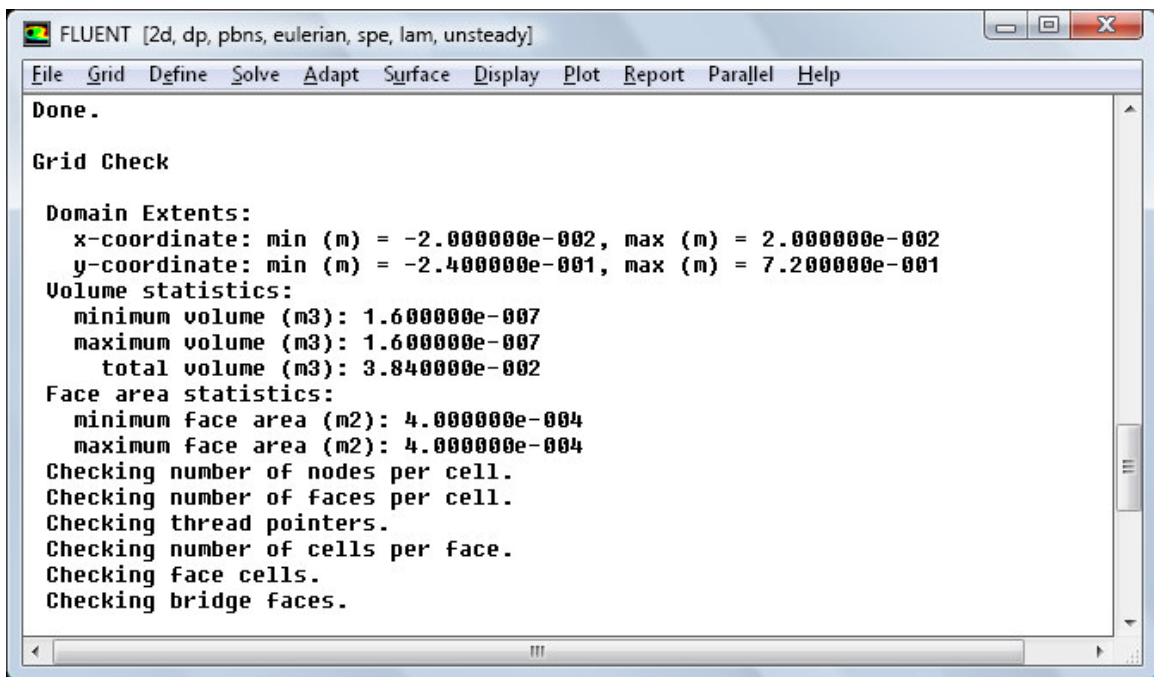
Scaling corrects the mesh dimensions to the required dimensions of the lab-scale reactor which is to be simulated (diameter = 4 cm, height = 96 cm)



→ **CHECK GRID**

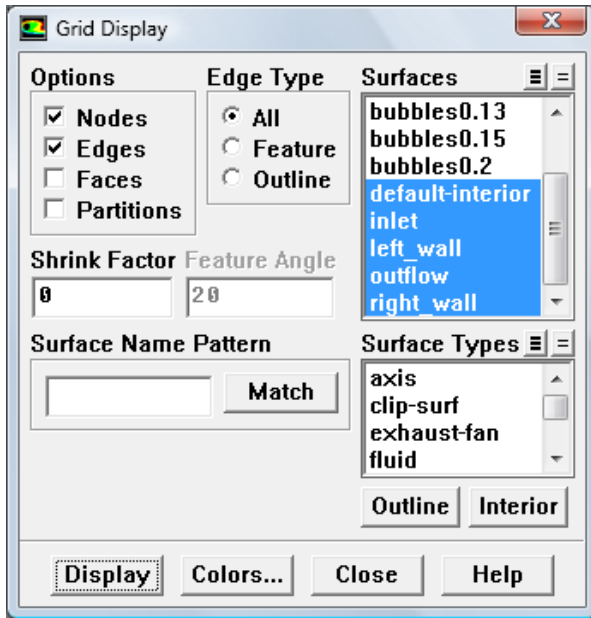
Grid---check---displays all information about the grid in the console

Basic check to make is that the minimum cell volume is non-zero

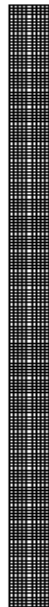


→ **GRID DISPLAY**

Display---Grid---opens the Grid Display panel, choose options and **Display**



View and check mesh

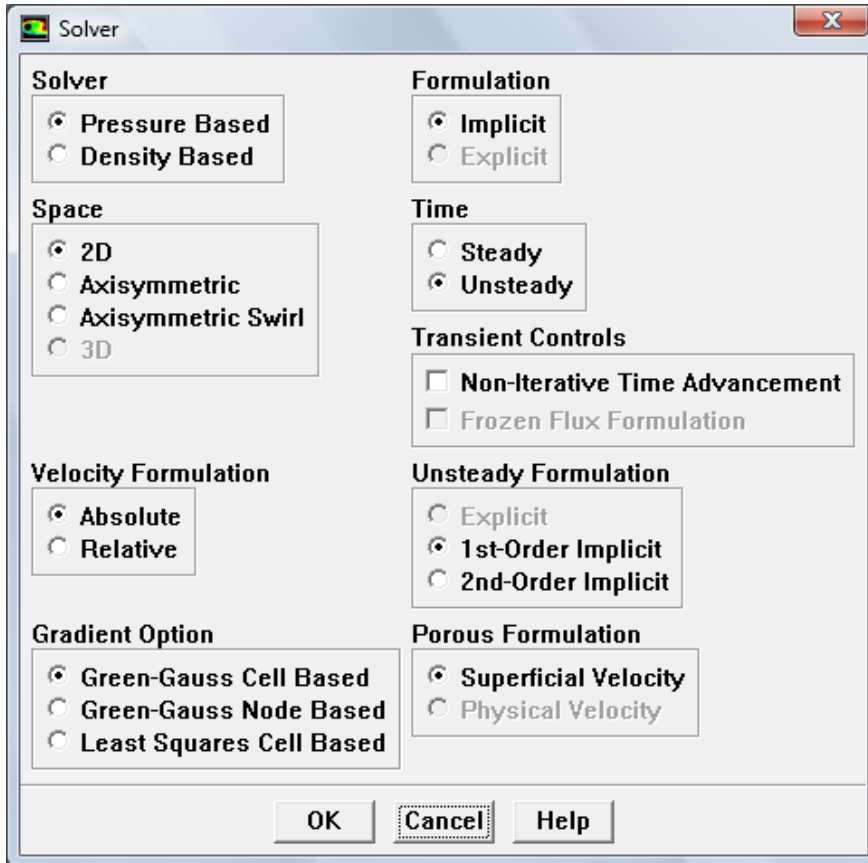


Grid (Time=0.0000e+00) Nov 13, 2014
 FLUENT 6.3 (2d, dp, pbns, eulerian, spe, lam, unsteady)

STEP 2: SOLVER

→ DEFINE SOLVER

Define----Models----Solver----opens the Solver panel, choose options and **OK**



***Solver:** The choice of solver depends on the speed of flow. Usually pressure based solver is suitable for low speed incompressible flows (FLUENT User's Guide 25.1.1). Since viscous regime was investigated the pressure based solver which solves equations in a segregated manner was chosen. In this approach the velocity field is corrected by the pressure field so as to satisfy continuity. In contrast, the density based solver solves equations in a coupled manner. This solver is suitable when the flow is highly coupled and Mach No.>4. FLUENT follows finite volume discretization technique for both approaches.*

Space: *Axisymmetric options are used when the flow solution expected is symmetric about a particular axis. This is not applicable for the fluidized bed so 2D was chosen.*

Absolute velocity: *The relative velocity formulation is appropriate when most of the fluid in the domain is rotating, as in the case of a large impeller in a mixing tank (FLUENT User's Guide 10.7.1). As this is not the case here, absolute velocity formulation was used.*

Gradient option: *The Green Gauss cell based method is sufficient for square mesh. Here gradients of scalars are constructed from face centroid values. Other options are more accurate for unstructured mesh (FLUENT User's Guide 25.3.3).*

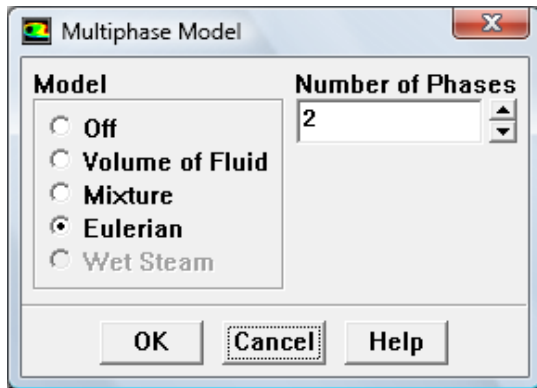
Time: *unsteady option was chosen to simulate the transient evolution of the bed from packed bed state*

Unsteady formulation: *only implicit methods for new time step calculations are available for pressure based solver (FLUENT User's Guide 32.3.1). First order accuracy was chosen to begin calculations and was later updated to second order accuracy as convergence behavior improved. This was one of the strategies employed to achieve convergence.*

STEP 3: MODELS

→ DEFINE MULTIPHASE MODELS

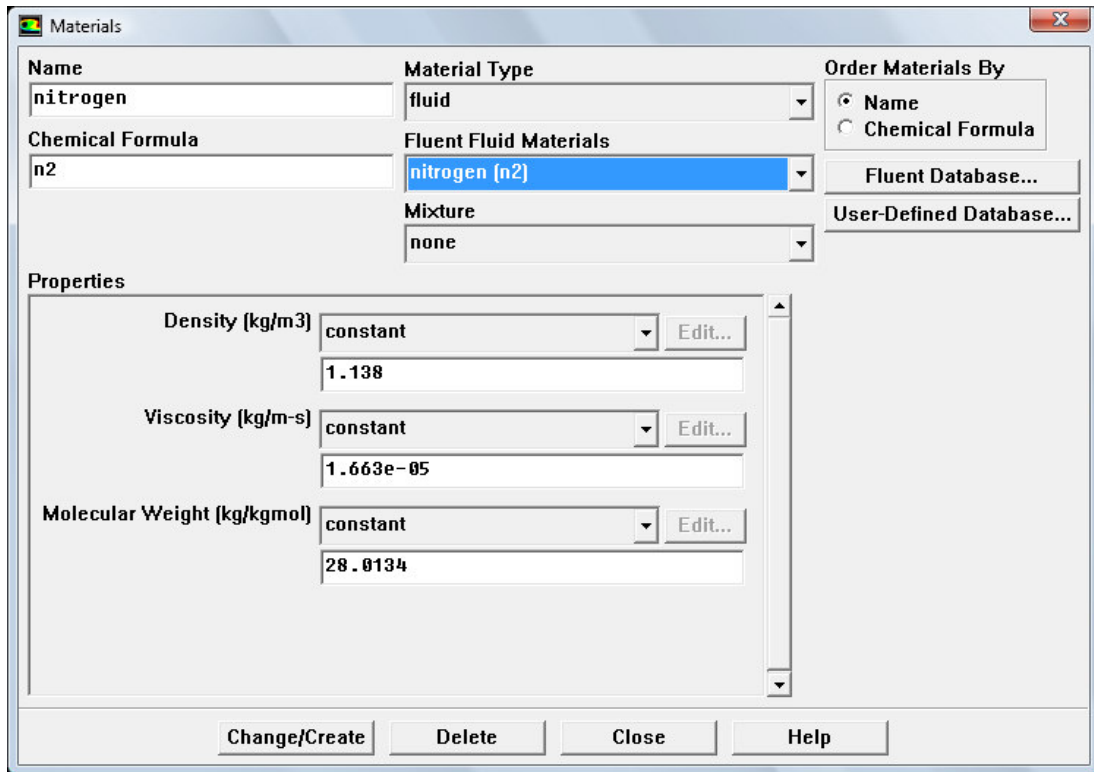
Define----Models----opens the Multiphase Model panel, choose Model, and enter Number of Phases and **OK**



***Multiphase model:** The Eulerian model is well accepted in the literature as the most rigorous multiphase model suitable for fluidized bed modeling (Wang, 2009). It solves momentum and continuity for individual phases, whereas in Mixture or Volume of Fluid models (VOF) only one set of equations are solved for all the phases combined.*

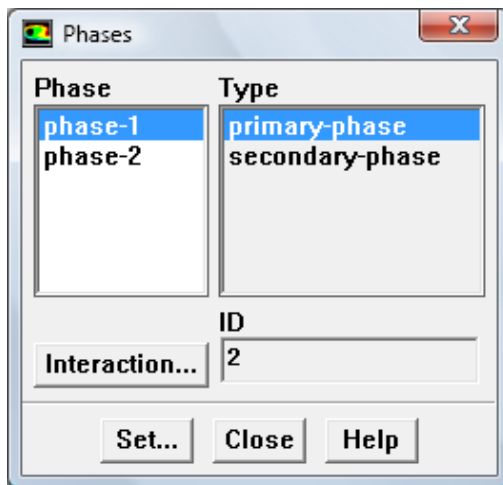
STEP 4: MATERIALS

Define----Materials----opens the Materials panel where nitrogen is added as a fluid material (main properties given are visible in the snapshot of Materials panel). Alumina was also created as a new material under **Material Type:** fluid. In FLUENT, there is no distinction between fluid-fluid and fluid-solid (granular) multiphase flows (FLUENT User's Guide 23.5.1). A granular flow is simply one that involves at least one phase that has been designated as a granular phase. Alumina will be designated as the granular phase but is created as a fluid material. Only density (2000 kg/m^3) is required for Alumina properties as it is the granular material.



STEP 5: PHASES

Define----Phases----opens the Phases panel where phase properties are set. No further input is required for primary phase defined as Nitrogen (gas phase)



→ **DEFINE SECONDARY PHASE PROPERTIES**

In Phases panel properties of secondary phase are **Set...** and Secondary Phase panel opens. All inputs are given by scrolling down in the Secondary Phase panel and are not visible in the snapshot shown. Table 3.3 defines all inputs (FLUENT User's Guide 23.5) along with reason for their choice. These inputs mainly relate to the detailed description of the solid phase stress

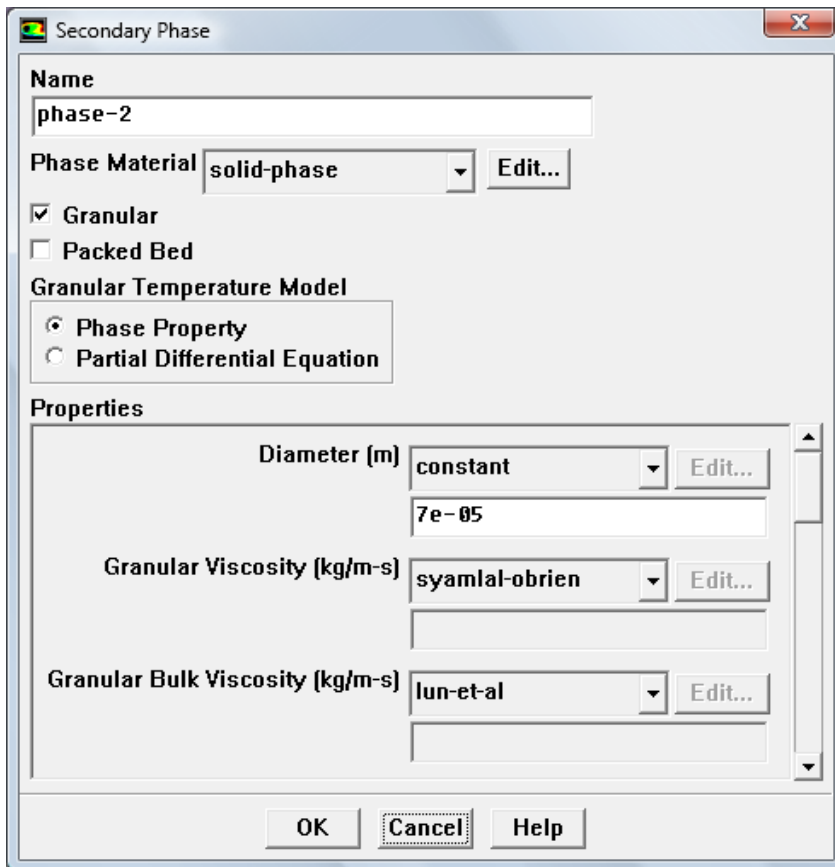
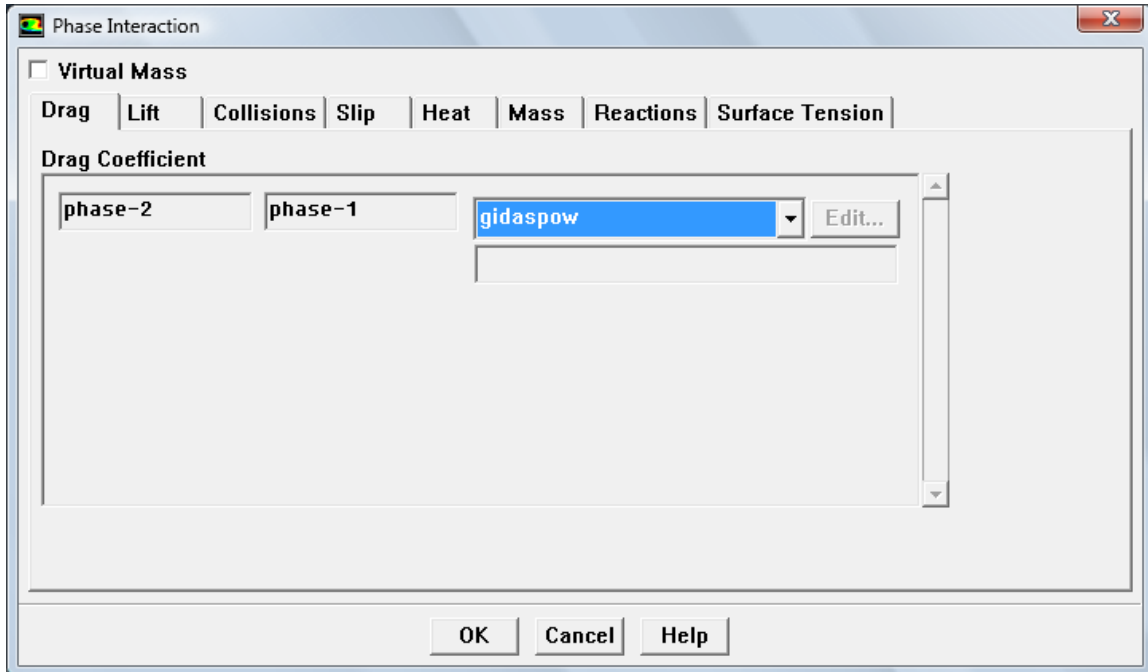


Table 3.3 Inputs for the granular (solid) phase.

Sl. No.	Physical quantity	Value / Model
1	Particle diameter: 7×10^{-5} m	<i>Typical Geldart A particle</i>
2	Granular Viscosity (kg/m-s) (Syamlal et al., 1993)	<i>The kinetic part of the granular viscosity is defined out of two options. The more recent Syamlal model was chosen over Gidaspow</i>
3	Granular Bulk Viscosity(kg/m-s) (Lun et al., 1984) <i>only option</i>	<i>This accounts for the resistance of the granular particles to compression and expansion</i>
4	Frictional Viscosity (kg/m-s) (Schaeffer, 1987)	<i>The other option is Johnson and Jackson model is and was also tested</i>
5	Angle of internal Friction: 30° (van Wachem et al., 2001)	<i>This is a material property required to calculate frictional viscosity</i>
6	Frictional pressure (Pa) (Syamlal et al., 1993)	<i>Model of Syamlal was consistent with friction viscosity from Schaeffer model</i>
7	Frictional modulus (Pa) Derived <i>only option</i>	<i>This is the partial differential of frictional pressure wrt solid volume fraction and is ≥ 0 in derived option</i>
8	Frictional Packing Limit: 0.53 (estimated)	<i>The frictional viscosity component is only calculated when packing exceeds this value</i>
9	Granular Temperature (m^2/s^2) Algebraic	<i>Granular temperature field is calculated from the particle velocity fluctuations (Algebraic). Other option is to impose a constant value</i>
10	Solids pressure (Pa) (Syamlal et al., 1993)	<i>Other options are Lun-et-al, and Ma-ahmadi models, but Syamlal is sufficient for dense particle laden flow (van Wachem et al., 2001)</i>
11	Radial Distribution (Syamlal et al., 1993)	<i>Models of Lun et. al, Ma-ahmadi and Arastoopour are also available but Syamlal is most commonly employed</i>
12	Elasticity Modulus(Pa) Derived <i>only option</i>	<i>This is the partial differential of solids pressure wrt solid volume fraction and is ≥ 0 in derived option</i>
13	Packing Limit: 0.55	<i>This is the maximum packing allowed in the simulation and represents packed bed state</i>

→ **DEFINE PHASE INTERACTION**

In phases panel **Interaction...** opens the Phase Interaction panel where we set only **Drag** and **Collisions** (restitution coefficient = 0.9 chosen as commonly used in DPM and having negligible effect in simulation (Wang et al., 2010)).

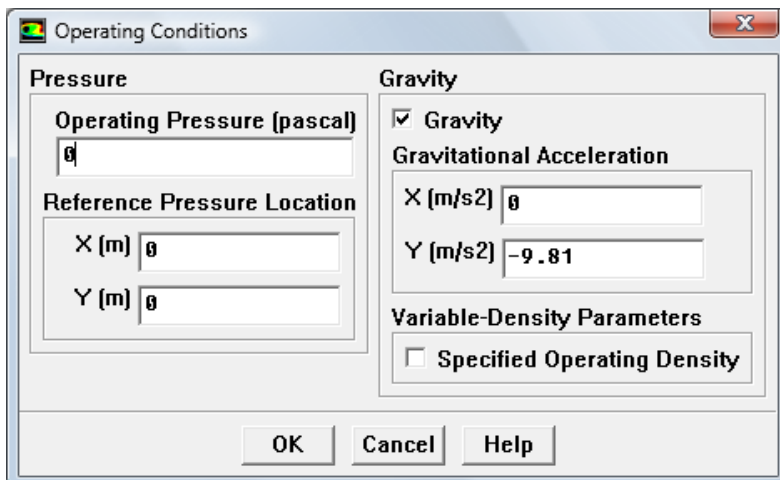


Drag Coefficient: *Gidaspow* the most commonly used model was mainly used, but *Syamlal* and *Wen Yu* models were also tested

STEP 6: OPERATING CONDITIONS

Define---Operating Conditions----opens the Operating Conditions panel where only gravity is the required input and **OK**.

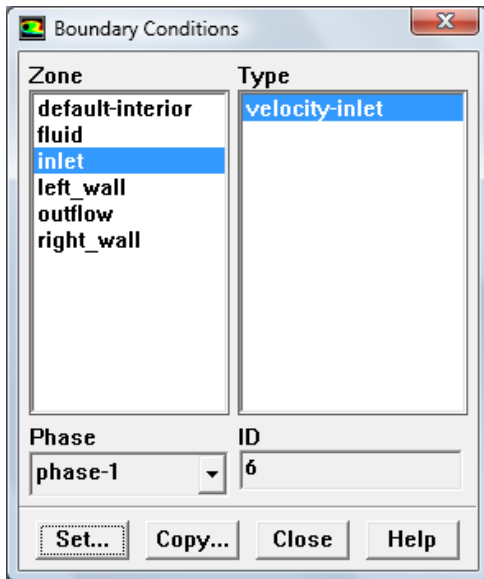
Operating Pressure: *The vessel is open to atmosphere so operating pressure (gauge) = 0*



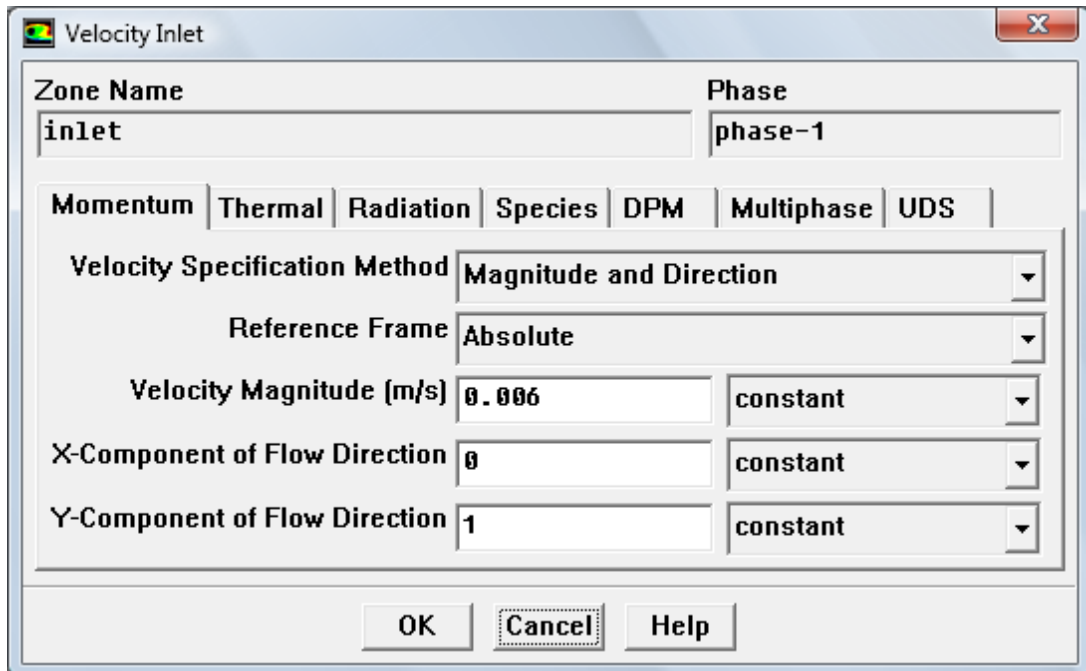
STEP 7: BOUNDARY CONDITIONS

→ DEFINE ZONAL BOUNDARY CONDITIONS

Define---Boundary conditions---opens the Boundary conditions panel where boundary conditions for each zone is **Set...**

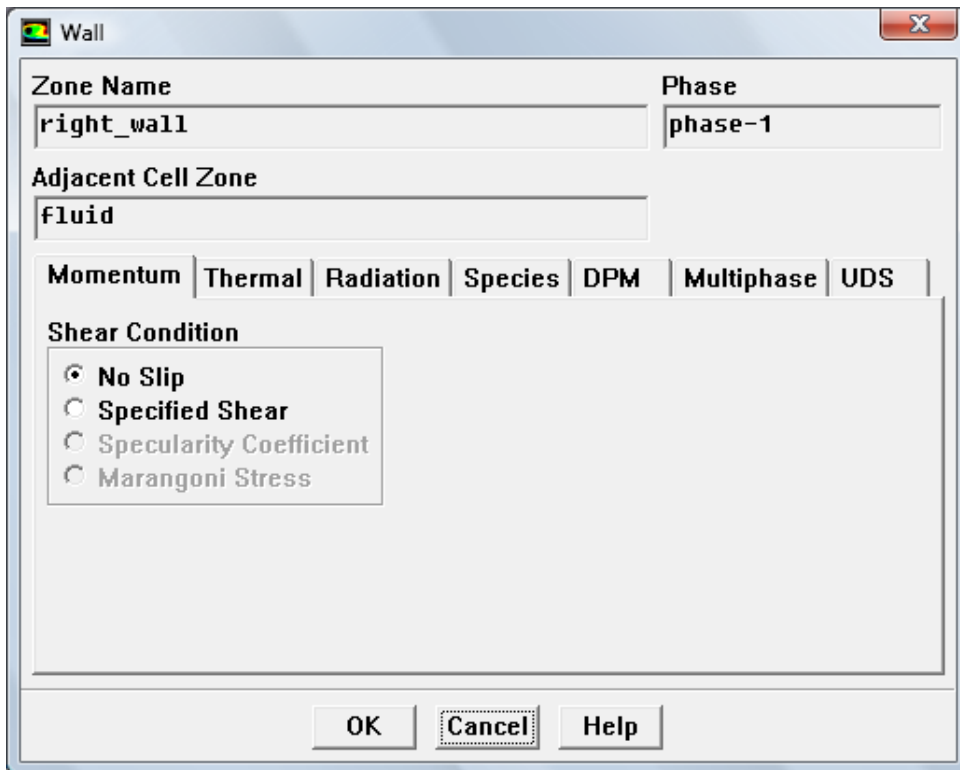


For **phase-1** at Inlet boundary, velocity is specified



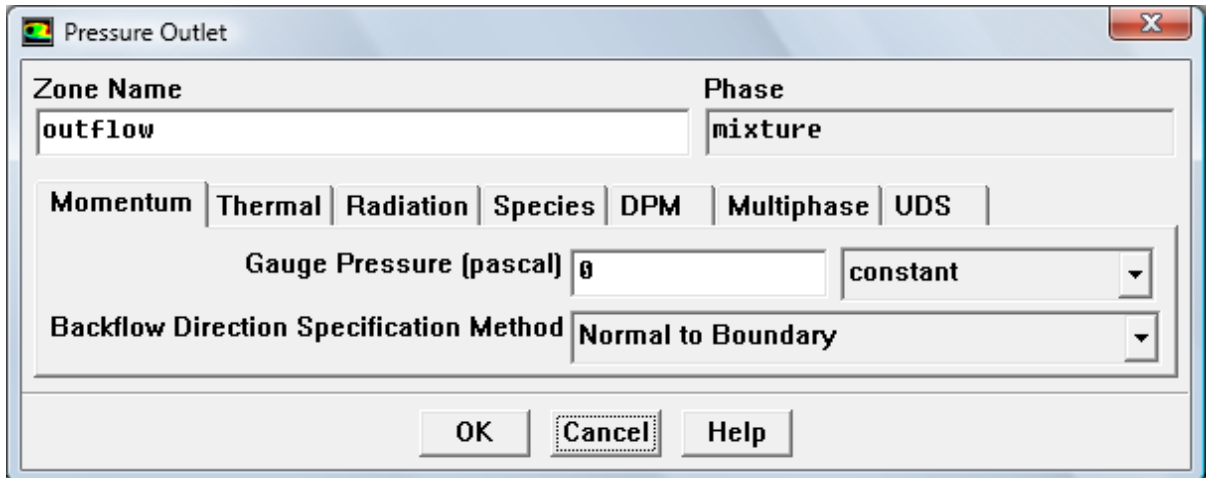
Velocity Specification Method: *Magnitude and Direction* option ensures that only the Y-component of velocity vector has magnitude (which is varied for different trials), to simulate the incoming gas flow only normal to the distributor. Other options are setting X and Y-components only or magnitude normal to the boundary

For phase-1 (gas phase) at **Wall**, no slip is specified on both left and right side. The only other available option is specified shear.

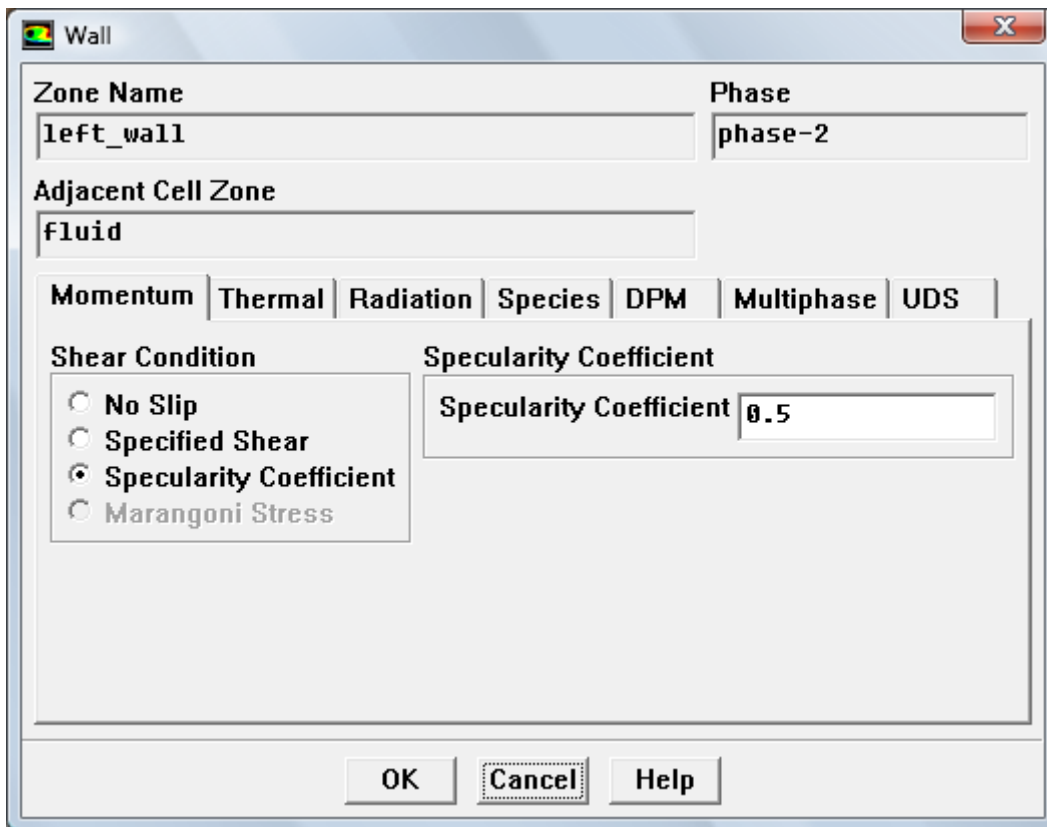


Shear Condition: *No slip* is commonly used for fluid at wall boundary in literature. Also specified shear data is not easily available or verifiable. In such cases we follow the heuristic that the commonly used rule or convention is followed. This makes the simulation results more conducive to comparison with literature data.

For mixture at the outflow (phase 1 and 2, should particles also move out of the vessel) zero gauge pressure is set, to simulate the vessel open to atmosphere. No other specification is needed.



For phase-2 (solids) at wall boundary, both left and right, specularity coefficient is set

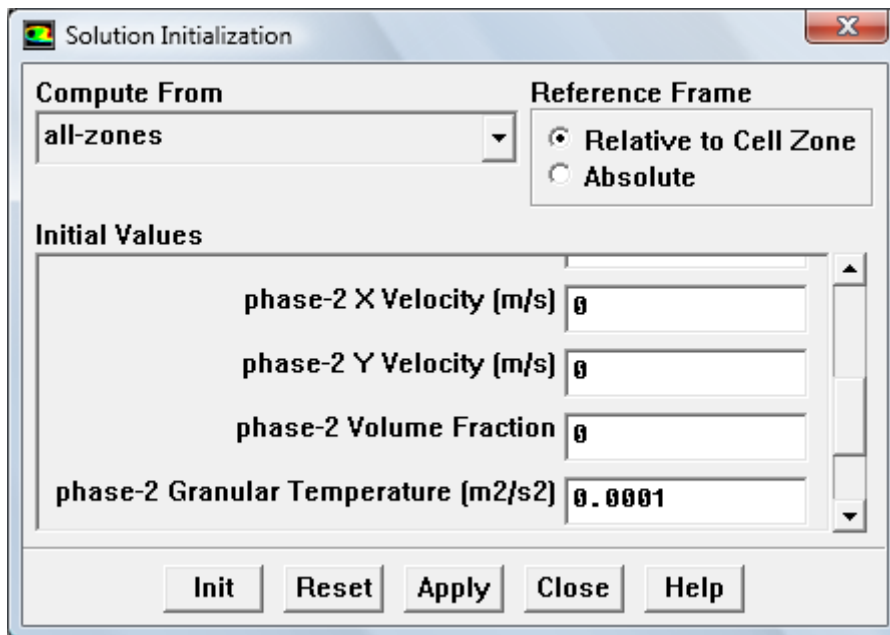


Shear Condition: The specularity coefficient is required to specify the Johnson and Jackson boundary condition which is commonly used to define granular shear at walls.

The specularity coefficient takes values between zero and unity and is a measure of the fraction of collisions which transfer momentum to the wall. its commonly used value is 0.5 (Johnson and Jackson, 1987).

→ **DEFINE INITIAL CONDITIONS**

Solve----initialize----opens the Solution Initialization panel where initial conditions are set for the interior cells. The Initial values displayed by the panel depend on the case built up. For this case inputs required are velocity components for both phases, gauge pressure, granular pressure for the mixture, and volume fraction for phase-2

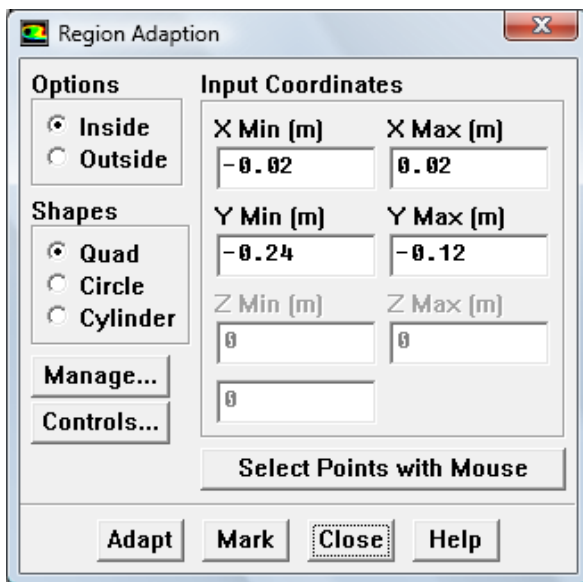


All initial conditions were zero except for phase-1 Y velocity. The interior cells need to be given an initial guess for velocity value of phase-1 (gas) to start the calculations. This value is usually close to but smaller than the gas velocity at the inlet boundary. For all trials we initialized 0.004m/s which is close to minimum fluidization velocity for the system. We also found that a negligible non-zero value of Granular Temperature helped

to start the calculations. It is important to initialize the phase-2 (solids) volume fraction to zero. Initial value is mandatory for cells that are intended to be patched later on

→ **MARK REGION FOR INITIAL PACKED BED**

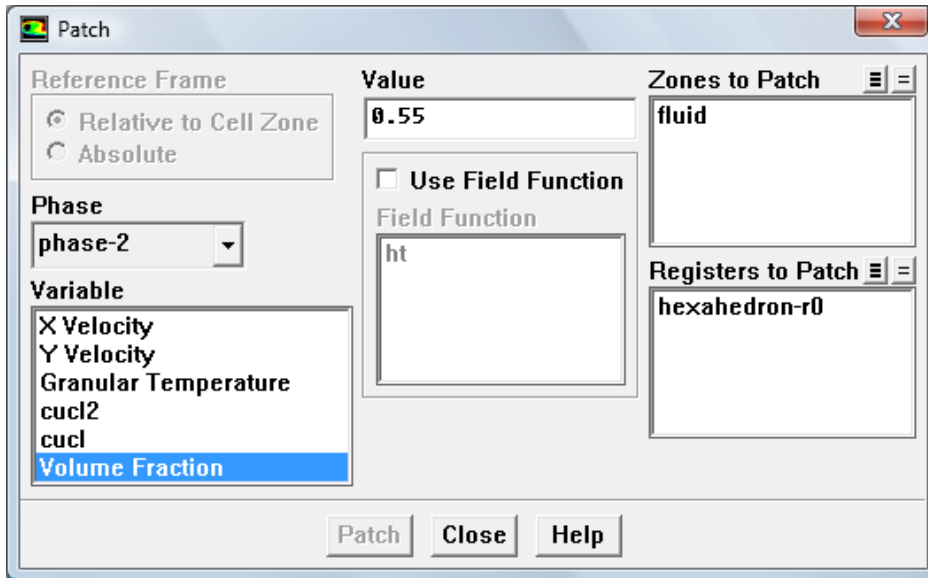
Adapt----Region----opens the Region Adaption panel where specific interior cells are marked or selected. We input the coordinates to mark all cells required to create the initial packed bed (4cm × 12cm). Then **Mark**. The number of cells marked appears in the console. Also a register name for the cells is created which can be viewed in **Manage...**



→ **PATCH INITIAL PACKED BED**

Solve----initialize----opens the Patch panel where the phase-2 Volume Fraction is patched with the value 0.55 to the register previously created

Patching is the process of initializing certain cells only to a particular value for a particular variable. In this case it is used to create an initial packed bed of solids with uniform initial solids packing (solid volume fraction) of 0.55, or voidage (gas volume fraction) of 0.45. The rest of the interior cells above the bed (freeboard), still have a solid volume fraction of zero as initialized previously.



Patch value of Volume Fraction: in the literature, values for the initial packed bed (maximum) solid volume fraction (ϵ_s^{\max}) vary from 0.4 to 0.6. the and higher values of ϵ_s^{\max} were shown to simulate more realistic drag predictions (Mazzei and Lettieri, 2007). Hence $\epsilon_s^{\max} = 0.55$ was chosen for the simulations.

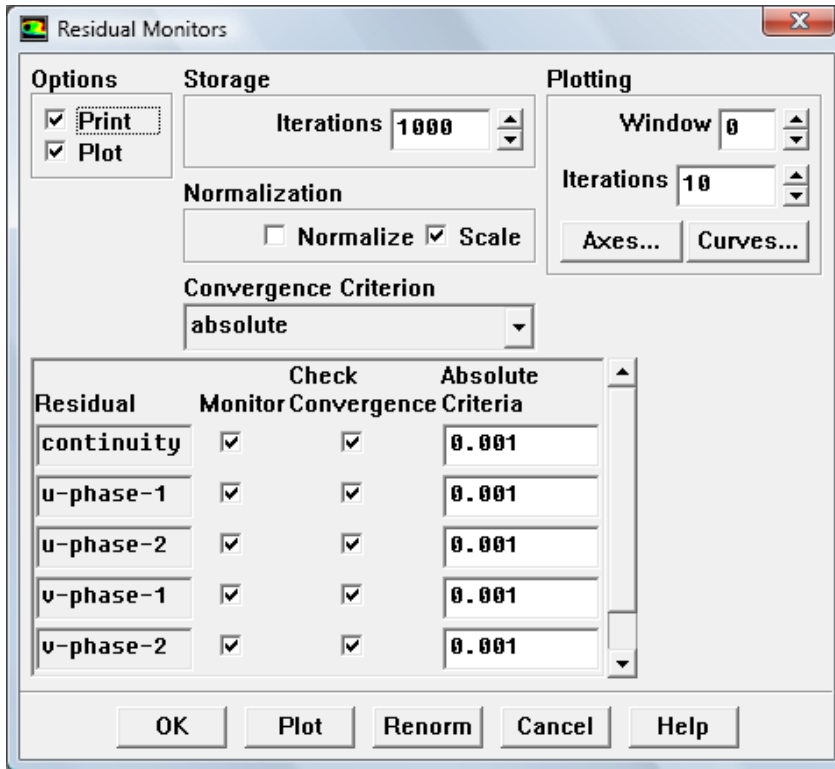
STEP 8: MONITORS

Solve----Monitor----Residuals opens the Residuals Monitors panel. Other quantities that are available to be monitored are based on statistics, force, surface and volume.

→ SET RESIDUAL MONITOR

Residuals represent the error in solving the partial differential equations. They are the difference between the LHS and RHS of the partial differential equations. The residuals set reflect the accuracy to which the equations are solved before the next iteration. They also represent a tolerance limit check before the next iteration. If residuals do not meet the criteria even after the **Maximum iterations per Time Step** (which will be set later n

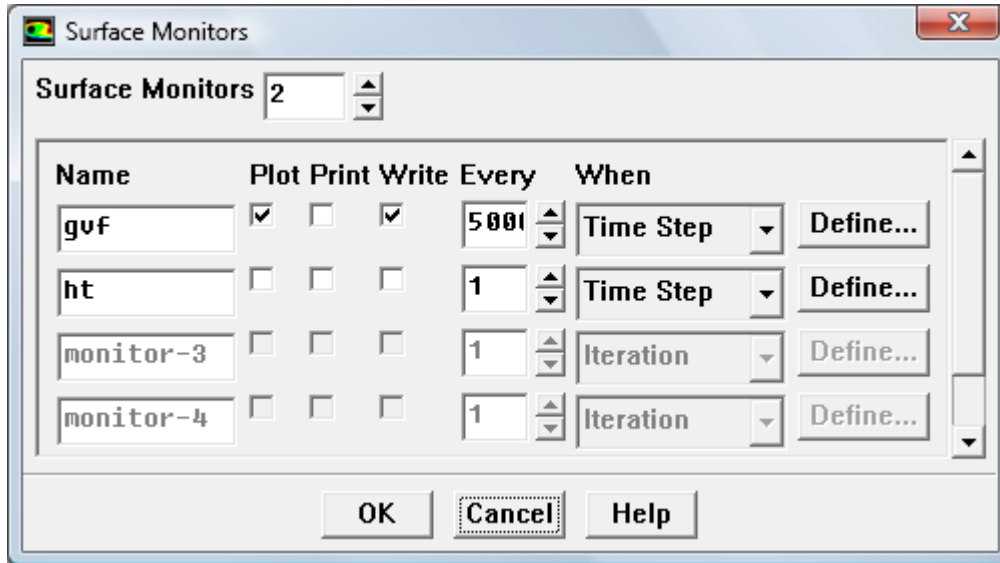
iteration panel to 80) the solver may proceed with the calculations but due to growing residuals divergence will occur.



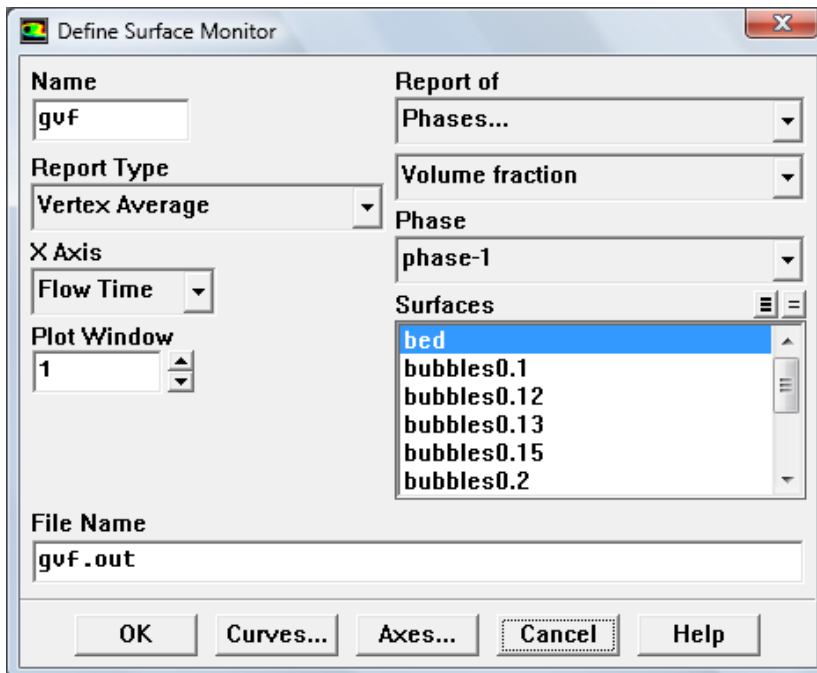
Monitor Convergence Criteria: We always maintained the residual values for all equations as low as 10^{-3} . According to FLUENT User Manual 25.22.1 this value is adequate for all the equations solved. Even at the beginning of calculations when convergence was difficult to achieve, the residuals restriction was not lifted. Instead time step was reduced to achieve convergence.

→ **SET SURFACE MONITORS**

Solve----Monitor----Surface----opens the Surface Monitors panel where the number of monitors and other options are set.



To set the quantities to be monitors **Define...** is used. In the Define Surface Monitor panel the report type can be the sum, maximum, minimum or average. The Surface is the collection of nodes over which the report type is calculated. On **X Axis** other options available are Iterations and Time Step.

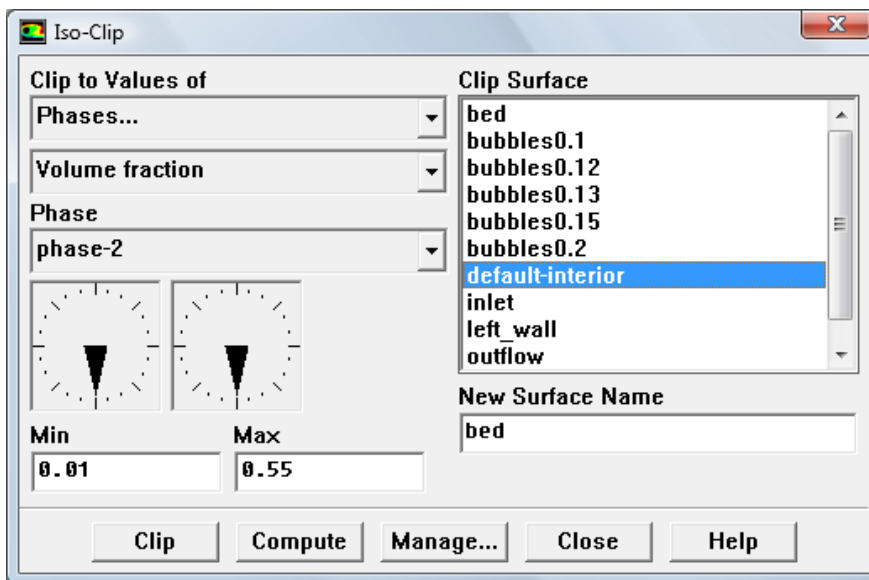


The main monitor created was for the bed gas volume fraction or voidage. The settings are shown in Define Surface Monitor panel. The node or vertex average of gas volume

fraction of all cells belonging to the surface called bed is calculated and plotted against the flow time. This monitor also represents the transient evolution of the bed voidage. Such plots are discussed in Chapter 5. They cannot be obtained from post-processing, but must be set up with the simulation case, and they get plotted as the simulation iterates.

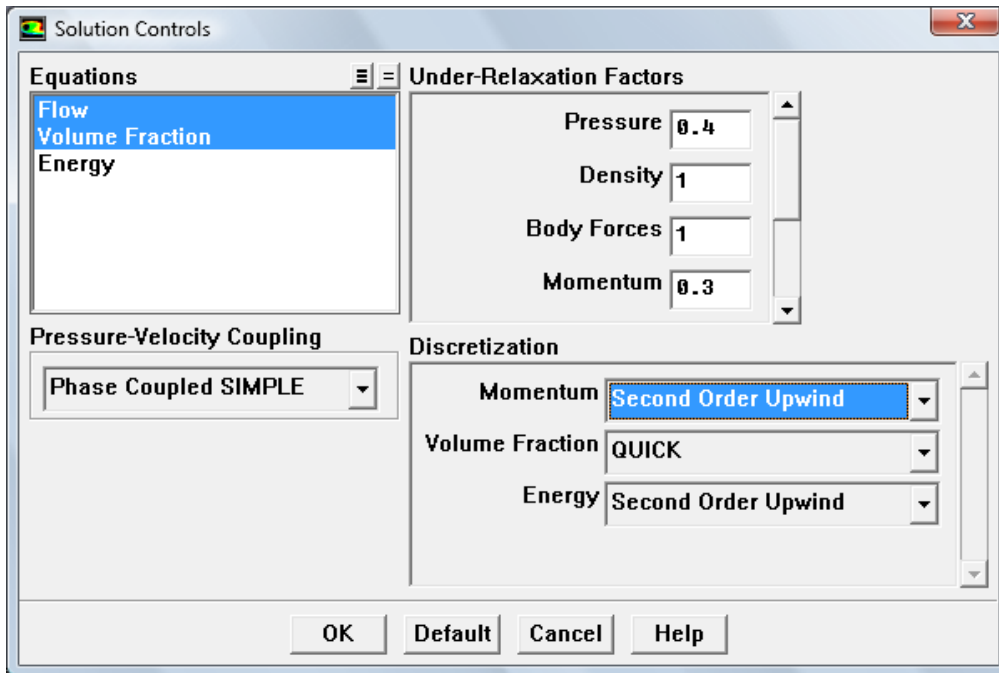
The **Surface** called 'bed' is a collection of cells within the domain (reactor) which represent the bed of particles. It is defined computationally as those cells in the domain with solid volume fraction% in the range of 1% to the maximum allowable value. The 1% limit was used instead of zero so that any dilute suspension above the bed (which usually has solids packing of 1% or less) would not be included in the bed. To create bed surface the following procedure is followed

Surface----Iso-clip----which opens the Iso-Clip panel where **Min** and **Max** inputs are the solids packing fraction limit of 0.01 and 0.55 (maximum solids packing allowed). **Clip** creates the **New Surface** bed from the cells of the default interior. Now bed appears under Surfaces in Define Surface Monitor panel.



STEP 9: SOLUTION CONTROLS

Solve----Controls----Solution----opens the Solution Controls Panel where the equations to be selected are solved. For **Discretization** the options available are First and Second Order Upwind, Power law, QUICK, and third-order MUSCL



Equations: Only the momentum and mass conservation equations are required to be solved for the isothermal case. Hence energy equation is not required for this problem. Isothermal assumption is justified for fluidization at ambient conditions where heat effects are small (Ye et al., 2005).

Under-relaxation factors are fractions by which the change in calculated variables are scaled before the next iteration. Under-relaxation factors therefore control the update of computed variables after each iteration, so that the solution progresses slowly. The calculations are therefore more stable and less likely to diverge because of sudden change in any variable.

Under-relaxation factors: We started the calculations cautiously with low under-relaxation factors (< 0.4) for the variables of pressure, momentum and volume fraction. Later under-relaxation factors were increased as convergence improved.

Discretization schemes are required to solve for the convection terms of each governing equation. Available options are First and second Order Upwind schemes, QUICK, Power law, and Third order MUSCL. When the flow is aligned with the grid (as with square and rectangular meshes) the first-order upwind discretization is acceptable. When the flow crosses the grid lines obliquely (as with triangular mesh) first-order scheme increases the numerical discretization error (numerical diffusion) and hence second-order scheme is required (FLUENT User's Guide 25.8.1). More advanced schemes are the QUICK and third-order MUSCL which may provide better accuracy than the second-order scheme for rotating or swirling flows. Power law scheme generally yields the same accuracy as the first-order scheme (FLUENT User's Guide 25.8.2).

Discretization: the more advanced QUICK scheme was used for volume fraction discretization since mass conservation affects all other equations. Second Order Upwind was deemed sufficient for all other equations. If convergence was difficult First Order Upwind scheme was used for all calculations to reduce calculations to some extent.

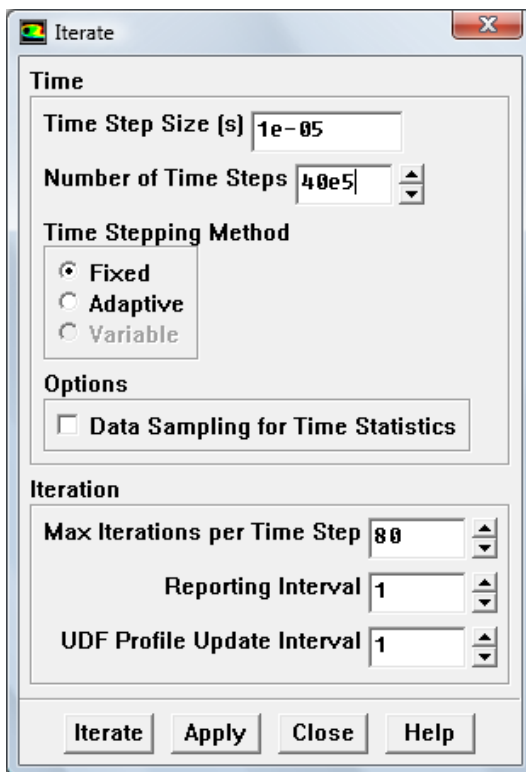
Pressure-based (segregated) solver is defined in step 2. Segregated solvers are of two types coupled and non-coupled algorithms. The non-coupled algorithm solves for velocity and pressure correction sequentially. SIMPLE is such an algorithm (FLUENT User's Guide 25.8.2).

Pressure-Velocity Coupling: The only available option is (pressure-based segregated algorithm) SIMPLE. It is called Phase-coupled SIMPLE because in Eulerian model a single pressure is shared by all phases.

STEP 10: ITERATE SOLUTION

→ **ITERATE**

Solve---Iterate ----opens the Iterate panel



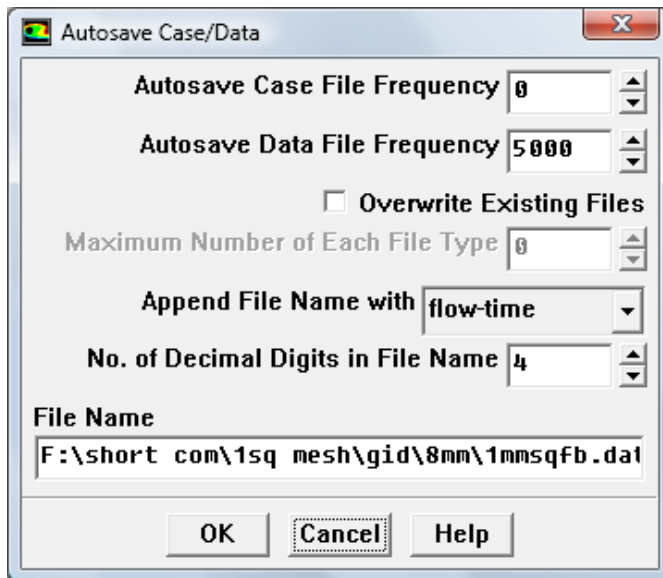
The Step Size required is closely related to the convergence behavior. When convergence behavior is 'good' the residuals do not vary much from iteration to iteration and are all lower than the limit prescribed (10^{-3}). In contrast if for one time step the residuals drop many orders of magnitude during the iterations within that time step, the convergence behavior is not good even if all residuals finally fall below the mandated limit. One way to alleviate poor convergence is to reduce time step. This reduces changes in the

calculated values and works analogous to the use of under-relaxation factors and increases solution stability. Solution is said to be stable when the monitors set do not vary by orders of magnitude but are near constant or have a definite trend.

From experience, we found that for that after one or two seconds of flow time a time step of 10^{-5} s always produced good convergence behavior. Initially, a time step as low as 10^{-8} s was required to start the calculations. This value was gradually raised as the convergence behavior improved. Hence all simulations were constantly monitored as flow-time progressed.

→ SAVE DATA

File----Write----Autosave opens the Autosave Case/Data panel which allows the saving of data files at any specified frequency of iterations or time steps. A data file contains all the calculated variables or fields for that time-step or iteration

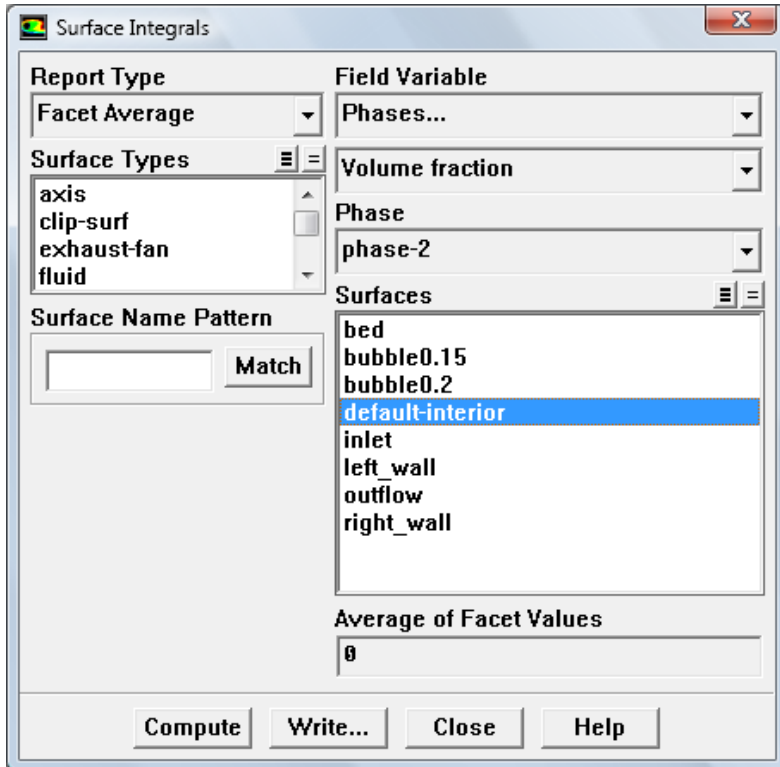


→ EXTRACT DATA FOR PLOTS

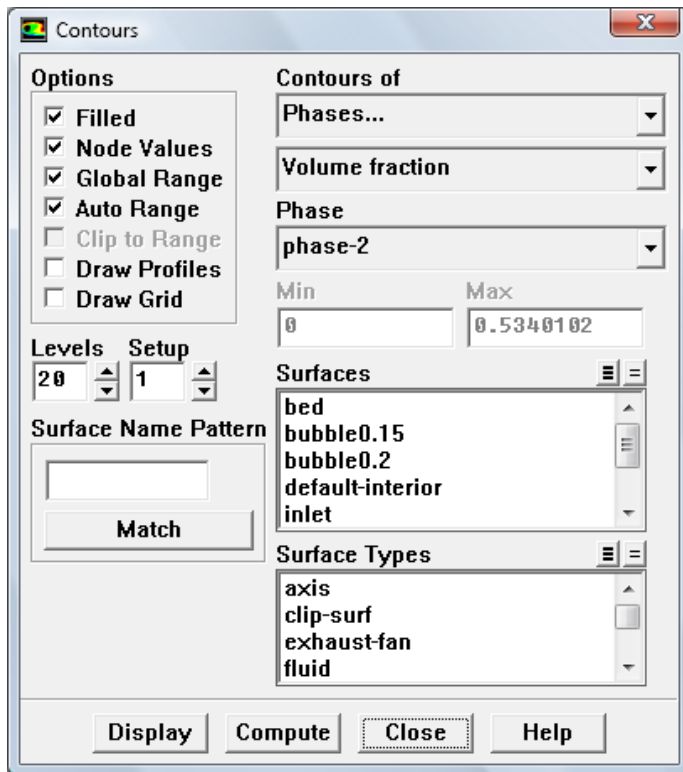
Plot tab in the FLUENT console allows for a variety of plots once the simulation is completed. We did not use this option however. We extracted all data required using

Report option and then made the plots in Origin software which afforded more control of plot details.

Report----Surface Integrals----opens the Surface Integrals panel where report or value of any variable from any data file can be calculated using **Compute** and is then displayed in the console



Display----contours----opens the Contours panel which allows the display of any field variables calculated at any time step or iteration. The required data file is read in and various contours obtained



→ **SIMULATION COMPLETE**

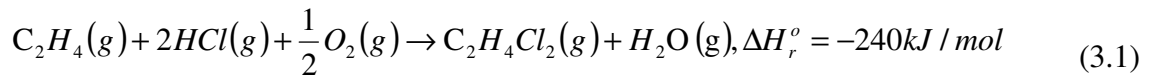
The Simulation trial was deemed completed when the monitored key variable (bed solids packing/ voidage) and therefore all other variables, reached pseudo-steady state. *This was usually reached within 5 s of flow-time, but we allowed the simulation to proceed for 20 to 40 s to be absolutely sure that pseudo-steady state was always reached.*

3.2 CFD procedure for simulation of reacting fluidized bed using Two-fluid model

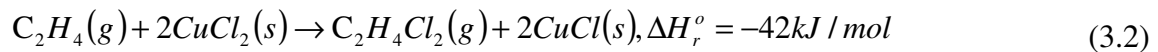
3.2.1 Heterogeneous oxychlorination of ethylene to Ethylene dichloride

3.2.1.1 Problem description

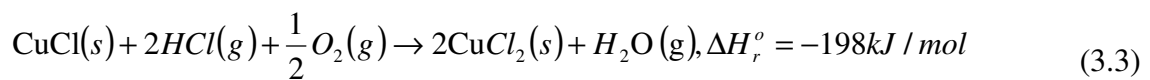
Ethylene dichloride (EDC) is a feed-stock for polyvinyl chloride which is one of the most mass produced thermo-plastics in chemical industries of the world. EDC is conventionally manufactured by the oxychlorination reaction of ethylene. The reaction takes place over copper dichloride catalyst and is carried out in fixed bed, and fluidized bed mode. The overall reaction is:



It was proposed (Go et al., 2010) to split this single reaction into two reactions, which occur sequentially, for the purpose of simpler separation of product gases downstream i.e. EDC would not have to be separated from unreacted oxygen and water vapour (see Eqs. 3.2 and 3.3). Also, since the EDC producing reaction would be less exothermic there would be less risk of sublimation of the catalyst over prolonged usage (see Eqs. 3.1 and 3.2). In the first reaction ethylene is chlorinated with copper dichloride catalyst to give EDC and reduced copper monochloride:



The copper monochloride is then re-oxidized to the original copper dichloride catalyst:



The kinetics of the reaction in Eq. 3.2 were reported (Wachi and Asai, 1994) to be of the Langmuir-Henshelwood type. The reaction was reportedly not limited by intraparticle diffusion.

$$r = \frac{k_r K_a [C_2H_4][CuCl_2]}{1 + K_a [C_2H_4]} \text{ mol / s.m}^3 \quad (3.4)$$

$$k_r = \left[269 \exp\left(\frac{-37.8}{RT}\right) \right] s^{-1}, K_a = 0.63 \text{ m}^3 / \text{mol} \quad (3.5)$$

The aim of the following procedure in FLUENT 6.3.26 is to simulate the lab-scale reacting (only Eq. 3.2) fluidized bed in homogeneous expansion regime, which was studied experimentally (Go et al., 2010). The kinetics mentioned in Eq.3.4 (Wachi and Asai, 1994) were implemented. The main system properties remain the same as given in Table 3.1 (except for the gas properties) which are described in step 4 on materials. A grid size of 1mm ×1 mm was used for this procedure. In addition, the system temperature was 523 K and pressure was atmospheric. The species properties at these operating conditions are defined in Table 3.5 and 3.6. Since the main steps of the simulation procedure overlap with those of the procedure in section 3.1.2, *only modifications* to procedure in section 3.1.2 (for non-reacting bed) will be outlined here. Table 3.4 summarizes these modifications.

3.2.1.2 Simulation procedure

In addition to the Preliminaries (1 to 2) mentioned just before procedure 3.1.2 the following are also applicable.

Preliminaries:

1. The kinetics (Wachi and Asai, 1994) given by Eq. 3.4 and 3.5 were coded in C++ (visual basic package) and saved as a .c file (APPENDIX – I and APPENDIX – II were both tested). This code is required to ‘hook-up’ to the FLUENT 6.3.26 case to incorporate the oxychlorination reaction.
2. It is ensured that the .c file is in the same directory as the FLUENT 6.3.26 case file.

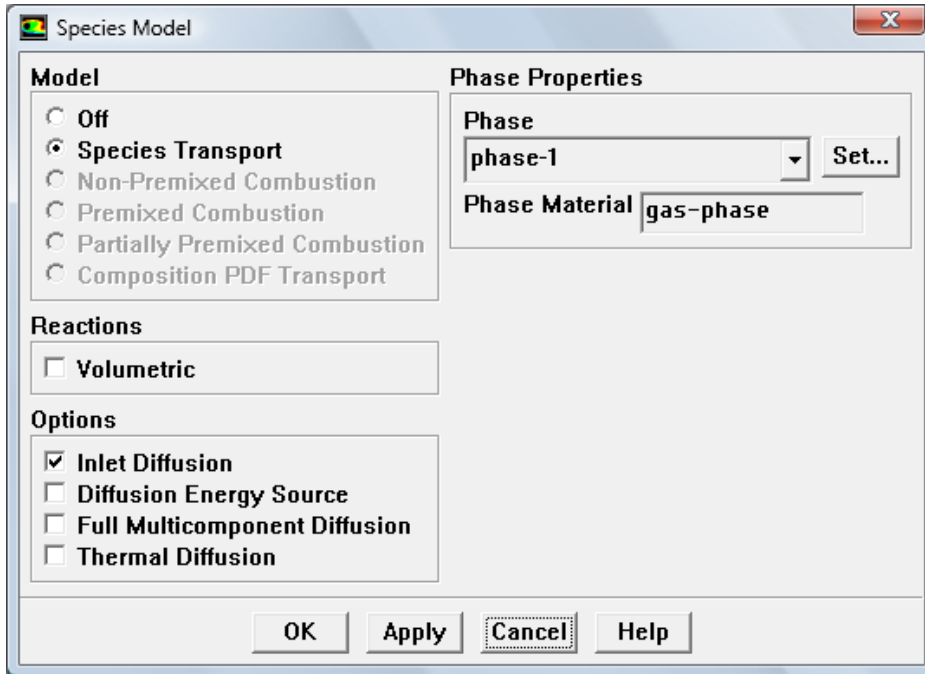
Table 3.4 Main steps of simulation procedure in FLUENT 6.3.26 for heterogeneous reacting bed

STEP1 to STEP 3	Same as in Procedure of section 3.1.2	
STEP 4	MATERIALS	Properties of all reactant and product species taking part in the oxychlorination reaction are defined. Two mixture materials called gas phase (all gaseous species) and solid phase (catalyst on alumina support) are created
STEP 4.1	USER DEFINED FUNCTION	A new step is incorporated which is not required in the procedure for non-reacting bed in 3.1.2. A UDF is built and loaded to simulate the heterogeneous reaction
STEP 5	PHASES	Under phase interaction stoichiometry of the heterogeneous reaction is defined and the rate function is <i>hooked in</i> from the UDF
STEP 6	OPERATION CONDITIONS	Same as in Procedure of section 3.1.2
STEP 7	BOUNDARY CONDITIONS	The species mass fractions entering from inlet are additionally defined
STEP 8	MONITORS	Additional monitor for species mass fraction (ethylene) at the outlet is set-up
STEP 9	SOLUTION CONTROLS	The species conservation equations are also solved
STEP 10	ITERARE SOLUTION	Additionally the data of mass fraction or mole fraction of each species on any domain surface can be extracted. Heterogeneous reaction rate data can also be extracted

STEP 3: MODELS

→ DEFINE SPECIES MODELS

Define---Models---Species---Transport & Reaction---opens the Species Model panel, choose options and **OK**, Phases are set later



Species transport: This enables the calculation of multi-species transport. The species conservation equations are now also included in the solver to predict the local mass fraction of each species, through the solution of a convection-diffusion equation for each species (FLUENT User's Guide 14.1.1).

Reactions: Volumetric reactions are those where all the reactants and products belong to a single mixture material and hence a single phase. Volumetric is not activated since we seek to model a heterogeneous reaction. This is done through a UDF as shown in steps 4.1 and 5.

Options (inlet diffusion only activated): species transport equations consists of both convection and diffusion components. The convection component is fixed by the inlet species mass fraction defined in step 7 on boundary conditions. The diffusion component is optional and we have enabled it at inlet. Full Multicomponent diffusion gives a detailed description of the species molecular transport processes in diffusion dominated flows. This was not deemed necessary for current case. Also thermal diffusion is not applicable for isothermal case.

STEP 4: MATERIALS

→ MIXTURE MATERIALS (GAS PHASE AND SOLID PHASE)

Define----Materials----opens the Materials panel where the fluid materials are created for all species in the case by defining their properties. The gas phase material properties are given in Table 3.5. For solid phase species only density is required as given in Table 3.6

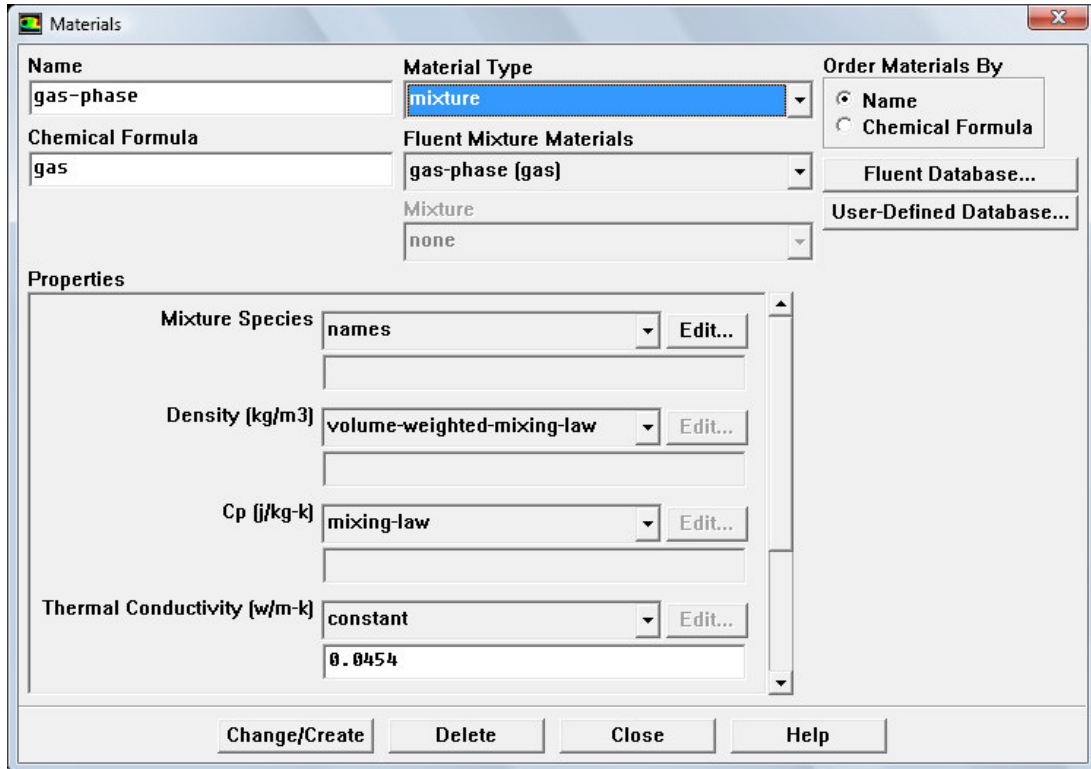
Table 3.5 Gas phase material properties

Gas-phase species	Density (kg/m ³)	Viscosity (kg/m.s) ×10 ⁵	Diffusivity (m ² /s) ×10 ⁵	Molecular weight (kg/kgmole)
C2H4	1.38 (Jahangiri et al., 1986)	1.03	3.4	28.050
C ₂ H ₄ Cl ₂ (EDC)	2.3 (ideal gas with Z correction)	1.72	2.2	98.960
N ₂ (bulk gas)	1.35 (STD Thermodynamic Tables)	1.663	3	28.013

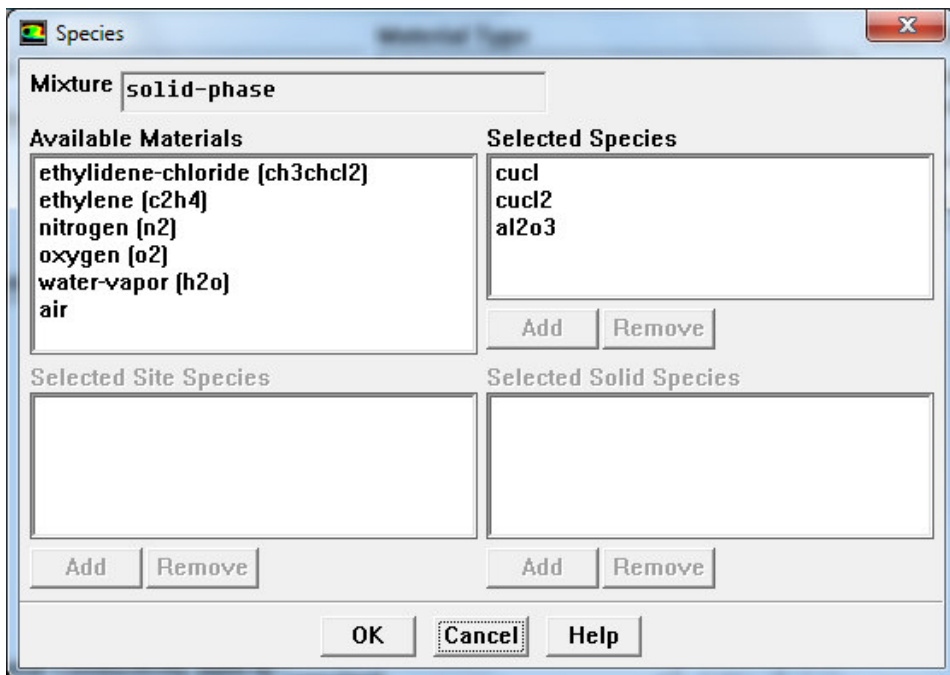
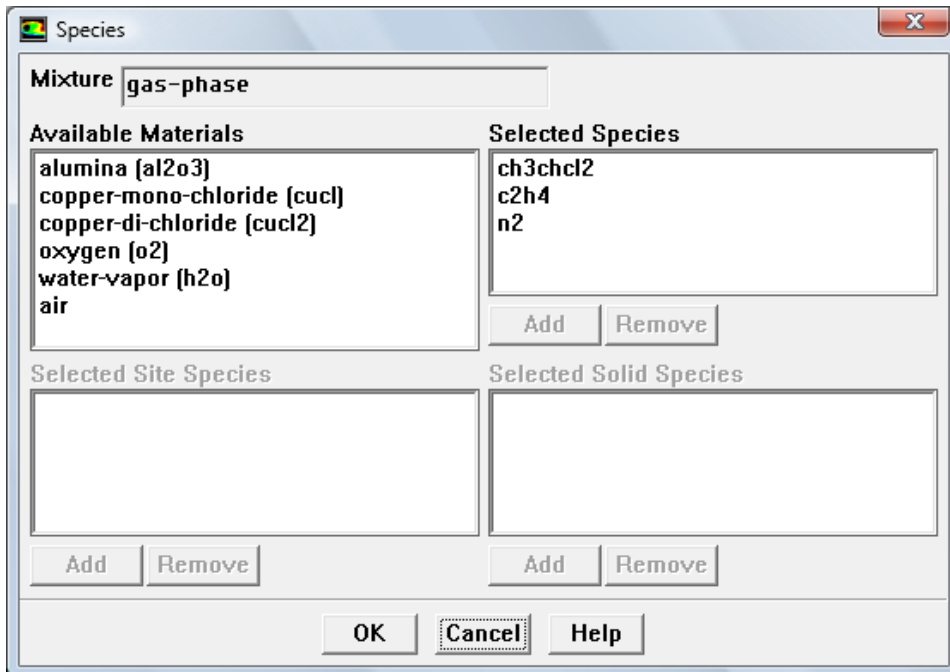
Table 3.6 Solid phase material properties

Solid-phase species	Density (kg/m ³)
CuCl	3530(Perry et al., 1999)
CuCl ₂ (2.14	3054(Perry et al., 1999)
Catalyst (4.12 wt % CuCl ₂ loading on Alumina support)	2000 (Go et al., 2010)

To create the mixture materials that represent the individual phases the **Material type** selected in Materials panel is mixture and the properties of the mixture are defined. The advantage of defining a mixture material which contains all the materials of that phase is that phase properties like density (listed in snapshot below) are then calculated by FLUENT, and separate UDFs are not required to define them.



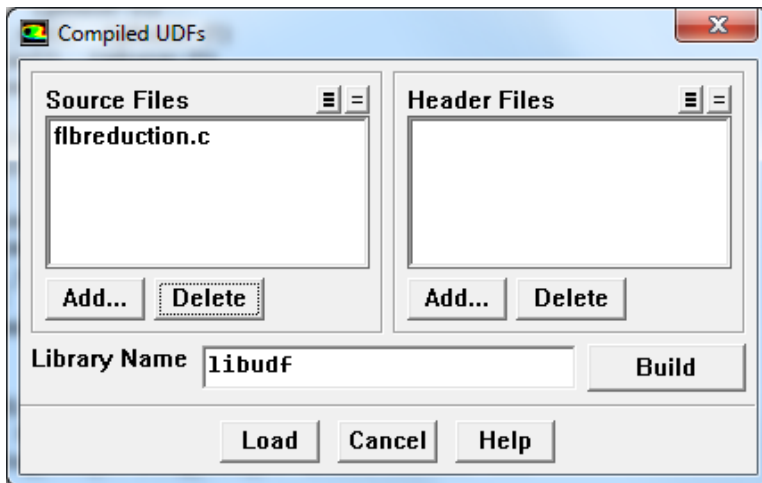
First the gas-phase mixture material is created. In Material panel the Mixture Species **Edit...** opens Species panel where the required species is selected from available materials previously created. The ordering of selected materials in the mixture species panel is important. The bulk material must always be put last to enable FLUENT to calculate its mass fraction in the phase with least error (FLUENT User's Guide 14.1.4). (The number associated with the each species in order is 0, 1, 2, 3 etc. is the species index: i , used to *call* the properties of a particular species in UDFs.) In a similar manner mixture material for the solid phase is created.



Now that materials are chosen, return to species model panel of **STEP 3** and **Set... phase-1 (gas phase)** as nitrogen and **phase-1 (solid phase)** as Alumina.

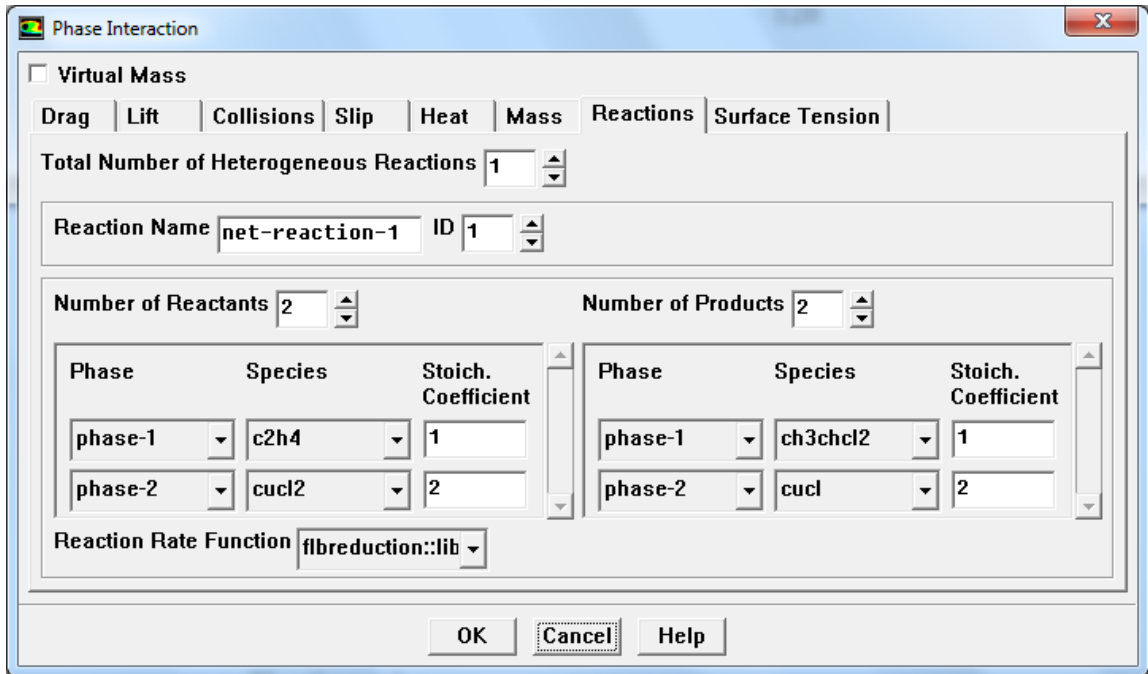
STEP 4.1: USER DEFINED FUNCTION

Define---User-defined---Functions---Compiled...-----opens the Compiled UDFs panel where the UDF or Source File called `flbreduction.c` is Added, Built and Loaded. It will later be *hooked up* in the Phase interaction panel so that it becomes part of the FLUENT code architecture. The UDF is used to calculate the rate of reduction of copper dichloride by ethylene, see Eqs 3.2 and 3.4.



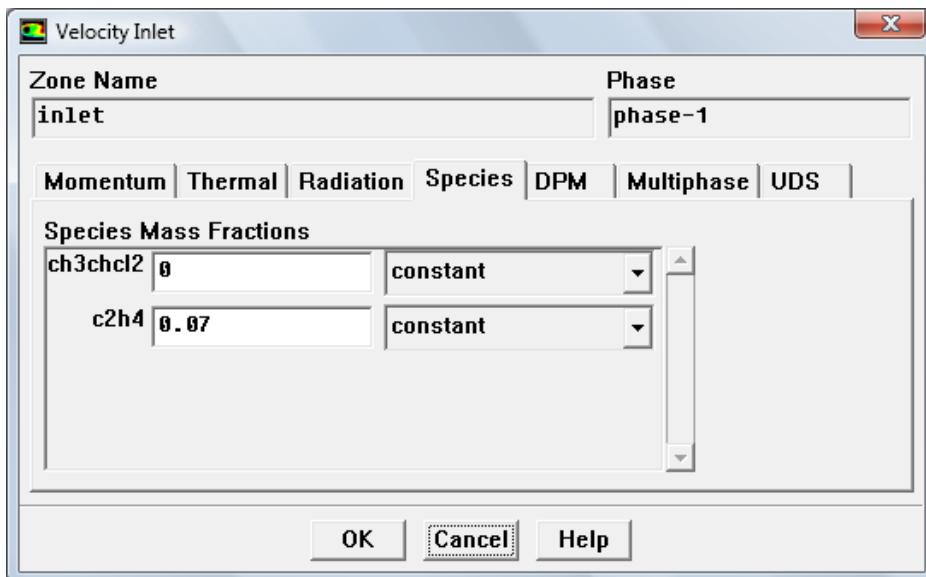
STEP 5: PHASES

Define---Phases---Interaction...opens the Phase Interaction panel where additionally reaction is defined. The reaction rate function contains the UDF that was compiled. The UDF is selected so that it is now hooked-up to the case.



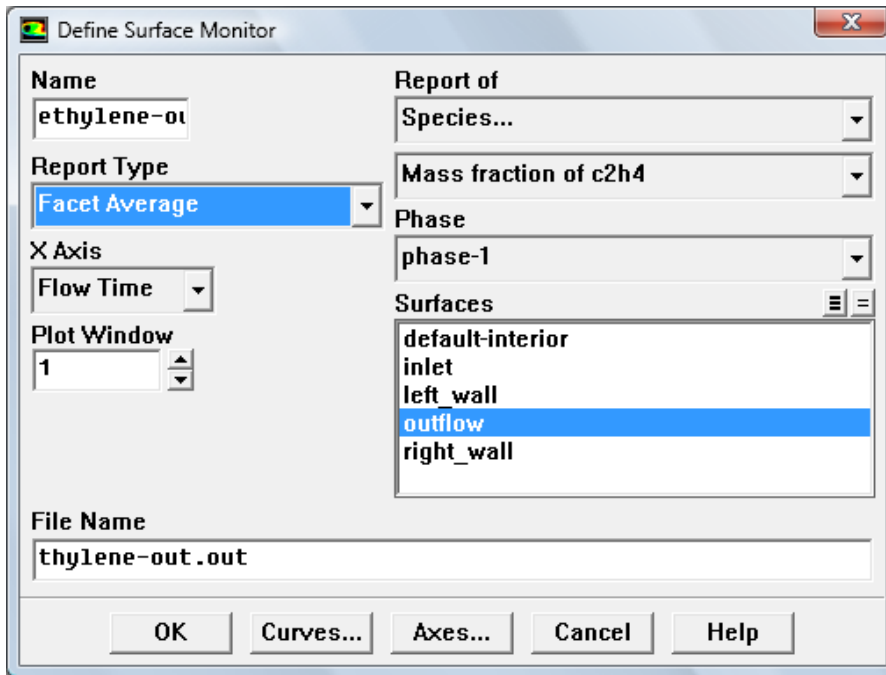
STEP 7: BOUNDARY CONDITIONS

The only additional boundary condition needed is for **phase-1** at inlet boundary. The ethylene mass fraction value to be tested (7%, 30%, 75% etc.) is defined. Since EDC is a product and does not enter with the feed, its mass fraction is zero. Nitrogen, the bulk or carrier gas is calculated by FLUENT from mass conservation and is not required to be set.



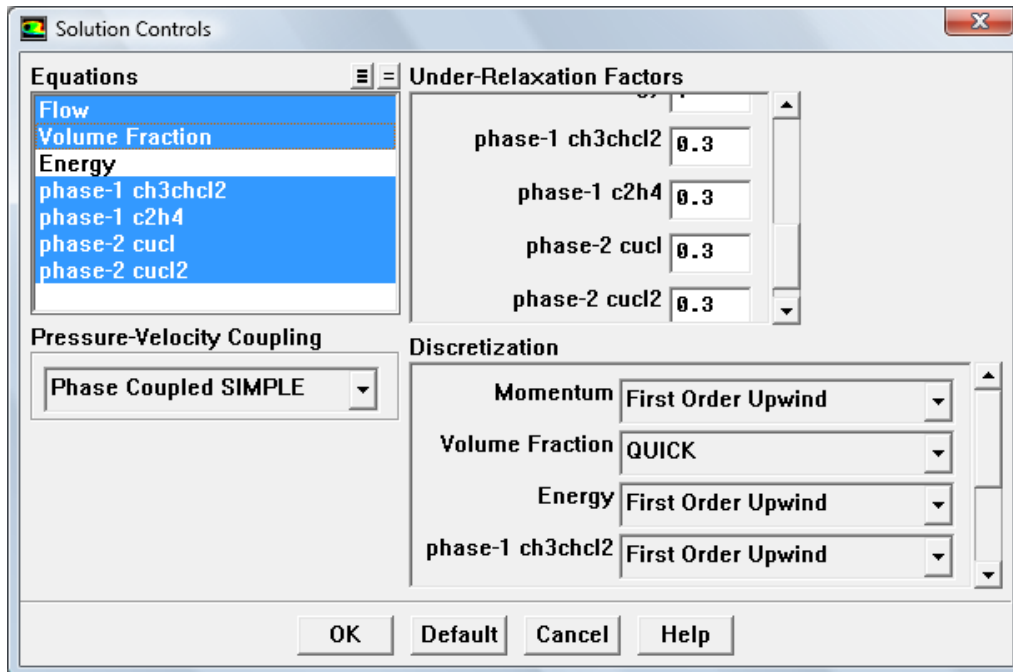
STEP 8: MONITORS

Monitors can now be set for all species. Since these materials have been created they appear in the lists. Below the monitor for average ethylene mass fraction at the outflow boundary is set



STEP 9: SOLUTION CONTROLS

The additional species equations are selected to be solved apart from mass and momentum conservation.



STEP 10: ITERATE SOLUTION

→ EXTRACT DATA FOR PLOTS

Additionally all species mass or mole fractions can be displayed as contours. Average values can be extracted to create various plots from any saved data file. The heterogeneous reaction rate data calculated from the UDF can also be extracted.

→ ACHIEVE CONVERGENCE

Achieving convergence for the reacting bed was very challenging. This was because the problem was inherently unsteady as described in the next step. As a consequence only very small time step (10^{-9} s to 10^{-11} s) allowed the simulation to converge. This means that although the case was error free and running and that the solution could theoretically be obtained given sufficiently long times, practically it was nearly impossible to achieve with the available CPU resources. Hence the pseudo-heterogeneous and steady state reaction was tested as described in section 3.2.2.

→ SIMULATION COMPLETE

It was observed that this case was inherently unstable as demonstrated by the residuals obtained. The resulting poor convergence mandated the use of very small time steps. At first it was thought that the instability emanated from the constraint that the species equations imposed on the solution. Since the reacting species belonged to both phases, the conservation equation for both phases experienced changes during the course of a single iteration and also needed to be satisfied before the next iteration. To cut down at least one constraint i. e. solid phase species balance equation, a single phase reaction was tested. The catalyst species (CuCl_2) was assigned to gas-phase and only alumina remained in the solid phase. This way, the species changes would be confined to one phase only. Of course, corrections had to be made in the UDF for reaction rate (Appendix II) to calculate the species concentrations with respect to their own respective phase. The addition of the catalyst reacting species to the gas phase reduces physical meaning of the simulation, but it was tested nonetheless. However, the instability persisted, and we inferred that the root cause is not just that the reaction is heterogeneous, but that it is unsteady. This case problem is inherently unstable because of the perpetual reduction of catalyst which is not instantaneously regenerated. Hence there is no steady state solution for the simulation to head towards. Since all species are changing at each time step, and never reach steady state the time step required for convergence was unrealistically low (10^{-9} s to 10^{-11} s). The simulation was verified as working by checking the loss and production of species and by checking that the reaction rate has a finite value. This simulation is still useful for future study if the time step can be increase to at least 10^{-7} s.

3.2.2 Pseudo-heterogeneous gas phase oxychlorination of ethylene to ethylene dichloride

3.2.2.1 Problem description

The reduction and regeneration reaction can be accomplished in a single step when oxygen and hydrochloric gases are fed to the reactor along with Ethylene. Using Copper dichloride as catalyst, the overall reaction (3.1) does not include the solid species because the copper monochloride is regenerated to the original copper dichloride due to the presence of oxygen and hydrogen chloride gases. The single stage oxychlorination reaction kinetics was studied in detail in the literature (Carrubba and Spencer, 1970) and the rate data at isothermal conditions of 457K (184°C) and atmospheric pressure fitted a power series correlation as follows:

$$r = 2.49e - 3 [C_2H_4]^{0.73} [O_2]^{0.34} [H_2O]^{-0.18}, mol / s.m^3 \quad (3.7)$$

We noted that this power law rate expression requires the concentration terms to be in partial pressure (mm Hg) of the respective species. The overall reaction does not contain any species belonging to the solid phase but still represents the rate data in presence of catalyst. From a computational point of view this reaction occurs purely in the gas phase, since solid phase species does not figure in the rate expression. The ‘Volumetric’ reaction option (where all species belong to one phase) in FLUENT was used. In the previous case we used the heterogeneous reaction option which is valid when reaction species belong to different phases. Since from a computational view point solid species calculations do not occur in the simulation this case was called the *pseudo-heterogeneous* oxychlorination of ethylene when actually the reaction rate takes into account the effect of the catalyst. The

participation of the solid phase in the reaction is computationally translated to the simulation by multiplying the reaction rate by the solid volume fraction in each cell. This ensures that the reaction does not take place in the gas phase devoid of solids but only where solids are present. The reaction rate is therefore scaled to the quantity of solid present. If this scaling factor were not included the reaction could occur even in the pure gas phase above the bed, which of course does not happen in the real reactor. Hence the modified rate expression to be incorporated as a UDF (Appendix III) is:

$$r = (1 - \varepsilon) \times (2.49e - 3 [C_2H_4]^{0.73} [O_2]^{0.34} [H_2O]^{-0.18}, mol / s.m^3) \quad (3.8)$$

Accordingly the UDF was coded to represent the volumetric reaction. It was then suitably hooked up to the case. We note that this reacting system simulation case is capable of reaching steady state since the catalyst is continuously and instantaneously regenerated. If the input variables like feed rate are steady state, then the reaction rate data ensures an eventual steady state. This was not the so in the previous case of Heterogeneous reaction where steady state was never reached due to continuous reduction of catalyst at every time step without simultaneous regeneration.

The major system properties are given in Table 3.7. The main steps of the simulation procedure for the system described are given below. **Only modifications** to the procedure in section 3.2.2 are described here. The rest of the steps remain the same as in 3.2.2. A summary of the modifications are presented in Table 3.8.

Table 3.7 System parameters (Carrubba and Spencer, 1970) simulated

Parameter	Simulation input
-----------	------------------

Domain size (cm)	38.1×1.905
Particle diameter (mm) for fixed bed reaction	3.175 (Geldart D)
Particle density (kg/m ³)	3800
Initial packed bed solid volume fraction	0.55
Isotherm maintained (K / °C)	457 / 184

3.2.2.2. Simulation procedure

In addition to the Preliminaries (1 to 2) mentioned just before procedure 3.1.2 the following are also applicable.

Preliminaries:

1. The kinetics (Carrubba and Spencer, 1970) given by Eq. 3.7 are coded in C++ visual basic and saved as a .c file (Appendix III). This code is *hooked-up* to the FLUENT 6.3.26 case to incorporate the homogeneous oxychlorination reaction in the simulation.
2. It is ensured that the .c file is in the same directory as the FLUENT 6.3.26 case file.

Table 3.8 Main steps of simulation procedure in FLUENT 6.3.26 for pseudo-heterogeneous reacting bed

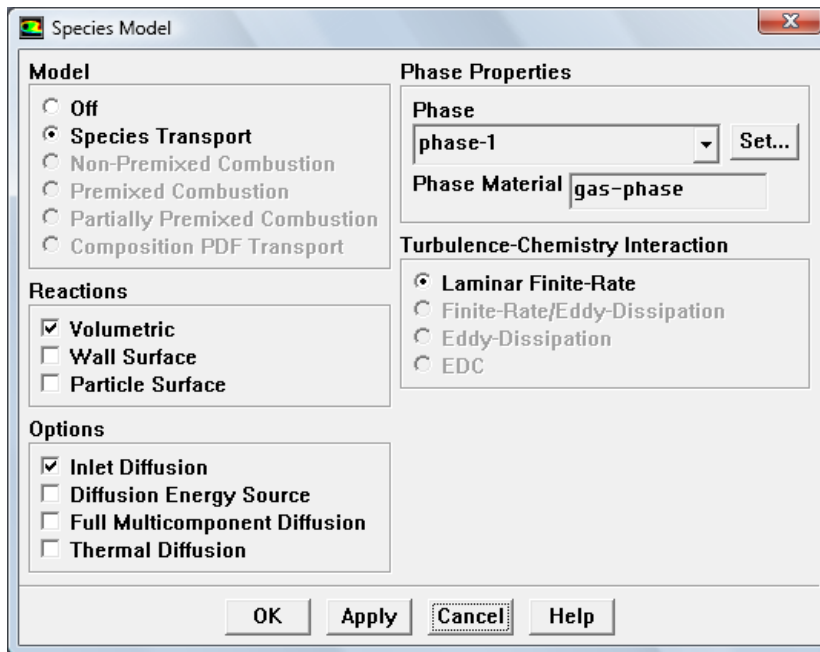
STEP1 to STEP 3	Same as in Procedure 3.1.2 except in STEP 3 while describing the models, Volumetric is activated under reactions. This action automatically activates Reaction panel in the Materials panel	
STEP 4	MATERIALS	All properties of reactant and product species taking part in the oxychlorination reaction are defined at 457K isotherm. Two mixture materials called gas phase (all gaseous species) and solid phase (catalyst on alumina support) are created
STEP 4.1	USER DEFINED	A UDF is built and loaded to simulate the homogeneous gas phase overall reaction in bed

	FUNCTION	
STEP 5 to STEP 6	Same as in Procedure of section 3.1.2	
STEP 7 to STEP 9	Same as in Procedure of section 3.1.2 except that the boundary condition values given in step 7 were different	
STEP 10	ITERARE SOLUTION	Additionally the data of mass fraction or mole fraction of each species on any domain surface can be extracted. Heterogeneous reaction rate data can also be extracted

STEP 3: MODELS

The only addition needed to procedure 3.2.1 in this step is to activate volumetric in species model panel. This automatically makes **Reaction** panel appear in Materials panel.

Reaction panel is addressed in the next step



STEP 4: MATERIALS

All material properties are defined at the system isotherm of 457K and atmospheric pressure. The species properties are given in Table 3.9 and Table 3.10.

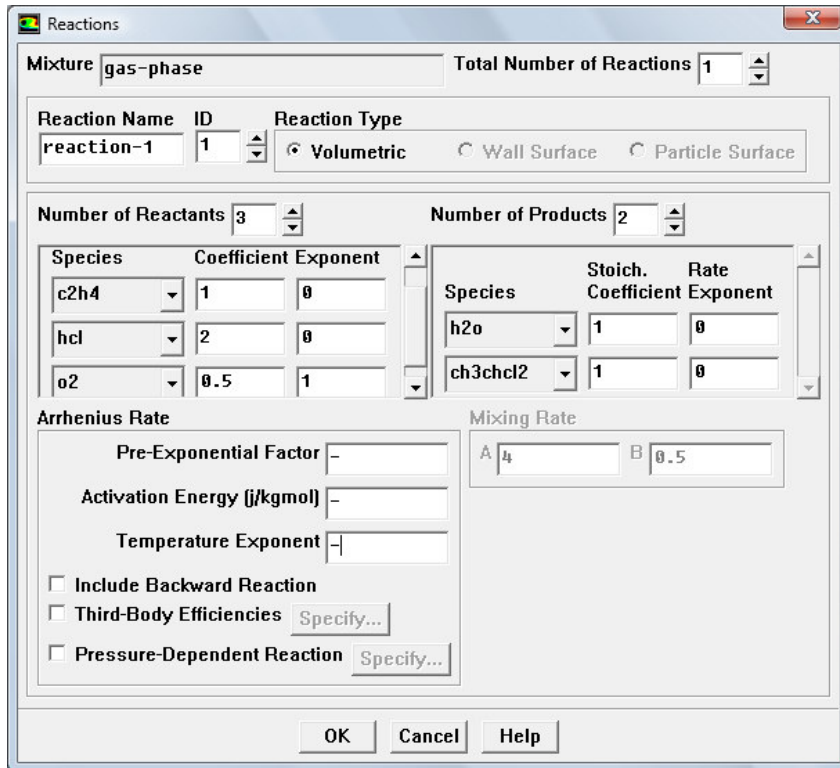
Table 3.9 Gas phase material properties

Gas-phase species	Density (kg/m ³)	Viscosity (kg/m.s) ×10 ⁵	Diffusivity (m ² /s) ×10 ⁵ (Carrubba, 1968)	Molecular weight (kg/kgmole)
HCl	0.9743 (ideal gas with Z correction)	1.72	3	36.461
C ₂ H ₄	0.761 (Jahangiri et al., 1986)	1.03	3.4	28.050
O ₂	0.54 (Stewart et al., 1991)	1.919	3	31.998
C ₂ H ₄ Cl ₂ (EDC)	2.7 (ideal gas with Z correction)	1.72	2.2	98.960
H ₂ O	0.4779 (STD Thermodynamic Tables)	1.34	3.6	18.015
N ₂ (bulk gas)	1.8776 (ideal gas with Z correction)	1.663	3	28.013

Table 3.10 Solid phase material property (only density is required)

Solid-phase species	Density (kg/m ³)
Harshaw Catalyst 10% CuCl ₂ / active alumina	3800 (Carrubba, 1968)

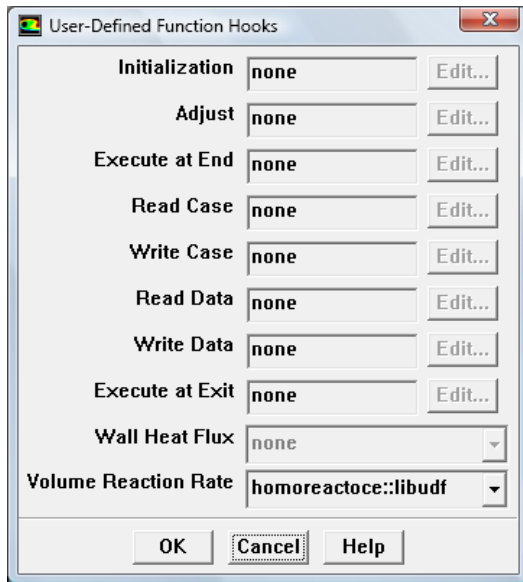
Mixture materials called gas phase and solid phase are created as described in the procedure of section 3.2.2. In the Materials panel showing gas-phase mixture material, the Reaction **Edit...** Opens the Reactions panel where the volumetric gas phase reaction is defined.



STEP 4.1: USER DEFINED FUNCTION

The volumetric (homogeneous) reaction rate as described by Eq. is coded (Appendix III) and compiled as a UDF in a manner similar to the procedure of section 3.2.2. To hook this UDF to the FLUENT case:

Define----User-Defined----Function Hooks...----opens the User-Defined Function Hooks panel where the compiled UDF which appears as an option under Volumetric Reaction Rate, is selected



STEP 7: BOUNDARY CONDITIONS

This simulation case was run initially keeping all conditions identical to the fixed bed system of Carrubba and Spencer (1970). The boundary conditions were set according to the simulation runs shown in Table 3.11. In the second case the same system was simulated but replacing the fixed bed with Geldart A particles. Velocity was kept the same as fixed bed case which fluidized the Geldart A particles in bubbling regime. In the third case the velocity was reduced to the range 6-12mm/s so that the Geldart A particles were fluidized in homogeneous regime. The three cases are compared and discussed in Chapter 4.

Table 3.11 Simulated feed conditions for inlet boundary (Carrubba and Spencer, 1970)

Gas-phase species	Feed mass fractions (Set-1: Ethylene rich)	Feed mass fractions (Set-2: Ethylene lean)	Inlet velocity (mm/s)
	For case I (Fixed bed), case II (Fluidized bubbling)		

	and case III (Fluidized homogeneous expansion)		
HCl	0.2774	0.2774	For case I and II:
C ₂ H ₄	0.1964	0.1122	159, 91, 58, 45
O ₂	0.0765	0.0765	For case III: 6, 8,
N ₂ (bulk gas)	0.4495	0.5339	10, 12

→ **ACHIEVE CONVERGENCE**

Achieving convergence for the reacting bed even with pseudo-heterogeneous reaction was challenging. This is because of the strong coupling between the mass and momentum balances and the species transport equations. A variety of strategies were employed to ensure a converged and steady state solution. A very small time step (10^{-7} s to 10^{-6} s) was used. Another strategy which proved beneficial was to turn on the volumetric reaction only once the inert bed reached a steady state i.e. mass and momentum balances had converged.

→ **SIMULATION COMPLETE**

This case problem is steady state and was deemed complete when the main species monitors or conversion rate became nearly constant with flow time.

3.3 Overcoming errors encountered with FLUENT 6.3.26 solver

The following are the main errors encountered during the process of simulation. These were overcome by a combination of experience and suggestions from technical help of

ANSYS FLUENT. The ability to overcome errors in a current simulation case rather than abandoning the case to start over increased our confidence in the solver.

i. Divergence in solver

FLUENT 6.3.26 is a stable solver. This means that if there are no sudden changes in the inputs, the simulation does not give any sudden changes in output and therefore divergence cannot easily occur. Divergence is judged by the magnitude and direction or trend of the residuals. If the residuals rise say, 4 to 5 orders of magnitude and cannot be brought down in subsequent iterations the solver diverges. FLUENT 3.6.26 usually gives 'Divergence in solver error' within the first 100 iterations of the simulation. If convergence can be achieved within the first 100 iterations and improved in the next 1000 iterations then divergence has been overcome. Divergence might mean that the problem is 'ill posed' and all inputs and models need to be rechecked. If the problem is 'well posed' it might simply mean that the time step is too large to calculate initial solution. Time steps as low as 10^{-11} s to 10^{-8} s was found to enable convergence. These time steps were later increased as convergence improved.

ii. Floating point error

This error usually occurs in the very first iteration. It happens because of a division by zero occurring somewhere in the sequence of solver calculations leading to an infinity value which cannot be handled by the solver. The infinity value occurs because many of the initial values given to start the problem are zero. An innovative way to overcome this error is to give a non-zero low value for the initial values instead of zero like 10^{-7} s to 10^{-

¹¹s. These values are so close to zero that they have a negligible effect on the solution and help the solver to initialize calculations without ‘Floating point error’.

iii. *‘nmake’ error*

This error occurs while attempting to compile a UDF. The UDF does not compile because of software inability to invoke the C++ compiler which should be installed on the system. The difficulty to invoke has to do with incompatibility between the Operating System and the version of C++ compiler installed. It was found that the C++ compiler (visual basic 6.0) compatible with FLUENT 3.6.26 was compatible with Windows XP and Vista but not Windows 7. Hence proper choice of compiler and Operating System alone can remove this error.

iii. *UDF not loaded error*

This error also occurs while attempting to compile a UDF. If the C++ compiler is correctly invoked, it compiles the .c file (UFD) provided. If there are any errors (syntax or logical) in the coding, then these errors will be displayed in the FLUENT console. These errors prevent the UDF from loading. Hence debugging the code and recompiling is the only way to remove this error.

iv. *‘not a pair’ error*

This error occurs because the monitor plotting is not correctly enabled. The variable to be plotted (Y-axis) and the choice of X-axis (time step, iteration or flow time) must be correctly defined to make this error go away.

v. *Fatal error*

This error occurs immediately after instructions are given by the user during monitoring of the simulation. Either the instructions were given so close in time that they appear to the solver to be required to be carried out instantaneously, or they are contradicting instructions. Either way, the error is overcome by reading afresh the data file and restarting iterations. If the simulation still does not proceed, the case file is also read afresh and the entire simulation restarted.

We were able to successfully overcome all the errors that occurred during the course of setting up simulations or post-processing. In case of unexpected shut-downs the simulations had to be restarted with the most recent data file saved. The precaution to save solver calculations in data files at frequent intervals proved very beneficial.

CHAPTER – 4

RESULTS AND DISCUSSION

In this chapter the CFD simulation results obtained using the TFM described in section 2.2.2.2 (Tables 2.3, 2.5 and 2.6) are presented. The TFM was implemented in FLUENT 6.3.26 solver as described in chapter 3, and summary of the simulation procedures are provided in Table 3.2, 3.4 and 3.8. The results and discussions in this chapter are presented under three headings (sections 4.1 to 4.3) in the context of fluidization of Geldart A particles. Section 4.1 presents a mesh study on homogeneous expansion and transition to bubbling. Section 4.2 presents a detailed fine mesh study on homogeneous expansion and transition to bubbling, with validation of simulation results. In section 4.3 the fluidized bed with reaction is simulated. The reaction considered was oxychlorination of ethylene to give ethylene di-chloride.

4.1 Mesh size study on gas-fluidization of Geldart A particles: Homogeneous expansion and transition to bubbling

The general consensus in the literature is that mesh sizes of the order of mm are acceptable for study of flow behavior of fluidization of Geldart A particles (Table 2.9). The size of the system and the flow regime also needs to be taken into consideration. Surveying the mesh sizes used in literature for dense particle flows, we either have very fine meshes advocated, of the order of 2-4 particle diameters i. e. 0.2mm × 0.2mm and 0.4mm × 0.4mm (Wang et al., 2009, 2010a) or commonly used sizes of the order of 4mm × 4mm (van Wachem and Sasic, 2008) and 5mm × 5mm (Mazzei and Lettieri, 2008;

McKeen and Pugsley, 2003; Ye et al., 2008) which we shall call coarse meshes. The commonly used coarse meshes are ten times or more the size of the fine meshes! Possible mesh size values in between have been largely unexplored as attested by Table 2.9 of section 2.2.2.2.1. It is important to test these mesh sizes for possible improvement in predictive capability of TFM (Wang et al., 2009, 2010a, 2011). As yet there has not been any systematic study on the effect of mesh size on TFM especially in context of homogeneous expansion and transition to bubbling, and specifically using a domain of lab-scale dimensions.

Refining the CFD mesh has the physical significance of resolving more and more details of the flow. This was shown by Igci et al. (2008) for riser flows which belong to turbulent régime. It was demonstrated that finer and smaller streamers and clusters were resolved on mesh refinement. These had an impact on the constitutive laws. Hence we adopt the process of mesh refinement as a research methodology to discover differences in flow details as the mesh is progressively reduced in size. Hence our aim in this section was to study the effect of mesh refinement while simulating homogeneous expansion regime and minimum bubbling velocity.

4.1.1 Mesh size study on homogeneous expansion

The following results emphasize transient profiles and select snapshots of gas volume fraction in the bed. We shall henceforth refer to the average bed gas volume fraction as simply ‘bed voidage’. To compute the same it was mandatory to computationally designate which cells belonged to the bed region. To discount the very dilute suspension in the freeboard, only cells with solid volume fraction (ϵ_s) greater than 0.01 were

designated as belonging to the bed. The following preliminaries include a more detailed discussion of the same.

i. Computational definition of bed

The bed voidage at any instant of time in the transient simulation is the averaged gas volume fraction values of all the cells which comprise the fluidized bed. To calculate this average bed voidage it is mandatory to computationally define which cells belong to the bed region. At gas-solid interface in a real fluidized bed, solids concentration decreases very rapidly with elevation to exceedingly low levels (Johnson and Jackson, 1987). We found this to be the case even in our simulations. With time an exponential solids concentration drop was observed at the bed interface. Moreover, if a very dilute suspension occupies the freeboard, it would be inappropriate to designate *all* cells with non-zero solid volume fraction as belonging to the bed. Hence, a solid volume fraction of 0.01 was chosen as threshold value, to distinguish the bed from any dilute suspension. The bed region therefore comprises all cells with solid volume of 1% or greater, and the voidage values of *only* these cells were averaged to give instantaneous bed voidage. An issue with this definition might arise in the event of formation of purely gas-phase bubble regions (cells with solid volume < 1%) which would incorrectly be excluded from the averaging to get bed voidage, even though they belong to bed. Such a case did not arise in any of our simulations as virtually *no* cells, within the bubble regions had less than 1% solid volume.

ii. Computational distinction between uniform and dilute regions

In the following discussions (sections 4.1 and 4.2) the distinction between ‘uniform’ and ‘dilute’ regions plays an important role. Uniform regions refer to those spaces in the bed

where the particles are more or less uniformly distributed in the gas phase to give a homogeneously expanded state of bed. Early researches believed this to be most representative of the bed structure (D'Amore et al., 1979; Donsi et al., 1975; Massimilla et al., 1972) hence the name 'homogeneous expansion'. Our CFD simulations however presented a more complex picture with the interplay of dilute regions, which can also be described as turbulent regions or slow instabilities. In CFD simulations the demarcation between solid volume fraction contours or solids packing contours is limited by the gradation of the concentration scale. The scale cannot be truly continuous but rather it is discrete. We therefore need a formalization to define a uniform region as distinct from other regions of the bed. In the absence of any literature, we defined uniform regions where solid packing differences were equal to or below either 1% or 4% (depending on the concentration scale chosen for a particular Figure). Depending on this threshold, the solid packing differences equal to or below either 1% or 4% appear uniform (same shade) in the simulations. From literature (Yates et al., 1994), bubbles were defined as having less than 20% solids packing and appear pure white in the simulations. Similarly, the regions near packed bed state (within 1% or 4% solids packing) appeared pure black. This left the remaining shades of grey to represent dilute or turbulent regions. Fig. 4.1 illustrates these distinctions for a concentration scale with 4% solids packing gradation.

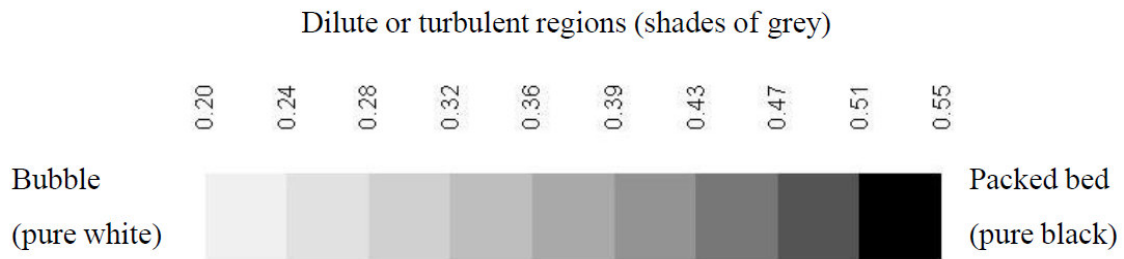


Fig. 4.1 Sample concentration scale with solids packing gradation of 4%.

iii. Mesh dimensions

To simulate realistic fluidization characteristics and rule out any effect of domain size, a typical lab scale size domain of 4cm diameter and 1m length was used. For fixed domain, as simulation resolution is inversely proportionate to cell area, we determined our mesh sizes from a sequence of cell areas in which each consecutive member has half the value of the previous. The first member chosen was 16mm^2 ($4\text{mm} \times 4\text{mm}$ mesh size), because it has been most commonly used in simulation studies of Geldart A/B particles (Wang et al., 2011). Applying the given rule, the remaining sequence is: 8mm^2 ($2.828\text{mm} \times 2.828\text{mm}$), 4mm^2 ($2\text{mm} \times 2\text{mm}$), 2mm^2 ($1.414\text{mm} \times 1.414\text{mm}$), 1mm^2 ($1\text{mm} \times 1\text{mm}$). These meshes will hence forth be identified to by their area (e.g. mesh size of $4\text{mm} \times 4\text{mm}$ will be called 16mm^2 mesh). Only the 8mm^2 mesh was not used in the study as we judged it redundant.

4.1.1.1 Transient voidage profiles in homogeneous expansion régime

For the various coarse mesh sizes, Fig. 4.2(a-d) illustrates transient bed voidage profiles for velocities in the range of 4-12mm/s. for our system this velocity range is of interest, as 8mm/s is the mean value of the range and also the approximate minimum bubbling velocity ($u_{mb,e}$) calculated from empirical correlation of Abrahamsen and Geldart (1980) given in Eq 1.2 (introduction chapter). Also, from the same work, 4mm/s is the approximate minimum fluidization velocity for our system. Hence, experimentally, the velocity range of 4-7mm/s covers the homogeneous expansion regime and 8-12mm/s covers the transition to bubbling.

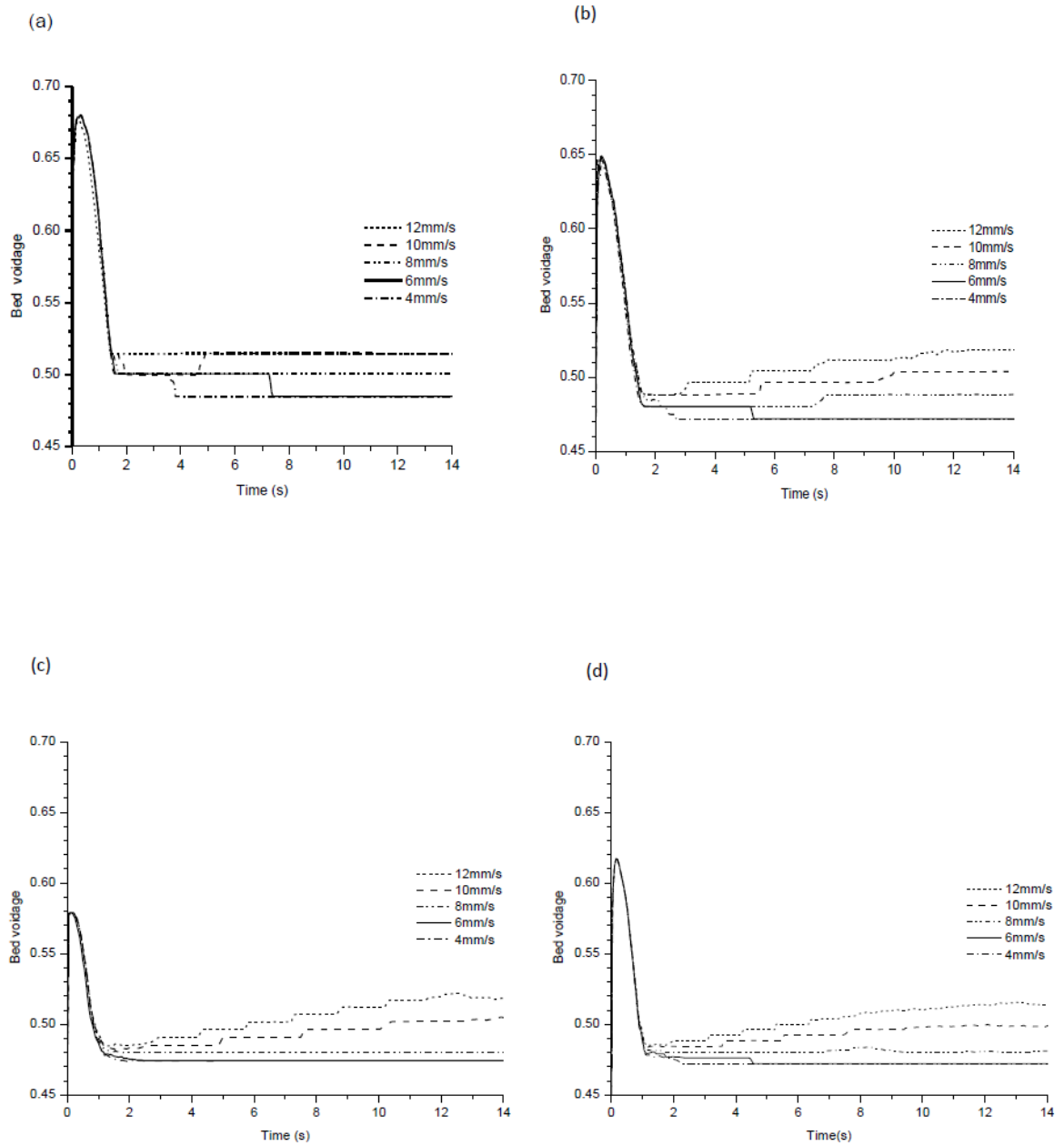


Fig. 4.2 Transient bed voidage profiles for velocities in range 4-12mm/s (experimental velocity range for homogeneous expansion and transition to bubbling) for different mesh sizes using Gidaspow drag law. (a) 16mm² mesh; (b) 4mm² mesh; (c) 2mm² mesh; (d) 1mm² mesh.

i. Transient profiles for 4-7mm/s inlet velocity

Due to shock to the bed at start-up (Jung et al., 2006) all the bed voidage profiles show a qualitatively similar initial 'jump' in the first 0.2s (Fig. 4.2(a-d)). During 0.2-1.5s the previously thrown up particle suspension is seen to settle and simultaneously the previously formed dilute regions are seen to rise up (Fig. 4.3(a)). Note that for Fig. 4.3(a), the voidage range on the grey scale was chosen so as to reveal the dilute suspension in freeboard and dilute regions in bed. The fate of these dilute regions or perturbations is an indicator of the predictive capability of the TFM. For Geldart A particles in homogeneous expansion regime, any finite perturbations, such as the one induced on start up because of velocity inlet boundary condition, must eventually disappear (Zhang et al., 2008). We found this to happen, for *all* mesh sizes, for inlet velocity between 4-7 mm/s (Fig. 4.5(a-d)). Snapshots in Fig. 4.3(b-c) and Fig. 4.4(a-b) are examples of this phenomenon shown transiently for 4mm^2 mesh and 1mm^2 mesh respectively. Note that grey scale voidage range on Fig. 4.3(b-d) and Fig. 4.4(a-c) were chosen so as to enhance visibility of dilute regions, and were kept consistent for a particular Figure, except in the case of Fig. 4.3(a) as explained before. For 4-7mm/s profiles (Fig. 4.2(a-d)) a step drop in bed voidage profile reflects the more continuous expulsion of dilute regions leaving behind an apparently homogeneous bed. Hereafter the transient bed voidage profiles remain straight horizontal lines which represent a steady state of bed voidage. At steady state, for 4mm/s and 6mm/s two homogeneous layers are seen due to the effect of gravity (Fig. 4.5(a-d)).

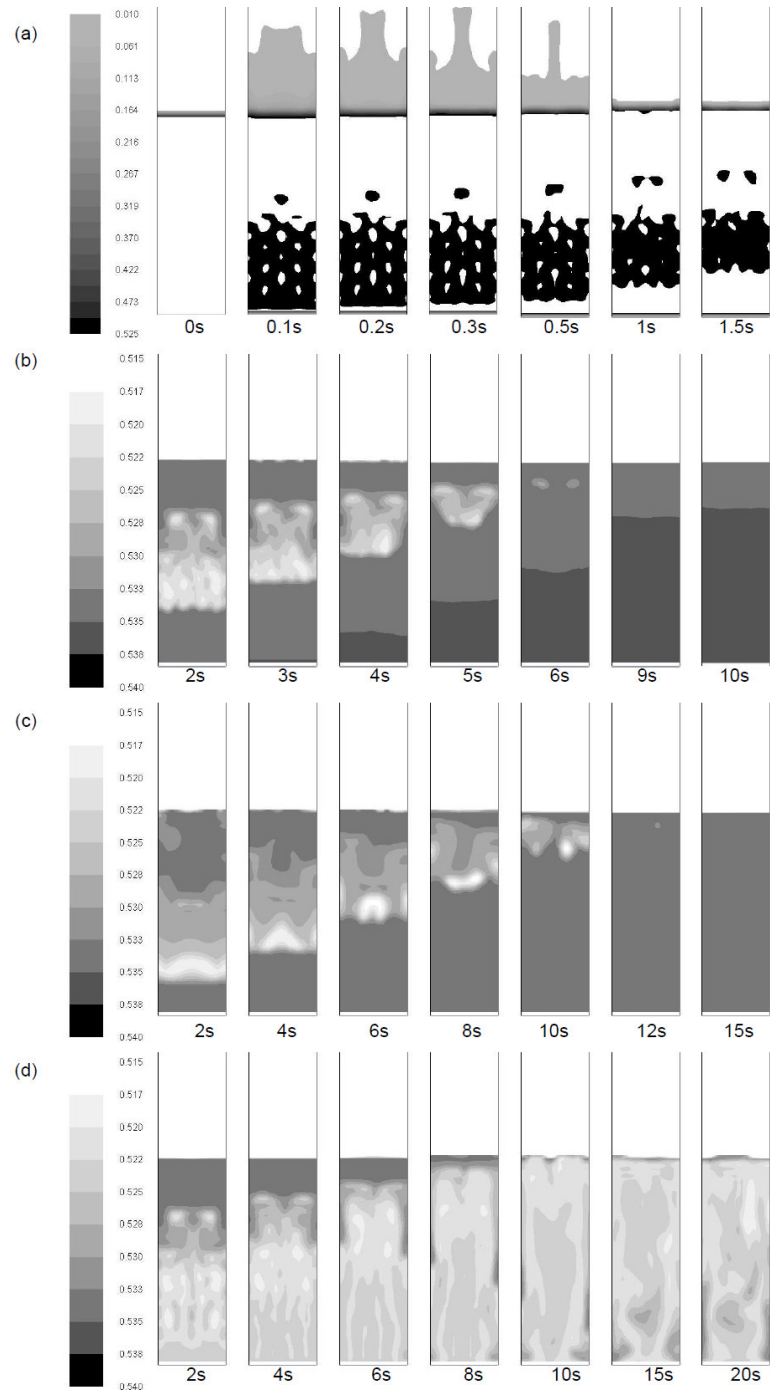


Fig. 4.3 Snapshots of transient solid volume fraction contours of the fluidized bed using 4mm^2 mesh and Gidaspow drag law. (a) Initial period bed expansion showing bed jump and settling for 6mm/s inlet velocity. (b) Evolution to pseudo steady state for inlet velocities of 6mm/s ; (c) 7mm/s ; (d) 8mm/s .

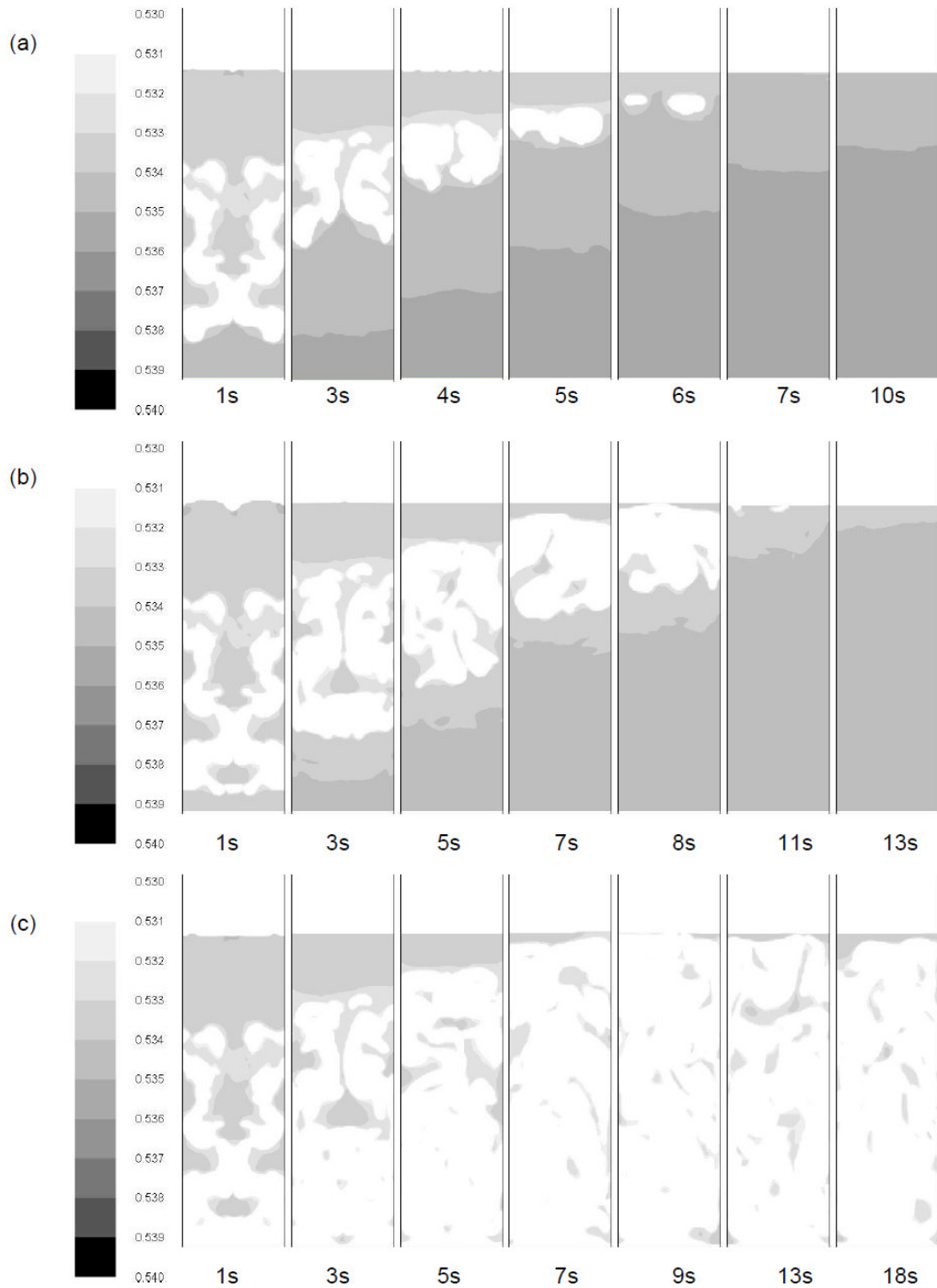


Fig. 4.4 Snapshots of transient solid volume fraction contours of the fluidized bed using 1 mm^2 mesh and Gidaspow drag law. (a) Evolution to pseudo steady state for inlet velocities of 6 mm/s ; (b) 7 mm/s ; (c) 8 mm/s .

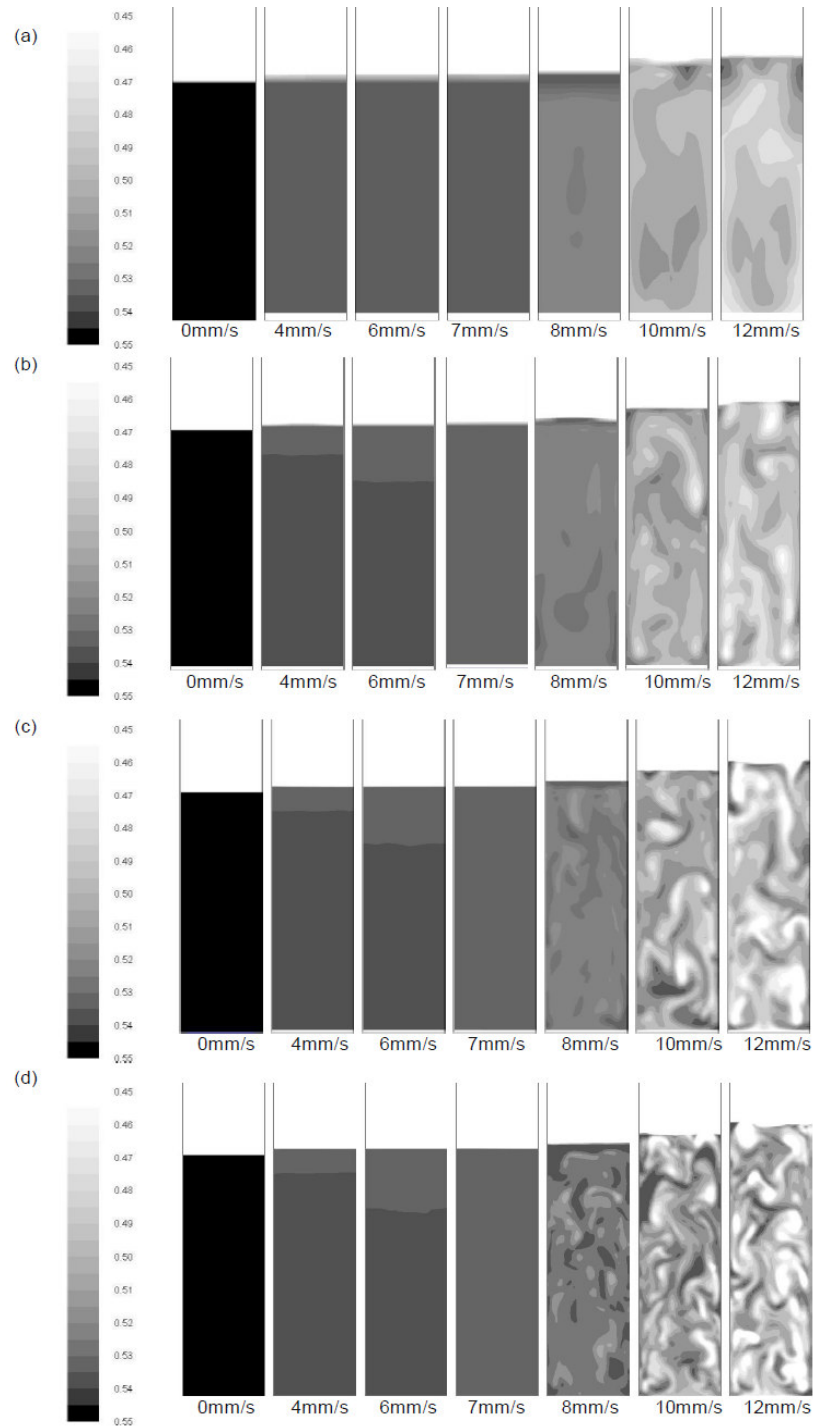


Fig. 4.5 Snapshots of solid concentration contours of the fluidized bed at pseudo steady state conditions for inlet velocities in the velocity range 4-12mm/s using Gidaspow drag law. Dilute regions are clearly visible only for 8mm/s and higher velocities, for all mesh sizes which are: (a) 16mm² mesh; (b) 4mm² mesh; (c) 2mm² mesh; (d) 1mm² mesh.

ii. Transient profiles for 8-12mm/s inlet velocity

For 8mm/s dilute regions which rise from the bottom of the bed do not simply get expelled with time (Fig. 4.3(d) and Fig. 4.4(c)). Instead they propagate upward to permeate the entire bed causing their steady state bed voidage profiles to be elevated from those of lower velocity values for all coarse mesh sizes (Fig. 4.2(a-d)). Once these dilute regions fill the entire bed cross-section they persist with time, displaying varying voidage and shapes but with little effect on over all bed voidage. We shall refer to this as 'dynamic steady state of dilute regions' which is observed for all mesh sizes, for 8mm/s and higher velocities (Fig. 4.5(a-d)). Transient profiles for 10 and 12mm/s show more number of step-like rises as mesh size decreases (Fig. 4.2(a-d)). These step-like rises mimic the continuous bed expansion due to the upward propagation of dilute regions. The dynamic steady state that follows this expansion is indicated by slightly fluctuating lines departing from the straight nature of the 8mm/s transient profile. The reason is the more pronounced dynamics as clearly seen from Fig. 4.5(a-d).

4.1.1.2 Effect of mesh size

For the 16mm² mesh, the simulated bed voidage values in experimental homogeneous expansion regime (4-7mm/s) are nearly constant (Table 4.1) thus indicating that increase in homogeneous expansion was not captured. The same was true even on reducing mesh size to 1mm², and the relationship between bed voidage and inlet velocity did not move closer to a Richardson and Zaki (1954) type expression (power law curve of Eq. 1.1) as we had expected. For a given mesh size, if the simulated bed voidage did not increase with velocity in the homogeneous regime, i.e. it did not mimic experimental

homogeneous expansion, we refer to it as being a ‘static bed’ for the said velocity range (third column in Table 4.1). Please note that minimum bubbling velocity (last column in Table 4.1) is discussed later in section 4.1.2.3.

Table 4.1 Summary of results from mesh size study.

Mesh	Drag law	Velocity range ^a (mm/s)	Static bed voidage	Next higher bed voidage ^b	Minimum bubbling velocity ^c (mm/s)
16mm²	Syamlal O’Brien	4 ^d -8	0.5005	0.5146	52
	Gidaspow	4-7	0.4848	0.5004	49
	Whe Yu	4-9	0.4848	0.5005	60
4mm²	Syamlal O’Brien	4-7	0.4719	0.4883	36
	Gidaspow	4-7	0.4719	0.4883	34
	Whe Yu	4-9	0.4719	0.4803	40
2mm²	Syamlal O’Brien	4-7	0.4742	0.4855	28
	Gidaspow	4-7	0.4742	0.4855	28
	Wen Yu	4-9	0.4742	0.4855	32
1mm²	Syamlal O’Brien	4-7	0.4721	0.4844	22
	Gidaspow	4-7	0.4720	0.4804	18
	Wen Yu	4-9	0.4720	0.4804	24

^a Static bed velocity range.

^b Bed voidage simulated at: highest velocity in static bed velocity range^a + 1mm/s.

^c Contour value of bubble boundary was 0.2 solid volume fraction.

^d For all meshes the reported bed voidage at 4mm/s did not adequately account for frictional stresses.

It must be noted that for all mesh sizes, solution for 4mm/s could not be obtained beyond 5s of flow time, due to convergence difficulties attributed to the frictional stress model invoked at high solid packing. The poor convergence as the bed compacted indicated that frictional stresses were not completely resolved. This problem was not encountered for higher velocities.

From the grid independence of bed voidage up to 1mm^2 mesh, we infer that there are no meso-scales (voids or clusters) present with size greater than 1mm, which is in contrast to riser flows. Though it is difficult to quantify, it seems that meso-scales of 0.5mm or less, if present, would have escaped resolution by 1mm^2 mesh or larger. Hence for homogeneous regime, we infer that 1- 4mm are suitable filter lengths, being smaller than the domain dimensions yet larger than the size of the meso-scales (Igci et al., 2008). In literature, filtered models were tested for riser flows (Igci et al., 2011).

4.1.1.3 Effect of Drag Law

Reduction of mesh size from 16mm^2 to 4mm^2 removed the effect of drag law on voidage and had negligible effect on static bed voidage (Table 4.1).

Clearly, 8mm/s ($u_{mb,e}$), was the lowest velocity value to create a bed voidage higher than the static bed voidage value using Gidaspow and Syamlal O'Brien drag law, for all coarse meshes. This threshold value was 10mm/s in the case of the Wen Yu drag law, again for all coarse meshes.

4.1.1.4 Effect of Frictional stress

In dense bed, frictional stress operates in a solid volume fraction range from a threshold value (ϵ_s^{min}) to the maximum packing limit (ϵ_s^{max}) (Zhang and Rauenzahn, 1997) and needs to be accounted for apart from kinetic and collision stress. Increasing frictional stress has the effect of increasing gas hold-up in fluidized bed (van Wachem et al., 2001). Fig. 4.6 clearly shows bed voidage values are lesser when frictional stress is omitted. Increasing the solid packing range by decreasing ϵ_s^{min} increased the overall stress in the bed as expected. Hence bed voidage was much higher for $\epsilon_s^{min} = 0.4$ (here only model of Johnson and Jackson (1987) converged), than $\epsilon_s^{min} = 0.53$ (were only model of Syamlal (1993) converged).

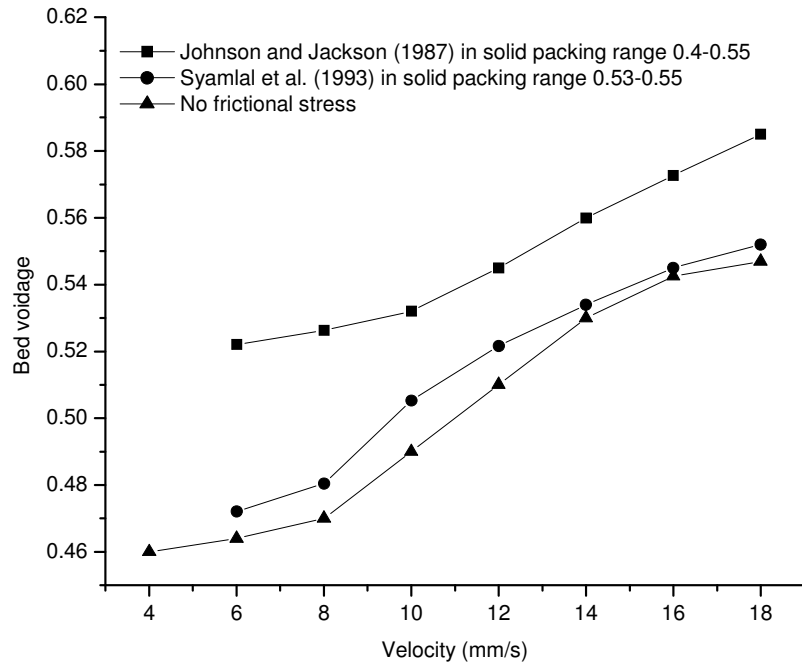


Fig. 4.6 Effect of frictional stress on bed voidage (1mm² mesh was used).

The difference in voidage with and without frictional stress model of Syamlal et al. (1993) is noticeably lower for velocities greater than 12mm/s which corresponds to freely bubbling bed. Wachem (van Wachem et al., 2001) et al. also reported that the predicted bed expansion in their freely bubbling fluidized bed was significantly less without frictional stress. They also observed poorer convergence when frictional stress was neglected, due to steepness of radial distribution function near ε_s^{max} . We observed no convergence difficulties when frictional stress was omitted. In fact, for the case of 4mm/s convergence was restored on omitting frictional stress, indicating that the frictional stress model could not be completely resolved with the default time step. When frictional stress was removed for 6-8mm/s, we observed fluctuations appearing in the transient voidage profiles. This implies that frictional stress contributes to bed stability in homogeneous expansion regime. 1mm² mesh was used for all simulations in this section, and this mesh size was found adequate for qualitative assessment.

4.1.2 Mesh study on Minimum bubbling velocity

Experimentally minimum bubbling has been probed by visualization of the first obvious bubble (Geldart, 1973; Geldart and Abrahamsen, 1978; Xie and Geldart, 1995a). Geldart (Geldart, 1973) stressed that the ‘first’ visible bubble should appear on ‘slowly’ increasing inlet gas velocity, and also qualified ‘clearly defined bubble’ as having diameter of about 5mm. In spite of this qualification the definition of minimum bubbling still remains subjective but there is consensus on the larger issue that increasing velocity beyond minimum bubbling causes a destruction of the apparently homogeneous bed structure and a heterogeneous structure ensues. Less subjective indicators of minimum

bubbling based on other bed variables have also been sought (De Jong and Nomden, 1974; Jacob and Weimer, 1987; Rhodes et al., 2001; Simone and Harriott, 1980; Wang et al., 2010b).

We used the most common method of visual observation to estimate minimum bubbling velocity, so that comparison to the experimental literature value (also obtained by visual method) could be made. Literature values of the bubble contour void fraction are either 0.15 (L. Cammarata, 2003) or 0.2 (Yates et al., 1994). We chose the value of 0.2 to define the computational bubble. Adopting the method of Wang et al. (Wang et al., 2010a) we observed the transient simulation animations for each mesh size during the first 1-2.5s of flow time, starting from a velocity of 6mm/s, to judge if the bubble had formed or not. If bubble had not formed, velocity was increased in small enough increments so as to obtain accuracy of U_{mb} up to 1mm/s.

4.1.2.1 Transient voidage profiles in bubbling regime

Fig. 4.7(a-c) illustrates transient bed voidage profiles for different meshes and for select inlet velocities which include $U_{mb, mesh-size}$. All the curves have a similar qualitative trend with three periods: an initial peak lasting no more than 2s, an expansion period (caused by upward propagating dilute regions), followed by the dynamic steady state of dilute regions (when bed voidage is in pseudo steady state).

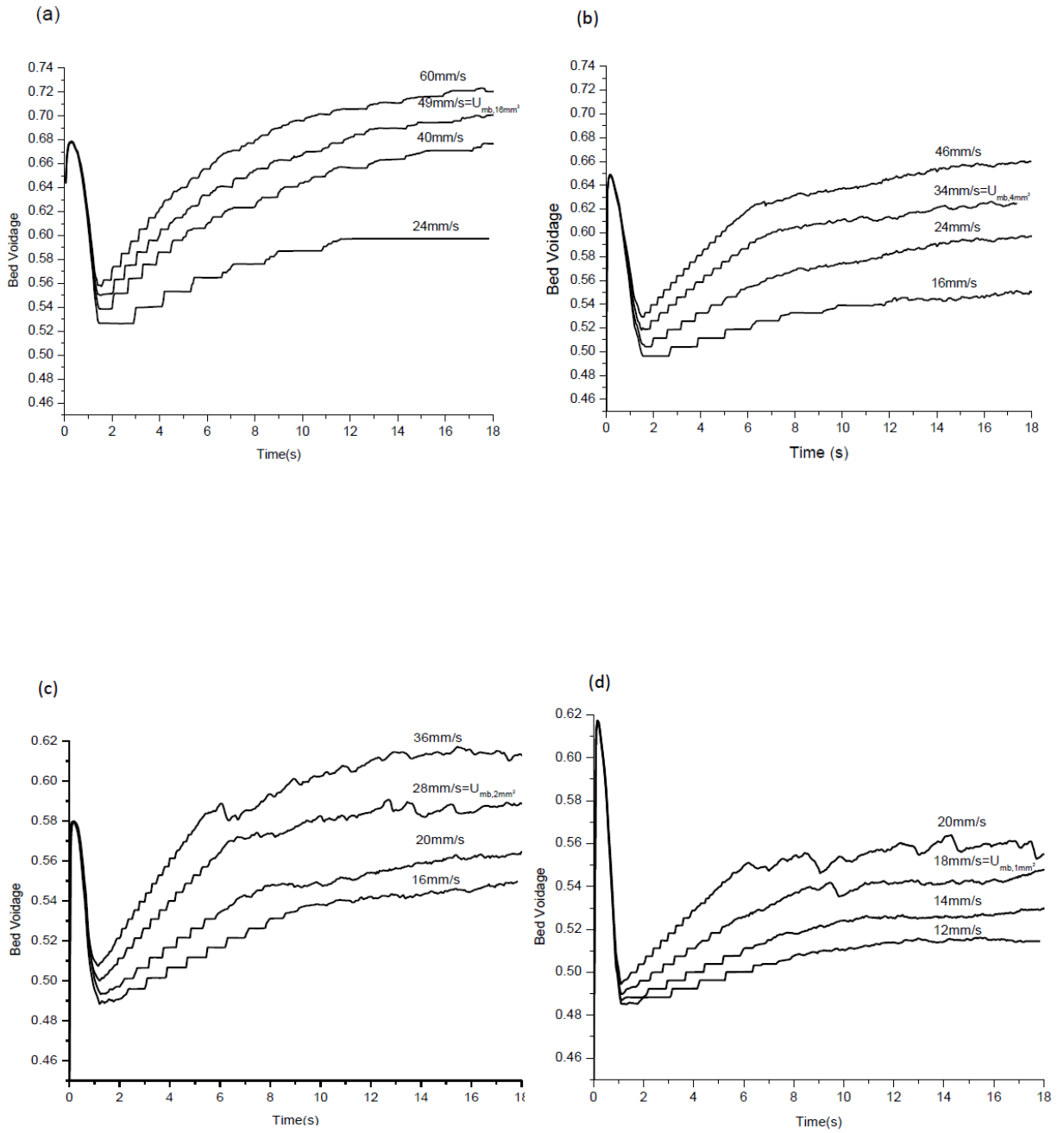


Fig. 4.7 Transient voidage profiles for higher velocities including the observed minimum bubbling for various mesh sizes using Gidaspow drag law (a) 16mm² mesh; (b) 4mm² mesh; (c) 2mm² mesh; (d) 1mm² mesh.

4.1.2.2 Effect of velocity

For coarse meshes the computational bubble is observed at a velocity much higher than $u_{mb,e}$. See for e.g. that $U_{mb,16mm^2}$ (Table 4.1) it is around 6 times $u_{mb,e}$. For $16mm^2$ mesh, (Fig. 4.7(a)) velocity profiles of 40mm/s & 80mm/s (before and after $U_{mb,16mm^2}$) have similar trends and qualitative fluctuations, indicating that the simulated $U_{mb,16mm^2}$ *did not* bring about the expected change in bed configuration which must accompany regime change, and hence fails as a regime change marker. Similar observations were made for all the coarse meshes.

For a particular mesh size increasing velocity creates smaller and smaller steps in second period, and higher fluctuations in third period reflecting smaller sized dilute regions with more and more varied voidage values.

4.1.2.3 Effect of mesh size

Taking the case of the Gidaspow drag model, reducing the mesh size from $16mm^2$ to $1mm^2$ caused a drop in minimum bubbling from 49 mm/s to 18 mm/s (Fig. 4.8). (Clearly the change is drastic for U_{mb} but not for average bed voidage, (taken at 8mm/s) implying that the bubble formation in the first 1-2.5s of flow time is a highly probably based event which should not be used to test for mesh independency.) We expect that meshes finer than $1mm^2$ (which we shall call fine meshes) would capture U_{mb} at a velocity lower than 18mm/s. It was reported (Wang et al., 2010a) that grid sizes of $0.2\text{ mm} \times 0.2\text{ mm}$ and $0.4\text{ mm} \times 0.4\text{ mm}$ captured $u_{mb,e}$ for domains sizes up to $3 \times 4\text{ cm}$. In section 4.1.3 we present one set of mesh simulations ($0.4\text{ mm} \times 0.4\text{ mm}$) for comparison with the coarse mesh simulations. In section 4.2 a detailed fine mesh study is presented.

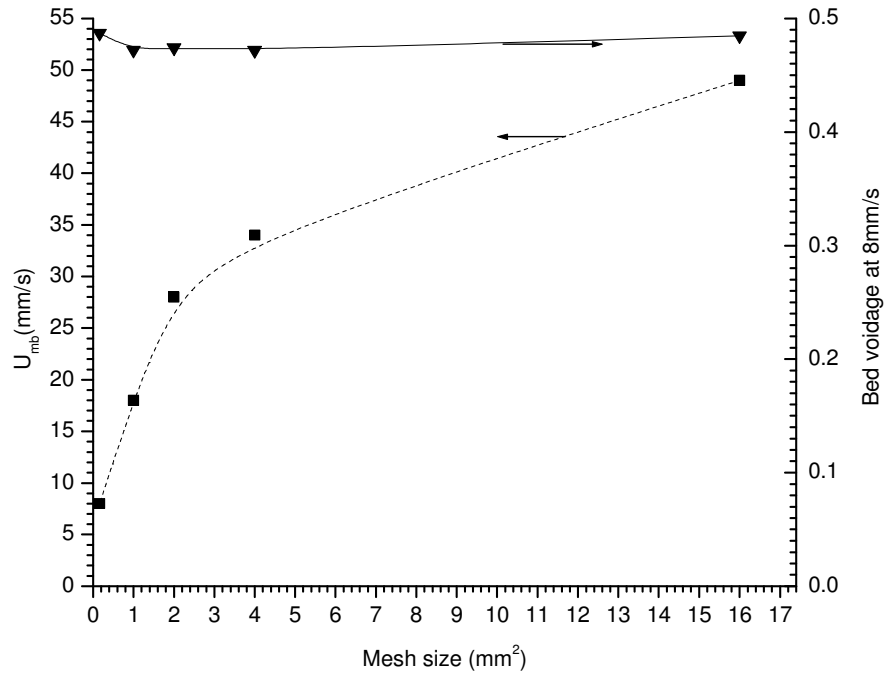


Fig. 4.8 Effect of mesh refinement on U_{mb} and bed voidage at 8mm/s

For velocities greater than 8mm/s, pseudo- steady state snapshots clearly show dilute regions, not present for velocities less than 8mm/s (Fig. 4.5(a-d)). On magnifying and inspecting many such dilute regions our observations matched the findings of others (Yates et al., 1994), that the cores of dilute regions have reduced voidage, with voidage reducing exponentially as we move away from the core. If the solid volume fraction in the core regions drops to 0.2 or less we have a ‘bubble’, but if the voidage in the core does not drop to such a low value we call it ‘dilute region’ to distinguish it from ‘bubble’. Hence every dilute region could potentially develop into a bubble. Therefore, dilute regions could have solid packing between 0.2 and ϵ_s^{\max} , and demarking them needs a formalized consensus to remove subjectivity. For a particular velocity, refining the mesh produced a larger number of dilute regions which occupied a larger bed area in total. This

is easily verified on comparing pseudo steady state snap shots of 12mm/s for reducing mesh sizes in Fig. 4.5(a-d), where the dilute regions (white regions) have solid volume fraction of 0.45 and lower. The reduced mesh size seems to influence in two ways to produce this result with time. Firstly, a finer mesh means increased number of cells at the inlet boundary which physically implies more inlet points for the incoming gas. This produces more *number* of independent dilute regions, having more varied shapes and voidage values (Fig. 4.9(a-d)), giving higher probability of one of them developing into a bubble. Secondly, finer meshes can better capture the meso- scale structural effects where their absence was cited as the reason for over prediction of bed voidage in coarse mesh bubbling bed simulations (Wang et al., 2011). We go further to explain that better resolution of dilute regions in the first two seconds of simulation Fig. 4.9(a-d), produces a drop in drag effect locally which forces more gas into the dilute regions further increasing their voidage. Both these factors have the effect of producing the first visible bubble at lower velocities as mesh is refined. In Fig. 4.9(a-d), pure white areas have solid packing less than 0.2, and are therefore bubbles.

In summary, reducing mesh size seems to influence bubble formation in two ways: Firstly, a finer mesh creates more inlet points for the incoming gas. This produces more *number* of dilute regions with greater diversity of shapes and voidages increasing probability of a bubble developing. Secondly, better resolution of dilute regions in the first two seconds produces a local drop in drag effect forcing more gas into the dilute regions. Both these factors have the effect of producing the first visible bubble at lower velocity on mesh refinement.

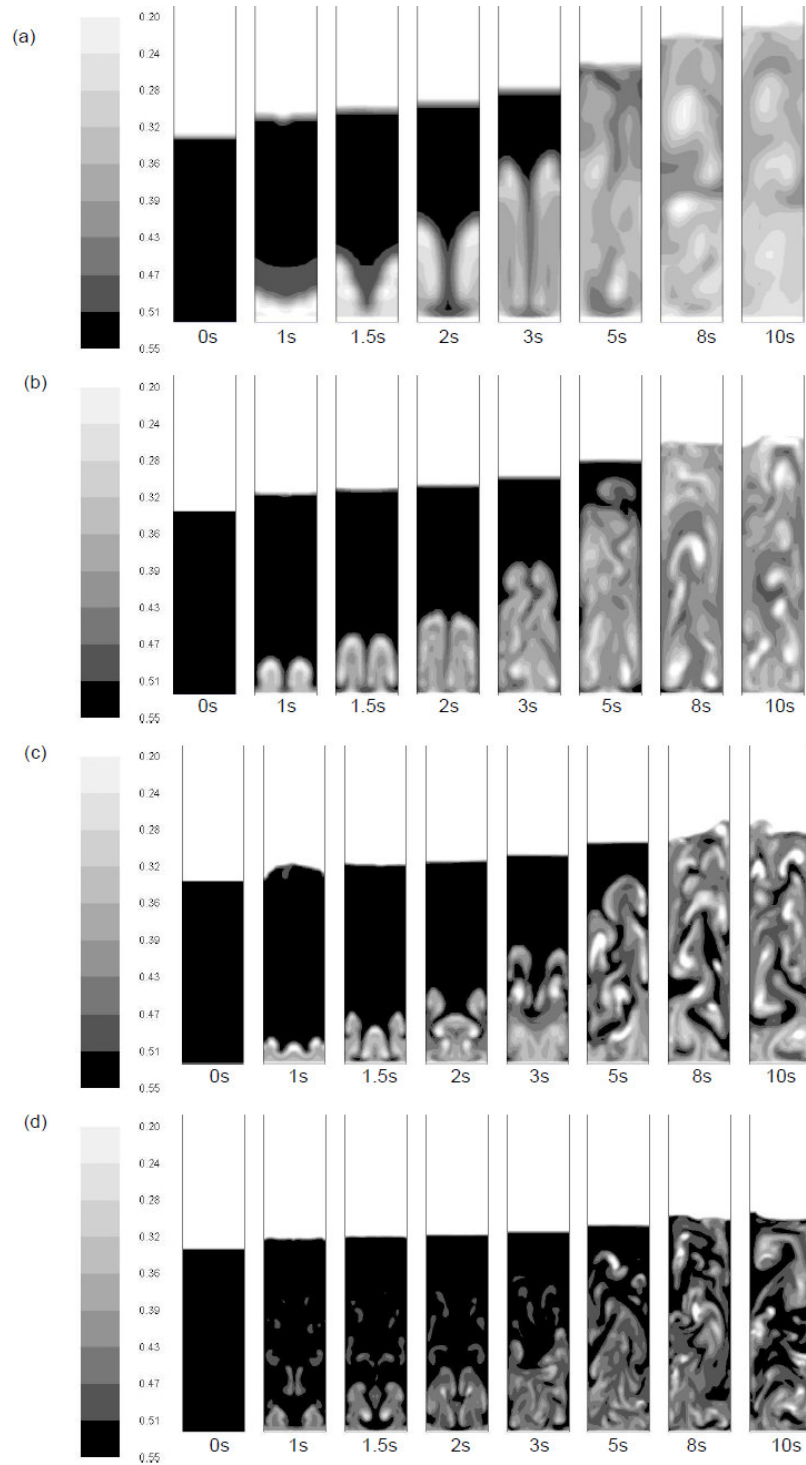


Fig. 4.9 Snapshots of transient simulations, using Gidaspow drag, for the observed minimum bubbling velocity values of 49mm/s, 34mm/s, 28mm/s and 18mm/s for the respective mesh sizes (a) 16mm² mesh; (b) 4mm² mesh; (c) 2mm² mesh; (d) 1mm² mesh.

4.1.2.4 Effect of wall boundary condition

The value of $U_{mb, 1mm2}$ obtained using no-slip and free-slip gas phase wall boundary condition (BC) were 18mm/s and 21mm/s respectively. Hence $U_{mb, 1mm2}$ was slightly delayed for the free-slip case. In contrast, DPM simulations of Ye et al (Ye et al., 2005), found that no-slip rather than free-slip BC delayed the transition. This could be because they simulated a much smaller domain. Also the transition was monitored by local porosity fluctuation and not visual method as in our simulations.

For particle-wall BC, Specularity Coefficient (SC) values of 0 (No wall shear on particles), and 1 (significant lateral momentum transfer) were trailed and $U_{mb, 1mm2}$ was 18mm/s and 20mm/s respectively. For Geldart A particles in riser flow, free-slip BC for both phases is considered a good first approximation in 2D simulations (Igci and Sundaresan, 2011). In our case, since no-slip gas boundary condition gave $U_{mb, 1mm2}$ value closer to $u_{mb,e}$, we infer that no-slip for gas phase is more realistic. Also since the flow is much denser than riser flow, this seems reasonable. By the same reasoning for particle BC we infer that free-slip (SC=0) was probably more realistic, but it is difficult to make a definitive statement.

When Frictional stress was omitted (using no-slip for gas), $U_{mb, 1mm2}$ was 20mm/s. The use of free-slip for gas, SC=1 for particle BC as well as omission of frictional stress produced a little more uniform packing in dilute region cores early on (1.5 s) and had the effect of delaying $U_{mb, 1mm2}$. $1mm^2$ mesh was used in all cases, but a finer mesh would bring out the effect better and confirm these qualitative results.

4.1.2.5 Effect of Drag Law

For each mesh size, Gidaspow drag law consistently produced lowest value of U_{mb} , which were closest to $u_{mb,e}$, while Wen Yu always gave the highest value (Table 4.1). Using this argument we confirm standard literature that Gidaspow it is more suitable for dense beds than stand alone Wen Yu which predicts a lower drag at same voidage. Also Syamlal O'Brien drag law behaves closer to Gidaspow than to Wen Yu.

4.1.2.6 Effect of time

The method of estimating minimum bubbling by inspection of snapshots does not include any consideration for 'time for persistence of first bubble' and no previous study has addressed this issue. In addition to observing animations of the simulation between 1-1.5s of flow time, to judge if the bubble had formed or not, we also noted the time for which it persisted. Taking the case of the 16mm^2 mesh and Gidaspow drag model, we found that the first bubble persisted only for 0.3s at the $U_{mb,16\text{mm}^2}$ value of 49mm/s. After this there was no bubble detected for the entire flow time. The time of persistence of the first bubble increased gradually with velocity, for a particular mesh size. Say for example at 60mm/s and the same mesh size of 16mm^2 it was 3s. After 100mm/s we found multiple bubbles in the initial period which were comparatively larger and also persist indefinitely i.e. if some were broken others were created, and there were always regions in the bed with less than 0.2 solid volume fraction. On reducing the mesh size we found a qualitatively similar behavior but manifesting at lower velocities. Hence time of persistence of computational bubble must be a consideration in this context and warrants further discussion and consensus in the literature.

4.1.3 Comparison with fine mesh simulation

Fine mesh simulations in (Fig. 4.10(c)) reveal some meso-scale structures not previously resolved. The fine mesh area was 0.16mm^2 (of order $6d_p$). Estimation of U_{mb} as per section 4.1.2, showed a ‘bubble’ for as low a velocity as 4mm/s and 6mm/s but inspection of snapshots revealed the equivalent diameters near 0.4mm and the minimum voidage contour was 0.15, making us judge these as small voids rather than first obvious bubble. For 8mm/s the bubble formed had diameter close to 1.6mm and contained voidage contour even less than 0.15. Ambiguity of designating ‘first obvious bubble’ has already been expressed by other researchers (Ye et al., 2005). However our simulations clearly show heterogeneous nature of the bed breaking out at 10-12mm/s (Fig. 4.10(c)), making 8mm/s a justifiable minimum bubbling velocity. Further, the dilute regions are visible at 8mm/s and not at lower velocities which reinforces our observations in section 4.1.4, that these dilute regions are potential regime transition markers. We note that the fineness of the dilute regions at 8mm/s make them difficult to perceive in print.

i. Extent of capture of homogeneous bed expansion

Even though fine mesh produces the highest expansion from packed bed state to 4mm/s gas velocity (Fig. 4.10(c)) the voidage increase from 4- 6mm/s and 6-8mm/s was only 0.006, showing that homogeneous expansion is still not adequately captured. One inference is that the homogeneous expansion is mainly due to ‘voids’ which are much smaller than bubbles with size of the order of the particles (such a bed structure is discussed in section 4.1.5). If the voids are of the order of $2-4d_p$ they would remain unresolved even with the fine mesh.

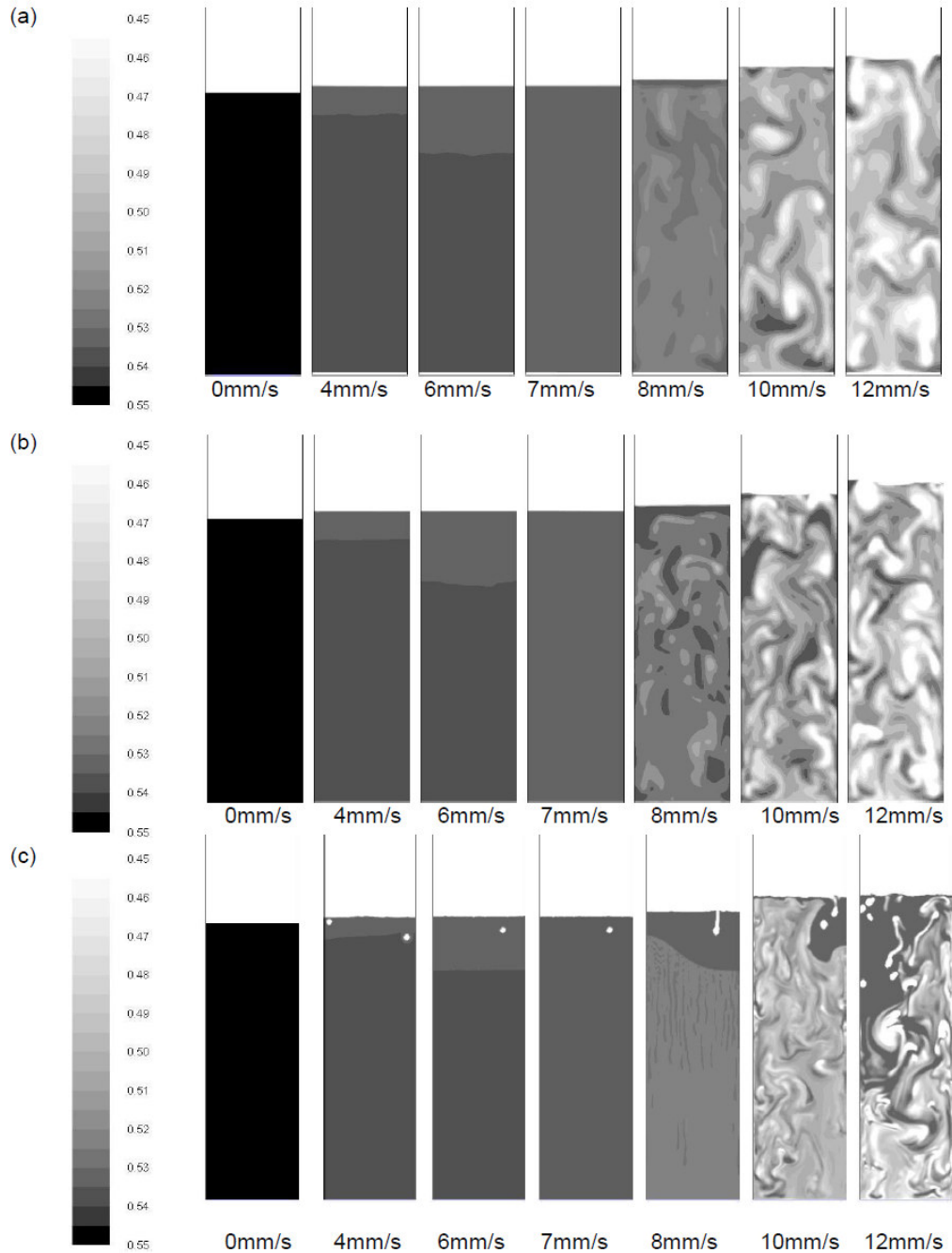


Fig. 4.10 Snapshots of solid concentration contours of the fluidized bed at pseudo steady state conditions for inlet velocities in the velocity range 4-12mm/s using Gidaspow drag law. Mesh sizes which are: (a) 2mm² mesh; (b) 1mm² mesh; (c) 0.16mm² mesh. Here (a) and (b) are repeated from Fig. 4.5 for the purpose of comparison with the fine mesh simulations in (c).

Secondly, the lack of increase in expansion might have to do with incorrect predictions of frictional stress mode. This is further investigated in the fine mesh study of section 4.2. A third explanation as to why the expansion was not adequately captured might proceed from effect of IPFs which are unaccounted for in TFM. For though our simulations like others (T. Kobayashi, 2002; Ye et al., 2005), confirm that IPFs are not the sole cause of expansion, their effect might not be negligible even for $d_p > 55\mu\text{m}$ (Geldart and Wong, 1984). However the effect of IPFs is to delay U_{mb} (Mazzei and Lettieri, 2008; Kobayashi, 2002) which already seems adequately predicted without the IPF contribution in our simulations and also in those of Wang et al. (Wang et al., 2010a). The detailed fine mesh study of section 4.2 investigates this more thoroughly.

ii. Simulation clock time

The number of CFD cells (and nodes) gets multiplied by the square of the mesh size divisor. Therefore the required CPU resources get multiplied with mesh refinement. Conversely, for a fixed CPU resource, the actual simulation time required to simulate equal flowtimes increases with mesh refinement. For 16mm^2 and 4mm^2 mesh, the wall clocked time required for simulation was no more than 24 hours. This increased to almost a week for 1mm^2 mesh, and the fine mesh of 0.16mm^2 required a total of six to twelve months of wall clocked time. The CPU configuration was Intel (R) Xenon core, 8GB, 2.33GHz. This shows that CPU time required increased exponentially with mesh refinement. The wall clocked time included occasional shutdowns and were applicable for simulation of 20s or more of flowtime.

4.1.4 A useful marker for regime change

Only fine meshes capture $u_{mb,e}$ accurately, but this comes at a huge computational cost. On reviewing several animations, we always observed the marked appearance of persisting dilute regions at around $u_{mb,e}$ (8mm/s) and after. We verified this by continuing several of the simulations for 40 seconds of actual flow time and confirmed that the bed did not evolve to a new homogeneous voidage field as occurred for velocities below 8mm/s. Pseudo steady state snapshots for each mesh size in Fig. 4.5(a-d) illustrate this. Transient voidage profile graphs for all coarse mesh size (Fig. 4.2(a-d)) also confirm that dilute regions appear at around 8mm/s, giving it a higher voidage than the static bed voidage. For the Wen Yu drag model this velocity value was 10mm/s as the static bed persisted till 9mm/s (Table 4.1).

Prediction of bed instability seems independent of mesh size. This reasoning is in line with that of other works (Glasser et al., 1996; Glasser et al., 1998; Igci et al., 2008) which state that the microscopic TFMs are robust in the sense that when they are augmented with physically reasonable closures, they do yield all the known instabilities in gas-particle flows, which in turn lead to persistent fluctuations that take the form of bubble-like voids in dense fluidized beds and clusters and streamers in dilute systems. Assuming loss of bed stability as a necessary condition for minimum bubbling, the observation of dilute regions may be considered a regime change marker, only for the purpose of extracting this useful information from coarse meshes at a much smaller computational cost. This in no way changes the definition of minimum bubbling, but only explores setting some computational formalization. Also, the definition of ‘dilute regions’ computationally requires consensus.

4.1.5 Inferences on homogeneous bed structure

Experimental studies in the literature reported on the average bed voidage in the homogeneous bed. CFD simulations can further provide information in terms of insight into bed structure. In this section we propose three views or models of the bed structure in homogeneous expansion, and report which of these views are validated by the fine mesh simulations of Fig. 4.10(c). In Fig. 4.11 an idealized representation of the three views is shown.

The first view of bed structure is a bubbling bed like model. We assume a bubble-emulsion like bed structure for the homogeneously expanded bed, except that the bubble dimensions are so much smaller that we will call them ‘voids’. Such a bed structure is in line with conclusions of 3D discrete particle model simulations of Ye et al. (2005). For this view to be valid, the void structures would have to be pervasive enough to contribute to bed expansion i.e. multiply in number with velocity increase. The growth in number of voids would have to be substantial enough to ensure that the ensuing bed expansion resembles the experimentally observed Richardson and Zaki type expansion. It remains to be seen if IPFs have a role or not in formation of these voids, and if so to what extent. Such a view of bed structure could explain the lack of change in bed voidage observed from our coarse mesh simulations i.e. no increase in expansion even on refining mesh up to 1mm^2 , as only finer meshes would capture these voids. However, this bed structure is not validated by the fine mesh simulations of Fig. 4.10(c). Here only one or two voids are visible for the homogeneously expanded bed (4-7mm/s).

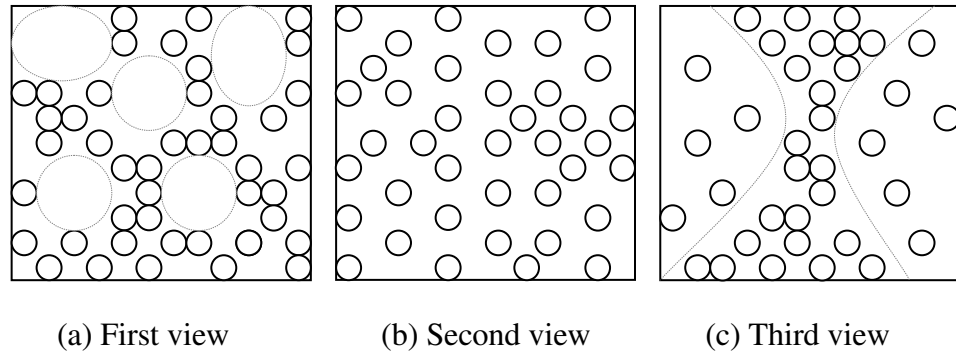


Fig. 4.11 Three Idealized representations of bed structure in homogeneous regime

A second view of bed structure in homogeneous regime is that the emulsion phase itself expands in the reactor more or less uniformly without any voids. This does not necessarily propagate a view of largely immobile particles suspended in gas phase as was envisioned by early works (Donsi et al., 1975; Mutsers and Rietema, 1977). Rather a dense particle laden gas is formed where particles move about locally and are likely to fluctuate. They might also have local contacts, but overall less than the other two views and even more less than in the packed bed state. This structure matches the fine mesh simulations for 4-7mm/s in Fig. 4.10(c). The expansion appears largely uniform from these simulations, subject to the chosen concentration scale.

A third view of bed structure is as follows: assuming the simulated expansion from 8-12mm/s (Fig. 4.10(a-c)) resembles homogeneous expansion qualitatively, one might expect dilute regions to be major contributors to homogeneous expansion. We attempt to computationally distinguish dilute regions from bubbles or voids as having comparatively much larger dimensions. Also the solids concentration is lower when compared to the largely prevalent and uniform emulsion phase but nowhere as low as the bubble. This is another view of the bed structure which appears similar to the fine mesh simulation at 8mm/s (see Fig.4.10(c)) where subtle instabilities permeate the largely

uniform distribution of particles (but are not so clear in print). Both the second and third views of bed structures are not invalidated by the fine mesh simulations of Fig. 4.10(c). They are also in line with the view that that homogeneous beds do not exist formally: they appear to be uniform, but are in fact subject to slow instabilities (Jackson, 2000). More number of fine mesh simulations, for varied particle properties, would be desirable to further confirm these inferences.

4.1.6 Limitations of the mesh size study

- i. The study was rigorous in terms of the number of mesh sizes studied and also the velocity range covered. However, only typical Geldart particle (70 μ m, 2000kg/m³) was considered. The Geldart classification enables us to extend behavior of the typical particle to all particles in that group. Yet it would be desirable to confirm observations for varied particle size and density within the Geldart A group. Densities of 1000 and 2500kg/m³ were tested with 1mm² and confirmed the observation about dilute regions as regime change marker.
- ii. Subjectivity of the definition of dilute regions in the simulation remains an issue. Uniform regions for a particular simulation appear so subject to the gradation on the given concentration grey scale. This was explained with the help of Fig. 4.1. The concentration scale can never be a true continuum which will always be a limitation. However, a consensus on the issue of threshold packing to define dilute and uniform regions, similar to the consensus on definition of bubble, is a requirement.

4.2 Fine mesh study on gas-fluidization of Geldart A particles: Homogeneous expansion and transition to bubbling

To rule out any effect of domain size and ensure realistic simulations, the typical lab-scale 2D domain of 4cm width (diameter) and 1m length which was used in the mesh size study, was also used here. Inspire of the computational intensity the domain dimensions were not compromised. A mesh as fine as $(2 - 4)d_p$ (i.e. $0.2\text{mm} \times 0.2\text{mm}$, as $d_p = 70 \mu\text{m}$) was recommended to accurately capture the true inter-phase drag force and bed expansion resulting thereof (Wang et al., 2009). However, simulations from a more recent work by the same authors (Wang et al., 2010a) revealed that even a mesh size of $0.4\text{mm} \times 0.4\text{mm}$ resolved sub-grid structures (voids and bubbles). These get annihilated by coarser mesh sizes such as $4\text{mm} \times 4\text{mm}$ which have hitherto been commonly used in simulation studies (Wang et al., 2011). Hence a mesh size of $0.4\text{mm} \times 0.4\text{mm}$ ($5.7d_p$) was deemed optimum in light of the large domain size adopted and the prohibitive computational cost entailed by a mesh size of $0.2\text{mm} \times 0.2\text{mm}$.

4.2.1 Fine mesh simulation of the transition from homogeneous to bubbling bed

4.2.1.1 Ambiguity in judging minimum bubbling point

i. By experiment

Visual method of determining minimum bubbling velocity from experiment ($u_{mb,e}$) relies on sighting the ‘first obvious bubble’ or ‘first clearly defined bubble’ upon slowly increasing inlet gas velocity. This makes it a subjective method as evidenced by the varied $u_{mb,e}$ values reported (Table 4.2) by different authors for similar particle properties. Some authors even cited the first appearance of *multiple* bubbles on the bed’s surface as

signaling minimum bubbling conditions (Lettieri et al., 2002; Sidorenko and Rhodes, 2004). Ambiguity in the visual method of detecting $u_{mb,e}$ was previously noted (Sidorenko and Rhodes, 2004) and non-visual indicators of $u_{mb,e}$ have also been sought (De Jong and Nomden, 1974; Simone and Harriott, 1980).

ii. By simulation

In simulation context, ‘a bubble’ is defined as a region within the bed with solid volume fraction less than either 0.15 (Kuipers et al., 1992; L. Cammarata, 2003) or 0.2 (Yates et al., 1994). We used the visual method to detect the minimum bubbling velocity from TFM simulation snapshots at pseudo steady state (U_{mb}). The detected value was found to vary depending on the threshold solid volume fraction chosen (Table 4.2). In addition to threshold solid volume fraction, detection of the computational bubble was also subjective in terms of (a) size of the bubble, and (b) time of persistence of the bubble. Experimentally a ‘distinct bubble’ is suggested as having a diameter of at least 5mm (Geldart and Abrahamsen, 1978). No such criterion exists in simulation where space is discretized into cells by the CFD mesh. Consequently a bubble can be considered present even if one cell in the fluidized bed domain (but not the freeboard) has solid volume fraction less than the selected threshold value. Further, even if a ‘clearly defined bubble’ appears but persists only for a fraction of a second (this can be definitively detected in simulation studies than by experimental observation) it would be difficult to justify occurrence of minimum bubbling. Such a ‘bubble’ might be better identified as a short lived void, no matter its size. In a previous work on coarse mesh TFM simulations we proposed the of ‘persisting dilute regions’ instead of ‘first bubble’ as a less ambiguous

marker of minimum bubbling conditions. A similar consideration will be analyzed for TFM fine mesh simulations, in the next section.

Table 4.2 Various minimum bubbling velocities reported by experimental works and compared with fine mesh TFM simulations

Authors	d_p (μm)	$u_{mb,e}$ (mm/s)	Comment on the visual method
Abrahamsen and Geldart (1980)	70	8.781	Empirical correlation based on 48 gas-solid systems
Xie and Geldart (1995)	68	5.37	Clearly defined bubble appeared at bed surface
Lettieri et al. (2002)	71	9.8	–
Our fine mesh TFM simulations	70	8 (svf<0.15)	U_{mb} dependant on threshold solid volume fraction (svf) contour selected
		4 (svf<0.2)	

4.2.1.2 A regime of transition to bubbling

In the mesh size study in section 4.1, five different mesh sizes were investigated. The triggering of dilute regions at minimum bubbling conditions was consistently observed. Hence in simulation context, appearance of dilute regions was proposed as a marker to signal the transition to bubbling regime. In this section we test this premise by examining TFM fine mesh simulations with different particle density (ρ_p) values. Fig. 4.12(a-c) presents the pseudo-steady state simulation snapshots for inlet gas velocities in range 4 – 12 mm/s and for ρ_p of 1, 2 and 2.8 g/cc. For a particular ρ_p with increasing gas velocity, the snapshots clearly show the appearance of dilute regions which destroy the homogeneous structure of the bed.

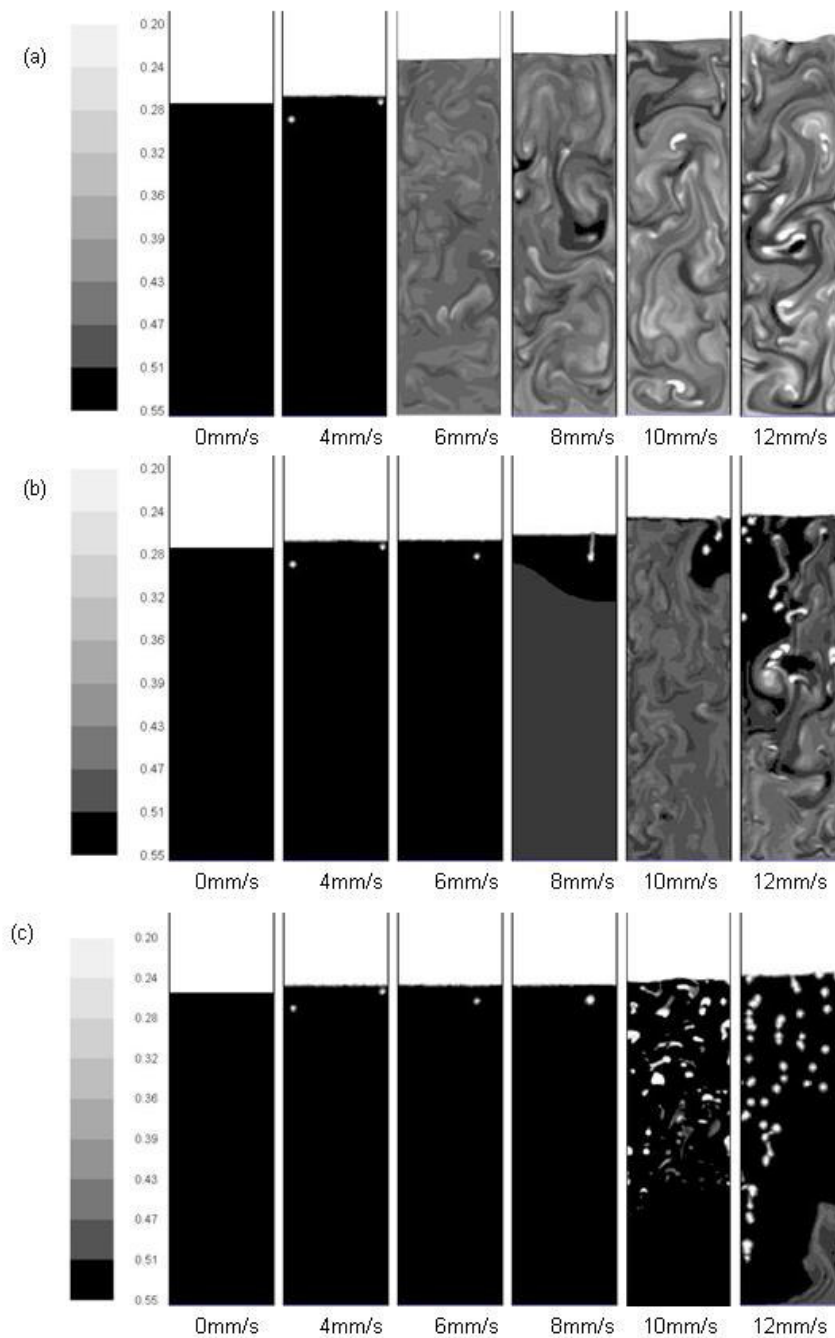


Fig. 4.12 Fine mesh simulation snapshots at pseudo-steady state in the homogeneous expansion and transition regime (4-12mm/s) for different particle densities (a) 1 g/cc; (b) 2 g/cc; and (c) 2.8 g/cc.

The velocity at which these dilute regions get simulated at pseudo steady state is designated: u'_{mb} to distinguish from U_{mb} , since dilute regions rather than ‘first simulated bubble’ was used as marker. The u'_{mb} detected for different ρ_p are given in Table 4.3, and resemble the trend of U_{mb} reported by Wang et al. (Wang et al., 2010a) from their fine mesh TFM simulations. They used visual method for bubble detection in the *first* 1.5 to 2.5s of simulation flow time while we ensure pseudo-steady state. We note that the empirical correlation of Abrahamsen and Geldart (Abrahamsen and Geldart, 1980) shows no change of $u_{mb,e}$ with ρ_p (Eq. 4.2). Snapshots in Fig. 4.12(a-c) show ‘bubbles’ (threshold solid volume fraction = 0.2) in the bed even for velocity as low as 4mm/s, but we judged these to be voids rather than the ‘first bubble’. This distinction was made whenever the homogeneous bed structure was intact i.e. solid volume fraction was nearly uniform (solid volume fraction variation not exceeding 0.004). For all values of ρ_p in Fig. 4.12(a-c), clearly visible multiple bubbles appear around 12mm/s, and this velocity marks the complete breakout of heterogeneous structures in the bed, giving way to a freely bubbling bed. We designate this velocity as: u'_b . Observation of clearly defined multiple bubbles at 12mm/s, was also reported from DEM simulations (Renzo and Maio, 2007). Hence for TFM simulations, transition to bubbling apparently occurs over a velocity range ($u'_{mb} - u'_b$) rather than at a single velocity, implying a regime of transition to bubbling, which we shall simply call *transition regime*. In their experimental observations Geldart and Wong (Geldart and Wong, 1984) describe the way bubbles destroyed the homogeneous bed structure on increasing gas velocity *slightly* above $u_{mb,e}$, clearly implying a transition regime. The velocity range over which this occurred was not mentioned. Further, transition regime from 9 – 12mm/s was clearly revealed by DEM

simulation snapshots of Renzo and Maio (Renzo and Maio, 2007) ($d_p = 70 \mu\text{m}$, $\rho_p = 1\text{g/cc}$). The simulated transition regime (Table 4.3) apparently contracts with increase in ρ_p . This might be explained as a consequence of the increasing Geldart B characteristics of the particles due to increase in ρ_p (at constant $d_p = 70 \mu\text{m}$).

Homogeneous expansion will be discussed in section 4.2.2, where the overall bed voidage will be analysed. Since Fig. 4.12 furnishes us with insight into bed structure, we discuss the same in this section. Since insights on bubbling bed structure has been extensively discussed in simulation studies in the literature (McKeen and Pugsley, 2003; Tsuji et al., 2008; Yujie et al., 2012) we will therefore largely restrict our discussion to the expansion that occurs before bubbling.

First we base the argument on the existence of a discrete end point to the homogeneous expansion velocity range. Assuming this end point is the minimum bubbling velocity proposed by Abrahamson and Geldart (1980), we fix 4-8mm/s as the velocity range. According to the same expression, this velocity range is independent of particle density. Then we see from (Fig. 4.12 (a-c)) that both the second and third views of bed structure presented in section 4.1.5 are validated i.e. a largely homogeneous dense bed and a bed with dilute regions or turbulent instabilities respectively. We note the limitation of the grey scale in defining particle packing. According to the chosen scale, only packing variation of more than 4% are made visible. Packing variations less than 4% therefore appear as uniform. Hence the 'uniform regions' may also be considered dilute regions with solid packing variation of less than 4%. This demonstrates the commonality of the two view points, as a purely homogeneous distribution is only theoretically possible for 'frozen' particles. In any case there is strong evidence from the simulation

snapshots for the idea of Jackson (2000) that homogeneously expanded beds are not truly homogeneous but subject to slow instabilities. Hence the term ‘homogeneous bed’ is something of a misnomer.

Second we analyzed the bed structure based on the hypotheses of this section that a transition regime does exist where the bed is neither homogeneous nor bubbling but rather transitioning from homogeneous expansion to freely bubbling. This means that *just* beyond the packed state the bed structure better resembles the second view of homogeneously distributed spheres (4mm/s for all ρ_p). The bed structure then evolves to instabilities or dilute regions (third view), which is the transition state. The dilute regions become pronounced at lower velocities for particles with less density e.g. 6mm/s for 1g/cc and for 2g/cc it is about 10mm/s. Hence this discussion on bed structure validates the second and third views of 4.1.5 and no evidence can be seen to support the first view. Further the non-bubble regions or emulsion phase becomes more packed and less turbulent or less varied in packing as particle density increases. This makes the bubbles appear more distinct for heavier particles.

Table 4.3 Velocity range for transition regime detected for different values of ρ_p

ρ_p (g/cc)	$(u'_{mb} - u'_b)$ mm/s
0.6	5 – 12
1	6 – 12
1.4	8 – 12
2	8 – 12
2.8	10 – 12

4.2.1.3 Comparison of TFM and DPM: non-visual minimum bubbling transition

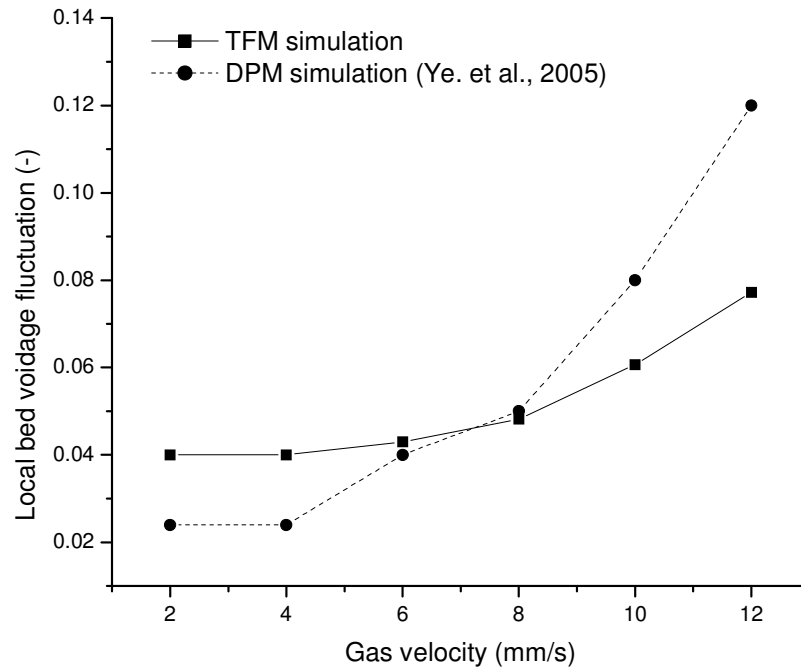


Fig. 4.13 Comparison of DMP and TFM: Variation of bed voidage fluctuation showing regime transition around the same gas velocity in both cases.

In literature, the minimum bubbling velocity values obtained from DPM simulations are closer to the higher, rather than the lower $u_{mb,e}$ values reported in Table 4.2. Take for example the 3D DPM simulations of Ye et al. (Ye et al., 2005) ($d_p = 75 \mu\text{m}$) where minimum bubbling values obtained by visual inspection were in the range 8 – 10 mm/s for ρ_p in the range 0.8 – 3g/cc.

Ye et al. (Ye et al., 2005) also used non-visual method of finding bubbling transition from DPM simulations. This was done by noting change in a key bed variable like local voidage fluctuations. Among key bed variables, the spatial fluctuations of local bed voidage was reported to be the most outstanding indicator of transition to bubbling

among others like temporal fluctuation of granular pressure and pressure drop (Ye et al., 2004). Fig. 4.13 compares local bed voidage fluctuations Vs inlet gas velocity from DPM simulations (Ye et al., 2005) with our TFM simulations (for same particle properties: $d_p = 75 \mu\text{m}$, $\rho_p = 1.4\text{g/cc}$). Here local voidage fluctuation (of the pseudo steady state bed) was defined equivalent to the expression used by Ye et al. (Ye et al., 2005) as:

$$\sqrt{\sum (\varepsilon_i^2)_{avg} - (\varepsilon)^2} \quad (4.1)$$

Where ε_i represents individual cell (local) values of gas volume fraction and ε is the average gas volume fraction of the bed. Averaging is done over all cells belonging to the bed. The bed comprises those cells with solid volume fraction ≥ 0.01 , to exclude the dilute suspension in freeboard.

A transition resembling a curve inflection was taken as indicative of regime change. The transition occurred around the same velocity (8mm/s) for both DPM and TFM simulations. However, we note that the first transition marking minimum fluidization velocity (u_{mf}) is more prominent in DPM simulations. Also, the curves are similar qualitatively but not quantitatively.

4.2.2 Simulation of homogeneous expansion

4.2.2.1 Validation of TFM with DEM: bed voidage expansion curves

The more rigorous *Eulerian-Lagrangian* (DPM/DEM) approach was reported to capture the main features of gas-fluidized Geldart A particles for theoretical domains (of the order of mm) (Renzo and Maio, 2007; Ye et al., 2005; Ye et al., 2008). As in our TFM simulations, qualitative homogeneous bed expansion was reported even in the absence of any IPF component (Renzo and Maio, 2007; T. Kobayashi, 2002). Fig. 4.14 shows the comparison of our TFM data with that of DEM (Renzo and Maio, 2007) for same input parameters (Table 4.4) without incorporation of IPF component in either case.

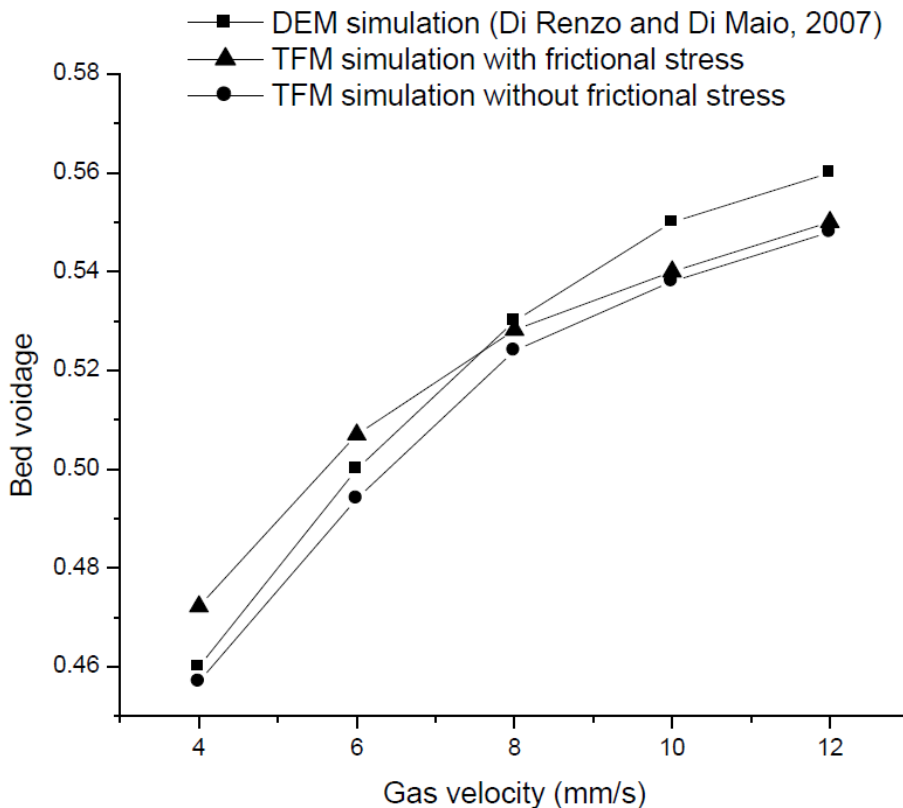


Fig. 4.14 Validation of our fine mesh TFM simulated expansion curves (with and without frictional stress) with DEM predictions.

Table 4.4

Main parameters used in DEM and TFM simulations

Parameter	DEM Simulation (Renzo and Maio, 2007)	TFM Simulation (This work)
Domain size	0.5×3×0.007 cm ³	4×12cm ²
No. of particles	10,000	-
Particle diameter (µm)	70	70
Particle density (g/cc)	1	1
Initial packed bed solid volume fraction	0.54	0.55
Friction coefficient	0.3	Syamlal O'Brien model (1993)
Time step (s)	5×10 ⁻⁷	^a 10 ⁻⁵
Restitution coefficient	0.9	0.9
Gas phase density (kg/m ³)	1.205	1.138
Gas phase viscosity (kg/m-s)	1.8×10 ⁻⁵	1.663×10 ⁻⁵
Minimum bubbling voidage (at 8.4 mm/s)	0.543	0.53 – 0.54
Velocity below which homogeneous distribution of particles is seen (mm/s)	9	6 (Fig. 4.12, sec 4.2.1.2)

^a Time step in range 10⁻⁸ to 10⁻⁵ was required during the initial 4 to 5s.

Both models show a good match overall but TFM voidages are lower than DEM values in the transition regime. In the homogeneous regime, the difference reduces. Clearly,

TFM with frictional stress model of Syamlal O'Brien (Syamlal et al., 1993) over predicts voidage when compared to DEM (2 – 4% error) which is in line with our findings in section 4.2.3. When correction for frictional stress (as described in section 4.2.3) is made, TFM exactly matches DEM in velocity range 4 – 8 mm/s (not shown in Fig. 4.14 for clarity). The DEM work reported that distinct bubbles appeared at 12mm/s (Renzo and Maio, 2007) which matches well with our TFM simulations (see Fig. 4.12(a) in section 4.2.1.2). In the DEM simulations, the minimum bubbling voidage was found at the condition of critical stability (Gibilaro, 2001) which corresponded to 8.4 mm/s. At this velocity, the voidage predicted by DEM is slightly higher (1.5%) than that of TFM. This is because the particle description in DEM can better capture the meso-scale voids which are most likely responsible for bed expansion at this point. Simulation predictions (Bolded values in Table 4.8) from both models show a good match. Hence the fine mesh TFM captures all the hydrodynamic forces adequately and accurately. This finding is the basis for the next section

4.2.2.2 Simulated bed voidage at minimum bubbling conditions and density effect

We first determined a common velocity range covering homogeneous expansion and transition regime for the particles studied (Table 4.5, p1 – p5). Minimum fluidization velocities (u_{mf}) calculated from the correlation of Abrahamsen and Geldart (Abrahamsen and Geldart, 1980) are given in Table 4.5. The u_{mf} values show that the Geldart A particles (p1 – p4) are fluidized for velocities ≥ 4 or 5mm/s. As discussed in section 4.2.1.2, multiple bubbles resembling a freely bubbling bed break out at gas velocity

12mm/s (u'_b). Hence fine mesh TFM simulations were conducted in velocity range 4 – 12mm/s, for different ρ_p .

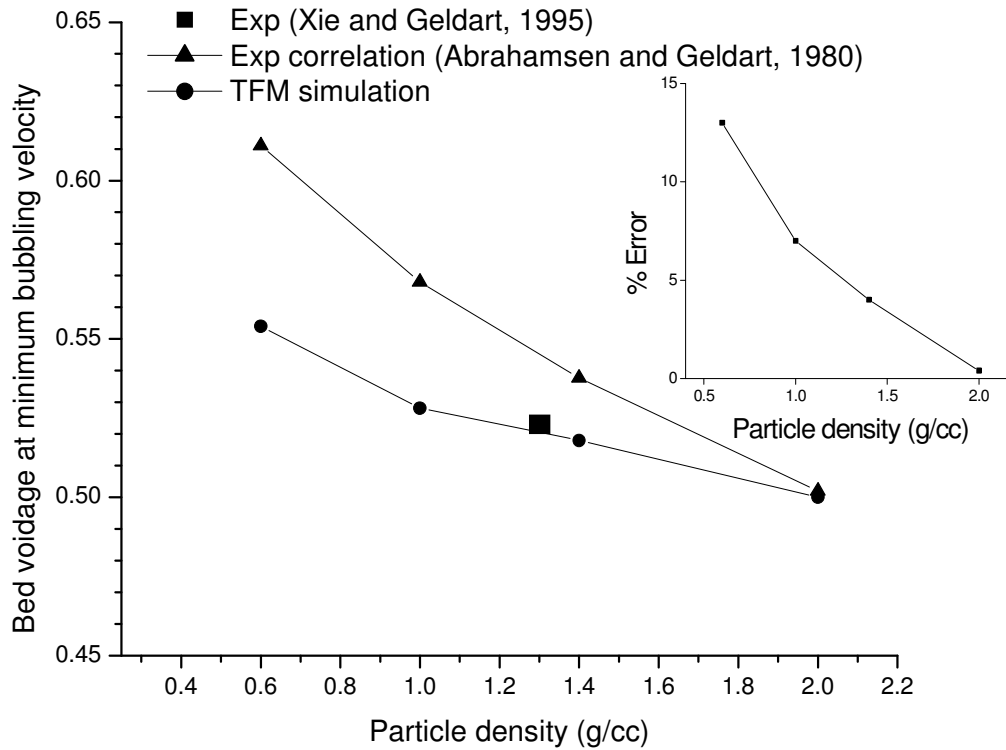


Fig. 4.15 Comparison of empirical and TFM simulated data: Variation of voidage at minimum bubbling velocity (9 mm/s) with particle density.

Bed voidage at minimum bubbling conditions is significance because it is the maximum expansion the homogeneous bed can attain. For the purpose of comparing minimum bubbling voidages at different ρ_p , the minimum bubbling velocity from empirical correlation of Abrahamsen and Geldart (Abrahamsen and Geldart, 1980) (Eq.

4.2) was considered. The calculated value ($\approx 9\text{mm/s}$) is independent of ρ_p for the particles studied.

$$u_{mb,e} = \frac{2.07d_p\rho_g^{0.06}}{\mu_g^{0.347}} \exp(0.716F_{45}) \quad (4.2)$$

$$\frac{H_{mb}}{H_{mf}} = \frac{5.50\rho_g^{0.028} \mu^{0.115} \exp(0.158F_{45})}{d_p^{0.176} g^{0.205} (\rho_p - \rho_g)^{0.205}} \quad (4.3)$$

Table 4.5 compares the experimental voidage (ε_{mb_exp}), calculated from the bed height (H) correlation of Abrahamsen and Geldart (Abrahamsen and Geldart, 1980) (Eq. 4.3), to simulated values (ε_{mb_sim}) for different ρ_p . It was found that ε_{mb_exp} was always higher than ε_{mb_sim} , by the % error reported in Table 4.5, for all the particles studied.

$$\%Error = \frac{\varepsilon_{mb_exp} - \varepsilon_{mb_sim}}{\varepsilon_{mb_exp}} \times 100 \quad (4.4)$$

Further, as seen from the inset in Fig. 4.15, %error drops exponentially with ρ_p . Clearly, ε_{mb_sim} approaches ε_{mb_exp} as ρ_p increases and the particles move towards the A/B boundary on the Geldart's classification chart i.e. B Group characteristics increase. The % error in simulated values may be attributed to the unaccounted fraction of expansion caused by IPFs. We discuss this in detail in section 4.2.3 where we attempt to quantify IPFs by the %expansion increase that they cause.

Table 4.5 Comparison of simulated minimum bubbling voidages with experimental values of Abrahamsen and Geldart (1980) for different particle densities.

Particle	ρ_p	Geldart	u_{mf} (mm/s)	$(H_{mb}/H_{mf})_{exp}$ ^b	$(H_{mb}/H_{mf})_{sim}$	ϵ_{mb_exp}	ϵ_{mb_sim}	% Error
Designation^a	(g/cc)	Group						
p1	0.6	A	1.41	1.4157	1.2880	0.6110	0.5540	13.3
p2	1	A	2.28	1.2748	1.1657	0.5680	0.5282	7
p3	1.4	A	3.12	1.1897	1.1411	0.5377	0.5180	3.7
p4	2	A	4.35	1.1058	1.1000	0.5020	0.5000	0.4
p5	2.8	A/B	5.96	1.0321	1.0577	0.3600	0.4800	-33.3

^a $d_p = 70\mu\text{m}$, for all particles

^b $F_{45} = 0$ was taken in Eq.3 because mono-sized particles were assumed in simulation

The -33.3% error for p5 may be ignored, as it was entailed because of the artificially imposed maximum solid packing ($\epsilon_s^{max} = 0.55$) in the bed domain which was required to model packed bed conditions.

As in Table 4.5, literature mainly compares CFD simulated values to predictions from correlations of Abrahamsen and Geldart (Abrahamsen and Geldart, 1980). For a broader comparison, Table 4.6 includes more recent experimental works. Simulation predictions of %expansion (Eq. 5) are comparable to those from the experimental works. Again we find the experimental voidages higher than simulated values, except in the case of Sidorenko and Rhodes (Sidorenko and Rhodes, 2004). This is due, at least in part, to their higher value of d_p .

$$\%Expansion = \frac{\epsilon_{mb} - \epsilon_{mf}}{\epsilon_{mf}} \times 100 \quad (4.5)$$

The ϵ_{mb} value reported from the work of Xie and Geldart (Xie and Geldart, 1995b) shows a very close match with simulation (Fig. 4.15). It must be noted that the $u_{mb,e}$ they reported (5.37mm/s) was lower than that from Abrahamsen and Geldart (Abrahamsen and Geldart, 1980) (8.781mm/s). In simulation, the aspect that 0.11 mass fraction of particles had $d_p < 45 \mu\text{m}$ ($F_{45} = 0.11$) was neglected due to mono-size particle assumption.

Table 4.6 Comparison of simulated expansion with experimental works other than Abrahamsen and Geldart (Abrahamsen and Geldart, 1980)

Work	ρ_p (kg/m ³)	d_p (μ m)	ε_{mf}	ε_{mb}	% Expansion
Our TFM simulation data	1400	70	0.45	0.52	15.56
Xie and Geldart (1995)	1310	68	0.45	0.525	16.67
Sidorenko and Rhodes (2004)	1330	77	0.42	0.47	11.9
Our TFM simulation data	1420	71	0.505	0.534	5.7
Lettieri et al. (2002)	1420	71	0.505	0.553	9.5

4.2.2.3 Homogeneous expansion in the Richardson–Zaki form

Fig. 4.16 shows the simulated pseudo steady state bed voidages in the velocity range 4 – 12mm/s. Pseudo steady state was usually reached after 5s of simulation flow time, but proper differentiation in voidage values was seen only after 15 – 20s. Transient voidage profiles shown in Fig. 4.17 illustrate this for p4. Hence voidage values obtained after 15 – 20s of flow time were plotted in Fig. 4.16. Each curve corresponds to a constant ρ_p value. Clearly the homogeneous expansion (4 – 9mm/s) was more for the lighter particles (p1, p2) than the heavier ones (p3, p4 and p5) as expected from the hydrodynamics.

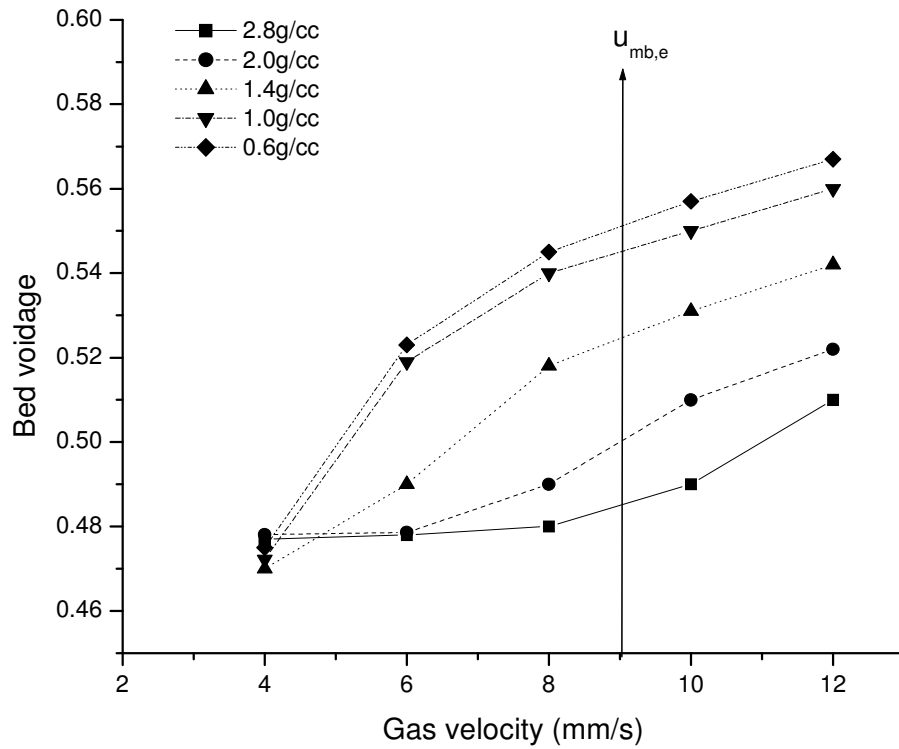


Fig. 4.16 Effect of particle density on bed expansion in homogeneous and transition regime. Particle diameter was constant at 70 μm .

In literature, homogeneous expansion of Geldart A particles is usually represented by the empirical expression of Richardson and Zaki (R-Z) (Richardson and Zaki, 1954) which follows the power law:

$$\ln u = n \ln \varepsilon + \ln u_t \quad (4.6)$$

Where u and ε are inlet gas velocity (cm/s) and bed voidage respectively and u_t (cm/s) is the single particle terminal velocity. The R-Z parameter: n is the slope of the $\ln(u)$ vs $\ln(\varepsilon)$ plot which we aim to determine and analyze in the rest of this section.

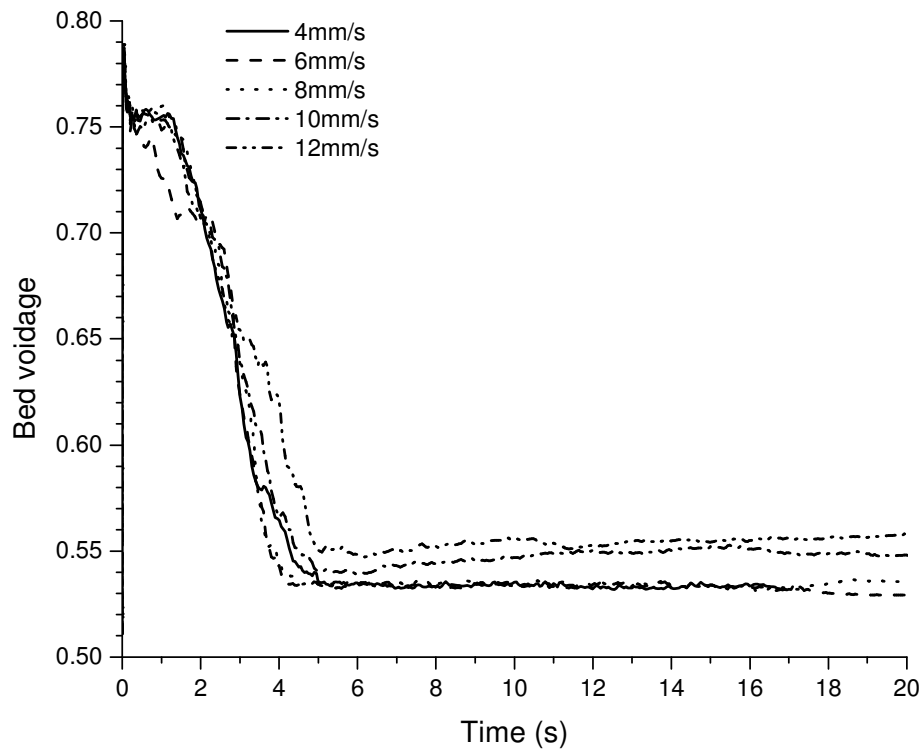


Fig. 4.17 Transient bed voidage profiles for p4 (70 μm , 2 g/cc): Proper differentiation in voidages seen after 20 s of flow time as voids/dilutes take time to develop or stabilize.

Despite the limitations in defining $u_{mb,e}$ as detailed in section 4.2.1.1, since the following treatment necessitated it, 9mm/s was taken from empirical correlation of Abrahamsen and Geldart (1980). Each simulated expansion curve (Fig.4.16) was fitted to the R-Z expression and the parameters reported in Table 4.7 (see n^o and u_i^o).

Table 4.7 Richardson-Zaki parameters for simulated expansion curves in Fig. 4.16

ρ_p (g/cc)	n^b	u_t^b (cm/s)	n^h	u_t^h (cm/s)	n^o	u_t^o (cm/s)
0.6	10.14	359.1	4.41	10.8	10.2	24.19
1	9.94	381.2	5.1	18.2	6.21	40.05
1.4	8.54	223.9	7.02	83.4	7.29	101.94
1.42	Exp – Lettieri et al. (2002)		R-Z (1954) correlation for liquids			
	9.6	245.4	4.6	19.5		
2	7.26	136.4	20.93	10^{32}	10.57	1277.67
2.8	5.04	34.1	76.2	10^{33}	10.81	1772.2

^b For the part of the expansion curve after $u_{mb,e}$ (i.e. velocity range of 9 – 12mm/s).

^h For the part of the expansion curve before $u_{mb,e}$ (i.e. velocity range of 4 – 9mm/s).

^o For the part of the entire expansion curve (i.e. velocity range of 4 – 12mm/s).

We observed that the part of the expansion curve before $u_{mb,e}$ fitted better with a different set of R-Z parameters than the part after $u_{mb,e}$. This amounted to constructing two straight lines with different slopes for one expansion curve. Fig. 4.18 illustrates this for the expansion curve with $\rho_p = 1.4\text{g/cc}$ from Fig. 4.16. By contrast, experimental expansion in R-Z form, shows only one slope (Fig. 4.18) signifying an apparent ‘continuity’ in expansion characteristics through the homogeneous expansion and transition to bubbling regime i.e. both regimes are best modeled by the same R-Z parameters. We attributed this ‘discontinuity’ in the simulated expansion to voidage over prediction by frictional stress

model which was operated only in the homogeneous regime. The difference between n^h and n^b (Table 4.7) can also be explained by this. Section 4.2.3 elaborates further.

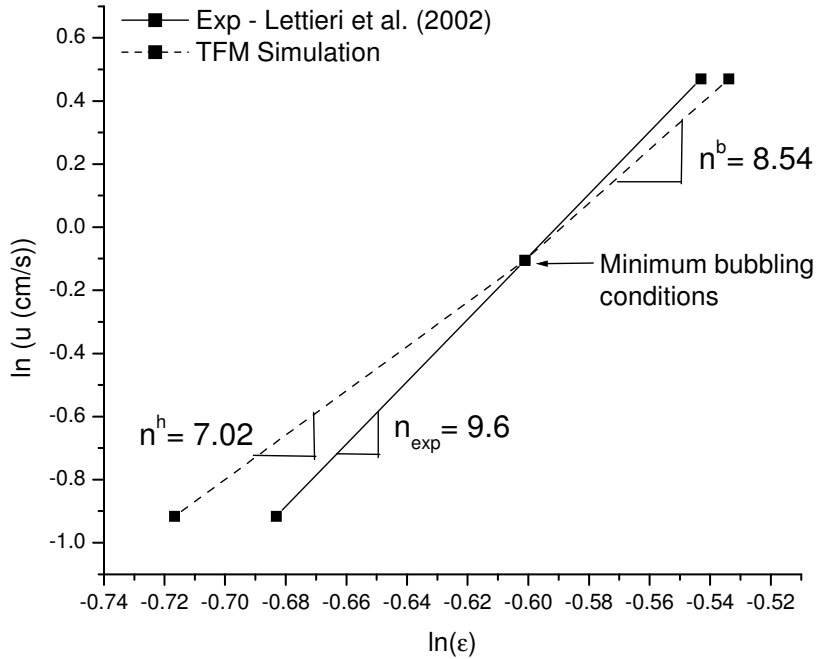


Fig. 4.18 Richardson and Zaki form of experimental and simulated expansion curves ($\rho_p= 1.4\text{g/cc}$) showing two slopes for the simulated data.

Particle properties used in the simulation and experimental work are listed in Table 4.8. Since the difference in ε_{mf} was not appreciable, its effect on n was neglected. Table 4.7 shows that the parameters (n^b , u_t^b for 1.4g/cc) for transition regime (9 – 12mm/s) matched much better with experimentally obtained values of Lettieri et al. (Lettieri et al., 2002), than the parameters (n^h , u_t^h for 1.4g/cc) for the homogeneous regime (4 – 9mm/s). The value of n (9.6) obtained from Lettieri et al. (Lettieri et al., 2002) was higher than Both n^b and n^h , which we attribute to IPFs causing expansion in the experimental system and unaccounted for in simulation.

Table 4.8 Bed parameters used in TFM simulation and experimental work of Lettieri et al. (Lettieri et al., 2002)

Powder	d_p (μm)	ρ_p (g/cc)	ε_{mf}	ε_{mb}	F_{45}^a
Exp – (Lettieri et al., 2002)	71	1.42	0.505	0.553	0.05
TFM Simulated	70	1.4	0.45	0.518	0

^a Mass fraction of particles with d_p less than 45 μm .

Other force interactions within the bed remaining same, a higher value of n was previously associated with manifestation of IPFs and lower values were predicted from the purely hydrodynamic correlations of liquid fluidization (Oyebanjo Oke et al., 2013). Prediction of u_t from Stokes law and n from R-Z correlation for liquids (Richardson and Zaki, 1954), as reported in Lettieri et al. (Lettieri et al., 2002), are also reported in Table 4.7 for comparison. Table 4.7 shows that u_t^o increases with ρ_p as predicted by Stokes law. For increase in ρ_p (0.6 – 1.4g/cc) n^o decrease from 10.2 to 7.3. This occurs because the increase in Re_t caused by increasing u_t^o , dampens the effect that change in average bed voidage has on average gas velocity in the bed i.e. n decreases. These findings show that n decreases with Re_t as in liquid sedimentation, but the n values themselves are clearly *higher*. For liquid system, n is expected to decrease from 4.65 to 2.39 as we move from viscous to inertial flow regime (Richardson and Zaki, 1954). This is valid when particle to vessel diameter is small enough to neglect wall effects, as in our case. For higher ρ_p (p4 and p5) expansion curves in Fig. 4.16 clearly *deviate* from the power law type R-Z expression. The aberrant parameters (italics in Table 4.7) simply

reflect poor logarithmic fit of data which we attribute to declining Geldart A characteristics. This is further discussed in section 4.2.4

4.2.3 Quantification of IPFs

In section 4.2.2.3, it was reasonable to compare n values obtained from simulation and experiment even though the initial packed bed voidage (ε_{mf}) in both cases differed (Table 4.8). In this section ε_{mf} was also kept identical with experimental work (Lettieri et al., 2002). We assumed mono-sized spheres in simulation since particle size distribution was reportedly narrow in experiment (Lettieri et al., 2002). Our aim in this section is not to model IPFs but rather to infer their effect on bed expansion, and thereby to quantify them via this indirect approach. Capability of TFM to accurately capture hydrodynamic forces in bubbling regime, when adequately fine mesh is used is well documented in the literature (Wang et al., 2009, 2011), and since the fine mesh of size $0.4\text{mm} \times 0.4\text{mm}$ ($5.7d_p$) afforded such a high density of CFD nodes, it was reasonable to assume that all the hydrodynamic forces were adequately and accurately captured in the simulation of bed voidage (validated for homogeneous regime in previous sections). The IPF effects were then determined by comparison with corresponding experimental bed voidages. It is also assumed that IPFs do exist in the homogeneous expansion regime as is well evidenced by the literature (Mutsers and Rietema, 1977; Rietema et al., 1993; Rietema and Piepers, 1990).

The forces that need to be accounted for in the gas-phase are interstitial gas stresses, gravity and the drag exerted on the gas phase by the particle surfaces. In the solid phase the drag of the fluid on the solid has to be represented and also the stress due

to particle-particle contacts as well as gravity. All of these stresses are represented by closures in the TFM. The most important among them is the inter-phase drag force which is the dominating force in gas-solid fluidization (Loha et al., 2012; Wang et al., 2011). The use of fine mesh resolved sub-grid or meso-scale structures and therefore adequately accounted for the drag in our TFM simulations. In addition to these stresses, in regions of the bed where the solids packing approaches packed bed state there is contact or rubbing between particles. The resulting frictional stresses must be accounted for in the description of the solid-phase stress. A threshold solids packing is required to demark regions in the bed where frictional stress must be accounted for in addition to other stresses. This threshold solid volume fraction was estimated from inspection of simulation snapshots to be $0.47(\epsilon_s^{min})$. Fig 4.19(b) shows the regions in the bed (coloured black) with solids packing from 0.47 to the maximum allowable value ($\epsilon_s^{max} = 0.495$) or packed bed state. This way frictional stress is accounted for in the most compacted 2.5% of the bed which includes the entire bed from 4- 8 mm/s, but only the black regions shown for 10-14mm/s. Fig. 4.20 shows the voidage curve obtained using frictional stress model (Syamlal et al., 1993) which operated in solid packing range 0.47- 0.495. Table 4.9 gives the voidages or average gas volume fractions calculated from the steady state simulations shown in Fig. 4.19(a).

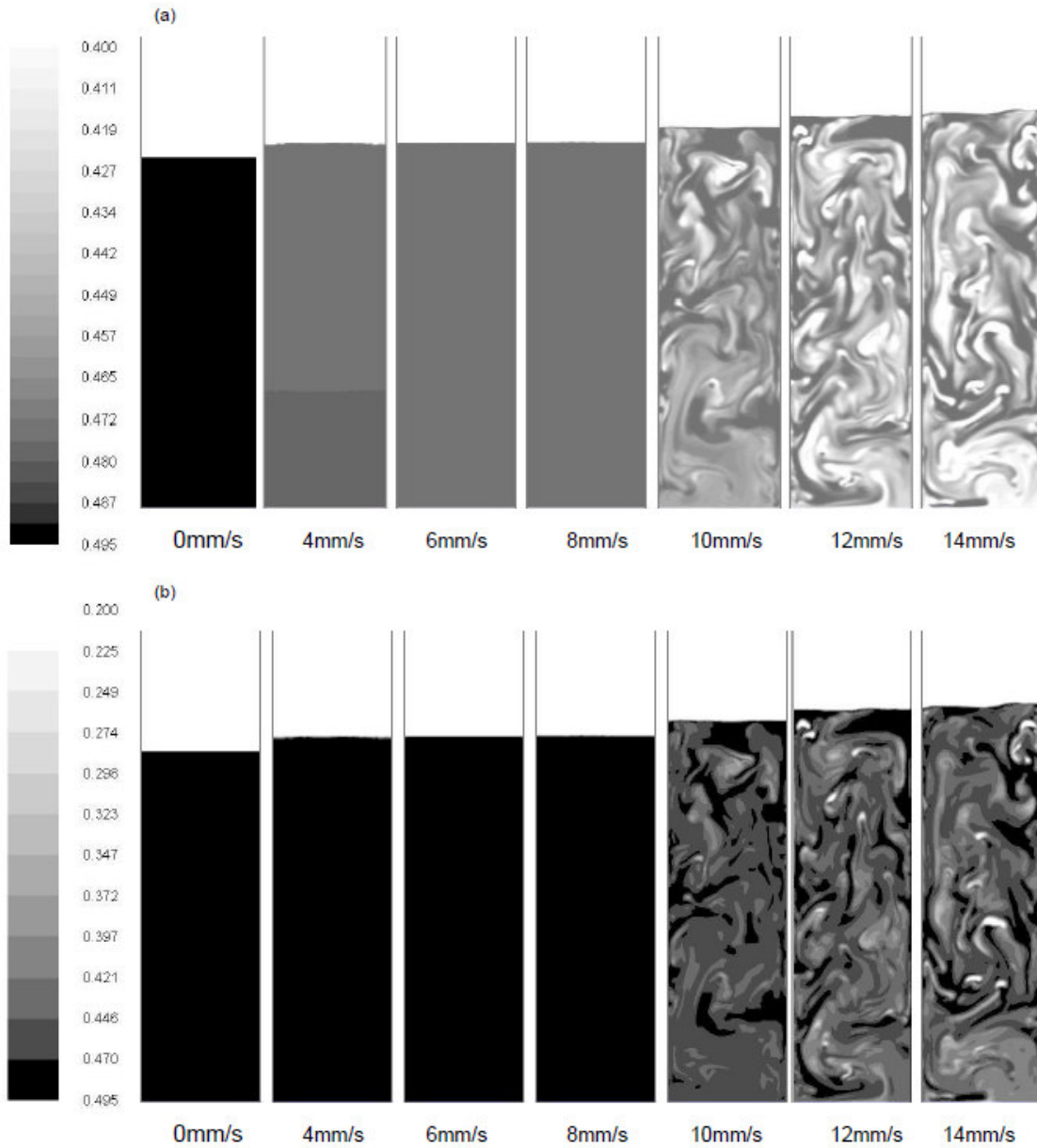


Fig. 4.19 Snapshots of solid concentration contours of the fluidized bed at pseudo steady state conditions for inlet velocities in the velocity range 4-12mm/s using Gidaspow drag law. Particle properties simulated are given in Table 4.8. Fine mesh (0.16mm^2) was used. (a) Reveals the extent of dilution; (b) Reveals the regions (coloured black) where frictional stress operates (solids packing in range 0.47-0.495).

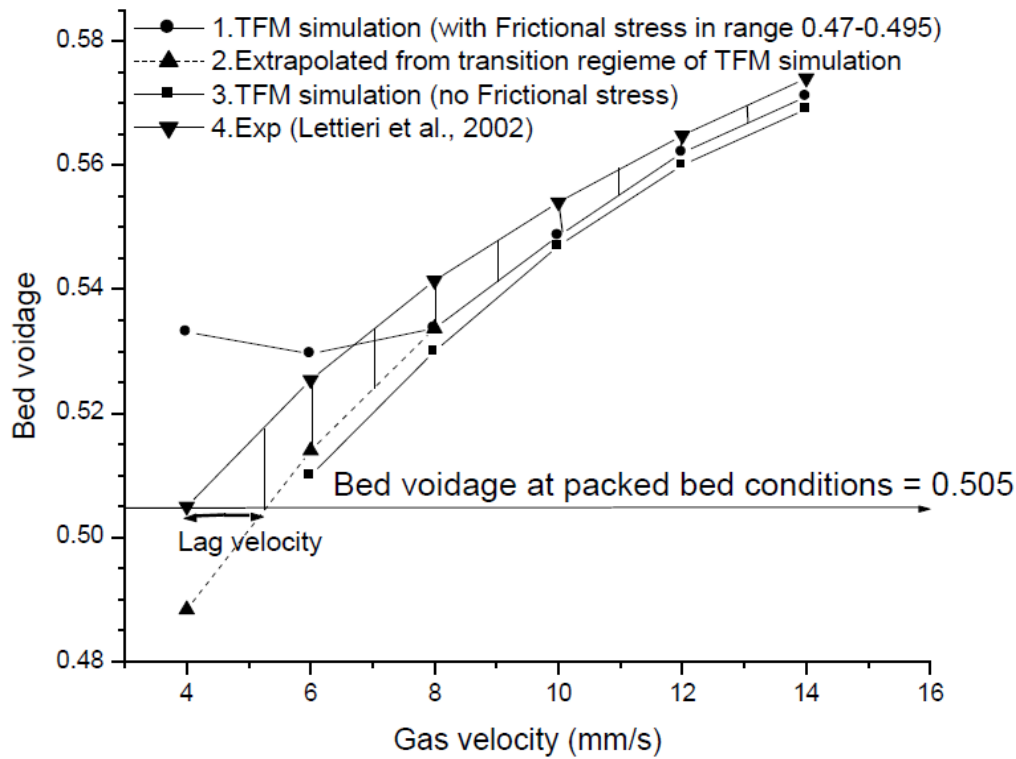


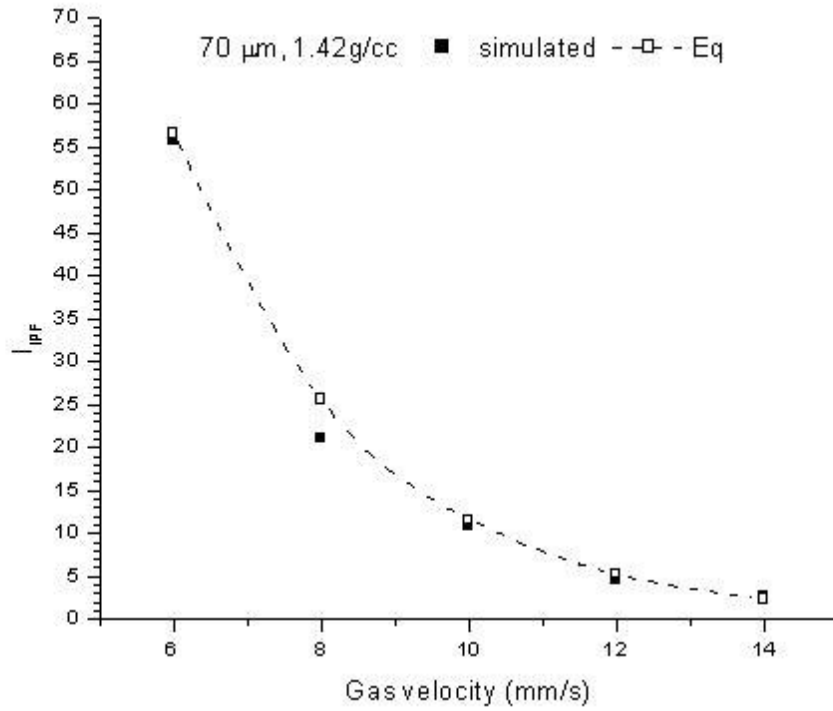
Fig. 4.20 Comparison of experimental and simulated expansion curves: The difference in expansion (stripped area) is attributed to IPFs.

Clearly the expansion curve (curve 1) is over estimated when compared to the experimental data (curve 4) in the homogeneous expansion regime, specifically in velocity range 4 - 6 mm/s. To make a correction for this, we extrapolated the curve from the transition regime with the aid of the R-Z parameters. This amounts to scaling down the frictional stresses in the homogeneous regime to a level proportional to their presence in transition regime. This assumption is in line with the trend of the experimental curve, where both regimes are modeled by the same R-Z parameters. The difference between the expansion curve due to the scaled down frictional stresses (curve 1 in transition regime and 3 in homogeneous regime) and *no* frictional stress seemed reasonable to attribute to frictional stresses alone. Since the frictional stresses were accounted for in this way, it

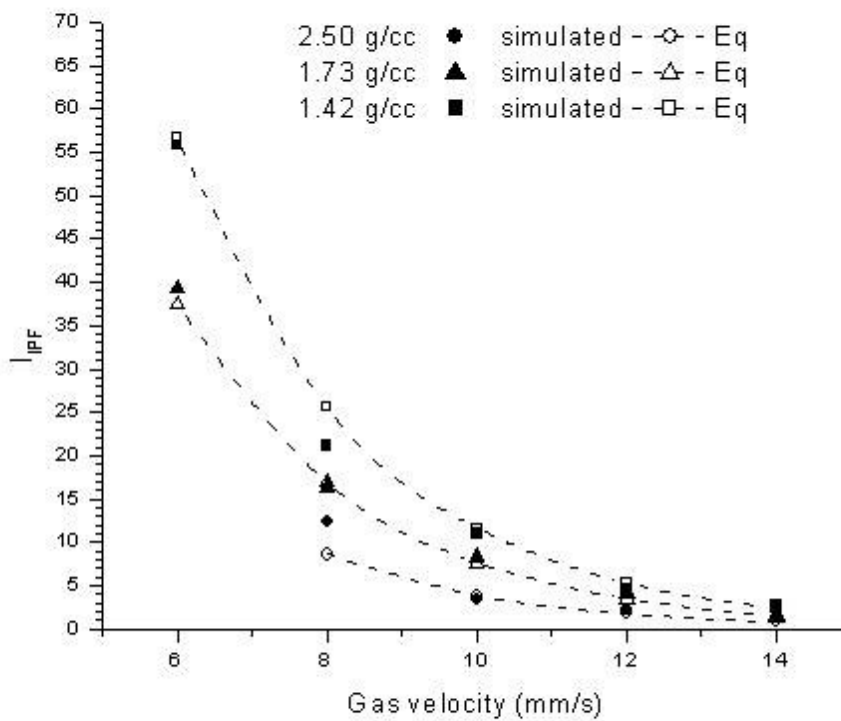
was reasonable to attribute the voidage difference between curve 4 and 2 in the homogeneous regime and curve 4 and 1 in the transition regime, to the only unaccounted forces, namely IPFs. Hence we define a dimensionless IPF index (I_{IPF}) which is that fraction of the total bed expansion (from the reference voidage: ϵ_{mf}) caused by the collaborative effect of IPFs.

$$I_{IPF} = \frac{(\epsilon_{exp} - \epsilon_{sim})}{(\epsilon_{exp} - \epsilon_{mf})} \times 100 \quad (4.7)$$

Implicit in this definition is the premise that IPFs are in fact present in homogeneous regime, which is well supported by literature. It was reported that moderately strong IPFs aid fluidization unlike very strong IPFs, such as those present in group C powders (Lee et al., 1999). This would explain why the experimental voidages are higher than simulated ones, except for the overestimation due to frictional stress model. Therefore we infer that the IPFs in homogeneously expanded Geldart A particles are moderately strong. Also, it was estimated that only the fourth decimal place of the voidage values was affected by numerical errors inherit in the calculations. These errors are truncation error during discretization and CPU round-off error. Hence the voidage difference between curves was outside the margin of error. Allowing for these errors as well as the fact that a conservative estimate of frictional stress was taken, the proposed I_{IPF} therefore quantifies a *maximum* limit of the effect of IPFs on bed expansion. The lag velocity delineated in Fig.4.20 is also a measurable effect of IPFs.



(a)



(b)

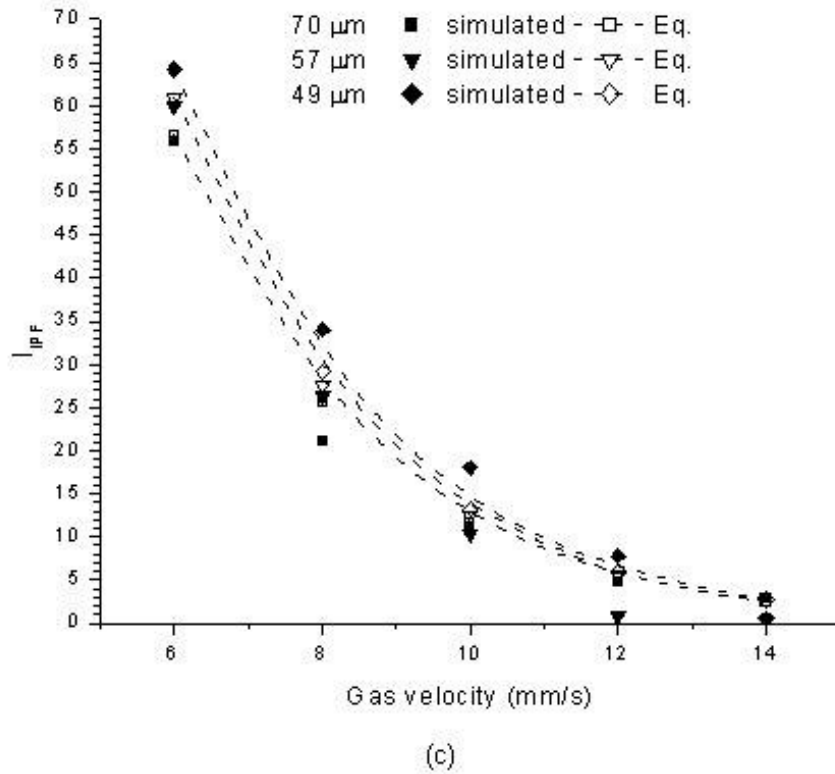


Fig. 4.21 I_{IPF} calculated from experimental voidages and our simulated voidages (Eq.7) for different particle systems, showing (a) effect of gas velocity for system 70 μm , 1.42 g/cc (Lettieri et al., 2002); (b) effect of particle density. Systems had similar particle diameter : 66 μm , 2.5 g/cc (Oke et al., 2015), 75.1 μm , 1.73 g/cc (Bruni et al., 2006), 70 μm , 1.42 g/cc (Lettieri et al., 2002); (c) effect of particle diameter. Systems had constant particle density of 1.42 g/cc and varying particle diameters of 70 μm , 57 μm and 49 μm (Lettieri et al., 2002).

Fig. 4.21 (a) shows that the I_{IPF} calculated from Fig. 4.20 drops exponentially with inlet gas velocity. The trend confirms that IPFs are negligible in bubbling region but present in the homogeneous expansion regime. I_{IPF} was likewise calculated for different

particle systems from our simulated bed voidages and corresponding experimental voidages from literature. Increase in particle density and diameter reduced the relevance of IPFs as shown by Fig. 4.21 (b) and (c) respectively. Clearly, for particle systems closer to the A/B boundary, I_{IPF} reduces. An expression to fit the I_{IPF} data in Fig. 4.21 (a-c) is presented (Eq. 8) for all parameters in SI units. The coefficient of determination or R^2 for the non-linear regression was 0.985. The expression shows that I_{IPF} is inversely proportional with gas velocity, particle density and particle diameter. Since I_{IPF} is dimensionless, the coefficient 3.2306×10^7 has units of $\text{kg}^{1.9691}/\text{m}^{5.5509}$ and the exponent -395.5306 has units of s/m . The expression would be unsuitable for particle diameters less than $45\mu\text{m}$ due to the effect of fines (Abrahamsen and Geldart, 1980).

$$I_{IPF} = 3.2306 \times 10^7 \exp(-395.5306u) \times \rho_p^{-1.9691} d_p^{-0.3564} \quad (4.8)$$

u (mm/s)	ε_{exp}	$^a \varepsilon_{sim_extrap}$	ε_{sim}					$\varepsilon_{exp} - \varepsilon_{sim_extrap}$ (% error ^f)	I_{IPF}
			With FS ^b	%OE ^c	%OE ^d	Without FS	%Diff ^e		
4	0.505	0.48836	0.5331	9.16	5.56	-	-	0.0166 (3.290)	-
6	0.525	0.51401	0.5296	3.03	0.80	0.510	3.84	0.0113 (2.167)	55.83
8	0.541	0.5337		-		0.530	0.70	0.0077 (1.422)	21.15
10	0.554	0.5486		-		0.547	0.30	0.0054 (0.970)	11.02
12	0.565	0.5620		-		0.560	0.35	0.0028 (0.490)	4.68
14	0.574	0.5710				0.569	0.35		

Table 4.9 Bed voidages for the expansion curves shown in Fig. 4.20 including % voidage differences between curves and index for IPF

^a Simulated + extrapolated voidages i.e. curve 1 in transition regime and curve 3 in homogeneous regime (Fig. 4.20).

^b FS is frictional stress

^c The %over estimation of ε_{sim} with frictional stress with respect to ε_{exp} .

^d The %over estimation of ε_{sim} with frictional stress with respect to ε_{sim_extrap} .

^e The %difference between ε_{sim} with FS and ε_{sim} without FS with respect to ε_{sim} without FS.

^f The %difference between ε_{sim} and ε_{sim_extrap} with respect to ε_{sim_extrap} .

4.2.4 The Geldart group A/B transition

In the Geldart chart for classification of powders (Geldart, 1973), the group A/B boundary is given by the line $(\rho_p - \rho_g)d_p = 225$ (Fig. 4.22) implying an abrupt transition. TFM simulations show a more gradual transition from group A to B behavior. We assume that the extent to which the bed expansion fits the R-Z curve as a measure of group A behavior. By this criterion Fig. 4.16 (section 4.2.2.3) suggests a reduction in group A behavior as ρ_p increases i.e. the powder properties approach the Geldart A/B boundary. The simulated powders are marked by triangles in Fig. 4.22.

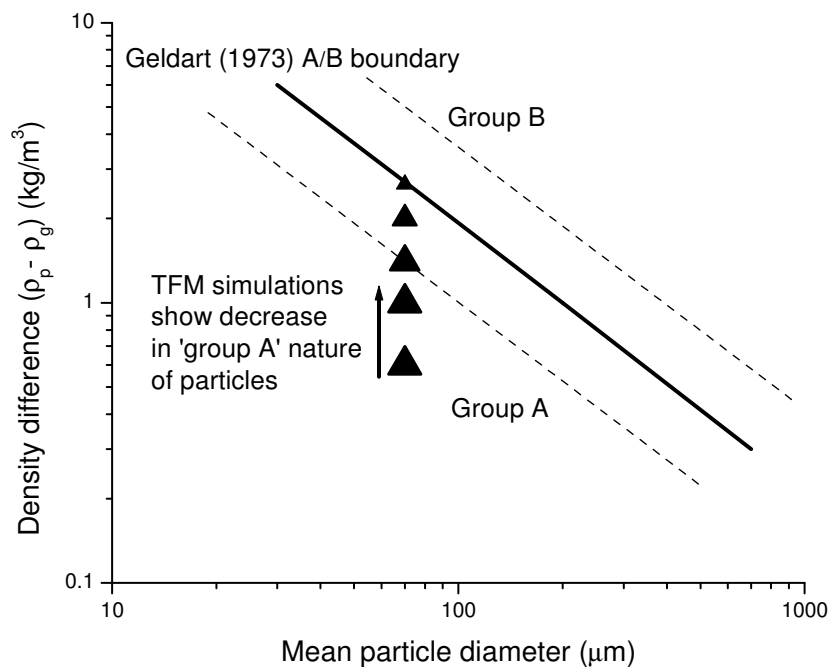


Fig. 4.22 Geldart, 1973, classification of Group A and B powders where the area between the dotted lines represents A/B transition as predicted by TFM.

The size of the triangles qualitatively relate to the extent of group A behavior observed. Beyond the dotted line group A behavior diminishes. Assuming a similar transition to group B behavior, a dotted line was constructed at the same distance from the A/B boundary, but in the group B region. The region between the dotted lines is the suggested A/B transition region as deduced from fine mesh TFM simulations.

Validation of these boundaries would require more simulations (especially for group B particles). Hence the dotted boundaries are presented only as preliminary findings.

4.2.5 Limitations of the fine mesh size study

- i. An ad hoc method was used to incorporate the frictional stress in the simulations. This was required to scale down the frictional stress model of Syamlal O'Brien (1993). It remains to test the more recent frictional stress models in literature for more realistic predictions of bed voidage.
- ii. It might be argued that a better way to gauge strength of IPFs would be to implement a closure for it (which is currently lacking in TFM), and find the level of cohesive strength which allows matching of simulated and experimental bed voidages. With further development of continuum model for IPFs, this could be done for future work.
- iii. The group A/B transition region on the Geldart chart was demarcated based on five particles of different densities. Different values of diameter must also be tested for a more comprehensive investigation. Further, sufficient particles in the group B region must also be tested to confirm these findings.

4.3 Reacting bed study on oxychlorination reaction of ethylene: Fixed bed, bubbling bed and homogeneous bed mode.

The experimental set-up and kinetics of the oxychlorination of ethylene from Carrubba, (1968), was simulated using TFM. All details of the reaction kinetics, set-up and modeling are presented in Chapter 3, section 3.2.2.1. For isothermal reaction of oxychlorination of ethylene in fixed or fluidized bed, four process variables exist: the feed mole fractions of ethylene, oxygen and hydrogen chloride as well as the gas residence time based on inlet gas velocity. In our study, the feed mole fractions of hydrogen chloride and oxygen were kept constant ($\text{HCl}/\text{O}_2 = 3.626$) and only ethylene mole fraction at inlet was varied for two values 0.1964 and 0.1122. These values are referred to as high and low ethylene mass fractions at inlet/ ethylene rich and ethylene lean feeds/ high and low ethylene concentration. For a fixed feed composition the residence time was varied in the simulations. Ethylene mass fraction in the feed and gas residence time were chosen to be varied from among the four process variables because the experimental study of Carrubba (1968) showed that they had the most effect on reaction rate. Details of simulation inputs are given in Table 3.11, and these were identical with the ‘spoke’ runs in experimental work of Carrubba (1968). N_2 gas was used as the bulk or ‘make-up’ gas to ensure that the total feed pressure added up to one atmosphere pressure.

The following sections discuss the results mainly of the simulated reaction rate and conversion for ethylene rich and ethylene lean feeds. Simulations were carried out in three modes (a) fixed bed (b) Bubbling bed (c) Homogeneous bed. The fixed bed

experimental reaction rates of Carrubba (1968) was used to validate corresponding simulated reaction rates.

4.3.1 Validation of TFM simulations of reacting bed: Fixed bed mode

Both the simulated and experimental values of reaction rate are presented for higher inlet ethylene mass fraction (0.1964) and a low inlet ethylene mole fraction (0.1122) in Fig. 4.23 and Fig. 4.24 respectively. The simulated reaction rate values plotted are the average value of reaction rate of all the cells in the bed, after near steady state was reached. Hence each point represents one simulation run. The parameters varied in the simulation were inlet gas velocity and ethylene inlet mass fraction (details are in Table 3.11)

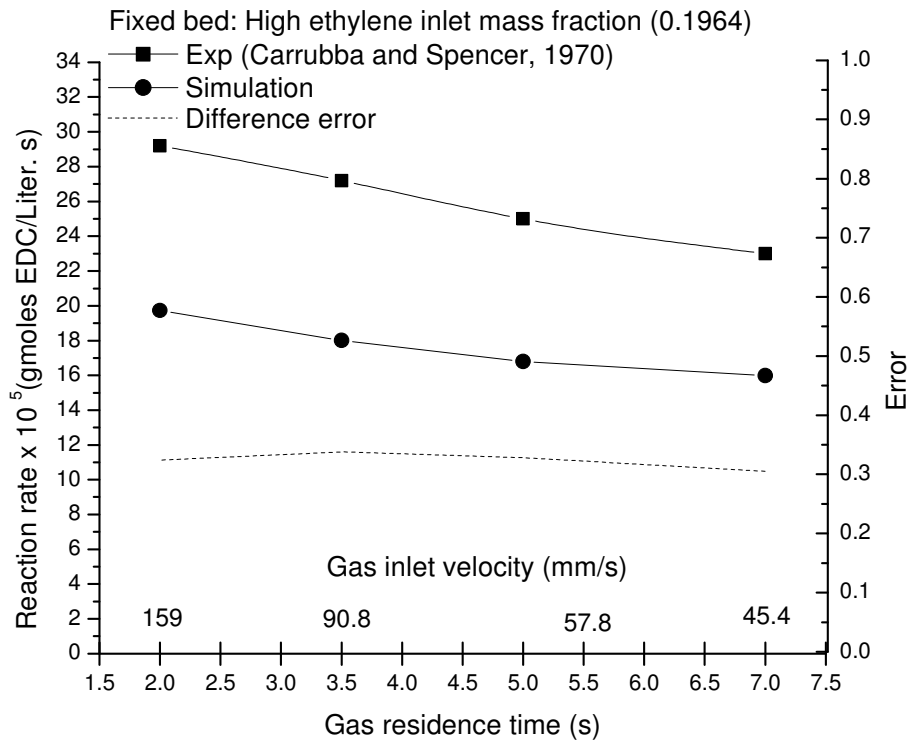


Fig. 4.23 Steady state reaction rates of oxychlorination of ethylene in fixed bed mode with high ethylene inlet mass fraction (0.1964): Comparison of experiment and TFM simulations is shown. The difference error is also reported.

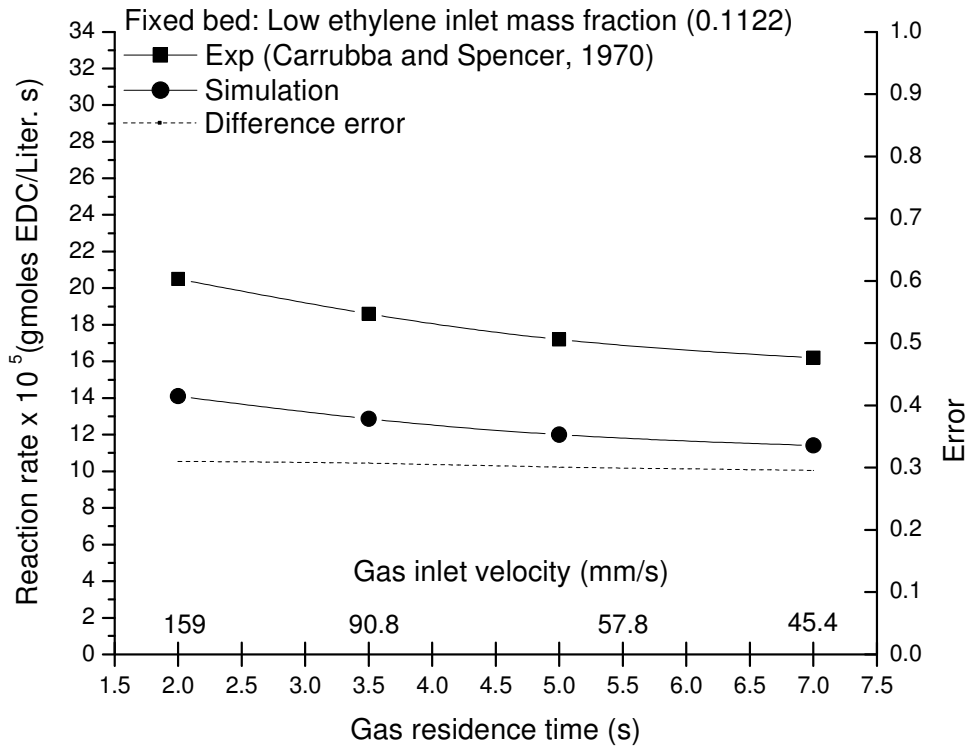


Fig. 4.24 Steady state reaction rates of oxychlorination of ethylene in fixed bed mode with low ethylene inlet mass fraction (0.1122): Comparison of experiment and TFM simulations is shown. The difference error is also reported.

4.3.1.1 Simulation of reaction rate of EDC in fixed bed

When the inlet ethylene mass fraction was lower, the reaction rates (both experimental and simulated) were also lower, because of the high power of ethylene concentration in rate expression (Eq. 3.8). Agreement in trend was found between the experimental and

simulated values of reaction rate. As the gas residence time increased the steady state reaction rate decreased as expected. The simulated reaction rate values were approximately 30% less than the experimental values and this remained nearly constant for all velocity values and also for the two values of inlet mass fraction of ethylene. It is inferred that the main reason for this could be the limitation imposed by the simulation in modeling the chemical interaction of the solid catalyst in the bed. In the simulation, the solid species did not take part in the reaction, since only the overall reaction was considered. The solid interaction was accounted for by scaling the reaction rate in each cell by the mass fraction of the solid. This ensured that no reaction took place in purely gas phase and that the cell reaction rate was directly proportional to the mass fraction of solid i.e. number of active sites. This method of scaling the reaction rate in each cell most likely produced a lesser value of reaction rate than in the experimental bed. Other simulation assumptions like 2D, perfectly isothermal conditions, perfectly uniform concentration of ethylene at inlet, and those relating to reactor hydrodynamics were also probable contributors to the difference error.

4.3.1.2 Simulation of ethylene conversion

The simulated conversions obtained for ethylene rich and ethylene lean feeds are presented in Fig. 4.25. When the ethylene mass fraction at inlet was lower the conversion was higher for the same gas residence time because more catalyst was available per mass of ethylene. Further the decrease in the inlet gas velocity caused increase of the gas residence time in the bed, making more provision for ethylene to convert to EDC. Hence

increase in gas residence time, and reduction in ethylene mass fraction in the feed contributes to higher ethylene conversion values. This trend is validated by the experimental work of Currubba (1968); however, the experimental values of ethylene conversion are marginally higher. Experimental conversions were reported in the range 5 - 18%, whereas simulated conversions (Fig. 4.25) were in the range 2 - 10%. These lower simulated values can be explained by the lower reaction rates resulting from the simulation as discussed in section 4.3.1.

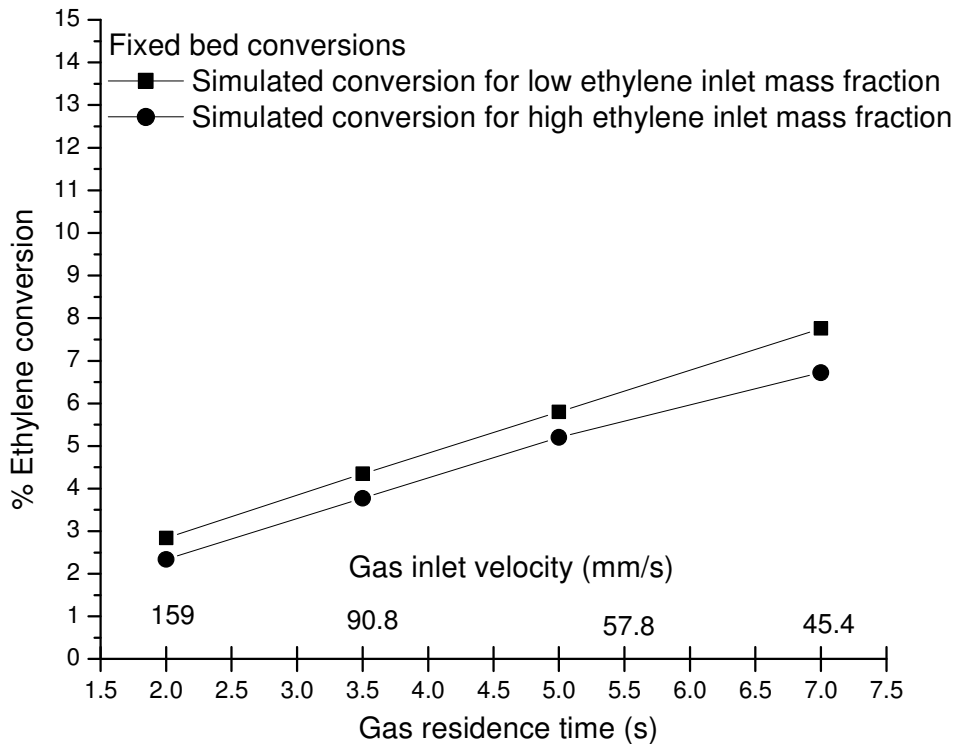


Fig. 4.25 Simulated ethylene conversion in fixed bed operation for low and high ethylene inlet mass fractions.

4.3.1.3 Effect of changing ethylene feed concentration on reaction rate and conversion in fixed bed

Fig. 4.26 presents the plot of the normalized difference of reaction rate and conversion against the gas residence time. The purpose of the plot is to reveal which parameter (reaction rate or conversion) is more affected by the same change in the ethylene feed mass fraction.

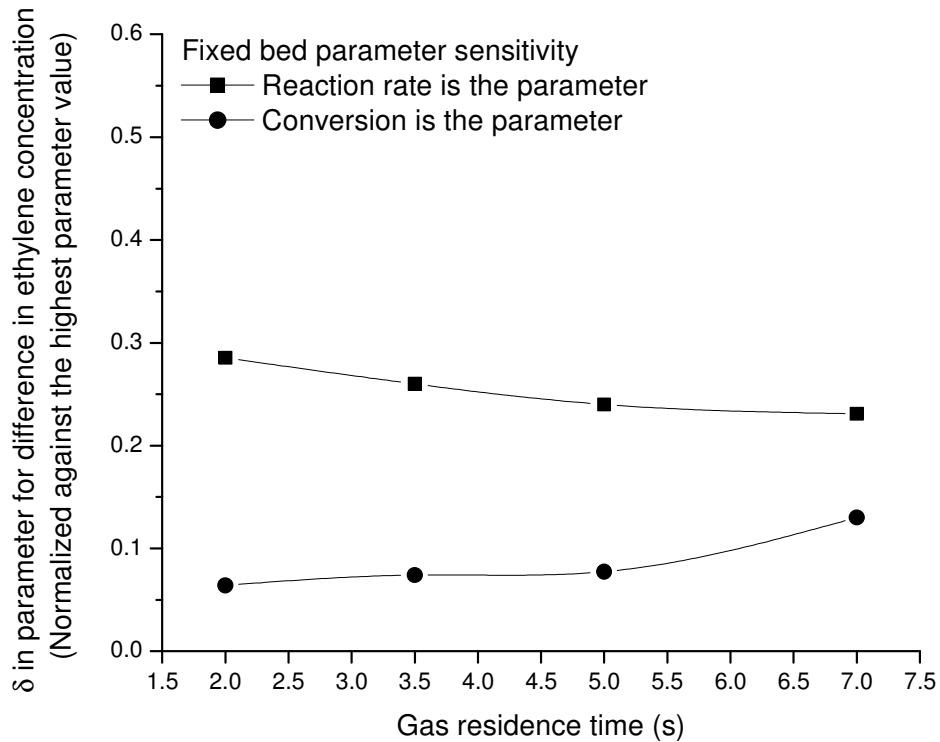


Fig. 4.26 The normalized difference in the parameter (reaction rate or conversion) for high and low ethylene feed concentration is plotted against gas residence time, for fixed bed operation. This indicates the effect of changing ethylene concentration on reaction rate or conversion.

The normalized difference in the parameter (reaction rate or conversion) was found as follows: the difference in the parameter value obtained for the case of ethylene rich and ethylene lean feed was obtained from simulation for each value of gas residence time. This difference was divided by the highest value of that parameter for the purpose of normalizing the difference. Clearly reaction rate is more affected than ethylene conversion in this regard. Hence an increase or decrease in ethylene feed mass fraction had greater effect on the magnitude of reaction rate than that of ethylene conversion.

4.3.2 TFM simulations of reacting bed: Bubbling bed of Geldart A particles

In the previous section (4.3.1) the TFM simulations of oxychlorination of ethylene occurring in the fixed bed was validated. The fixed bed mode employed Geldart D particles characterized by large diameter (3.175 mm) particles of high density (3800 kg/m^3) in the bed. If the fixed bed particles (Geldart D) used in experiment are replaced with particles of Geldart A, then for the same velocity range, the bed can be expected to operate in the bubbling regime. The purpose of this section is to simulate the bubbling bed and compare the simulated reaction rates and conversions with those of the fixed bed mode. Accordingly only the particle properties of the fixed bed were changed to those of typical Geldart A particles ($70\mu\text{m}$, 2000kg/m^3). All the remaining simulation details were kept unchanged to enable comparison of the bubbling bed mode of operation with that of the fixed bed.

4.3.2.1 Simulation of reaction rate of EDC in bubbling regime

The average steady state reaction rates in the bubbling beds are clearly lower than those of the fixed bed (Fig. 4.27 and Fig. 4.28). The reason for this could be attributed to a higher bed expansion.

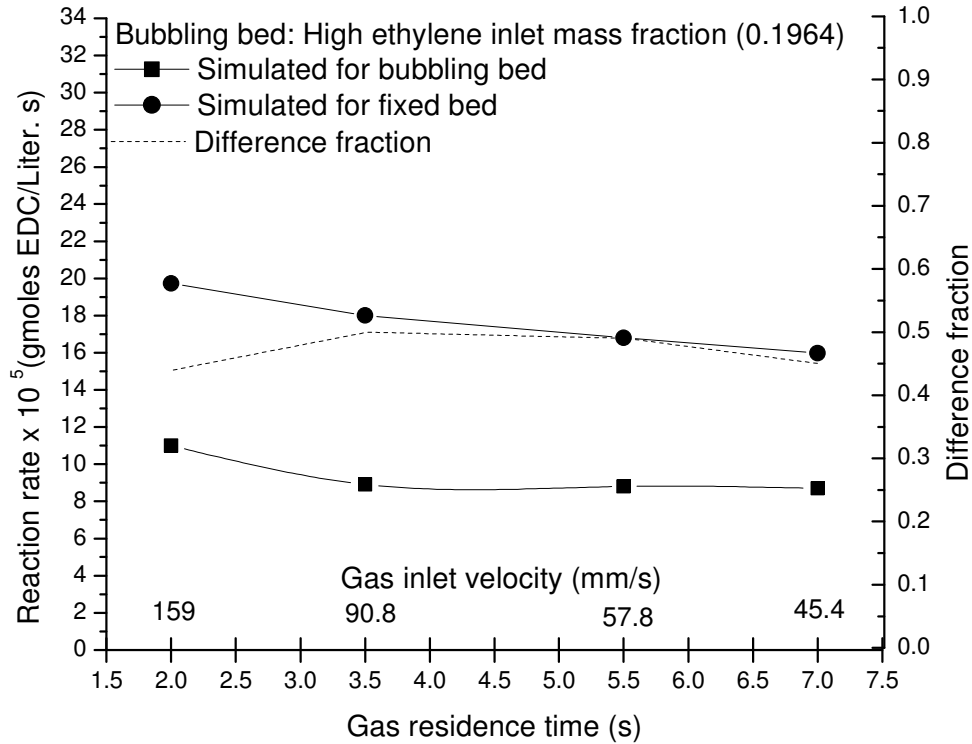


Fig. 4.27 Steady state reaction rates of oxychlorination of ethylene in bubbling bed mode with high ethylene inlet mass fraction (0.1964): Comparison of simulated values in fixed bed and bubbling bed is shown. The difference error is also reported.

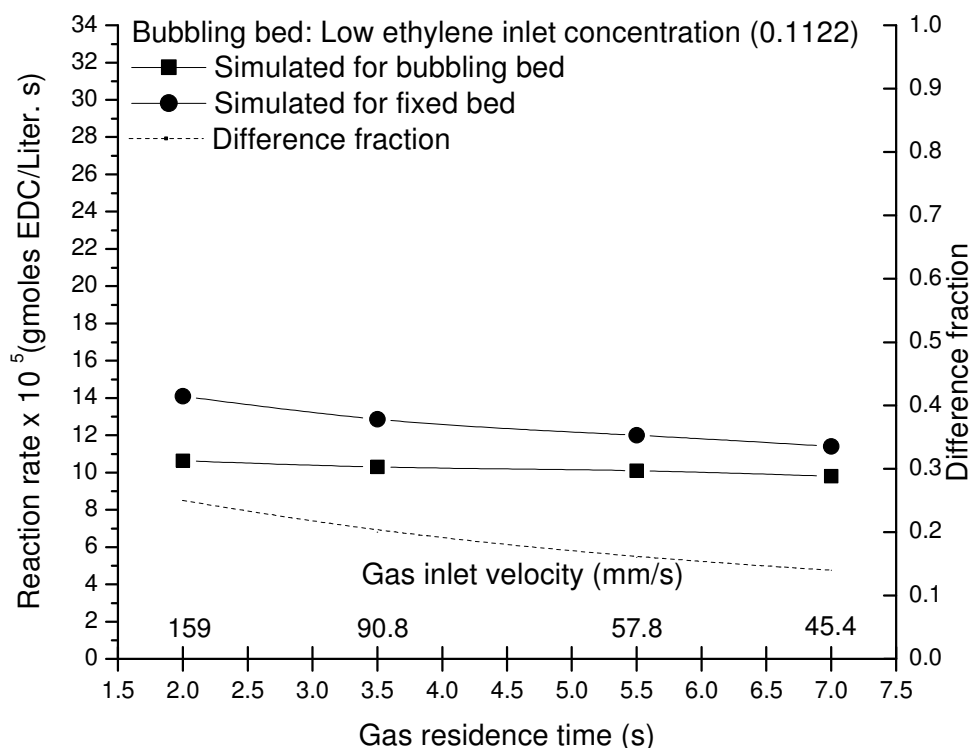


Fig. 4.28 Steady state reaction rates of oxychlorination of ethylene in bubbling bed mode with low ethylene inlet mass fraction (0.1122): Comparison of simulated values in fixed bed and bubbling bed is shown. The difference error is also reported.

Since the bubbling bed of Geldart A particles produced higher gas hold-up than the fixed bed (Fig. 4.29), reaction rates dropped because of the lower average solid packing in bubbling bed when compared to fixed bed. However, since a larger volume of bed was available for reaction in the case of bubbling bed, overall conversion of ethylene was found higher than in the fixed bed (shown in following section) in spite of the lower reaction rate. This can be visualized from comparing the steady state contours of ethylene

mass fraction (Fig. 4.30) in the fixed bed and bubbling bed. For same inlet velocity, comparison between fixed and bubbling beds shows lower ethylene concentration towards the top of the bed. For EDC (product) concentration the reverse is true. This is clearly seen from Fig. 4.31. The finding that conversion in bubbling bed is higher than in fixed bed given same conditions is contrary to what is normally observed and needs to be confirmed by 3D simulations in future work.

The difference in reaction rates from fixed and bubbling beds, is more pronounced for high ethylene feed concentration (0.4 to 0.5 from Fig. 4.27) than for low ethylene feed concentration (in range of 0.15 to 0.25 from Fig. 4.28). To attribute this to any one factor is difficult, since the solid mass fraction *as well as* the ethylene mass fraction per CFD cell was changing from fixed to bubbling bed. The lower size and density of the Geldart A particles also affected the hydrodynamics which impacted reaction rate. Hence a collaboration of these factors was probably responsible for the result that reaction rate of the bubbling bed was closer to that of fixed bed for lower ethylene feed mass fraction. Hence, higher ethylene feed mass fraction created more disparity in the reaction rates between fixed and bubbling beds.

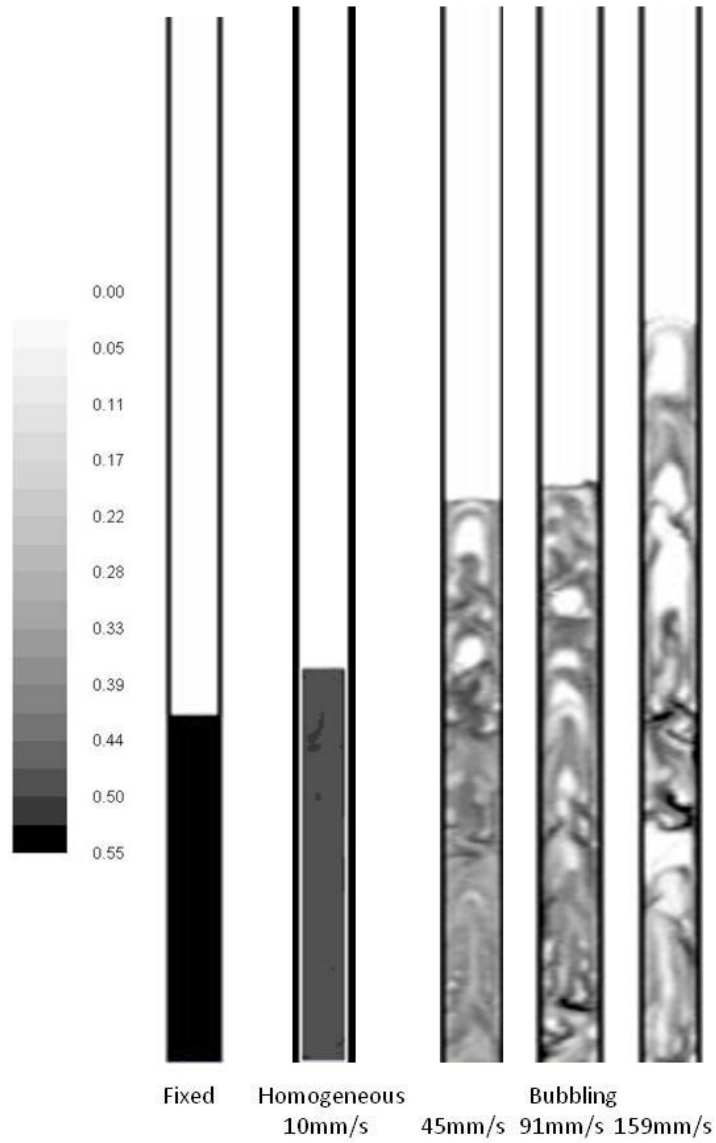


Fig. 4.29 Snapshots of solid concentration contours for fixed, homogeneous and bubbling beds (different inlet gas velocities) which are undergoing reaction of oxychlorination of ethylene.

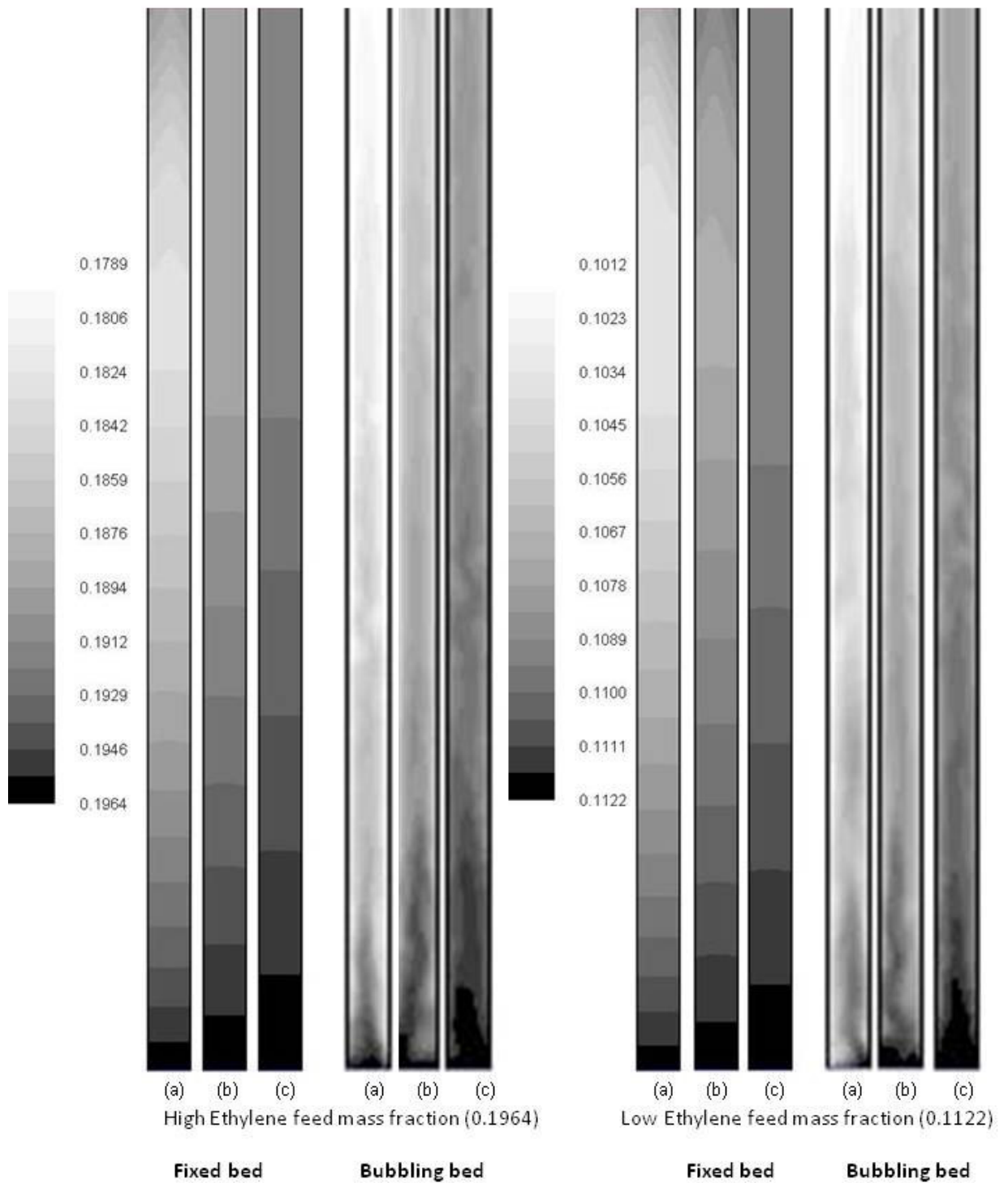


Fig. 4.30 Steady state contours of ethylene mass fraction for fixed and bubbling beds at three different inlet gas velocities (a) 45mm/s; (b) 92mm/s; and (c) 159mm/s.

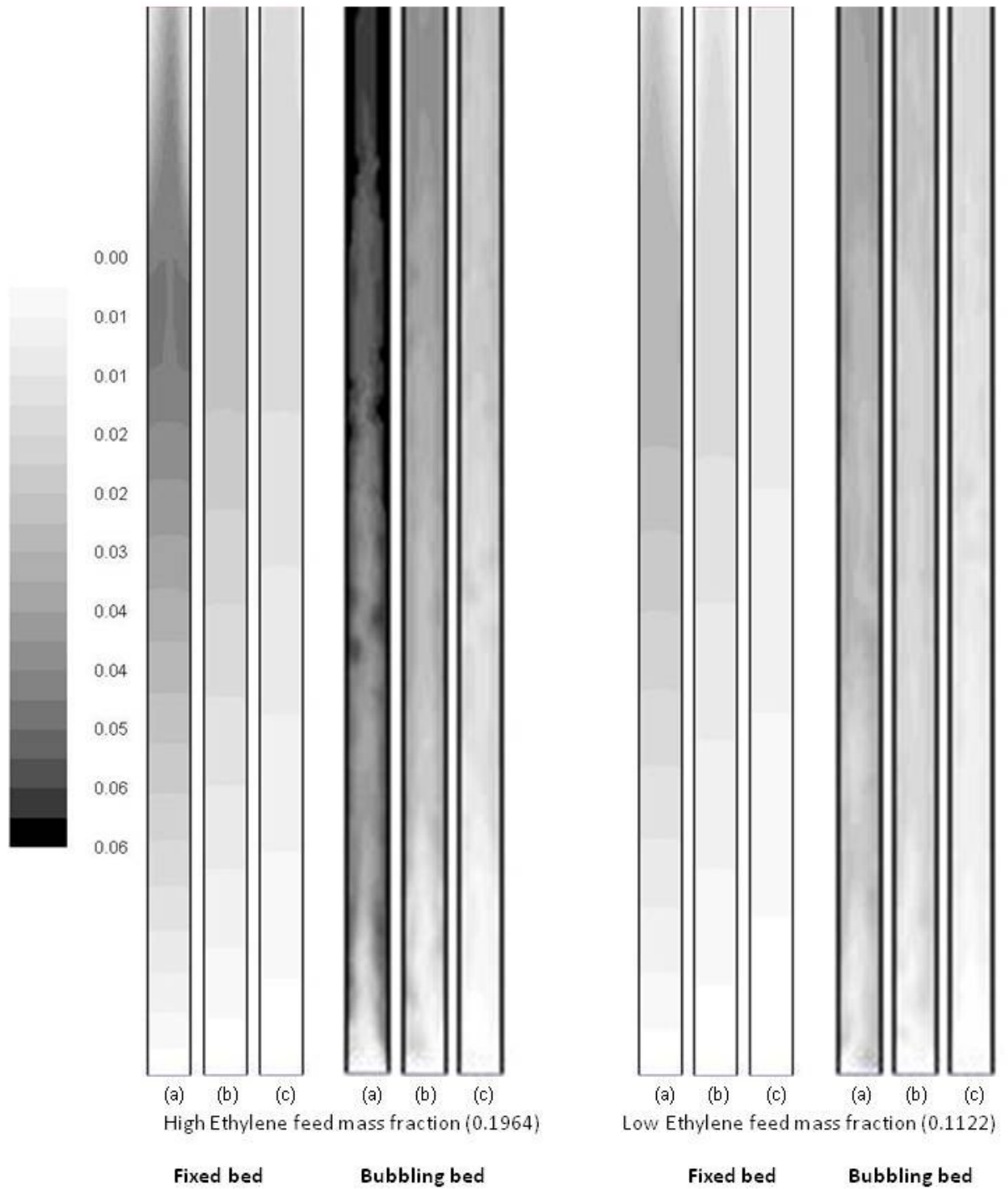


Fig. 4.31 Steady state contours of EDC mass fraction for fixed and bubbling beds at three different inlet gas velocities (a) 45mm/s; (b) 92mm/s; and (c) 159mm/s.

4.3.2.2 Simulation of ethylene conversion in bubbling regime

Overall, the ethylene conversion values are higher in bubbling bed than in fixed bed (Fig. 4.32) since higher ethylene conversion results from longer gas residence time experienced in the bubbling bed when compared to fixed bed for same inlet gas velocity. Further, low ethylene inlet mass fraction results in marginally higher conversions when compared to high ethylene inlet mass fraction, which can be explained in the same way as for the fixed bed in section 4.3.1.2.

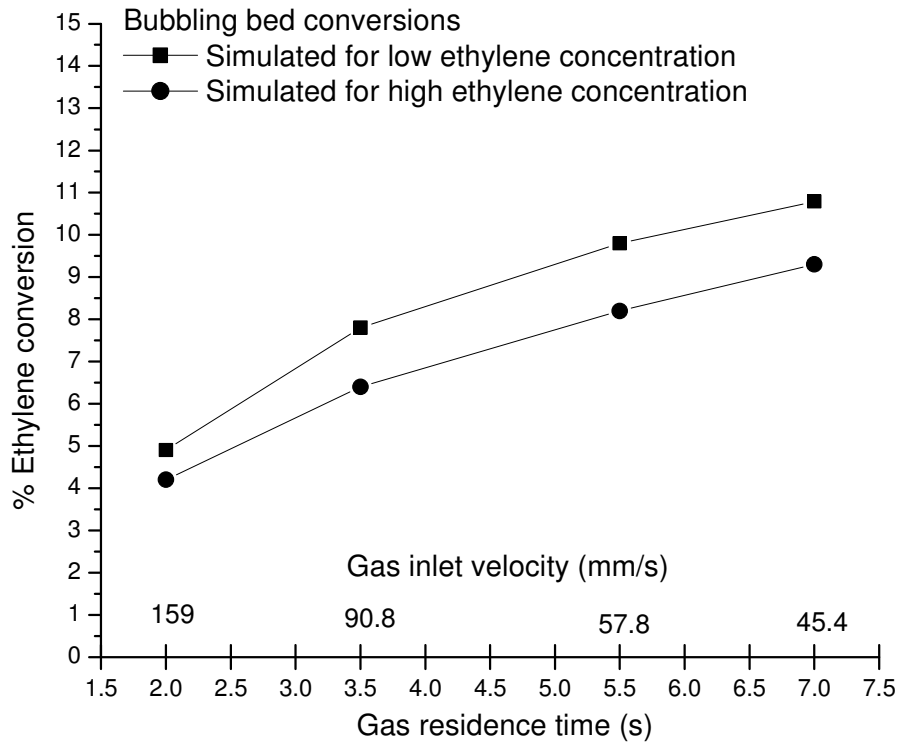


Fig. 4.32 Simulated ethylene conversion in bubbling bed operation for low and high ethylene inlet mole fractions.

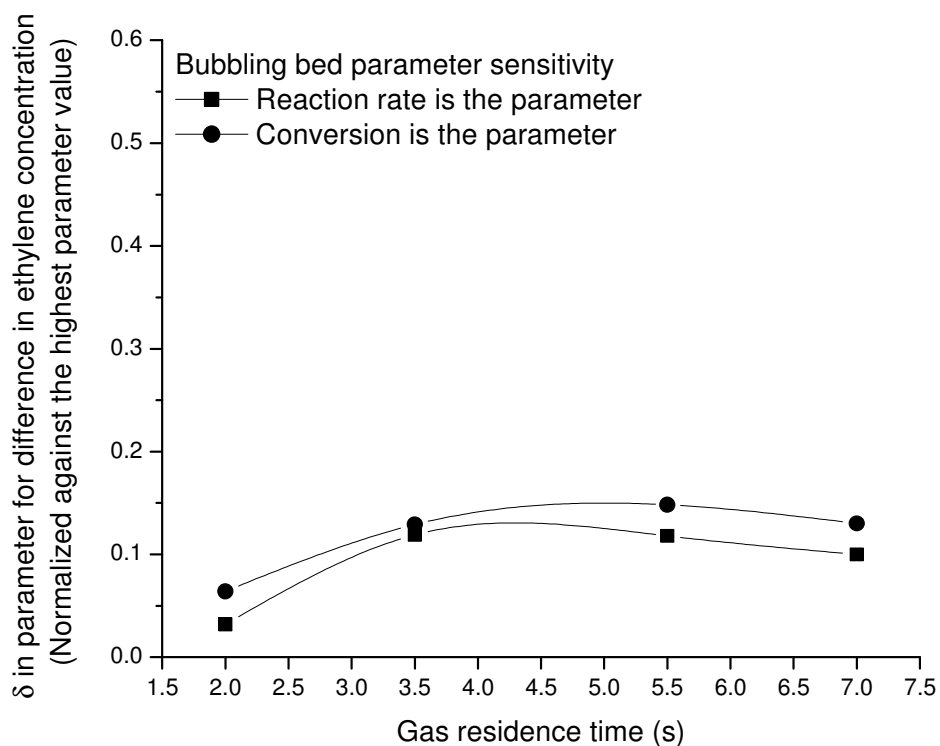


Fig. 4.33 The normalized difference in the parameter (reaction rate or conversion) for high and low ethylene feed concentration is plotted against gas residence time, for bubbling bed operation. This plot indicates the effect of changing ethylene concentration on reaction rate or conversion.

4.3.2.3 Effect of changing ethylene feed concentration on reaction rate and conversion in bubbling bed

Fig. 4.33 presents the plot of the normalized difference of reaction rate and conversion against the gas residence time. The purpose of the plot is to reveal which parameter (reaction rate or conversion) is more affected by the same change in the ethylene feed

mass fraction as explained in section 4.3.1.3. For the bubbling bed, the effect of changing feed ethylene mass fraction clearly has a lower effect on reaction rate, than in the case of fixed bed (Fig. 4.26). In general, it is observed that the better gas mixing caused by the particle fluidization in bubbling bed, tends to suppress the difference in conversion or reaction rate caused by change in ethylene feed mass fraction. Therefore, such changes affect fixed bed more acutely.

4.3.3 TFM simulations of reacting bed: Homogeneous bed of Geldart A particles

To simulate the homogeneously expanded bed with simultaneous reaction all simulation details were kept the same as in the case of bubbling bed simulations, except the inlet gas velocities which were: 4, 6, 8, 10, and 12 mm/s. These velocities ensured that the bed was in homogeneous expansion regime. these low velocities (compared to the velocity range of the bubbling bed which was 45.4 – 159 mm/s) took an inordinate amount of time (150 - 200s of flow time) for the inert bed to come to steady state, after which reaction was activated in the simulation and more time was required for the reacting bed to come to a steady state. The monitors of reaction rate and exiting ethylene mass fraction were seen to approach steady state asymptotically, requiring long flow times to reach steady state. Hence the results presented in this section were obtained after around 200s of flow time, which was estimated to be close to steady state conditions.

4.3.3.1 Simulation of ethylene conversion in homogeneous regime

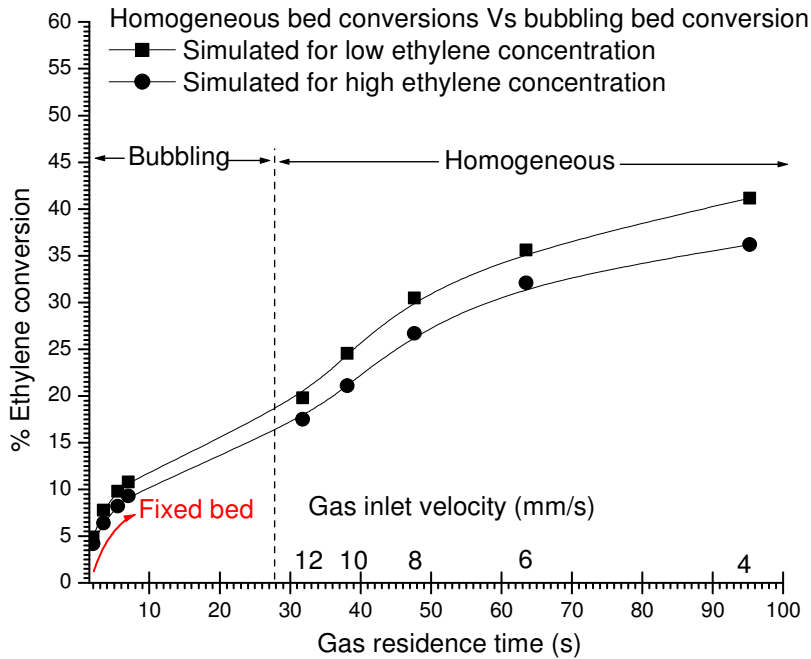


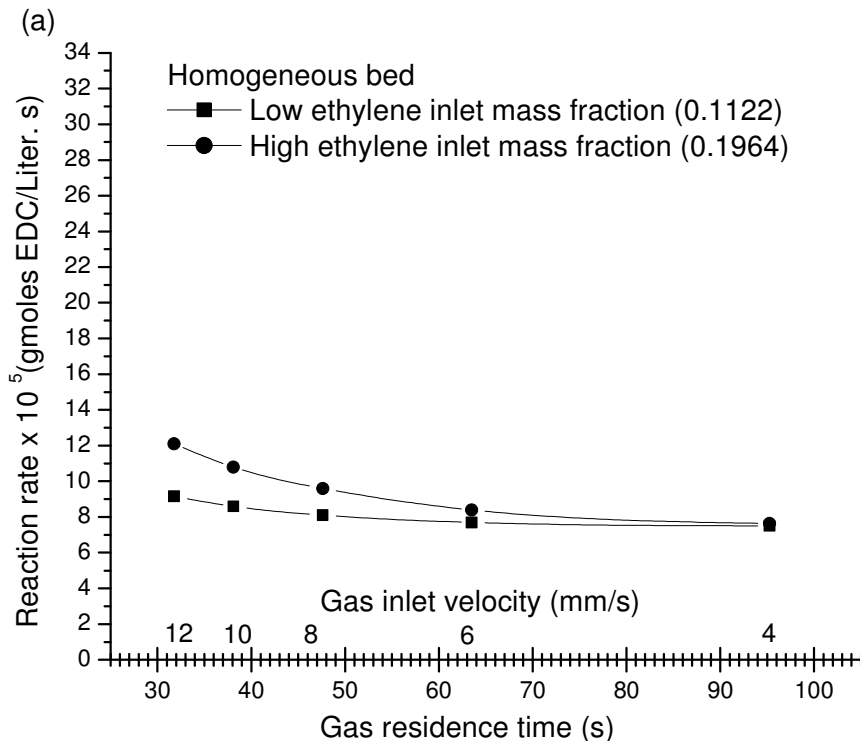
Fig. 4.34 Simulated ethylene conversion in bubbling bed vs. homogeneous bed for low and high ethylene inlet mole fractions. Average conversion for fixed bed is also given for comparison.

Fig. 4.34 gives conversion rates for the bubbling and homogeneous bed operations for low and high ethylene feed concentrations. Average conversion for fixed bed is also shown. For a particular mode of operation, the low ethylene feed concentration gave higher conversion than the higher feed concentration. This is expected since a smaller mass of ethylene would have the same gas residence time to react as a larger mass of ethylene, making conversion in the former case higher. Clearly the conversion rates are the highest for the homogeneous bed. The reason for this is the bed structure shown in Fig. 4.29 which has an expansion (and therefore gas hold-up) in between that of packed bed and bubbling bed, thereby providing optimum concentration of solid catalyst, feed

gas and residence time. Note that the inlet gas velocity required for homogeneous bed expansion is much lower than bubbling bed, making the higher conversion for homogeneous bed when compared to bubbling bed an expected conclusion.

4.3.3.2 Simulation of reaction rate of EDC in homogeneous regime

The homogeneous regime reaction rates are shown in Fig. 4.35. Fig 4.35 (a) shows variation between high and low ethylene; as inlet velocity reduces the effect of feed concentration reduces i.e. as bed becomes packed reaction rates become independent of the feed concentration.



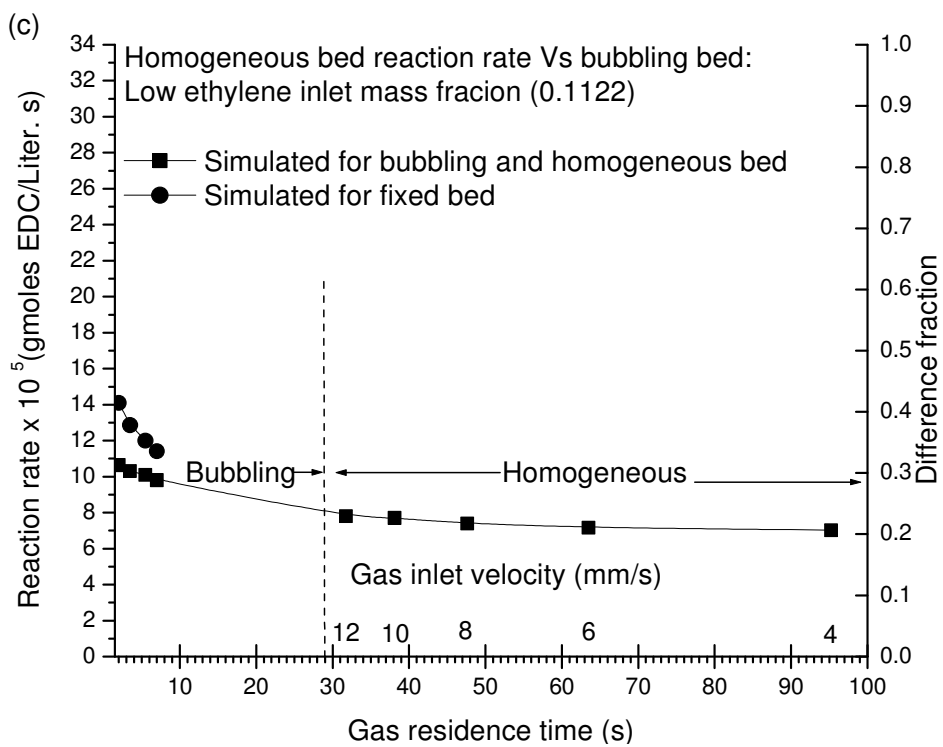
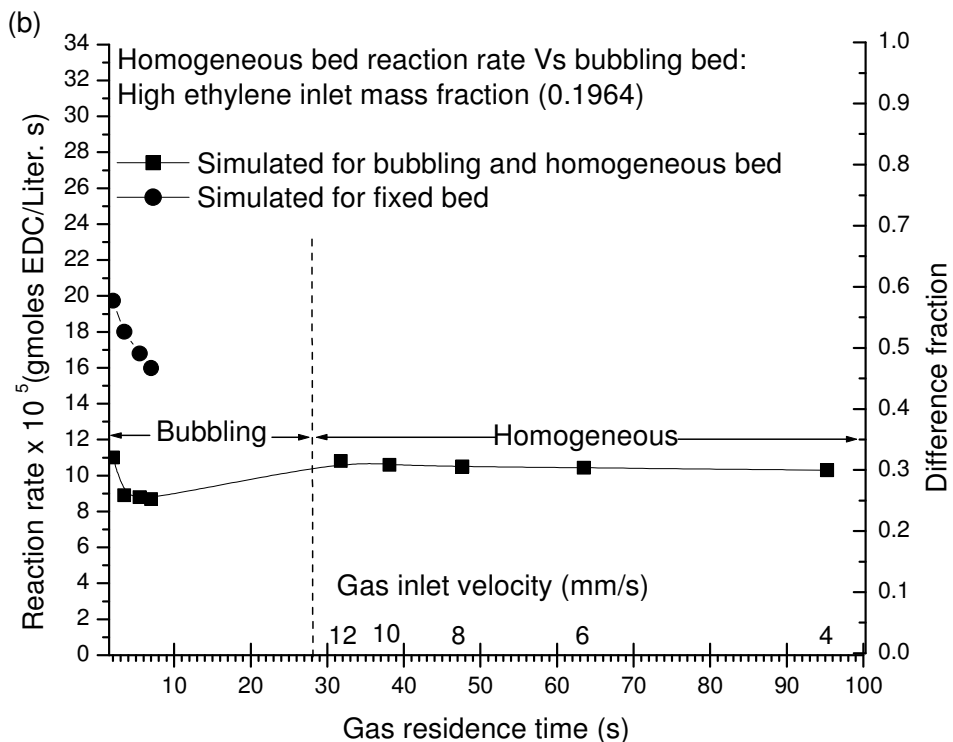


Fig. 4.35 Reaction rates of oxychlorination of ethylene for (a) Homogeneous bed, varying ethylene feed concentration. (b) All three modes with high ethylene feed concentration (c) All three modes with low ethylene feed concentration.

Fig 4.35 (b) compares the reaction rates for all three modes, but only high ethylene feed mass fraction, showing that homogeneous bed has a marginally higher reaction rate than bubbling bed. The reaction rate for fixed bed is the highest. Fig 4.35 (c) compares the reaction rates for all three modes, but only low ethylene feed mass fraction, showing that bubbling bed has a marginally higher reaction rate than homogeneous bed. Clearly the reaction rates for homogeneous bed is comparable to bubbling bed and as seen from section 4.3.3.1 the conversion rates are higher, making homogeneous regime more attractive than bubbling regime given same conditions.

4.3.4 Limitations of the reacting bed study on oxychlorination reaction of ethylene

- i. Before every iteration the species concentration changed in the reacting bed. Hence there had to be good coupling between the species concentration equations and the mass transport equations to obtain accurate solution. Poor convergence was observed in the reacting bed, which was not so for inert bed. Need for robust coupling needs to be addressed by the numerical methods.
- ii. The heterogeneous oxychlorination of ethylene was modeled in FLUENT 6.3.26 as detailed in section 3.2.1, but simulations could not be executed with current speed of computational facilities. Hence results presented were for the pseudo-heterogeneous gas phase oxychlorination of ethylene (section 3.2.2).

CHAPTER – 5

CONCLUDING REMARKS

5.1 Conclusions

Based on the simulation results obtained in this work, the following conclusions were drawn:

1. Refining mesh size from 16mm^2 to 1mm^2 does not capture the R-Z type expansion which is reported experimentally. This is attributed to the coarseness of the mesh and also to the inaccuracy of commonly used frictional stress model (Syamlal O'Brien).
2. Using drag law of Gidaspow and Syamlal O'Brien, the velocity range in which the qualitative homogeneous fluidization is observed is 4-7mm/s which matched experiment. For Wen Yu drag law this range is 4-9mm/s.
3. The resolution of meso-scale structures in homogeneous expansion requires meshes finer than 1mm^2 area.
4. Reduction of mesh size from 16mm^2 to 4mm^2 removes the effect of changing drag law, which was only seen for 16mm^2 , and presumably larger mesh sizes.
5. Determination of minimum bubbling velocity by observation of first bubble i. e. detection of bubble in 1.5-2.5s of simulated flow time, improves drastically with mesh refining ($U_{mb, 16\text{mm}^2} = 49\text{mm/s}$, $U_{mb, 1\text{mm}^2} = 18\text{mm/s}$).
6. Based on the definition of minimum bubbling velocity as persistence of dilute regions, the value of the same was approximately 8mm/s in case of Gidaspow and

Syamlal drag law and 10mm/s in case of Wen Yu drag law. And this was found irrespective of mesh size used.

7. Assuming loss of bed stability as a necessary condition for minimum bubbling, the observation of dilute regions is proposed as an alternative and less subjective marker of minimum bubbling when compared to the observation method.
8. The proposed marker for minimum bubbling has the advantage of being applicable to coarse mesh simulations as well, which have a drastically lower computational cost when compared to fine mesh simulations.
9. The use of free-slip instead of no-slip boundary condition for gas-phase had the effect of delaying observed minimum bubbling velocity.
10. The use of specular coefficient = 1 (for particle boundary condition) instead of lesser values, had the effect of delaying observed minimum bubbling velocity.
11. The use of frictional stress model as opposed to absence of frictional stress model in the simulation had the effect of delaying observed minimum bubbling velocity.
12. Using TFM simulations as basis, the most probable view of bed structure during homogeneous expansion is dynamic coexistence of dilute regions of varying voidages. The second most probable view is a largely uniform emulsion phase of particles and gas. The structure of uniformly distributed voids pervading an otherwise intact emulsion phase is least applicable.
13. TFM fine mesh simulations reveal that transition from a homogeneous to a bubbling bed occurs gradually over a velocity range. Hence rather than a discrete minimum bubbling velocity a 'transition regime' is envisioned. The transition regime contracts with increase in particle density. As the powder transitions to group B, further

contraction of transition regime occurs, culminating in the break out of bubbling at a discrete velocity i.e. the minimum fluidization velocity.

14. Fine mesh simulations confirmed that dilute regions or turbulent instabilities rather than voids are the dominant sub-grid structures or meso-scales in homogeneous regime. Expansion was considered uniform for solid packing variations of 4% and below. A consensus is required on the value of solid packing threshold to distinguish dilute regions from uniform expansion.
15. TFM expansion curves are simulated for different particle densities, and the obtained R-Z parameter values (n) were analyzed. The simulated n values decrease with terminal Reynolds number as observed in liquid systems. However, the n values themselves were higher than in liquid systems.
16. The conventional frictional stress model of Syamlal O'Brien caused over prediction of bed voidage in homogeneous regime. More recent frictional stress models in literature need to be tested for more realistic predictions of bed voidage.
17. After correcting for frictional stress, the simulated voidages is found to be under predicted (outside margin of error) when compared to experimental data and this was a consistently observation throughout the study. This under prediction of voidage was reasonably attributed to the effect of IPFs which were quantified using the proposed index (I_{IPF}) which dropped exponentially with velocity, becoming negligible in bubbling regime ($I_{IPF} < 10$, when velocity reaches 12mm/s, for systems studied). Also as the particle density and diameter increased I_{IPF} decreased showing a drop in the relevance of IPFs as the particle moves towards Geldart B type.

18. As in DEM simulations from literature, fine mesh TFM simulations also revealed the appearance of multiple bubbles at 12mm/s. Using change in key bed variable as an indicator of bubbling transition, both DPM and TFM simulations predicted regime transition around 8mm/s. The TFM without IPF contribution can adequately predict transition to bubbling implying negligible effect of IPF during the transition.
19. TFM simulations show that the transition from Geldart group A to B occurs more gradually and in a more continuous manner than is indicated by the Geldart (1973) classification chart. The area on the chart where this occurs is proposed.
20. The heterogeneous (two-step) oxychlorination of ethylene with copper dichloride catalyst to give ethylene dichloride and reduced copper monochloride (first step) is successfully modeled. However the continuous catalyst decay makes the reaction inherently unsteady state, requiring unrealistically long simulation times.
21. The pseudo heterogeneous oxychlorination of ethylene to give ethylene dichloride and water is successfully modeled and simulated for fixed bed, bubbling bed and homogeneously expanded bed. Simulated reaction rate data for fixed bed is validated with experimental data.
22. Simulated ethylene conversion is higher in bubbling bed of Geldart A particles than in fixed bed and homogeneously expanded bed affords the highest conversion.
23. Corresponding steady state reaction rates are lower in bubbling bed than in fixed bed, and homogeneous bed affords reaction rates only marginally lower than bubbling bed in spite of its much higher conversion.

24. High ethylene feed concentration results in higher reaction rates, but only marginally higher conversion rates, for both fixed and bubbling mode of operation.
25. The reaction rates of the bubbling bed are closer to that of fixed bed for lower ethylene feed concentration. Higher ethylene feed concentration creates more difference in the reaction rates between fixed and bubbling bed operations.
26. In fixed bed operation, reaction rate is found to be more sensitive to change in feed ethylene concentration than conversion. For bubbling bed, sensitivity of both parameters is nearly same and lower than for fixed bed.

5.2 Major Contributions

1. Conducted a systematic study on effect of mesh size (5 different mesh sizes were used) on TFM simulations of fluidized Geldart A particles. Effect of mesh refinement on the industrially important phenomenon of transition to bubbling and on the standard drag laws was investigated in detail. The study encompassed results from over 200 simulation runs using the coarse meshes.
2. Proposed a new marker (based on observation of over 12 sets of transient simulation runs) to predict onset of minimum bubbling: The marked appearance of persisting dilute regions. This marker was tested and verified using fine mesh simulations.
3. Conducted fine mesh study for high accuracy, which was highly CPU intensive. With available computational facilities the simulations took 6 – 12 months of wall-clock time. Around 30 fine mesh simulations were conducted.

4. Proposed microscopic structure of homogeneously expanded bed of Geldart A particles, based on fine mesh simulations. The approximation to idealized view proposed, has theoretical significance.
5. Obtained visual matrix from over six sets of fine mesh simulations showing the effect of density change (industrially important particle property) on homogeneous expansion, transition to bubbling and transition from Group A to B powder. Existence of a ‘transition regime’ was shown, which was envisioned as precursor to bubbling regime in lieu of the conventional minimum bubbling velocity.
6. Quantified IPFs in homogeneous expansion regime via an IPF index, and developed an expression for the Index which is applicable to Geldart A particles in general. This throws some light on the long standing issue in the literature of IPFs in homogeneous regime.
7. Successfully modeled and simulated simultaneous reaction and hydrodynamics in three modes: Fixed bed, bubbling bed and homogeneously expanded bed. This constituted validation of the CFD approach and multi-phase flow theory to further extend to other reactions and industrial size scale.

5.3 Future Scope of Research

The future scope of this work is enumerated below:

1. Development of closures mainly for IPFs and also for physics of static stresses (which remains when velocity gradients near zero) are required to improve the

capability of TFM. A common theory applicable to all flow regimes is required in the long term.

2. With further development of continuum model for IPFs, the level of cohesive strength allowing matching of simulated with experimental voidage curves must be obtained.
3. More experimental observations are needed to validate the existence of 'transition regime'.
4. Simulation of the heterogeneous phase reaction of oxychlorination of ethylene is required. Modeling was successfully developed in this work.

REFERENCES

- Abrahamsen, A. R., & Geldart, D. (1980). Behaviour of gas-fluidized beds of fine powders part I. Homogeneous expansion. *Powder Technology*, 26, 35-46.
- Al-Zahrani, S. M., Aljodai, A. M., & Wagialla, K. M. (2001). Modelling and simulation of 1,2-dichloroethane production by ethylene oxychlorination in fluidized-bed reactor. *Chemical Engineering Science*, 56, 621-626.
- Albadawi, A., Donoghue, D. B., Robinson, A. J., Murray, D. B., & Delauré, Y. M. C. (2014). On the assessment of a VOF based compressive interface capturing scheme for the analysis of bubble impact on and bounce from a flat horizontal surface. *International Journal of Multiphase Flow*, 65, 82-97.
- Anderson, J. (1995). *Computational Fluid Dynamics*: McGraw-Hill Education.
- Anderson, T. B., & Jackson, R. (1967). Fluid Mechanical Description of Fluidized Beds. Equations of Motion. *Industrial & Engineering Chemistry Fundamentals*, 6, 527-539.
- Andrews, Loezos, P. N., & Sundaresan, S. (2005). Coarse-Grid Simulation of Gas-Particle Flows in Vertical Risers. *Industrial & Engineering Chemistry Research*, 44, 6022-6037.
- Barreto, G. F., Yates, J. G., & Rowe, P. N. (1983). The measurement of emulsion phase voidage in gas fluidized beds of fine powders. *Chemical Engineering Science*, 38, 345-350.
- Bruni, G., Lettieri, P., Newton, D., & Yates, J. (2006). The influence of fines size distribution on the behaviour of gas fluidized beds at high temperature. *Powder Technology*, 163, 88-97.
- C.Y. Wen, Y. H. Y. (1966). Mechanics of fluidization. In (Vol. 62, pp. 100–111).
- Carrubba, R. V. (1968). Kinetics and Mechanism of the Oxychlorination of Ethylene.
- Carrubba, R. V., & Spencer, J. L. (1970). Kinetics of the Oxychlorination of Ethylene. *Industrial & Engineering Chemistry Process Design and Development*, 9, 414-419.
- Chialvo, S., Sun, J., & Sundaresan, S. (2012). Bridging the rheology of granular flows in three regimes. *Physical Review E*, 85, 021305.
- Chu, B. (1967). *Molecular Forces*. New York: Wiley.
- Cundall, P. A., & Strack, O. D. L. (1979). A discrete numerical model for granular assemblies. In *Géotechnique* (Vol. 29, pp. 47-65).
- D'Amore, M., Donsi, G., & Massimilla, L. (1979). The influence of bed moisture on fluidization characteristics of fine powders. *Powder Technology*, 23, 253-259.
- Das Sharma, S., Pugsley, T., & Delatour, R. (2006). Three-dimensional CFD model of the deaeration rate of FCC particles. *AIChE Journal*, 52, 2391-2400.
- Davidson, D. L. (2001a). The Enterprise-Wide Application of Computational Fluid Dynamics in the Chemicals Industry. In *Proceedings of the 6th World Congress of Chemical Engineering*. Melbourne, Australia.
- Davidson, D. L. (2001b). Spin Expert: The Digital Expert for the Design and Analysis of Fiber Spinning Operations. In *3rd International ASME Symposium on Computational Technology (CFD) for Fluid/Thermal/Chemical/Stress Systems and Industrial Applications* (pp. 219 - 226). Atlanta, Ga.: American Society of Mechanical Engineers.

- De Jong, J. A. H., & Nomden, J. F. (1974). Homogeneous gas—solid fluidization. *Powder Technology*, 9, 91-97.
- Di Felice, R. (1994). The voidage function for fluid-particle interaction systems. *International Journal of Multiphase Flow*, 20, 153-159.
- Ding, J., & Gidaspow, D. (1990). A bubbling fluidization model using kinetic theory of granular flow. *AIChE Journal*, 36, 523-538.
- Donsi, G., Moser, S., & Massimilla, L. (1975). Solid—solid interaction between particles of a fluid bed catalyst. *Chemical Engineering Science*, 30, 1533-1535.
- Dou, B., & Song, Y. (2010). A CFD approach on simulation of hydrogen production from steam reforming of glycerol in a fluidized bed reactor. *International Journal of Hydrogen Energy*, 35, 10271-10284.
- Dry, R. J., Judd, M. R., & Shingles, T. (1983). Two-phase theory and fine powders. *Powder Technology*, 34, 213-223.
- Ergun, S. (1952). Fluid flow through packed columns. *Chem. Engng. Prog.*, 48, 89.
- Foscolo, P. U., & Gibilaro, L. G. (1984). A fully predictive criterion for the transition between particulate and aggregate fluidization. *Chemical Engineering Science*, 39, 1667-1675.
- Foscolo, P. U., Gibilaro, L. G., & Waldram, S. P. (1983). A unified model for particulate expansion of fluidised beds and flow in fixed porous media. *Chemical Engineering Science*, 38, 1251-1260.
- Gao, J., Chang, J., Xu, C., Lan, X., & Yang, Y. (2008). CFD simulation of gas solid flow in FCC strippers. *Chemical Engineering Science*, 63, 1827-1841.
- Geldart, D. (1973). Types of gas fluidization. *Powder Technology*, 7, 285-292.
- Geldart, D., & Abrahamsen, A. R. (1978). Homogeneous fluidization of fine powders using various gases and pressures. *Powder Technology*, 19, 133-136.
- Geldart, D., & Wong, A. C. Y. (1984). Fluidization of powders showing degrees of cohesiveness—I. Bed expansion. *Chemical Engineering Science*, 39, 1481-1488.
- Gerber, S., Behrendt, F., & Oevermann, M. (2010). An Eulerian modeling approach of wood gasification in a bubbling fluidized bed reactor using char as bed material. *Fuel*, 89, 2903-2917.
- Gibilaro, L. G. (2001). *Fluidization-Dynamics*. In. Oxford: Butterworth-Heinemann.
- Gibilaro, L. G., Di Felice, R., Waldram, S. P., & Foscolo, P. U. (1985). Generalized friction factor and drag coefficient correlations for fluid-particle interactions. *Chemical Engineering Science*, 40, 1817-1823.
- Gidaspow, D. (1994.). *Multiphase Flow and Fluidization: Continuum and Kinetic Theory Description*, . New York: Academic Press.
- Gidaspow, D., Jung, J., & Singh, R. K. (2004). Hydrodynamics of fluidization using kinetic theory: an emerging paradigm: 2002 Flour-Daniel lecture. *Powder Technology*, 148, 123-141.
- Glasser, B. J., Kevrekidis, I. G., & Sundaresan, S. (1996). One- and two-dimensional travelling wave solutions in gas-fluidized beds. *Journal of Fluid Mechanics*, 306, 183-221.
- Glasser, B. J., Sundaresan, S., & Kevrekidis, I. G. (1998). From Bubbles to Clusters in Fluidized Beds. *Physical Review Letters*, 81, 1849-1852.

- Go, K. S., Kim, Y., Real Son, S., & Kim, S. D. (2010). 1,2-Dichloroethane production by two-step oxychlorination reactions in a fluidized bed reactor. *Chemical Engineering Science*, 65, 499-503.
- Goldhirsch, I. (2008). Introduction to granular temperature. *Powder Technology*, 182, 130-136.
- Government. (2014). Chemicals and Petrochemicals statistics at a glance: 2014. In: Government of India, Ministry of Chemicals and Fertilizers, Department of Chemicals and Petrochemicals statistics and monitoring division, Janpath Bhavan.
- Grace, J. R., & Clift, R. (1974). On the two-phase theory of fluidization. *Chemical Engineering Science*, 29, 327-334.
- Hansen, K. G., Solberg, T., & Hjertager, B. H. (2004). A three-dimensional simulation of gas/particle flow and ozone decomposition in the riser of a circulating fluidized bed. *Chemical Engineering Science*, 59, 5217-5224.
- Hejazian, M., Moraveji, M. K., & Beheshti, A. (2014). Comparative study of Euler and mixture models for turbulent flow of Al₂O₃ nanofluid inside a horizontal tube. *International Communications in Heat and Mass Transfer*, 52, 152-158.
- Herzog, N., & Egbers, C. (2013). Numerical prediction of pressure drop and particle separation efficiency of some vane-type dust filters. *Powder Technology*, 245, 265-272.
- Hosseini, S., Rahimi, R., Zivdar, M., & Samimi, A. (2009). CFD simulation of gas-solid bubbling fluidized bed containing FCC particles. *Korean Journal of Chemical Engineering*, 26, 1405-1413.
- Hrenya, C. M., & Sinclair, J. L. (1997). Effects of particle-phase turbulence in gas-solid flows. *AIChE Journal*, 43, 853-869.
- Igci, Y., Andrews, A. T., Sundaresan, S., Pannala, S., & O'Brien, T. (2008). Filtered two-fluid models for fluidized gas-particle suspensions. *AIChE Journal*, 54, 1431-1448.
- Igci, Y., Pannala, S., Benyahia, S., & Sundaresan, S. (2011). Validation Studies on Filtered Model Equations for Gas-Particle Flows in Risers. *Industrial & Engineering Chemistry Research*, 51, 2094-2103.
- Igci, Y., & Sundaresan, S. (2011a). Constitutive Models for Filtered Two-Fluid Models of Fluidized Gas-Particle Flows. *Industrial & Engineering Chemistry Research*, 50, 13190-13201.
- Igci, Y., & Sundaresan, S. (2011b). Verification of filtered two-fluid models for gas-particle flows in risers. *AIChE Journal*, 57, 2691-2707.
- J. Kuipers, W. v. S. (1998). *Computational Fluid Dynamics Applied to Chemical Reaction Engineering*. *Adv. Chem. Eng.*, 24, 227-328.
- J.F. Davidson, R. C., D. Harrison. (1985). *Fluidization*. London: Academic Press.
- Jackson, R. (1997). Locally averaged equations of motion for a mixture of identical spherical particles and a Newtonian fluid. *Chemical Engineering Science*, 52, 2457-2469.
- Jackson, R. (2000). *The Dynamics of Fluidized Particles* (1st ed.): Cambridge University Press.
- Jacob, K. V., & Weimer, A. W. (1987). High-pressure particulate expansion and minimum bubbling of fine carbon powders. *AIChE Journal*, 33, 1698-1706.

- Jahangiri, M., Jacobsen, R. T., Stewart, R. B., & McCarty, R. D. (1986). Thermodynamic Properties of Ethylene from the Freezing Line to 450 K at Pressures to 260 MPa. *Journal of Physical and Chemical Reference Data*, 15, 593-734.
- Jajcevic, D., Siegmann, E., Radeke, C., & Khinast, J. G. (2013). Large-scale CFD–DEM simulations of fluidized granular systems. *Chemical Engineering Science*, 98, 298-310.
- Jing, Q., Lou, H., Fei, J., Hou, Z., & Zheng, X. (2004). Syngas production from reforming of methane with CO₂ and O₂ over Ni/SrO–SiO₂ catalysts in a fluidized bed reactor. *International Journal of Hydrogen Energy*, 29, 1245-1251.
- Johnson, P. C., & Jackson, R. (1987). Frictional–collisional constitutive relations for granular materials, with application to plane shearing. *Journal of Fluid Mechanics*, 176, 67-93.
- Jung, J., Gidaspow, D., & Gamwo, I. K. (2006). BUBBLE COMPUTATION, GRANULAR TEMPERATURES, AND REYNOLDS STRESSES. *Chemical Engineering Communications*, 193, 946-975.
- Khoe, G. K., Ip, T. L., & Grace, J. R. (1991). Rheological and fluidization behaviour of powders of different particle size distribution. *Powder Technology*, 66, 127-141.
- Klinzing, G. E., Rizk, F., & Marcus, R. (2011). *Pneumatic Conveying of Solids: A theoretical and practical approach*: Springer.
- Kobayashi, T., Kawaguchi, T., Tanaka, T., & Tsuji, Y. (2002). DEM analysis on flow pattern of Geldart's group A particles in fluidized bed. In *Proceedings of the World Congress on Particle Technology 4 (CD-ROM)*. Sydney, Australia,.
- Kobayashi, T., Tanaka, T., Shimada, N., & Kawaguchi, T. (2013). DEM–CFD analysis of fluidization behavior of Geldart Group A particles using a dynamic adhesion force model. *Powder Technology*, 248, 143-152.
- Kopyscinski, J., Schildhauer, T. J., & Biollaz, S. M. A. (2011). Methanation in a fluidized bed reactor with high initial CO partial pressure: Part I—Experimental investigation of hydrodynamics, mass transfer effects, and carbon deposition. *Chemical Engineering Science*, 66, 924-934.
- Kuipers, J. A. M., Tammes, H., Prins, W., & van Swaaij, W. P. M. (1992). Experimental and theoretical porosity profiles in a two-dimensional gas-fluidized bed with a central jet. *Powder Technology*, 71, 87-99.
- Kunii, D., & Levenspiel, O. (1991). *Fluidization Engineering*: Butterworth-Heinemann.
- L. Cammarata, P. L., G. Micale, D. Colman. (2003). 2D and 3D CFD simulations of bubbling fluidized beds using Eulerian-Eulerian models. *Int J Chem Reactor Eng.*, 1 1-19.
- Lee, W.-K., Jovanovic, G., & Kim, H. (1999). The effect of interparticle forces on fluidization regimes in the magnetized fluidized beds. *Korean Journal of Chemical Engineering*, 16, 362-370.
- Lettieri, P., Newton, D., & Yates, J. G. (2001). High temperature effects on the dense phase properties of gas fluidized beds. *Powder Technology*, 120, 34-40.
- Lettieri, P., Newton, D., & Yates, J. G. (2002). Homogeneous bed expansion of FCC catalysts, influence of temperature on the parameters of the Richardson–Zaki equation. *Powder Technology*, 123, 221-231.

- Lettieri, P., Yates, J. G., & Newton, D. (2000). The influence of interparticle forces on the fluidization behaviour of some industrial materials at high temperature. *Powder Technology*, 110, 117-127.
- Li, J., Ge, W., Wang, W., Yang, N., Liu, X., Wang, L., He, X., Wang, X., Wang, J., & Kwauk, M. (2013). *From Multiscale Modeling to Meso-Science: A Chemical Engineering Perspective*: Springer.
- Li, T., Gopalakrishnan, P., Garg, R., & Shahnam, M. (2012). CFD-DEM study of effect of bed thickness for bubbling fluidized beds. *Particuology*, 10, 532-541.
- Li, T., Pougatch, K., Salcudean, M., & Grecov, D. (2008). Numerical simulation of horizontal jet penetration in a three-dimensional fluidized bed. *Powder Technology*, 184, 89-99.
- Li, Y. H., Lu, G. Q., & Rudolph, V. (1998). The kinetics of NO and N₂O reduction over coal chars in fluidised-bed combustion. *Chemical Engineering Science*, 53, 1-26.
- Lindborg, H., Lysberg, M., & Jakobsen, H. A. (2007). Practical validation of the two-fluid model applied to dense gas-solid flows in fluidized beds. *Chemical Engineering Science*, 62, 5854-5869.
- Liu, M., Li, J., & Kwauk, M. (2001). Application of the energy-minimization multi-scale method to gas-liquid-solid fluidized beds. *Chemical Engineering Science*, 56, 6805-6812.
- Liu, X., Zhu, C., Geng, S., Yao, M., Zhan, J., & Xu, G. (In press). Two-fluid modeling of Geldart A particles in gas-solid micro-fluidized beds. *Particuology*.
- Loha, C., Chattopadhyay, H., & Chatterjee, P. K. (2012). Assessment of drag models in simulating bubbling fluidized bed hydrodynamics. *Chemical Engineering Science*, 75, 400-407.
- Lun, C. K. K., & Savage, S. B. (1986). The effects of an impact velocity dependent coefficient of restitution on stresses developed by sheared granular materials. *Acta Mechanica*, 63, 15-44.
- Lun, C. K. K., Savage, S. B., Jeffrey, D. J., & Chepurniy, N. (1984). Kinetic theories for granular flow: inelastic particles in Couette flow and slightly inelastic particles in a general flow field. *Journal of Fluid Mechanics*, 140, 223-256.
- Ma, D., Liu, M., Zu, Y., & Tang, C. (2012). Two-dimensional volume of fluid simulation studies on single bubble formation and dynamics in bubble columns. *Chemical Engineering Science*, 72, 61-77.
- Makkawi, Y. T., Wright, P. C., & Ocone, R. (2006). The effect of friction and interparticle cohesive forces on the hydrodynamics of gas-solid flow: A comparative analysis of theoretical predictions and experiments. *Powder Technology*, 163, 69-79.
- Massimilla, L., Donsì, G., & Zucchini, C. (1972). The structure of bubble-free gas fluidized beds of fine fluid cracking catalyst particles. *Chemical Engineering Science*, 27, 2005-2015.
- Mazzei, L., & Lettieri, P. (2007). A drag force closure for uniformly dispersed fluidized suspensions. *Chemical Engineering Science*, 62, 6129-6142.
- Mazzei, L., & Lettieri, P. (2008). CFD simulations of expanding/contracting homogeneous fluidized beds and their transition to bubbling. *Chemical Engineering Science*, 63, 5831-5847.

- McKeen, T., & Pugsley, T. (2003). Simulation and experimental validation of a freely bubbling bed of FCC catalyst. *Powder Technology*, 129, 139-152.
- Mills, P. L., Randall, H. T., & McCracken, J. S. (1999). Redox kinetics of VOPO₄ with butane and oxygen using the TAP reactor system. *Chemical Engineering Science*, 54, 3709-3722.
- Molerus, O. (1982). Interpretation of Geldart's type A, B, C and D powders by taking into account interparticle cohesion forces. *Powder Technology*, 33, 81-87.
- Moreira, J. C. S., & Pires, C. A. M. (2010). Modelling and simulation of an oxychlorination reactor in a fluidized bed. *The Canadian Journal of Chemical Engineering*, 88, 350-358.
- Movahedirad, S., Dehkordi, A. M., Molaie, E. A., Haghi, M., Banaei, M., & Kuipers, J. A. M. (2014). Bubble Splitting in a Pseudo-2D Gas-Solid Fluidized Bed for Geldart B-Type Particles. *Chemical Engineering & Technology*, 37, 2096-2102.
- Mutsers, S. M. P., & Rietema, K. (1977). The effect of interparticle forces on the expansion of a homogeneous gas-fluidized bed. *Powder Technology*, 18, 239-248.
- Oke, O., Lettieri, P., & Mazzei, L. (2015). An investigation on the mechanics of homogeneous expansion in gas-fluidized beds. *Chemical Engineering Science*, 127, 95-105.
- Owoyemi, O., & Lettieri, P. (2008). Stability analysis and CFD validation of a new fluid-particle interaction force for mono-component gas-solid fluidized beds. *Powder Technology*, 183, 27-36.
- Oyebanjo Oke, Luca Mazzei, & Lettieri, P. (2013). Theoretical investigation of the behavior of cohesive homogeneous gas- fluidized beds. In 14th International Conference on Fluidization. Noordwijkerhout, The Netherlands.
- Parmentier, J.-F., Simonin, O., & Delsart, O. (2012). A functional subgrid drift velocity model for filtered drag prediction in dense fluidized bed. *AIChE Journal*, 58, 1084-1098.
- Perry, R. H., Green, D. W., & Maloney, J. O. (1999). *Perry's Chemical Engineers' Handbook*: McGraw-Hill.
- Raman, V., Fox, R. O., Harvey, A. D., & West, D. H. (2001). CFD Analysis of Premixed Methane Chlorination Reactors with Detailed Chemistry. *Industrial & Engineering Chemistry Research*, 40, 5170-5176.
- Renzo, A. D., & Maio, F. P. D. (2007). Homogeneous and bubbling fluidization regimes in DEM-CFD simulations: Hydrodynamic stability of gas and liquid fluidized beds. *Chemical Engineering Science*, 116 – 130.
- Rhodes, M. J., Wang, X. S., Nguyen, M., Stewart, P., & Liffman, K. (2001). Use of discrete element method simulation in studying fluidization characteristics: influence of interparticle force. *Chemical Engineering Science*, 56, 69-76.
- Richardson, J. F., & Zaki, W. N. (1954). Sedimentation and fluidisation. Part 1. *Trans.Inst.Chem.Eng.*, 32, 35-53.
- Rietema, K., Cottaar, E. J. E., & Piepers, H. W. (1993). The effects of interparticle forces on the stability of gas-fluidized beds—II. Theoretical derivation of bed elasticity on the basis of van der Waals forces between powder particles. *Chemical Engineering Science*, 48, 1687-1697.

- Rietema, K., & Piepers, H. W. (1990). The effect of interparticle forces on the stability of gas-fluidized beds—I. Experimental evidence. *Chemical Engineering Science*, 45, 1627-1639.
- S. Ogawa, A. U., N. Oshima. (1980). On the Equation of Fully Fluidized Granular Materials. 31, 483-495.
- Sai Prasad, P. S., Prasad, K. B. S., & Ananth, M. S. (2001). Parameter Estimation in a Fixed-Bed Reactor Operating under Unsteady State: Oxochlorination of Ethylene†. *Industrial & Engineering Chemistry Research*, 40, 5487-5495.
- Schaeffer, D. G. (1987). Instability in the evolution equations describing incompressible granular flow. *Journal of Differential Equations*, 66, 19-50.
- Schneiderbauer, S., Puttinger, S., & Pirker, S. (2013). Comparative analysis of subgrid drag modifications for dense gas-particle flows in bubbling fluidized beds. *AIChE Journal*, 59, 4077-4099.
- Shang, Z., Lou, J., & Li, H. (2013). A novel Lagrangian algebraic slip mixture model for two-phase flow in horizontal pipe. *Chemical Engineering Science*, 102, 315-323.
- Shuai, W., Huilin, L., Guodong, L., Zhiheng, S., Pengfei, X., & Gidaspow, D. (2011). Modeling of cluster structure-dependent drag with Eulerian approach for circulating fluidized beds. *Powder Technology*, 208, 98-110.
- Sidorenko, I., & Rhodes, M. J. (2004). Influence of pressure on fluidization properties. *Powder Technology*, 141, 137-154.
- Simone, S., & Harriott, P. (1980). Fluidization of fine powders with air in the particulate and the bubbling regions. *Powder Technology*, 26, 161-167.
- Sinclair, J. L., & Jackson, R. (1989). Gas-particle flow in a vertical pipe with particle-particle interactions. *AIChE Journal*, 35, 1473-1486.
- Snider, D., & Banerjee, S. (2010). Heterogeneous gas chemistry in the CFPD Eulerian–Lagrangian numerical scheme (ozone decomposition). *Powder Technology*, 199, 100-106.
- Srinivasan, V., Salazar, A. J., & Saito, K. (2010). Modeling the disintegration of cavitating turbulent liquid jets using a novel VOF–CIMP approach. *Chemical Engineering Science*, 65, 2782-2796.
- Stewart, R. B., Jacobsen, R. T., & Wagner, W. (1991). Thermodynamic Properties of Oxygen from the Triple Point to 300 K with Pressures to 80 MPa. *Journal of Physical and Chemical Reference Data*, 20, 917-1021.
- Syamlal, M., Rogers, W., & O'Brien, T. J. (1993). MFIX documentation: Theory guide. Technical Note, DOE/METC-94/1004, NTIS/DE94000087, National Technical Information Service, Springfield, VA.
- T. Kobayashi, T. K., T. Tanaka, Y. Tsuji (2002). DEM analysis on flow pattern of Geldart's group A particles in fluidized bed. In *Proceedings of the World Congress on Particle Technology 4 (CD-ROM)*. Sydney, Australia,.
- Tsuji, T., Yabumoto, K., & Tanaka, T. (2008). Spontaneous structures in three-dimensional bubbling gas-fluidized bed by parallel DEM–CFD coupling simulation. *Powder Technology*, 184, 132-140.
- van Wachem, B., & Sasic, S. (2008). Derivation, simulation and validation of a cohesive particle flow CFD model. *AIChE Journal*, 54, 9-19.

- van Wachem, B. G. M., Schouten, J. C., van den Bleek, C. M., Krishna, R., & Sinclair, J. L. (2001). Comparative analysis of CFD models of dense gas–solid systems. *AIChE Journal*, 47, 1035-1051.
- Wachi, S., & Asai, Y. (1994). Kinetics of 1,2-Dichloroethane Formation from Ethylene and Cupric Chloride. *Industrial & Engineering Chemistry Research*, 33, 259-264.
- Wang, J. (2009). A Review of Eulerian Simulation of Geldart A Particles in Gas-Fluidized Beds. *Industrial & Engineering Chemistry Research*, 48, 5567-5577.
- Wang, J., & Liu, Y. (2010). EMMS-based Eulerian simulation on the hydrodynamics of a bubbling fluidized bed with FCC particles. *Powder Technology*, 197, 241-246.
- Wang, J., van der Hoef, M. A., & Kuipers, J. A. M. (2009). Why the two-fluid model fails to predict the bed expansion characteristics of Geldart A particles in gas-fluidized beds: A tentative answer. *Chemical Engineering Science*, 64, 622-625.
- Wang, J., van der Hoef, M. A., & Kuipers, J. A. M. (2010). CFD study of the minimum bubbling velocity of Geldart A particles in gas-fluidized beds. *Chemical Engineering Science*, 65, 3772-3785.
- Wang, J., van der Hoef, M. A., & Kuipers, J. A. M. (2011). The role of scale resolution versus inter-particle cohesive forces in two-fluid modeling of bubbling fluidization of Geldart A particles. *Chemical Engineering Science*, 66, 4229-4240.
- Wang, W., & Li, J. (2007). Simulation of gas–solid two-phase flow by a multi-scale CFD approach—of the EMMS model to the sub-grid level. *Chemical Engineering Science*, 62, 208-231.
- Wang, W., Lu, B., Zhang, N., Shi, Z., & Li, J. (2010). A review of multiscale CFD for gas–solid CFB modeling. *International Journal of Multiphase Flow*, 36, 109-118.
- Wang, Y., Zou, Z., Li, H., & Zhu, Q. (2014). A new drag model for TFM simulation of gas–solid bubbling fluidized beds with Geldart-B particles. *Particuology*, 15, 151-159.
- Xie, H., & Geldart, D. (1995). Fluidization of FCC powders in the bubble-free regime: effect of types of gases and temperature. *Powder Technology*, 82, 269-277.
- Xie, H. Y., & Geldart, D. (1995). Fluidization of FCC powders in the bubble-free regime: effect of types of gases and temperature. *Powder Technology*, 82, 269-277.
- Xu, Y., Liu, M., & Tang, C. (2013). Three-dimensional CFD–VOF–DPM simulations of effects of low-holdup particles on single-nozzle bubbling behavior in gas–liquid–solid systems. *Chemical Engineering Journal*, 222, 292-306.
- Yang, N., Wang, W., Ge, W., & Li, J. (2003). CFD simulation of concurrent-up gas–solid flow in circulating fluidized beds with structure-dependent drag coefficient. *Chemical Engineering Journal*, 96, 71-80.
- Yates, Y. G., Cheesman, D. J., & Sergeev, Y. A. (1994). Experimental observations of voidage distribution around bubbles in a fluidized bed. *Chemical Engineering Science*, 49, 1885-1895.
- Ye, M., van der Hoef, M. A., & Kuipers, J. A. M. (2004). A numerical study of fluidization behavior of Geldart A particles using a discrete particle model. *Powder Technology*, 139, 129-139.
- Ye, M., van der Hoef, M. A., & Kuipers, J. A. M. (2005). The effects of particle and gas properties on the fluidization of Geldart A particles. *Chemical Engineering Science*, 60, 4567-4580.

- Ye, M., Wang, J., van der Hoef, M. A., & Kuipers, J. A. M. (2008). Two-fluid modeling of Geldart A particles in gas-fluidized beds. *Particuology*, 6, 540-548.
- Yujie, Z., Mingyan, L., Yonggui, X., & Can, T. (2012). Three-dimensional volume of fluid simulations on bubble formation and dynamics in bubble columns. *Chemical Engineering Science*, 73, 55-78.
- Zhang, D. Z., & Rauenzahn, R. M. (1997). A viscoelastic model for dense granular flows. *Journal of Rheology*, 41, 1275-1298.
- Zhang, K., Brandani, S., Bi, J., & Jiang, J. (2008). CFD simulation of fluidization quality in the three-dimensional fluidized bed. *Progress in Natural Science*, 18, 729-733.
- Zhang, S.-p., Li, X.-j., Li, Q.-y., Xu, Q.-l., & Yan, Y.-j. (2011). Hydrogen production from the aqueous phase derived from fast pyrolysis of biomass. *Journal of Analytical and Applied Pyrolysis*, 92, 158-163.
- Zhuang, Y.-Q., Gao, X., Zhu, Y.-p., & Luo, Z.-h. (2012). CFD modeling of methanol to olefins process in a fixed-bed reactor. *Powder Technology*, 221, 419-430.
- Zimmermann, S., & Taghipour, F. (2005). CFD Modeling of the Hydrodynamics and Reaction Kinetics of FCC Fluidized-Bed Reactors. *Industrial & Engineering Chemistry Research*, 44, 9818-9827.

APPENDIX – I

User Defined function (C++) for heterogeneous reaction occurring in two phases.

```
#include "udf.h"
DEFINE_HET_RXN_RATE(flbreduction, c, t, hr, mw, yi, rr, rr_t)
{
int i, j; /* i, j are apecies index for ethylene in gas and cucl2 in solid phase*/
double k, m,n;
Thread **pt;
Thread *tg;
Thread *ts;

/* d is domain ID */
pt=THREAD_SUB_THREADS(t);/* returns array of pointers tp phase level threads*/

tg=pt[0]; /* thread pointer to gas phase */

ts=pt[1];/* thread pointer to solid phase*/

k=94.7625; /* raction rate constant*/
```

```

i=1; /* index of species in gas phase */
j=1; /* index of species in solid phase */
m=28.05; /* molecular weight of gas species */
n=134.48; /* molecular weight of solid species */

```

```

*rr = (k * (C_YI(c,tg,i)/m) * C_R(c,tg) * (C_YI(c,ts,j)/n) * C_R(c,ts))/(1+(0.63 *
(C_YI(c,tg,i)/m) * C_R(c,tg)));
}

```

```

Microsoft Visual C++ - [flbreduction.c *]
File Edit View Insert Project Build Tools Window Help
/*gas species is ethylene- active solid species in solid phase is CuCl2 */
#include "udf.h"
DEFINE_HET_RXN_RATE(flbreduction, c, t, hr, mw, yi, rr, rr_t)
{
  int i, j; /* i, j are species index for ethylene in gas and cucl2 in solid phase*/
  double k, m, n;
  Thread **pt;
  Thread *tg;
  Thread *ts;

  /* d is domain ID */
  pt=THREAD_SUB_THREADS(t); /* returns array of pointers to phase level threads*/

  tg=pt[0]; /* thread pointer to gas phase */

  ts=pt[1]; /* thread pointer to solid phase*/

  k=94.7625; /* reaction rate constant*/
  i=1; /* index of species in gas phase */
  j=1; /* index of species in solid phase */
  m=28.05; /* molecular weight of gas species */
  n=134.48; /* molecular weight of solid species */

  *rr = (k * (C_YI(c,tg,i)/m) * C_R(c,tg) * (C_YI(c,ts,j)/n) * C_R(c,ts))/(1+(0.63 * (
}
Ready Ln 10, Col 12 REC COL OVR READ

```

APPENDIX – II

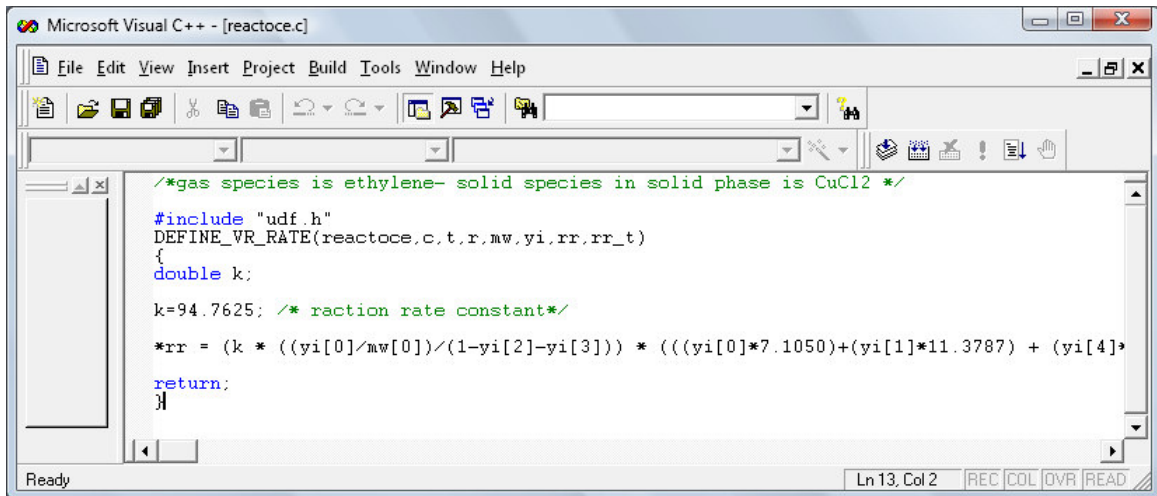
User Defined function (C++) for heterogeneous reaction with phase correction to make reaction occur in single phase.

```
#include "udf.h"
DEFINE_VR_RATE(reactoce,c,t,r,mw,yi,rr,rr_t)
{
double k;

k = 94.7625; /* raction rate constant*/

*rr = (k * ((yi[0]/mw[0])/(1-yi[2]-yi[3])) * (((yi[0]*7.1050)+(yi[1]*11.3787) +
(yi[4]*6.4938))/(yi[0]+yi[1]+yi[4])) * ((yi[3]/mw[3])/(1-yi[0]-yi[1]-yi[4])) *
(((yi[2]*3530)+(yi[3]*3054)+(1*2000))/(yi[2]+yi[3]+1)))/(1+(0.63 *(yi[0]/mw[0])/(1-
yi[2]-yi[3])));

return;
}
```



```
Microsoft Visual C++ - [reactoce.c]
File Edit View Insert Project Build Tools Window Help
/*gas species is ethylene- solid species in solid phase is CuCl2 */
#include "udf.h"
DEFINE_VR_RATE(reactoce,c,t,r,mw,yi,rr,rr_t)
{
double k;

k=94.7625; /* raction rate constant*/

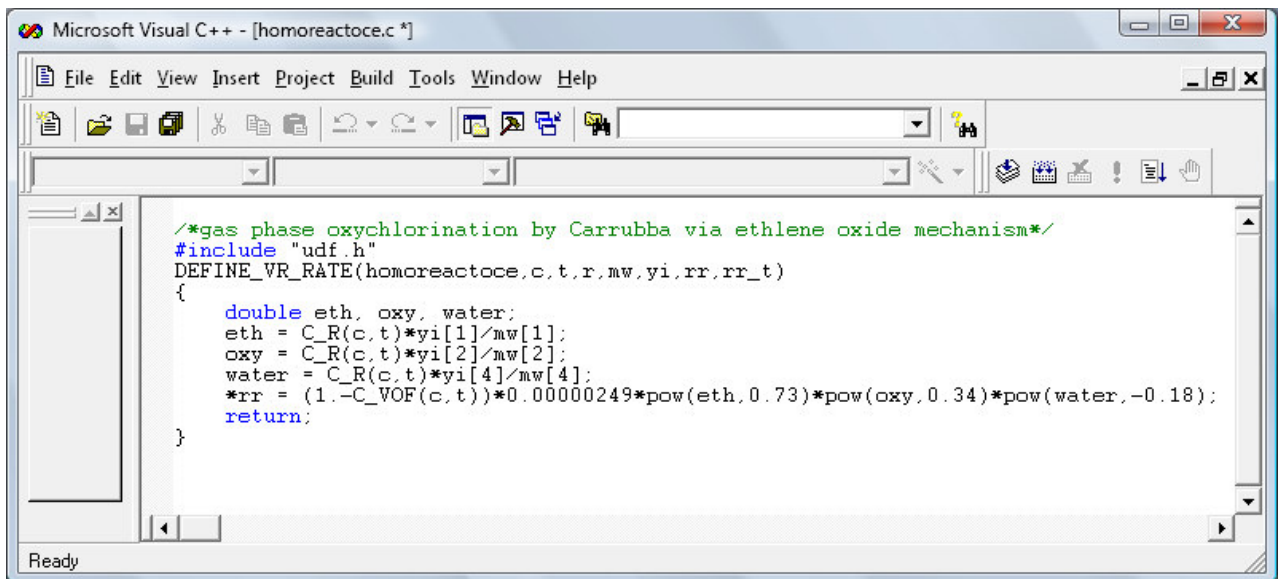
*rr = (k * ((yi[0]/mw[0])/(1-yi[2]-yi[3])) * (((yi[0]*7.1050)+(yi[1]*11.3787) + (yi[4]*
return;
}
```

Ready Ln 13, Col 2 REC COL OVR READ

APPENDIX – III

User Defined function (C++) for single phase homogeneous reaction to form EDC.

```
/*gas phase oxychlorination by Carrubba via ethlene oxide mechanism*/
#include "udf.h"
DEFINE_VR_RATE(homoreactoce,c,t,r,mw,yi,rr,rr_t)
{
    double eth, oxy, water;
    eth = C_R(c,t)*yi[1]/mw[1];
    oxy = C_R(c,t)*yi[2]/mw[2];
    water = C_R(c,t)*yi[4]/mw[4];
    *rr = (1.-C_VOF(c,t))*0.00000249*pow(eth,0.73)*pow(oxy,0.34)*pow(water,-
0.18);
    return;
}
```



The image shows a screenshot of the Microsoft Visual C++ editor window. The title bar reads "Microsoft Visual C++ - [homoreactoce.c *]". The menu bar includes "File", "Edit", "View", "Insert", "Project", "Build", "Tools", "Window", and "Help". The toolbar contains various icons for file operations and editing. The main text area displays the following C++ code:

```
/*gas phase oxychlorination by Carrubba via ethlene oxide mechanism*/
#include "udf.h"
DEFINE_VR_RATE(homoreactoce,c,t,r,mw,yi,rr,rr_t)
{
    double eth, oxy, water;
    eth = C_R(c,t)*yi[1]/mw[1];
    oxy = C_R(c,t)*yi[2]/mw[2];
    water = C_R(c,t)*yi[4]/mw[4];
    *rr = (1.-C_VOF(c,t))*0.00000249*pow(eth,0.73)*pow(oxy,0.34)*pow(water,-0.18);
    return;
}
```

The status bar at the bottom left shows "Ready".

LIST OF PUBLICATIONS

International Journals (Referred)

1. Sande, P.C., Ray, S., 2014. Mesh size effect on CFD simulation of gas-fluidized Geldart A particles. *Powder Technology*, 264, 43-53.
2. Sande, P.C., Ray, S., 2015. Fine mesh CFD study on gas-fluidization: homogeneous expansion and bubbling transition. *Industrial and Engineering Chemistry Research*. *Under revision*.
3. Sande, P.C., Ray, S., 2015. Computational fluid dynamic study on bed structure of gas-fluidized Geldart A particles using Two-fluid model. *Communicating*.
4. Sande, P.C., Ray, S., 2015. A Computational fluid dynamic approach to simulating oxychlorination of ethylene reaction in fluidized bed. *Communicating*.

Conference papers

5. Sande, P.C., Ray, S., 'Modeling and simulation of a nitrogen fluidized bed of copper-dichloride using Computational Fluid Dynamics', National Conference on Modeling, Computational Fluid Dynamics and Operations Research, 4th-5th Feb, 2012, Dep. of Mathematics, BITS Pilani, Pilani campus. .
6. Sande, P.C., Ray, S., Symposium on, Recent Trends in Chemical Sciences, 25th March, 2012, Dep. of Chemistry BITS Pilani. Simulation of Reactive and Inert Fluidized Bed using CFD Approach.

International Conference

7. Sande, P.C., Ray, S., 2015. 'Computational fluid dynamic study on bed structure of gas-fluidized Geldart A particles using Two-fluid model '. 2015, 4th International Conference on Chemical and Process Engineering (ICCPE 2015) to be held during June 15th -16th , 2015, Madrid, Spain. *Accepted*.

Miscellaneous

1. Conducted workshop session for internal and external candidates on 'Simulation of gas-solid fluidized bed', for National Workshop on Modeling and Computation, BITS Pilani, Pilani campus, Feb 23rd - 24th , 2013
2. Published articles 'Get FLUENT with CFD' in student Chemical Engineering magazines to inspire students to explore CFD simulation tools.
3. Given talks to undergraduate students, BITS Pilani, on applications of CFD in Chemical Engineering.
4. Guided Design projects for undergraduate students, BITS Pilani, using CFD as simulation tool.

BIOGRAPHIES

Biography of the Candidate

Priya Christina Sande is currently working as Lecturer in the Department of Chemical Engineering at Birla Institute of Technology and Science (BITS) – Pilani campus, and is carrying out research in Fluidization Technology using Computational Fluid Dynamics (CFD) as a simulation tool. Along with her guide she has international journal publications in the field. She teaches undergraduate and post graduate courses in Science and Chemical Engineering such as Thermodynamics, Material Science, Fluid Mechanics, Heat Transfer, and Petroleum Refinery Engineering.

P.C. Sande completed her 10th class studies from Sacred heart Girls' High School, Bangalore. ICSE Board examinations are known for their high standards in Mathematics, Science and English. She went on to secure 90% (in each) Mathematics, Physics, Chemistry, and Biology and received merit certificates for the same. She also won accolades for debate and public speaking. She then completed her pre-university plus two from Mount Carmel College, Bangalore. She secured 90% (in each) Mathematics, Physics, Chemistry and Electronics., She ranked among the top 2000 (Out of 1.2 lakh candidates) in the Common Entrance Test examination and secured a free seat in Chemical Engineering discipline in BMS College of Engineering, Bangalore. BMS College ranks among the top three colleges of the state along with R.V. College and M.S. Ramaiah College. *She was the only student in her class to complete the Bachelor of Engineering degree with distinctions (above 70% average) in every semester and distinction overall.* In the final year she did her dissertation in the field of interfacial phenomenon and two papers from the project won first place in student symposiums in RV College and MS Ramaiah College. She then completed a six month internship in a Pharmaceutical company in Bangalore where she improved the working of unit operations, specifically sugar pills production and coating unit. She secured high ranks in competitive examinations like GRE and GATE. She got admission into the M.E. Program in Chemical Engineering in BITS, Pilani, Pilani campus, and was also selected as teaching assistant. She did her ME Dissertation in simulation of reactive extraction residual curves. In 2008 she was appointed as a Lecturer after clearing the PhD qualifying examination. She was elected member of Institution of Engineers, India (IEI) and Indian Institute of Chemical Engineers (IChE).

Biography of the Supervisor

Prof. Saumi Ray, Associate Professor, Department of Chemistry at Birla Institute of Technology and Science (BITS) – Pilani campus, has over 10 years of teaching, and research experience. She completed her B Tech from Calcutta University and did her PhD from Indian Institute of Science (IISc), Bangalore in 2003.

Her current research interests are in the field of Materials Chemistry and Simulation using Computational Fluid Dynamics (CFD). She has publications in reputed international journals and has completed projects funded by external agencies. She has been guiding three Ph. D candidates. She is an active member of various academic boards, and has mentored probation students who have later come out of probation. She has an exemplary teaching record with good peer and student feedback for her courses.